UNIVERSITY OF READING
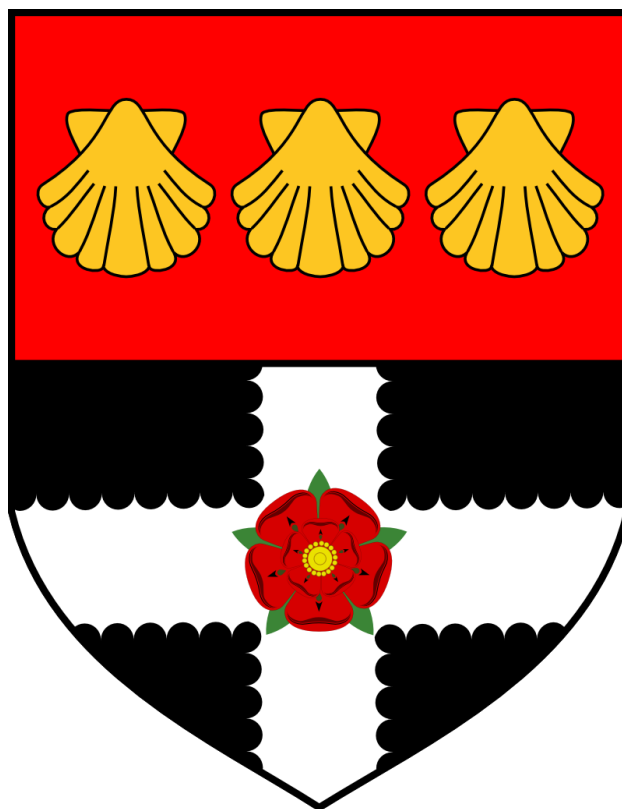
Artificial lipid membranes to study the platelet CLEC-2-podoplanin interaction

A thesis submitted for the degree of Doctor of Philosophy

By Marcin Andrzej Sowa

Institute for Cardiovascular and Metabolic Research

School of Biological Sciences

September 2021

Declaration

I confirm that this is my own work and the use of all material from other sources has been properly and fully acknowledged.

Signed: Marcin Sowa

Date: 20/09/2021

Abstract

The C-type lectin-like receptor-2 (CLEC-2) is a platelet receptor for the endogenous ligand podoplanin. This interaction contributes to several pathophysiological roles, such as lymphangiogenesis, preservation of blood and lymphatic vessel integrity, organ development and tumour metastasis, however the mechanism of this interaction is poorly understood. The aims of this thesis were to develop a reconstituted artificial lipid membrane platform as an experimental approach to investigate what determinates the biochemical properties of platelet signalling; and to identify a small-molecule inhibitor of the CLEC-2-podoplanin interaction and to characterise their effect on human platelet activation. To achieve the aims, supported lipid bilayers were used to mimic the platelet membrane. Fluorescent recovery after photobleaching and total internal reflection fluorescence microscopy were used to investigate bilayer mobility and platelet-mediated clustering of human podoplanin. The AlphaScreen-based high-throughput screen with 18,476 compounds from Pivot Park Screening Centre library was used to identify a small-molecule inhibitor of the CLEC-2-podopolanin interaction. Molecular docking and bio-layer interferometry were used to predict the binding sites and affinity between small molecule and CLEC-2. Light transmission aggregometry, flow cytometry, platelet spreading, and phosphorylation assays were used to evaluate the effect of the small molecule on CLEC-2-mediated platelet activation. Human dermal lymphatic endothelial cells were used to investigate the small molecule effect on platelet adhesion to cells endogenously expressing podoplanin. A semi-high-throughput artificial lipid membrane platform has been successfully developed as an experimental approach to investigate CLEC-2-mediated clustering of its endogenous ligand, podoplanin. An identified small molecule inhibitor of the CLEC-2-podoplanin interaction, MAS9, showed an inhibitory effect on the human platelet function and

selectivity for the CLEC-2 receptor. This study provides the opportunity to take full advantage of the supported lipid bilayer model to understand CLEC-2-mediated signalling and clustering. Identified in a high-throughput screen, MAS9, may be a good candidate for a novel anti-platelet drug having therapeutic potential.

Acknowledgements

I would first like to thank my supervisor and mentor, Alice Pollitt. I am very thankful and appreciative for all the help, support and encouragement. I couldn't ask for a better supervisor, that's for sure. Without you, I would not have achieved what I have achieved.

Thanks also to Ángel García, my second supervisor who has been a source of great help and advice.

A huge thank you to Jon Gibbins, Craig Hughes and Chris Jones for your support. Thanks also to members of Reading Platelet Lab, it wouldn't have been the same without you all! Thanks to Neline, Tanya, Renato, Alex, Kirk, Jo, Daniel, Taysseer, Fahd, Yasmin, Abdul, Zannah and Salihah for being so kind and helpful! A very special thanks go to Charlie, Danni and Anatol for sharing the lab space together and being amazing people.

Many thanks for an amazing year in Spain to Platelet Proteomics Group members, María, Lidia, Luis, María "chiquita" and Sara! Thanks also to Alberto, Yaiza and Leticia for being in Santiago for me! I would also acknowledge Edu, David and Rocío for cooperation and suggestions.

Huge thanks to members of Pivot Park Screening Centre: Jan and Helma.

Massive shoutout to all TAPAS-ESRs: Ale, Xueqing, Jingnan, Natalie, Ilaria, Helena, Isabella, Zahra, Chu, Hilaire and Stefano. Thank you also to all TAPAS supervisors and members! Big thanks to Delia for helping me to survive in the Netherlands.

I would especially like to thank Eva Maria Soriano Jerez for going through this PhD journey, from the very first day, together! Thank you for your friendship and support! I couldn't imagine a better friend during a PhD.

Many thanks to all my other lab mates. In no particular order, Sophie for teaching me how to be a British. Gemma for talking about musicals and making me laugh. Safa for convincing me that I am a great person and making me special. Carly for asking me every day 'How are you?' and being a lovely person. I love you guys! Thank you for everything!

Huge thanks to my valued friends! Ewa for being my committed conversational partner, willingly offering help in overcoming my problems. Grzegorz for being my buoyant travel companion and huge mental support in times of distress and need. Janusz for making me happy and being my motivation at the last stage of my PhD.

Last but not least, I would like to thank my family. My mum and dad for supporting me throughout the years of my education and believing in me. My sister and brother for their endless encouragement and help.

Publications

Published:

Dunster, JL, Unsworth, AJ, Bye, AP, Haining EJ, **Sowa MA**, Di Y, Sage T, Pallini C, Pike JA, Hardy AT, Nieswandt B, García Á, Watson SP, Poulter NS, Gibbins JM, Pollitt AY; Interspecies differences in protein expression do not impact the spatiotemporal regulation of glycoprotein VI mediated activation. J Thromb Haemost. 2020; 18: 485– 496.

d'Alessandro E, Becker C, Bergmeier W, Bode C, Bourne JH, Brown H, Buller HR, Ten Cate-Hoek AJ, (…), **Sowa MA**, (…), Ten Cate H; Scientific Reviewer Committee; Thrombo-Inflammation in Cardiovascular Disease: An Expert Consensus Document from the Third Maastricht Consensus Conference on Thrombosis. Thromb Haemost. 2020 Apr;120(4):538-564.

Submitted:

Morán LA, Di Y, **Sowa MA**, Hermida-Nogueira L, Barrachina M, Martin E, Clark JC , Mize TH, Eble, JA, Moreira D, Pollitt AY, Loza MI, Domínguez E, Watson SP, García Á; Katacine is a new ligand of CLEC-2 that acts as a platelet agonist. Thromb Haemost. 2021

In preparation:

Sowa MA, van Groningen J, Di Y, Gibbins JM, García Á, Pollitt AY; MAS9 – a novel small molecule inhibitor of CLEC-2-Podoplanin interaction.

Presentations

Oral communication

June 2021: **School of Biological Sciences PhD Symposium (University of Reading, UK).**

Sowa MA, van Groningen J, Di Y, Gibbins JM, García Á, Pollitt AY. MAS9 – a novel small molecule inhibitor of CLEC-2-Podoplanin interaction.

June 2020: **School of Biological Sciences PhD Symposium (University of Reading, UK).**

Sowa MA, van Groningen J, Di Y, Gibbins JM, García Á, Pollitt AY. Identification of small-molecule inhibitors of the CLEC-2-Podoplanin interaction using high-throughput screening.

Poster presentation

July 2021: **XXIX Congress of the International Society on Thrombosis and Haemostasis (ISTH 2021, Philadelphia, U.S.)**

Sowa MA, van Groningen J, Di Y, Gibbins JM, García Á, Pollitt AY. MAS9 – a novel small molecule inhibitor of CLEC-2-Podoplanin interaction.

March 2021: **2nd Platelet Society Online Meeting (Keele University, UK).**

Sowa MA, van Groningen J, Di Y, Gibbins JM, García Á, Pollitt AY. MAS9 – a novel small molecule inhibitor of CLEC-2-Podoplanin interaction.

July 2020: **III annual CIMUS Workshop (Santiago de Compostela, Spain).**

Sowa MA, Di Y, Watson SP, Gibbins JM, Pollitt AY, García Á. Reconstitution of C-type lectin receptor 2 (CLEC-2)-mediated clustering od podoplanin using supported lipid bilayers.

June 2020: **XXVIII Congress of the International Society on Thrombosis and Haemostasis (ISTH 2020, Milan, Italy)**.

Sowa MA, Di Y, Watson SP, Gibbins JM, García Á, Pollitt AY. An artificial lipid membrane platform as an approach to study CLEC-2 receptor clustering.

October 2019: **1st Platelet Society Meeting, University of Cambridge, UK**

Sowa MA, Di Y, Watson SP, García Á, Gibbins JM, Pollitt AY. Supported lipid bilayers as an innovative platform to investigate platelet receptor clustering.

June 2019: **School of Biological Sciences PhD Symposium (University of Reading, UK)**

Sowa MA, García Á, Gibbins JM, Pollitt AY. Artificial lipid membranes as a novel platform to study platelet signalling receptor.

Abbreviations

αIIbβ3	Glycoprotein IIb/IIIa
5-HT	5-hydroxytryptamine
Å	Angström
ACD	Acid-citrate-dextrose
ADP	Adenosine diphosphate
AlphaScreen	Amplified luminescent proximity homogeneous assay
ATP	Adenosine triphosphate
ATPase	Adenosine 5'-triphosphatase
Bcl-xL	B-cell lymphoma-extra large
Biotin-Cap-PE	1,2,-dioleoyl-sn-glycero-3-phophoethanolamine-N-(cap-biotinyl)(sodium-salt)
BLI	Bio-layer interferometry
BSA	Bovine serum albumin
Btk	Bruton's tyrosine kinase
cAMP	Cyclic adenosine monophosphate
CD9	Cluster of differentiation 9
CLEC-2	C-type lectin-like receptor-2
Co-HP	Cobalt-hematoporphyrin
COX-1	Cyclooxygenase 1
COX-2	Cyclooxygenase 2
CRP	Collagen-related peptide
CTLD	C-type lectin-like domain
CV	Column volume

DAG	Diacyl glycerol
DGS-NTA	1,2,-dioleoyl-sn-glycero-3-[(N-(5-amino-1-carboxypentyl)iminodiacetic acid)succinyl (nickel salt)
DMEM	Dulbecco's Modified Eagle's Medium
DMSO	Dimethyl sulfoxide
DNA	Deoxyribonucleic acid
DOPC	1,2,-dioleoyl-sn-glycero-3-phosphocholine
DPBS	Dulbecco's phosphate buffered saline
DTS	Dense tubular system
DTT	Dithiothreitol
ECM	Extracellular matrix
EDTA	Ethylenediaminetetraacetic acid
ELISA	Enzyme-linked immunosorbent assay
EMA	European Medical Agency
EMT	Epithelial-mesenchymal transition
ERM	Ezrin, radixin and moesin
FACS	Fluorescence-activated cell sorting
FBS	Fetal bovine serum
FcRγ	Fc receptor γ-chain
FCS	Fluorescence correlation spectroscopy
FDA	Food and Drug Administration
FLIPR	Fluorescent imaging plate reader
FRAP	Fluorescent recovery after photobleaching
Gads	Grb2 Related Adaptor Protein Downstream of Shc
GAPDH	Glyceraldehyde-3-phosphate dehydrogenase

GEFs	Guanine nucleotide exchange factors
GLIDE	Grid-based ligand docking with energetic
GPCRs	G-protein coupled receptors
GPI	Glycosylphosphatidylinositol
GPO	Glycine-proline-hydroxyproline
GPVI	Glycoprotein VI
Grb2	Growth-factor receptor-bound protein 2
H2-PP	Protoporphyrin IX
HDLECs	Human dermal lymphatic endothelial cells
HEK293T	Human endothelial kidney 293T cells
hemITAM	Hemi-immunoreceptor-tyrosine-based activation motif
HIT	Heparin induced thrombocytopenia
HTRF	Homogenous time resolved fluorescence
HTS	High-throughput screening
IC_{50}	Half maximal inhibitory concentration
IVC	Inferior vena cava
IF	Immunofluorescence
Ig	Immunoglobulin
IP	Immunoprecipitation
IP_3	Inositol 1,4,5-trisphosphate
IPTG	Isopropyl β-D-1-thiogalactopyranoside
ITAM	Immunoreceptor-tyrosine-based-activation-motif
k_a	Association constant
K_D	Affinity constant
k_d	Dissociation constant

kDa	Kilodalton
KO	Knockout
LAT	Linker of activated T cells
LB	Lysogeny broth
LogP	Partition coefficient
LTA	Light transmission aggregometry
MESF	Molecules of Equivalent Soluble Fluorochrome
MFI	Median fluorescence intensity
MWCO	Molecular weight cut-off
NHS	N-Hydroxysulfosuccinimide
NO	Nitric oxide
OCS	Open canalicular system
PAF	Platelet activating factor
PC	Phosphatidylcholine
PCR	Polymerase chain reaction
PDB	Protein Data Bank
PDGF	Platelet derived growth factor
PE	Phosphatidylethanolamine
PECAM-1	Platelet endothelial cell adhesion molecule-1
PF4	Platelet factor 4
PGI2	Prostaglandin I2
PI	Phosphatidylinositol
PI3K	Phosphoinositide 3-kinase
PIP_2	Phosphatidylinositol 4,5-bisphosphate
PKA	Protein kinase A

PKC	Protein kinase C
PLAG	Platelet aggregation-stimulating
PLCβ	Phospholipase C-β
PLCγ2	Phospholipase Cγ2
PPP	Platelet poor plasma
PRP	Platelet-rich plasma
PS	Phosphatidylserine
PVDF	Polyvinylidene difluoride
PxxP	Proline-rich region
pY	Phosphotyrosine
RCF	Relative Centrifugal Force
RDG	Arginine-glycine-aspartic acid
ROI	Region of interest
rPA	Reverse passive Arthus reaction
RPM	Revolutions per minute
S/B	Signal-to-background
S/N	Signal-to-noise
SD	Standard deviation
SDS-PAGE	Sodium dodecyl sulphate–polyacrylamide gel electrophoresis
SFK	Src family kinase
SH2	Src Homology 2
SH3	Src Homology 3
SLB	Supported lipid bilayer
SLP-76	SH2 domain containing leukocyte protein of 76kDa
SPA	Scintillation proximity assay

STORM	Stochastic Optical Reconstruction Microscopy
TAE	Tris-acetate-EDTA
TBS-T	Tris-buffered saline with Tween 20
Tec	Tec family kinase
TGF-β	Transforming growth factor β
TIRF	Total Internal Reflection Fluorescence
TP	Thromboxane
TPO	Thrombopoietin
tPSA	Topological polar surface area
TxA2	Thromboxane A_2
vHTS	Virtual High Throughput Screening
VWF	Von Willebrand factor
WB	Western blot
WP	Washed platelet
WPBs	Weibel-Palade bodies

Table of Contents

List of Figures

List of Tables

Chapter 1

Introduction

1.1. Thesis overview

Platelets play an important role in wound healing and blood clot formation. During vessel injury, they are involved in the first wave of haemostasis (platelet activation) and form a haemostatic plug to stop the bleeding. Conversely, uncontrolled and excessive platelet activation is detrimental to human health and can lead to thrombotic disorders, such as stroke and myocardial infarction (Nguyen and Coull, 2017). The physiological role of the platelets is to maintain primary haemostasis. The platelets circulate through the vessel near the vessel wall, which allows for a quick response when the injury occurs (Whittle *et al.*, 1978). During a bleeding event, plasma von Willebrand factor binds to exposed collagen at the site of injury. The platelet response starts with adhesion on the subendothelial extracellular matrix through the GPIb-IX-V complex on platelet surface which binds to von Willebrand factor. This binding mediates platelet tethering, enabling GPVI and integrin $\alpha_2\beta_1$ to interact with collagen (Li *et al.*, 2010). Following this initial tethering of the platelet to the vessel wall, subsequent firm adhesion results in signal transduction within the platelet, resulting in secretion of α- and dense granules. Release of TxA_2 and ADP from the dense granules activates G-protein coupled receptors ($P2Y_1$, $P2Y_{12}$ and thromboxane receptor),
leading to incorporation of new platelets from circulation through platelet-platelet interactions mediated by the integrin receptor $\alpha_{IIb}\beta_3$, resulting in a thrombus formation (Rivera *et al.*, 2009). More loosely associated platelets in the shell of thrombus become activated through positive feedback of the secondary mediators via cyclooxygenase COX-1 and small molecules from the dense granules. The initial platelet thrombus consists of tightly-packed P-selectin positive platelets that require secondary feedback through COX-1 and $P2Y_{12}$ receptor. The platelets surrounded by a thrombus shell (in a

core) are more sensitive to antiplatelet therapies using COX-1 and $P2Y_{12}$ receptor inhibitors (Holinstat, 2017).

In addition to playing a role in haemostasis, platelets also have a role in angiogenesis (Kisucka *et al.*, 2006), inflammation (Wagner and Burger, 2003), antimicrobial activity (Tang *et al.*, 2002), tumour growth and metastasis (Takagi *et al.*, 2013).

Available antiplatelets therapies are used for treatment of diseases that involve arterial thrombosis and require the use of aspirin, which inhibits cyclooxygenase COX-1, leading to decreased production of prostaglandins and TxA_2. Aspirin treatment can be enhanced by using $P2Y_{12}$ receptor inhibitors, such as ticagrelor, clopidogrel or prasugrel. These antiplatelet medications may affect other platelet activation pathways, including ITAM signalling, that are crucial for haemostasis and may increase the risk of major bleeding (Grove *et al.*, 2015). One of the ITAM receptor, CLEC-2, interacts with its endogenous ligand podoplanin and plays a major role in thrombo-inflammation, which has been shown in mouse models of deep venous thrombosis and *Salmonella* infection (Thomas and Storey, 2015; Rayes *et al.*, 2017). Additionally, CLEC-2-podoplanin interaction is important in arterial thrombosis, blood lymphatic development and cancer (Harbi *et al.*, 2021). That is why CLEC-2 may be a promising target for long-term prevention of pathologies such as arterial thrombosis, deep venous thrombosis, sepsis, and cancer, with a decreased bleeding risk relative to current therapies. There are currently no clinical trials targeting CLEC-2. A potent anti-CLEC-2 antibody AYP1, which blocks platelet activation by podoplanin, is not oral bioavailable and expensive to produce (Gitz *et al.*, 2014). The development of other drugs, such as small molecule inhibitors, is highly challenging. There has been identified a small molecule inhibitor of CLEC-2-podoplanin interaction, called Cobalt-hematoporphyrin, which blocked tumour metastasis and thrombosis in mice. However,

because of its low potency, toxicity, and lack of oral availability, it cannot be pursed for clinical development (Tsukiji *et al.*, 2018). CLEC-2 provides a promising alternative target for identification of novel antiplatelet medications, with a low toxicity and oral availability, and the role in thrombosis, thrombo-inflammation, and cancer.

Many cell surface receptors coalesce into micron and submicron clusters, following the initiation of signalling cascades. Assembly of cell surface receptors into clusters is a common feature of cell membranes (Dustin and Groves, 2012; Garcia-Parajo *et al.*, 2014). Receptor clustering has also been found to involve downstream signalling molecules that appear to undergo protein condensation phase transitions (Case *et al.*, 2019; Huang *et al.*, 2019). When receptors are packed together, signal-enhancing phenomena can occur, such as ligand receptor switching, or improved ligand-receptor and receptor-effector encounter probabilities (Caré and Soula, 2013). However, the effect of clustering on receptor-ligand binding dynamics and afterwards cell response is poorly understood. Interesting seems to be also question how declustering may affect signalling upon the inhibition.

Cluster formation to initiate signalling followed by assembly in a larger central cluster is characteristic of ITAM-containing immunoreceptors. It enhances the intracellular signal and has the advantage of restricting the diffusion of molecules at the membrane, such as the exclusion of membrane associated negative regulators like CD45 (Davis and van der Merwe, 2011). Clustering may be associated also with signal termination (Varma *et al.*, 2006), maintenance (Yokosuka *et al.*, 2008), or enhancement (Salaita *et al.*, 2010) in different systems.

The interaction between CLEC-2 and its endogenous ligand podoplanin may play a crucial role in a receptor clustering, however this process is poorly understood. Pollitt et al. proposed a model of CLEC-2 mediated clustering of podoplanin. The proposed

model assumes that interaction of CLEC-2 with podoplanin enhances platelet adhesion to lymphatic endothelial cells (LECs) through CLEC-2-mediated clustering involving Syk. This mechanism may possibly lead to clustering of podoplanin on LECs (Pollitt *et al.*, 2014).

Pollitt et al. showed that platelet mouse CLEC-2 clusters mouse podoplanin incorporated into supported lipid bilayer, which is one of the methods to investigate the clustering (Pollitt *et al.*, 2014). Receptor signalling components reconstituted on artificial lipid membranes enables the dynamics of macromolecular assembly to be measured and the molecular behaviour of signalling components to be studied in ways that cannot be achieved using intact platelets. Receptor clustering reconstituted on supported lipid bilayer can be followed by using microscopy techniques, such as Total Internal Reflection Fluorescence microscopy and Stochastic Optical Reconstruction Microscopy imaging. The microscopy methods have some limitation, such as multicolour tracking of signalling components in experimental throughput or restrictions of the brightness and photostability of organic dyes (Zhang and Reinhard, 2019).

This thesis is a collaborative work between University of Reading (United Kingdom), University of Santiago de Compostela (Spain) and Pivot Park Screening Centre (Netherlands).

1.2. Platelet production

Platelets are produced through thrombopoiesis. The main regulator of platelet production is thrombopoietin (TPO), which supports the proliferation and differentiation of bone marrow megakaryocytes – the platelet precursor cells (De Sauvage *et al.*, 1994; Kaushansky *et al.*, 1994). Megakaryocytes develop from multipotential hematopoietic stem cells through their differentiation into specialized progenitors in the bone marrow osteoblastic niche (Kaushansky, 2005). The thrombopoiesis process requires binding of TPO to the megakaryocyte-specific receptor c-MPL on the megakaryocyte surface (Choi *et al.*, 1995; Ito *et al.*, 1996). The binding of TPO induces the process of chromosome division without cell division which results in an increased number of chromosomes in the cell – endomitosis, also called polyploidization (Ebbe, 1976). Then polyploid megakaryocytes undergo a maturation process in which their cytoplasm is packaged into proplatelets, and the nucleus is extruded. Platelets receive their organelle and granule content from particles transported from the megakaryocyte cell body (Italiano *et al.*, 1999). Maturation and proplatelet formation are dependent on the cellular migration of the megakaryocyte from the osteoblastic to the vascular niche, where they interact with sinusoidal endothelial cells (Tavassoli and Aoki, 1989). At the end of the maturation, proplatelets form platelets through the fragmentation process and they are released into the bloodstream (Harker and Finch, 1969; Jackson and Edwards, 1977).

It has been recently demonstrated that the lungs might also contribute to platelet biogenesis. Lefrançais et al. showed, using intravital microscopy, that a large number of megakaryocytes circulate through the mouse lungs, where they dynamically release platelets. It has been estimated that the lungs contribute to platelet biogenesis by producing approximately 50% of total platelets in mice (Lefrançais *et al.*, 2017).

1.3. Platelet structure

Human platelets are the smallest cells circulating in the blood, with diameter between 2 to 5 μm, 0.5 μm in thickness and a discoid shape in the inactive state. Each platelet possesses a mean cell volume of 6 to 10 femtoliters (White, 2013). The number of platelets produced per day is approximately 10^{11}. Additionally, they have a relatively short life-span, circulating in the blood between 7 to 10 days before removal and clearance by the reticuloendothelial system in the liver and spleen (Josefsson et al., 2013). Platelets can be cleared through opsonization by anti-platelet antibodies, Fc-receptor mediated recognition, and subsequent clearance (Cines and McMillan, 2007). Another mechanism is removal of platelets by scavenger receptors in the liver by controlled apoptosis which depends on the balance between anti-apoptotic Bcl-x_L and pro-apoptotic molecules Bax and Bak (Mason et al., 2007; Josefsson et al., 2011; Debrincat et al., 2012). Recent studies showed the role of glycan modifications on platelets in mediating their clearance. As platelets lose sialic acid and β-galactose residues from their surface, they are cleared by the hepatic Ashwell-Morell receptor (Quach et al., 2018).

The platelet plasma membrane has three layers: the glycocalyx, phospholipidic and submembranous layer. The glycocalyx contains surface receptors involved in platelet activation and aggregation. These receptors include integrins, adhesion receptors and G-protein-coupled receptors (GPCRs) (Kamath et al., 2001). The glycocalyx is supported by a cytoskeleton composed of microtubules and actin filaments which are responsible for the discoid shape of the platelet (Erlandsen et al., 2001). During platelet activation the shape of the platelet changes through the depolymerisation, reorganisation and polymerisation of the cytoskeleton network (Sandmann and Köster, 2016). Platelets possess two membrane channel structures: the open canalicular system (OCS),

responsible for granule release and substance entry into the platelet; and the dense tubular system (DTS), responsible for sequestration and release of calcium ions (Ca^{2+}), involved in platelet activation (White, 1972). The DTS also contains adenosine 5'-triphosphatases (ATPases), which are crucial for adenylyl cyclase activity in the regulation of GPCRs downstream signalling (Cutler *et al.*, 1978).

Platelets contain three types of granules: α-granules, dense granules, and lysozymes. α-granules contain biologically important molecules, such as growth factors (platelet derived growth factor PDGF and transforming growth factor TGF-β), chemokines (platelet factor 4 PF4) and proteins (fibronectin, fibrin, and von Willebrand factor). In addition, they contain transmembrane receptors, such as platelet endothelial cell adhesion molecule-1 (PECAM-1), glycoprotein Ib-IX-V (GPIb-IX-V) complex and integrin αIIbβ3 (Golebiewska and Poole, 2015). Dense granules store lower molecular weight molecules, including adenosine triphosphate (ATP), adenosine diphosphate (ADP), calcium, serotonin, and inorganic phosphate. Platelets have a small number of lysozymes that contain phospholipases, guanine, acid hydrolases and kinases, acting like hydrolytic and proteolytic enzymes (Polasek, 2005). Dense granules release their contents through the OCS or the surface plasma membrane, leading to platelet activation. Platelets also contain mitochondria (energy generation) and glycogen particles (energy source) (Aibibula *et al.*, 2018). A schematic of the human platelet structure is presented in Figure 1.1.
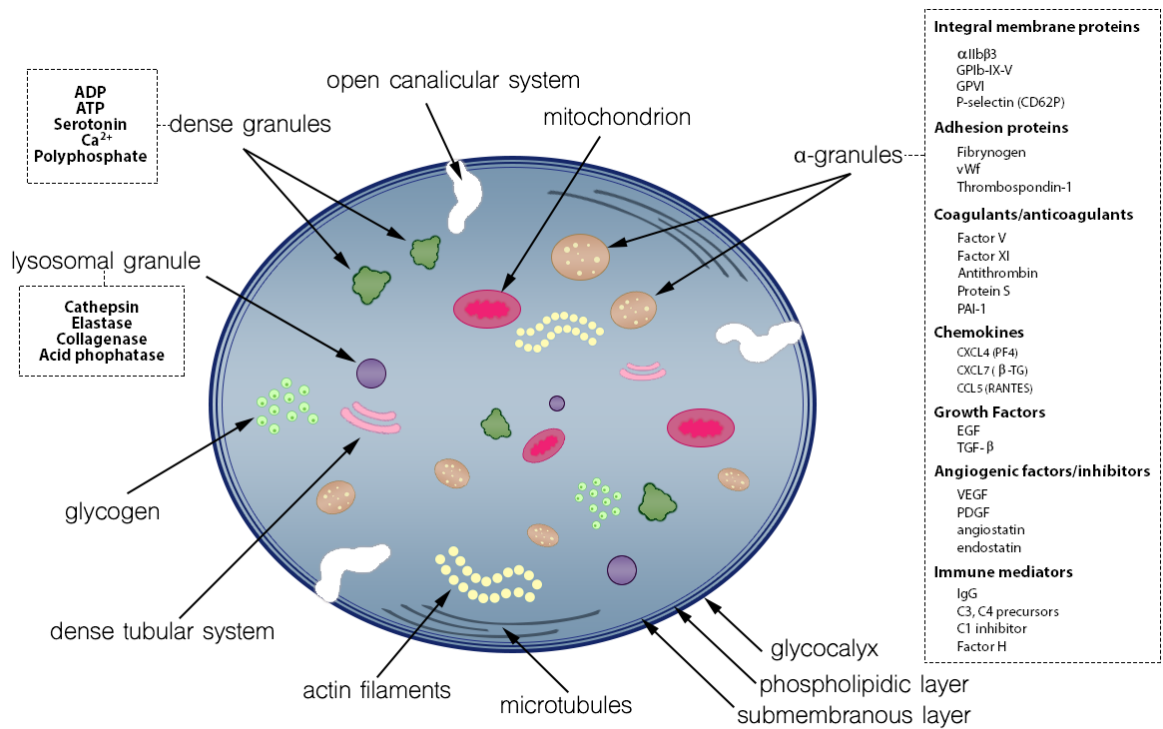
Figure 1.1. Human platelet structure.

The plasma membrane of platelets has 3 layers (glycocalyx, phospholipidic and submembranous layer). Platelets contain microtubules, actin filaments, mitochondria, three types of granules (alpha, dense and lysosomal), an open canalicular system, a dense tubular system, and small factors like glycogen. α-granules contain integral membrane proteins, adhesion proteins, coagulants and anticoagulants, chemokines, growth factors, angiogenic factors and inhibitors and immune mediators. Dense granules store ADP, ATP, serotonin, calcium, and polyphosphate. Lysosomal granules contain cathepsin, elastase, collagenase and acid phosphatase.

1.4. Haemostasis and thrombosis

1.4.1. Haemostasis

Under normal conditions, platelets circulate through the bloodstream in a resting state near the vessel wall. The resting (or inactive) state is maintained thanks to molecules, such as nitric oxide (NO) and prostaglandin I_2 (PGI_2) produced by the endothelium, that inhibit platelet function (Whittle *et al.,* 1978). Due to endothelium damage or the rupture of an atherosclerotic plaque, different subendothelial components of the extracellular matrix, including collagen, fibronectin and laminin are exposed, resulting in platelet recruitment and activation (Singh *et al.*, 2002). This process is divided into three phases: adhesion, activation, and aggregation.

1.4.2. Adhesion, activation, and aggregation

Several proteins, located on the platelet membrane surface play a role in the platelet adhesion process, including the platelet receptors GPIbα (GPIb-IX-V), integrin $\alpha_2\beta_1$ and GPVI (Bryckaert *et al.,* 2015). During the rupture of an atherosclerosis plaque or damage to the vessel wall , plasma VWF binds to exposed collagen at the site of injury (Wagner *et al.,* 1984). This permits the reversible platelet adhesion between the receptor GPIb-IX-V and VWF, which allows for translocation (rolling) of platelets on the surface of the collagen. This leads to a reduction in the speed of circulating platelets, favouring the interaction between the collagen and the GPVI and integrin $\alpha_2\beta_1$ on the platelet surface (Li *et al.*, 2010).

Interaction between collagen and the GPVI activates platelets, allowing a firm adhesion via collagen receptors GPVI and $\alpha_2\beta_1$, resulting in secretion of α- and dense granules by platelets. In addition, this interaction promotes receptor clustering, triggering of signalling pathways mediated by phosphorylation through tyrosine kinases (Poulter *et*

al., 2017). GPVI signalling leads to the activation of PLCγ2, which increases intracellular Ca^{2+} levels and causes platelet degranulation. It allows a conformational change of the integrin $\alpha_{IIb}\beta_3$ to its active form, thus favouring the "inside-out" signalling (Watson *et al.*, 2005; Senis *et al.*, 2014). On the other hand, α-granules and dense granules contain many positive reinforcing factors such as fibrinogen, VWF, ADP, TxA_2, and serotonin, which promote complete activation of the pathway (Rivera *et al.*, 2009).

Once the $\alpha_{IIb}\beta_3$ integrin is in its active conformation, platelet recruitment begins. These adhere to each other thanks to the bridges formed by fibrinogen, fibrin and VWF. The receptor-ligand binding triggers the activation of the receptor "outside-in" signalling that culminates in powerful platelet activation, responsible for the remodelling of the cytoskeleton and leads to the formation of initial clot (Hynes, 2002). More loosely associated platelets in the shell of thrombus become activated through positive feedback of the secondary mediators via cyclooxygenase COX-1 and small molecules from the dense granules. When the initial thrombus has been formed, it activates the coagulation cascade, leading to the stabilization of the clot. Prothrombin is cleaved to thrombin, which mediates the formation of fibrinogen through PAR1 receptor, and this is then converted to fibrin (Rand and Israels, 2017). The platelet thrombus consists of tightly-packed P-selectin positive platelets that promote platelet aggregation through platelet-fibrin and platelet-platelet binding, leading to the stable thrombus formation (Holinstat, 2017).

The process of platelet adhesion, activation and aggregation is illustrated in Figure 1.2.
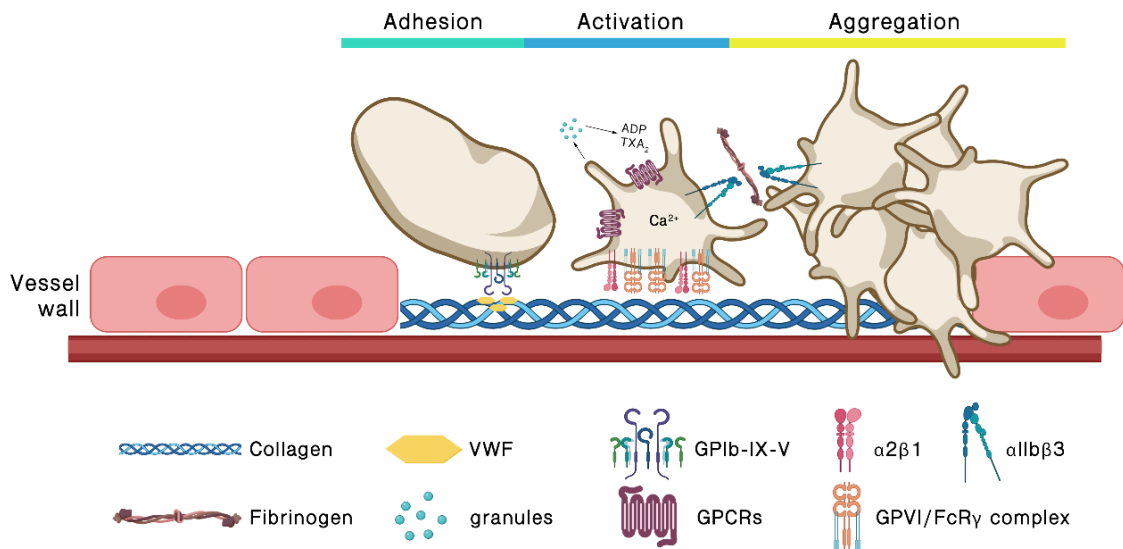
Figure 1.2. Platelet adhesion, activation and aggregation on the ECM.

During a damage to the vessel wall, plasma VWF binds to exposed collagen at the site of injury. Interaction between GPIb-IX-V and VWF mediates platelet tethering, enabling GPVI and integrin $\alpha_2\beta_1$ interaction with collagen. This allows firm adhesion, resulting in platelet activation, secretion of α- and dense granules by platelets and release of TxA_2 and ADP. Secreted soluble agonists activate GPCRs, leading to further $\alpha_{IIb}\beta_3$ activation and the formation of a stable thrombus.

1.4.3. Platelet receptors

Platelet receptors play a key role in the normal function of platelets. They can initiate intracellular signalling to activate platelets as well as behave like adhesion molecules, interacting with the other platelets, damaged endothelium or leukocytes (Yun *et al.*, 2016). The main groups of receptors on the platelet surface that initiate early platelet activation are G protein-coupled receptors and immunoreceptor-tyrosine-based-activation-motif (ITAM) receptors. These, as well as the platelet specific adhesion receptors and integrins are presented in Figure 1.3.
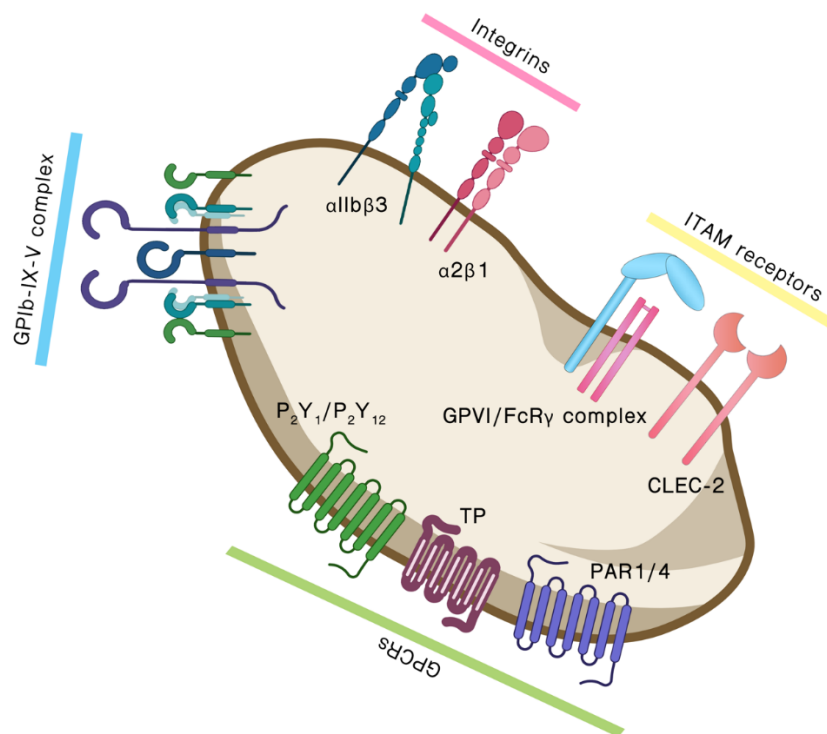
Figure 1.3. The main receptors on the platelet surface involved in platelet activation.

The main groups of platelet receptors that initiate early platelet activation are G protein-coupled receptors (P_2Y_1, P_2Y_{12}, TP, PAR1 and PAR4), immunoreceptor-tyrosine-based-activation-motif receptors (GPVI, CLEC-2), integrins $\alpha_{IIb}\beta_3$ and $\alpha_2\beta_1$ and GPIb-IX-V complex.

1.4.3.1. GPIb-IX-V complex

The GPIb-IX-V complex is composed of four type 1 transmembrane proteins: GPIbα, GPIbβ, GPIX, and GPV (Du *et al.*, 1987; Modderman *et al.*, 1992). The main function is to mediate the interaction between the platelet and the vascular wall during the bleeding injury by binding to VWF that is immobilized on the collagen surface of the subendothelial matrix. After binding, activation begins downstream of the receptor, where the following intervene sequentially: phosphorylation of the Src kinases (SFKs), the activation of PLCγ2, the formation of DAG and the activation of PKC (Ozaki *et al.*, 2005). It is also known that GPIb activates the p38-MAP (mitogen-activated protein) kinase pathway leading to changes in the cytoskeleton, platelet degranulation and the conformational change of the $\alpha_{IIb}\beta_3$ integrin (Z. Li *et al.*, 2006). Bernard-Soulier syndrome relates to dysfunction or lack of GPIb-IX-V complex. It is a congenital bleeding disorder characterised by giant platelets and mild thrombocytopenia (López *et al.*, 1998). Lack of interaction between VWF and GPIb-IX-V contributes towards of Bernard-Soulier syndrome progression. It has been reported that GPIb-IX-V interacts with coagulation factors, such as thrombin, factor VII, XI and XII. The absence of these interactions, as well as the absence of the interaction with VWF, may play a role in the bleeding defects related to Bernard-Soulier syndrome patients (Lanza, 2006; Andrews and Berndt, 2013).

1.4.3.2. Integrins

Integrins are a family of transmembrane heterodimeric proteins made up of two α and β subunits and play an important role in platelet adhesion and aggregation. Platelets express five different types of integrins ($\alpha_2\beta_1$, $\alpha_5\beta_1$, $\alpha_6\beta_1$, $\alpha_{IIb}\beta_3$ and $\alpha_v\beta_3$). The most important role in platelet activation during haemostasis have the fibrinogen receptor $\alpha_{IIb}\beta_3$ and collagen receptor $\alpha_2\beta_1$.

Integrin $\alpha_{IIb}\beta_3$ (also called GPIIb/IIIa) is considered an essential receptor for platelet activation and aggregation. It is a heterodimeric glycoprotein composed of non-covalently associated α and β subunits. Integrin $\alpha_{IIb}\beta_3$ is the most abundant glycoprotein on the human platelet surface with the expression of 40,000-80,000 copies per cell (Wagner *et al.*, 1996). Integrin $\alpha_{IIb}\beta_3$ can bind to several arginine-glycine-aspartic acid (RGD)-containing ligands, including fibrin, VWF and fibronectin, however the major ligand for $\alpha_{IIb}\beta_3$ is fibrinogen. Similarly to $\alpha_2\beta_1$, $\alpha_{IIb}\beta_3$ in resting platelets is presented in a 'low affinity' state. Once the stimulus occurs, $\alpha_{IIb}\beta_3$ undergo a structural change that initiates a high affinity conformation for the ligands through "inside-out" signalling (Hato *et al.*, 1998). Once $\alpha_{IIb}\beta_3$ is activated by ligand binding, it begins "outside-in" signalling, leading to the generation of a cascade of intracellular signalling events that mediate platelet adhesion, spreading, cytoskeletal reorganization, aggregation, and subsequent thrombus growth (Hynes, 2002).

Disruption of αIIb or β3 subunit or the absence of $\alpha_{IIb}\beta_3$ can cause a rare autosomal recessive bleeding disorder, called Glanzmann's thrombasthenia. It is characterised by defective normal platelet function, such as adhesion, spreading and aggregation (Hodivala-Dilke *et al.*, 1999; Nurden, 2006).

Integrin $\alpha_2\beta_1$ (also called GPIa/IIa) is a heterodimer of the $\alpha2$ integrin subunit non-covalently associated with the $\beta1$ subunit (Dickeson *et al.*, 1998). There are between 2,000-4,000 $\alpha_2\beta_1$ copies per human platelet (Best *et al.*, 2003). $\alpha_2\beta_1$ is normally presented in a 'low affinity' state in resting platelets, and in response to collagen-mediated "inside-out" signalling, it is converted into 'high-affinity' state (Jung and Moroi, 2000). $\alpha_2\beta_1$ has the function of mediating the adhesion of platelets to the vascular wall, reinforcing GPVI-collagen binding, although it has a limited role in platelet activation (Holtkötter *et al.*, 2002).

1.4.3.3. ITAM receptors

Another important group of platelet receptors are immunoreceptor-tyrosine-based-activation-motif receptors. The ITAM motif is located in the intracellular region of the receptor and is defined as two Yxx(L/I) sequences separated by 6-12 amino acid residues (Gibbins *et al.*, 1997; Watson *et al.*, 2005). In human platelets we can distinguish 3 different types of receptors containing ITAMs: the complex of Glycoprotein VI (GPVI) and the Fc receptor γ chain (GPVI/FcRγ), C-type lectin-like receptor-2 (CLEC-2) which has a truncated form of an ITAM called a hemITAM, and FcγRIIA receptor (Boulaftali *et al.*, 2014).

The major collagen receptor expressed in platelets is GPVI. It is a 62 kDa type I transmembrane collagen receptor expressed in platelets and megakaryocytes (Clemetson *et al.*, 1999). It belongs to the immunoglobulin superfamily and is located on chromosome 19 of the human genome. The expression and signalling of GPVI depend on its association with dimeric FcRγ which contains an ITAM motif (Nieswandt and Watson, 2003). Human GPVI consists of 319 amino acids with a 20 amino-acid signal sequence. The expression has been estimated as 3,000-4,000 copies per cell (Best *et al.*, 2003) or 25,384 ± 3,639 (Dunster *et al.*, 2019) copies per cell, using antibody-based flow cytometry approaches. This difference in GPVI copy number may be due to the different antibodies used: Best et al. used a mouse monoclonal anti-GPVI antibody (204-11) and measured the copy number in platelet-rich plasma (PRP), whereas Dunster et al. used mouse monoclonal anti-GPVI antibody (HY-101) and measured the copy number in washed platelets (WPs). The proteomic approach reported that platelets express 9,600 copies of GPVI per cell. The GPVI structure, ligands and signalling are described in detail in Chapter 1.5.

CLEC-2 is a 32 kDa type II transmembrane protein and belongs to group V subfamily of C-type lectin receptors, and is expressed on platelets and megakaryocytes, and also on dendritic cells (Suzuki-Inoue *et al.*, 2006). It is located on chromosome 12 in the human genome, with six other C-type lectin receptors in the Dectin-1 gene cluster (Huysamen and Brown, 2009). CLEC-2 is a receptor for the transmembrane ligand podoplanin. Podoplanin is not present in the vasculature, which is why CLEC-2 may not play a major role in normal haemostasis. However, it may play a role in lymphangiogenesis, preservation of blood and lymphatic vessel integrity, organ development and tumour metastasis (Suzuki-Inoue *et al.*, 2010). Recently, a new endogenous ligand for CLEC-2, hemin, has been identified (Bourne *et al.*, 2021), however, it has not been well-described yet. In contrast to GPVI-FcRγ-chain complex, CLEC-2 contains a single YxxL, which is downstream of a tri-acidic amino acid region (DEDG), which has been demonstrated to be important for signal initiation *(Watson et al.,* 2010). There are between 2,000-4,000 CLEC-2 copies per cell on the human platelet surface and around 40,000 copies per cell in mouse platelets (Burkhart *et al.*, 2012; Zeiler *et al.*, 2014; Dunster *et al.*, 2019). As CLEC-2 is the main receptor investigated in this thesis, it is described in detail in Chapter 1.6.

FcγRIIA (CD32a) is a human platelet receptor for the Fc region of IgG. It is a 40 kDa type 1 transmembrane glycoprotein that belongs to the class II of FcγRs, alongside FcγRIIB and FcγRIIC. It consists of 317 amino acids with a 33 amino-acid signal sequence and expression levels range from 1350, estimated using dimeric IgG_1 (Karas *et al.*, 1982), to 3060 copies per cell, estimated by using the Fab from the monoclonal antibody (mAb) IV.3 (Tomiyama *et al.*, 1992) in a flow cytometry experiments. The extracellular domain is composed of two Ig-like domains, with the second domain

mediating binding to IgG (Maxwell *et al.*, 1999). The cytoplasmic region contains an ITAM, with 12 amino acids between the two YXXL motifs (Brooks *et al.*, 1989).

The most commonly used ligands for FcγRIIA include aggregated IgGs, IgG-coated beads, crosslinked IV.3 mAb, and FcγRIIA-dependent activating antiplatelet antibodies (Arman *et al.*, 2014). These ligands lead to phosphorylation of the FcγRIIA ITAM, which provides a docking site for Syk, leading to Syk tyrosine kinase activation. Syk activation begins a cascade of phosphorylations involving linker of activated T cells (LAT) and phospholipase Cγ2 (PLCγ2) (Blake *et al.*, 1994; Bodin *et al.*, 2003). Activation of PLCγ2 subsequently induces the production of the second messengers IP_3 and DAG, followed by elevation of intracellular Ca^{2+} levels and activation of protein kinase C (PKC), which are essential for platelet secretion and aggregation (Gratacap *et al.*, 1998).

The physiologic role of platelet FcγRIIA is uncertain. It has been proposed as an amplifier of "outside-in" signalling mediated by integrin $\alpha_{IIb}\beta_3$. Boylan et al. demonstrated that platelet spreading on fibrinogen and clot retraction can be inhibited by using antibodies against the extracellular domain of FcγRIIA. Additionally, they showed that the cytoplasmic domain of the integrin β3 subunit is required for phosphorylation of FcγRIIA (Boylan *et al.*, 2008). Since mouse platelets do not express FcγRIIA, Zhi et al. demonstrated that transgenic FcγRIIA-positive murine platelets had increased spreading on fibrinogen, as well as tyrosine phosphorylation of Syk and PLCγ2 compared to the murine WT control platelets. Moreover, murine platelets expressing FcγRIIA retracted a fibrin clot faster and increased thrombus formation and fibrin deposition in electrolytically injured femoral veins (Zhi *et al.*, 2013).

FcγRIIA plays a pathological role in processes mediating the interaction between platelets and immune complexes. It has been shown that platelet FcγRIIA induces pro-

inflammatory cytokines important in Kawasaki disease and Graves' disease (Smith and Clatworthy, 2010; Yu and Lazarus, 2016), participates in immune mediated heparin induced thrombocytopenia (HIT) (Baroletti and Goldhaber, 2006) and responds to diverse IgG-opsonized pathogens (Riaz *et al.*, 2012).

1.4.3.4. GPCRs

G-protein-coupled receptors are a family of membrane proteins that possess seven transmembrane domains, which, when activated trigger intracellular signalling through G proteins. The main ligands that activate platelets via GPCRs are thrombin and ADP (Simon *et al.*, 1991).

Thrombin is the most effective activators of platelets. It is formed during the exposure of tissue factor to plasma coagulation factors after vascular endothelium disruption. Platelet activation by thrombin is mediated by protease-activated receptors PAR-1 and PAR-4 in humans (or PAR3 and PAR4 in mice), which couple to G_q, $G_{12/13}$ and G_i (Kahn *et al.*, 1999; Holinstat *et al.*, 2006). PAR-1 is a high-affinity signalling receptor in human platelets, while PAR4 plays a role in thrombin signalling at high thrombin concentration (Kahn *et al.*, 1999). Platelets stimulation with thrombin increase the level on intracellular calcium Ca^{2+} and decrease in intercellular cyclic adenosine monophosphate (cAMP), which plays an essential role in maintaining the inactive state of platelets. It also stimulates ADP and other contents release from dense granules, and P-selectin exposure (Offermanns, 2006).

ADP is a soluble agonist that acts as a powerful amplifier of the prothrombotic signal and can be recognized by $P2Y_1$ (coupled to G_q) and $P2Y_{12}$ (coupled to G_i), It is released from dense granules during platelet activation. Like platelets stimulated with thrombin, platelets stimulated with ADP increase the level on intracellular calcium and decrease in intracellular cAMP concentration (Woulfe, 2005).

Thromboxane A_2 (TxA_2) is another important activator of platelets. It is produced from arachidonic acid through the conversion of COX-1. It activates the thromboxane receptor (TP) coupled to G_q and $G_{12/13}$. Like thrombin and ADP, it increases the level

on intracellular calcium and decrease in intracellular cAMP concentration (Gurbel *et al.*, 2015).

A platelet shape change is the initial response of platelet to thrombin, ADP or TxA$_2$. This process is based on the cytoskeleton reorganization, leading to the formation of submembranous actin filament network and the extension of filopodia (Hartwig, 1992). In addition, G$_q$-coupled receptors, once activated, bind to phospholipase C-β (PLC-β), which catalyses a hydrolysis of phosphatidylinositol 4,5-bisphosphate (PIP$_2$) generating inositol 1,4,5-trisphosphate (IP$_3$) and diacyl glycerol (DAG) (Bailey *et al.*, 2000; Shah *et al.*, 2001).

1.5. GPVI

1.5.1. GPVI structure

The intracellular domain (C-terminus) of human GPVI is relatively short and is 51 amino acids in length. The murine GPVI intracellular domain is shorter than the human one and is only 27 amino acids in length (Best *et al.*, 2003; Nieswandt and Watson, 2003; Moroi and Jung, 2004). The intracellular domain contains a basic amino-acid rich region, that can bind calmodulin (Andrews *et al.*, 2002) and a proline-rich motif, which brings the Src homology 3 (SH3) domains of Lyn and Fyn to the Fc receptor (FcR)γ-chain ITAM, initiating an activation signal through GPVI (Suzuki-Inoue *et al.*, 2002).

The transmembrane domain of GPVI possesses an arginine residue (Arg273), which is responsible for the formation of a salt bridge with the aspartic acid pair of the transmembrane domains of the homodimer FcRγ-chain (Zheng *et al.*, 2001; Feng *et al.*, 2005). Each chain of FcRγ contains an ITAM defined as two Yxx(L/I) sequences separated by 6-12 amino acids, which are responsible for signal transduction after collagen binding to GPVI (Gibbins *et al.*, 1997; Watson *et al.*, 2005).

The extracellular region (N-terminus) of GPVI consists of two immunoglobulin domains – D1 and D2, linked by a single peptide strand (Smethurst *et al.*, 2004). GPVI has only one N-glycosylation site at Asn-93 which contributes to maximal adhesion to collagen related peptide (CRP) and type I collagen (Miura *et al.*, 2000). Numerous threonine and serine residues located in a mucin-like stalk are potential O-glycosylation sites, however the function of this modification for GPVI in unknown (Wandall *et al.*, 2017). Described features and domains of GPVI are illustrated in Figure 1.4.
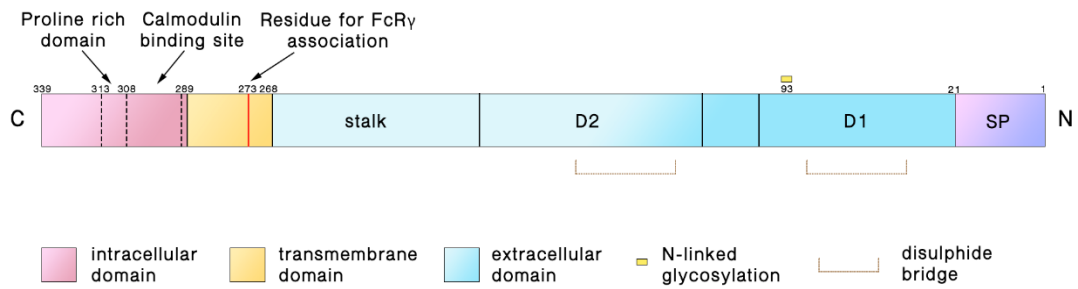
Figure 1.4. GPVI domain structure.

GPVI contains a C-terminal intracellular domain (pink) with proline-rich domain and calmodulin binding site. This is followed by a transmembrane domain (orange) which contains a critical arginine residue for FcRγ association, and a C-terminal extracellular domain (blue) which contains a stalk region and two IgG-like domains D1 and D2. The structure ends with a N-terminal signal peptide (purple). An N-linked glycosylation site and disulphide bridges are also highlighted.

1.5.2. GPVI ligands

GPVI is the main signalling receptor in platelet activation by collagen. The major feature of collagen is a presence of glycine-proline-hydroxyproline (GPO) repeats (Huggins, 1954). It has been shown that a synthetic CRP, which consists of cross-linked multiple GPO repeats activates platelets through GPVI (Gibbins *et al.*, 1997), whereas its non-crosslinked, monomeric version does not (Asselin *et al.*, 1999). These results suggest the presence of multiple binding sites in the quaternary structure of collagen for interaction with GPVI. Val54, Leu56 and Lys79 residues of D1 extracellular domain of GPVI have been identified using site-directed mutagenesis as the collagen binding region of human GPVI (Lecut *et al.*, 2004; Smethurst *et al.*, 2004).

It was reported that collagen binds to recombinant dimeric but not monomeric GPVI. GPVI-specific dimeric antibodies can block platelet activation, suggesting that collagen binds to dimeric GPVI (Miura *et al.*, 2002; Jung *et al.*, 2009; Loyau *et al.*, 2012a). Additionally, the crystal structure of the D1 and D2 domains of GPVI showed that it can dimerize through the D2 domains, however the protein does not dimerize in solution (Horii *et al.*, 2006). A recent study showed that GPVI is expressed as a mixture of monomers and dimers, when transfected to the HEK293T cells and the level of dimeric form of GPVI increased upon stimulation by CRP. Additionally, a Förster resonance energy transfer (FRET) experiment performed using platelets showed that GPVI is partially expressed as a dimer on resting platelets and the dimerization did not significantly increase upon the activation with CRP (Clark *et al.*, 2021).

Another endogenous ligand for GPVI is fibrin. It can induce a similar profile of tyrosine phosphorylation to that induced by collagen (Alshehri *et al.*, 2015). Moreover, it has been demonstrated that fibrin binds to dimeric GPVI (Mammadova-Bach *et al.*, 2015). In contrast, a recent study showed that plasma fibrin contains different proteins,

compared to the recombinant fibrin. Super resolution imaging demonstrated differences in the recombinant and plasma fibrin network. In a flow experiment, platelets adhered to the recombinant fibrin were of irregular shape and showed long pseudopods, suggesting they were activated, whereas on plasma fibrin the platelets were rounder and had shorter pseudopods, suggesting no activation (Zhang *et al.*, 2020). These data do not support plasma fibrin as a GPVI ligand.

Next to collagen and fibrin, fibrinogen has also been proposed as an endogenous ligand for GPVI. It has been demonstrated that spreading of human platelets on fibrinogen was abolished in GPVI-deficient human platelets. This result suggests that fibrinogen can bind and activate platelets through GPVI. Moreover, human-GPVI-transgenic mouse platelets spread on fibrinogen, whereas wild-type (WT) mouse platelets did not (Mangin *et al.*, 2018).

1.5.3. GPVI signalling

GPVI activation by collagen (or other ligands) initiates phosphorylation of two conserved tyrosines in the FcRγ-chain ITAM by SFKs Lyn and Fyn within the lipid rafts (Senis *et al.*, 2014b). The conserved proline-rich region (PxxP) of GPVI enables the binding of Lyn's and Fyn's SH3 domains. This places the receptor in a "ready-to-go" state (Nieswandt and Watson, 2003) with Lyn and Fyn held in close proximity to the receptor. Although Lyn and Fyn both are required for the GPVI signalling, Lyn, but not Fyn, binds GPVI receptors in resting platelets, suggesting the role in initial events of activation (Schmaier *et al.*, 2009). Lyn and Fyn are held in an inactive confirmation and during platelet activation change into their active confirmation through the dephosphorylation of an inhibitory tyrosine residue by the protein tyrosine phosphatase CD148 (Senis *et al.*, 2009).

The phosphorylated ITAM by SFKs recruits tyrosine kinase Syk via its SH2 domains. Syk is an essential kinase for the signal transduction and undergoes a series of auto- and trans-phosphorylations by SFKs, leading to recruitment and phosphorylation of the adaptor protein LAT (Gibbins *et al.*, 1998; Pasquet *et al.*, 1999). It leads to recruitment of LAT pathway effectors, such as Grb2, Gads, SLP76, tyrosine kinases Btk and Tec, the Vav family of guanine nucleotide exchange factors and the small GTPase Rac. This recruitment catalyses the production of phosphatidylinositol 3,4,5-triphosphate (PIP_3) from phosphatidylinositol 4,5-trisphosphate (PIP_2). The signalling cascade ends in the phosphorylation and activation of PLCγ2, binding to phosphorylated LAT and PIP_3 on the plasma membrane. Additionally, Btk and Tec are recruited by PIP_3, and it causes phosphorylation of PLCγ2 (Watson *et al.*, 2005). Activation of PLCγ2 initiates hydrolysis of phosphatidylinositol 4,5-biphosphate, which leads to formation of the secondary messengers DAG and IP_3. It activates PKC and release of Ca^{2+} which leads

to platelet activation (Suzuki-Inoue *et al.*, 2003). The schematic GPVI signalling pathway is presented in Figure 1.5.

A number of studies showed that GPVI activation is highly dependent on lipid rafts. These are defined as a small, heterogenous and highly dynamic membrane domains highly enriched in sphingolipids and cholesterol. They are involved in many cellular processes, as well as signal transduction (Simons and Ikonen, 1997). Wonerow et al. found permanent co-localisation of GPVI- FcRγ-chain complex and Lyn and Fyn in lipid rafts, suggesting a critical role in the initiation of GPVI signalling (Wonerow *et al.*, 2002), whereas Locke et al. found no GPVI- FcRγ-chain complex associated to lipid rafts in resting platelets but massive recruitment to lipid rafts when platelets were activated with convulxin (Locke *et al.*, 2002). The differences in these results may be attributed to different lipid rafts isolation procedures, for example the type of detergent used to lyse the platelets. Wonerow et al. used Brij® 58, whereas Locke et al. used Triton-X100. Selection of the detergent is significantly cell type-dependent (Schuck *et al.*, 2003). Recent studies using LC-MS/MS proteomic analysis of lipid rafts isolated using Brij® 58 from platelets activated through GPVI, as well as from resting platelets, showed a higher amount of GPVI isolated in lipid rafts from GPVI-activated platelets, although a small amount of GPVI was also recovered from basal samples. Additionally, the studies demonstrated that Brij® 58 is more efficient in lipid raft enrichment from platelets than Triton-X100 (Izquierdo *et al.*, 2019). It confirms that GPVI is partially associated to lipid rafts in resting platelets, and that GPVI activation leads to its enrichment in these membrane fractions.
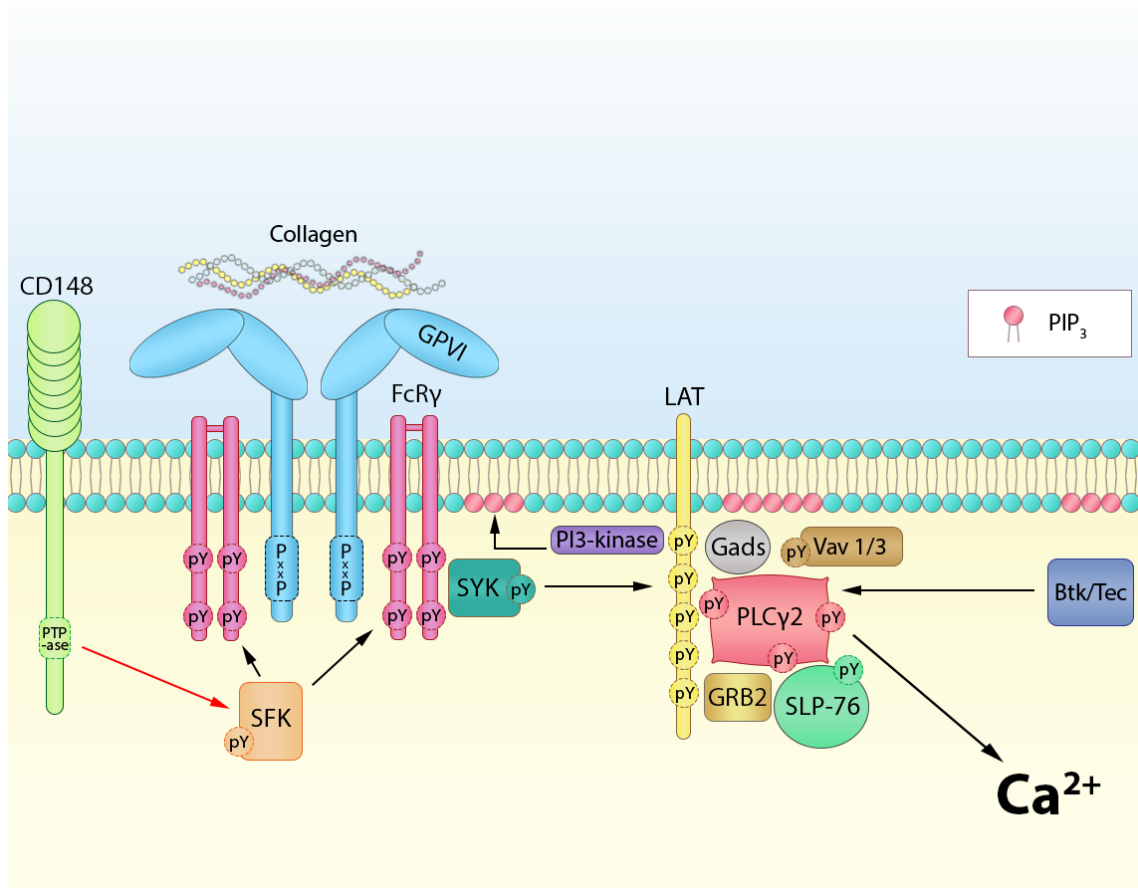
Figure 1.5. GPVI signalling pathway.

GPVI activation by collagen initiates phosphorylation of two immunoreceptor tyrosine-based activation motifs (ITAM) by Src family kinases and allows the recruitment and docking of Syk's SH2 domains. Recruitment of Syk contributes to series of phosphorylations by Src family kinases, leading to the formation of the 'LAT signalosome' and resulting in PLCγ2 activation, leading to calcium release and platelet activation.

1.5.4. GPVI functions

Deficiency of GPVI in humans is rare and usually characterised by normal platelet size and number, prolonged bleeding time and response normally to all agonists except collagen (Sugiyama *et al.*, 1987). Moreover, platelets from patients with GPVI-deficiency are unable to adhere to collagen under flow, suggesting a crucial GPVI dependent role in platelet thrombus formation (Goto *et al.*, 2002). Similarly to humans, GPVI-deficient mice have a normal platelet count with a mildly prolonged bleeding time following tail incision (Nieswandt *et al.*, 2000; K. Kato *et al.*, 2003).

Although GPVI's primary function is haemostasis, it has a role in non-haemostatic function. Dovizio et al. demonstrated that GPVI can bind to galectin-3 presented on colon cancer cells (HT29). Inhibitors of galectin-3 function, Gal-3C and anti-galectin-3 antibody M3/38 or an inhibitor of the GPVI receptor, revacept, prevented aberrant COX-2 expression in the colon cancer cells. These data suggest that inhibition of collagen binding sites via GPVI may be important in the prevention of colon cancer metastasis. Mammadova-Bach et al. showed by injecting colon (MC38 or MC38-CEA) or breast (AT-3) cancer cells into genetic GPVI-deficient mice that metastasis is decreases. Similarly to Dovizio et al., they identified galactin-3 as the major counterreceptor of GPVI on tumour cells and demonstrated that the GPVI-galectin-3 interaction promotes tumour cell-induced platelet activation, degranulation and trans-endothelial cell migration. Finally, they showed that inhibition of GPVI function using JAQ1 F(ab')$_2$ can efficiently impair platelet-tumour cell interaction and tumour metastasis (Mammadova-Bach *et al.*, 2020).

1.6. CLEC-2

1.6.1. CLEC-2 structure

CLEC-2 was identified originally in immune cells through a computational screen. However, a surface expression of CLEC-2 has been only shown on platelets and dendritic cells (Colonna *et al.*, 2000; Suzuki-Inoue *et al.*, 2006). Human and mouse CLEC-2 share a 62% amino acid sequence identity and the same domain structure (Colonna *et al.*, 2000).

Human CLEC-2 consists of 229 amino acids with an N-terminal intracellular domain, a single transmembrane region, and a C-terminal extracellular domain. The intracellular domain is 33 amino acids long and contains a hemITAM, a single YxxL sequence with a tri-acidic amino acid region (DEDG) upstream and the tyrosine residue at position 7. The extracellular domain possesses a stalk region, which contains a putative N-linked glycosylation site and disulphide bond, which may be responsible for stabilization of CLEC-2 dimerization through non-covalent interaction (Watson *et al.*, 2009). Besides a stalk region, there is also a carbohydrate-like recognition domain (also called a C-type lectin-like domain or CTLD). This domain contains WIGL and WXW motifs and a triplet of disulphide bonds which are typical for the group V subfamily of C-type lectin receptors (Watson *et al.*, 2008; Nagae *et al.*, 2014), however it lacks the Ca^{2+} binding residues required for binding carbohydrates (Colonna *et al.*, 2000). In addition, the CTLD of CLEC-2 is post translationally modified at two conserved asparagine residues (at position 120 and 134) by glycosylation which is important for receptor expression at the cell surface. It has been demonstrated, that point mutations of both, N120 and N134, abolished the translocation of CLEC-2 to the cell surface in HeLa cells (Wang *et al.*, 2012). Described features and domains of CLEC-2 are illustrated in Figure 1.6.
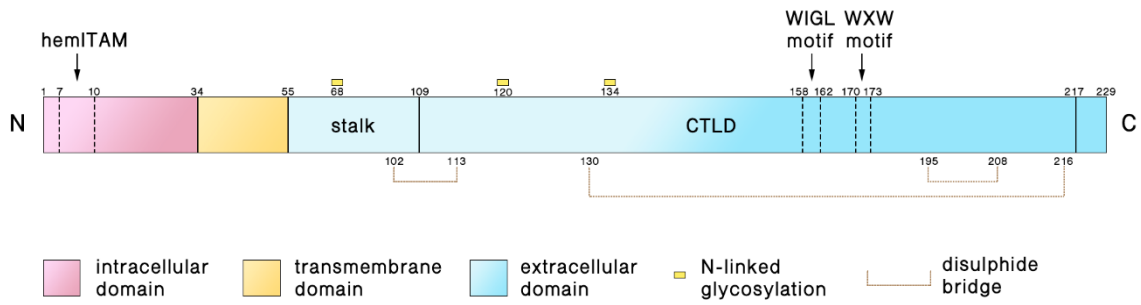
Figure 1.6. Domain structure of CLEC-2.

It contains an N-terminal intracellular domain (pink) with a hemITAM motif. This is followed by a transmembrane domain (orange) and a C-terminal extracellular domain (blue) which contains a stalk region and the C-type lectin domain (CTLD). N-linked glycosylation sites and disulphide bridges are also highlighted.

1.6.2. CLEC-2 ligands

Rhodocytin, podoplanin, fucoidan and hemin have been identified as ligands for CLEC-2.

Rhodocytin (also known as aggretin), the first identified exogenous ligand for CLEC-2, is a snake venom protein derived from the Malayan pit viper *Calloselasma rhodostoma* (Chung *et al.*, 1999). It has been classified as a snake venom C-type lectin, with a tetrameric structure containing two α (136 amino acids) and two β (146 amino acids) subunits, linked covalently with a disulphide bond at position 83 and 98 respectively (Clemetson, 2010). Both subunits multimerise and lead to CLEC-2 clustering and platelet activation. Described features and domains of rhodocytin are illustrated in Figure 1.7A. In addition, rhodocytin induces platelet aggregation with a characteristic lag phase and the aggregation is dependent on SFKs, Syk and PLCγ2 (Suzuki-Inoue *et al.*, 2007). The characteristic lag phase is likely related to the time required to form a cluster of CLEC-2 to start platelet activation.

Podoplanin is an endogenous ligand for CLEC-2. It is expressed outside the blood vasculature, including on kidney podocytes, lymphatic endothelial cells, choroid plexus cells, and lung epithelial cells (Breiteneder-Geleff *et al.*, 1999). Due to this, the podoplanin-CLEC-2 interaction possibly does not play a role in classical primary haemostasis and arterial thrombosis but may be important in many other pathologies, such as in cancer (Suzuki-Inoue *et al.*, 2010). Podoplanin has been classified as a type-I transmembrane sialomucin-like glycoprotein that consists of an extracellular domain with abundant Serine/Threonine residues as potential O-glycosylation sites, a single transmembrane domain, and a short cytoplasmic tail (Kunita *et al.*, 2007).

The extracellular domain contains three tandemly repeated motifs EDXXVTPG at positions 29-36, 38-45 and 47-54 and additional highly conserved EDXXT motif at position 81-85 (Kato *et al.*, 2003; Sekiguchi *et al.*, 2016). They have been described as the PLatelet AGgregation-stimulating (PLAG) domains (PLAG1-4). The O-linked glycosylation site (Thr52) within the PLAG3 domain, contains a sialic acid residue, which is essential for CLEC-2 binding (Kaneko *et al.*, 2007). In addition, deletion of this region or a point mutation in the PLAG4 domain drastically suppressed its binding to CLEC-2 and podoplanin-induced aggregation, suggesting the importance of this region (Sekiguchi *et al.*, 2016). Described features and domains of podoplanin are illustrated in Figure 1.7B. Just as with rhodocytin, platelets stimulated with podoplanin showed a characteristic lag phase (Suzuki-Inoue *et al.*, 2007)
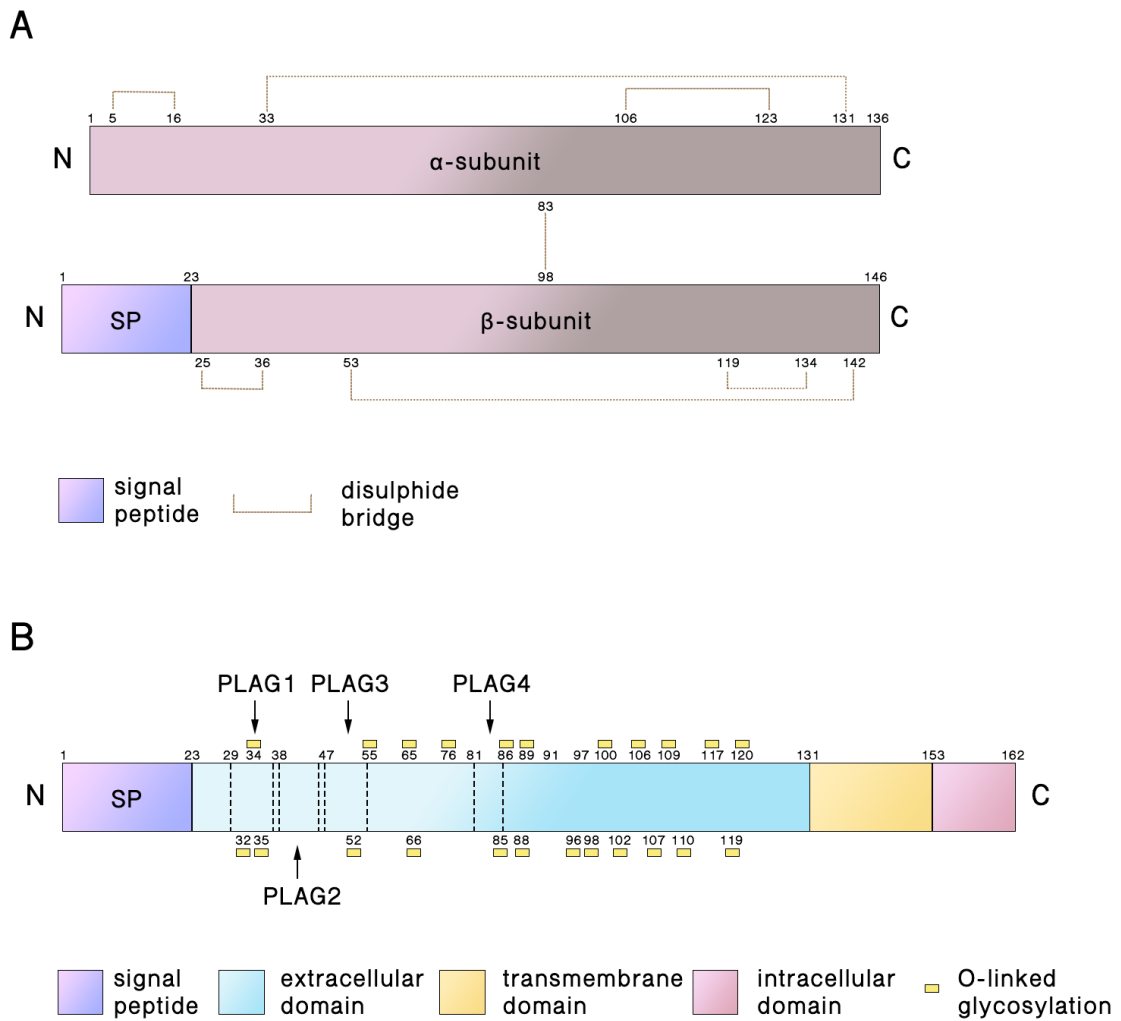
Figure 1.7. Domain structure of rhodocytin and podoplanin.

Rhodocytin (A) contains α and β subunits, linked covalently with a disulphide bond at position 83 and 98. In addition, β subunits contains a signal peptide (purple). Podoplanin (B) contains a N-terminal signal peptide (purple) followed by extracellular domain (blue) with the four PLAG motifs, transmembrane domain (orange) and C-terminal intracellular domain (pink). O-linked glycosylation sites and disulphide bridges are highlighted.

The comparative crystallographic studies of rhodocytin and podoplanin in complex with CLEC-2 showed that both of the proteins bind to the noncanonical "side" face of CLEC-2, as well as a common interaction mode between consecutive acidic residues on the ligands and the same arginine residues on CLEC-2 (Nagae *et al.*, 2014a). The common binding sites to induce CLEC-2 activation by podoplanin and rhodocytin are four arginine residues (Arg107, Arg118, Arg152, Arg157).

Podoplanin binds to CLEC-2 through the previously described PLAG domains. The side chains of podoplanin Gly47 and Asp48 make electrostatic contact with three CLEC-2 arginine residues; Arg107, Arg152 and Arg157. In addition, the podoplanin Asp48 side chain is connected by hydrogen bonds with the side chain of Thr153 and the backbone of His154 in CLEC-2, the carboxyl group of the sialic acid binds to the side chain and backbone of Arg118 in CLEC-2, the *N*-acetyl oxygen atom of sialic acid interacts with the side chain of Asn105 in CLEC-2, and the hydroxyl groups OH8 and OH9 of sialic acid make hydrogen bonds with the side chains of His119 and Tyr129 in CLEC-2. The side chain of Arg118 of CLEC-2 makes a hydrogen bond with the main chain atoms of Asp49-Val50-Val51 in podoplanin (Nagae *et al.*, 2014).

Regarding rhodocytin, four arginine residues of CLEC-2 (Arg107, Arg118, Arg152, Arg157) form electrostatic interactions with negatively charges residues Glu3, Asp4 and Asp6 in the α-subunit of rhodocytin. In addition, the carboxyl group of the C-terminal Tyr136 in the α subunit of rhodocytin appears close to Arg118 of CLEC-2 (Nagae *et al.*, 2014).

Another ligand for CLEC-2, fucoidan, is a non-anticoagulatory sulphated polysaccharide derived from the brown seaweed *Fucus vesiculosus* (Manne *et al.*, 2013). It is a polymer of α-(1→3) linked fucose with sulphate groups substituted at the C-4 position on some of the fucose residues (Figure 1.8A) (Patankar *et al.*, 1993). Just

as podoplanin and rhodocytin, platelets stimulated with fucoidan showed a characteristic lag phase. It has also been shown that key signalling molecules, SFKs and Syk, are crucial for fucoidan-induced platelet activation. In the CLEC-2 knockout, but not GPVI knockout mouse platelets, the aggregation was lost at low concentrations of fucoidan. However, at higher concentrations of fucoidan partial aggregation was maintained in CLEC-2 knockout mice, suggesting the role of other receptors in fucoidan-mediated platelet activation (Manne *et al.*, 2013). Additionally, in a double knockout model of CLEC-2 and GPVI, the platelet aggregation was abolished even at high fucoidan concentrations (Alshehri *et al.*, 2015). These data suggest that fucoidan can stimulate CLEC-2-mediated platelet activation, and partially GPVI-mediated activation.

Hemin, a product of haemolysis, released during red blood cell destruction, has recently been discovered as a ligand for CLEC-2. It is a protoporphyrin IX containing a ferric iron (Fe^{3+}) ion with a coordinating chloride ligand (Li *et al.*, 2006). The chemical structure of hemin is shown in Figure 1.8B. It was first shown that hemin induces activation and death of human platelets through ferroptosis. Hemin significantly and dose-dependently reduced platelet viability, however this effect of hemin is rescued when platelets were pre-incubated with ferroptosis inhibitors. Moreover, scanning electron microscopic analysis showed that hemin at doses of 5 to 10 μM induced filopodia-like structures formation, however, at concentration 25 μM, filopodia were destroyed (NaveenKumar *et al.*, 2018).

Bourne et al. investigated hemin-mediated human and mouse platelet activation *in vitro*. They demonstrated that hemin leads to platelet aggregation through activation of integrin $\alpha_{IIb}\beta_3$ at low concentrations and agglutination at high concentrations. In addition, the selectivity of hemin to CLEC-2 over the other platelet receptor, GPVI, was

shown using dimeric recombinant forms of these receptors. When hemin was pre-incubated with a recombinant dimeric form of CLEC-2, hemin-induced platelet aggregation was abolished, but this did not occur with a recombinant dimeric form of GPVI (Bourne *et al.*, 2021). Oishi et al. showed that hemin activates platelets through a SFK-Syk-PLCγ2 signalling pathway by binding to CLEC-2 and GPVI. In aggregation assays, hemin dose-dependently increased light transmittance of washed platelets and it could be abolished by using the SFK inhibitors PP2 and SU6656, and Syk inhibitor R406. Moreover, a western blot analysis demonstrated that Syk and PLCγ2 phosphorylation was upregulated by hemin, and these were inhibited by PP2 to a basal level. A surface plasmon resonance spectrometry study showed that hemin binds to human CLEC-2 and human GPVI, with an affinity constant of 0.915 μM and 29.4 μM, respectively (Oishi *et al.*, 2021). Bourne et al. showed that the affinity constant of the interaction between hemin and mouse or human CLEC-2 is 0.210 μM and 0.191 μM, respectively. Platelet activation by hemin requires further studies as the mechanism is still unclear.
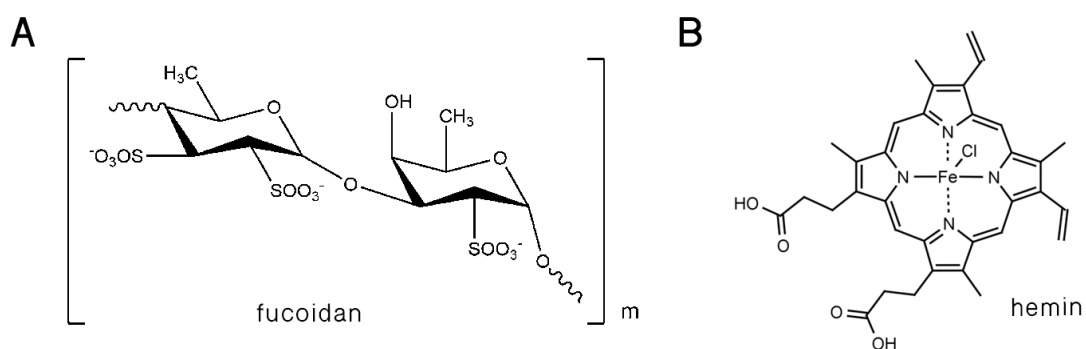
Figure 1.8. Chemical structure of fucoidan and hemin.

Fucoidan (A) is a polymer of α-(1→3) linked fucose with sulphate groups substituted at the C-4 position on some of the fucose residues. Hemin (B) is a protoporphyrin IX containing a ferric iron (Fe^{3+}) ion with a coordinating chloride ligand.

1.6.3. CLEC-2 signalling

Ligand binding to CLEC-2 triggers the phosphorylation of the tyrosine residue in its cytoplasmic hemITAM domain. CLEC-2 may be phosphorylated independently of SFKs activation by Syk (Séverin *et al.*, 2011) or phosphorylated by both – Syk and SFKs (Spalton *et al.*, 2009). It has been shown that CLEC-2 is initially phosphorylated by Syk, and this is then increased by a pathway that involves Btk and ADP (Nicolson *et al.*, 2020). After phosphorylation of the CLEC-2 hemITAM, inactive Syk and semi-active SFK bind via their SH2 domains, leading to activation of these kinases and initiating the "LAT signalosome" (Séverin *et al.*, 2011).

Syk phosphorylates the LAT, which interacts with PI3K and PLCγ2 via their SH2 domains (Moroi and Watson, 2015). Vav1/3 and SLP-76 also bind the phosphorylated cytoplasmic domain of LAT. However, in contrast to GPVI, SLP-76 is partially involved in CLEC-2-mediated platelet activation (Judd *et al.*, 2002; Pearce *et al.*, 2004; Suzuki-Inoue *et al.*, 2006). Fully activated phosphoinositol-3-kinase (PI3K) converts phosphatidylinositol 3,4,5-triphosphate from phosphatidylinositol 4,5-trisphosphate , which recruits Btk/Tec (Hyvönen and Saraste, 1997). Btk is required for CLEC-2-mediated platelet activation (Nicolson *et al.*, 2020). Activated Btk/Tec by SFKs activates PLCγ2 (Moroi and Watson, 2015), which induce hydrolysis of phosphatidylinositol 4,5-biphosphate, leading to formation of the second messengers DAG and IP_3 (Berridge *et al.*, 2003). It stimulates PKC and release of Ca^{2+}. These changes result in secretion of the contents of dense granules and α-granules and "inside-out" signalling activation of integrin $\alpha_{IIb}\beta_3$, leading to platelet aggregation (Ma *et al.*, 2007). The schematic CLEC-2 signalling pathway is presented in Figure 1.9.

CLEC-2 activation and release of ADP (from dense granules) and TxA_2 (formed in the COX-1-dependent pathway) results in the involvement of the P_2Y_1 and TP receptors,

respectively (Kauskot and Hoylaerts, 2012). In contrast to GPVI, to induce CLEC-2 signalling there is a requirement for secondary mediators, which are released from platelets upon activation (Pollitt *et al.*, 2010a; Manne *et al.*, 2015; Izquierdo *et al.*, 2019). Stimulation of these by G_q protein transmits the signal to PKCα, activates a number of phosphatases which transform SFKs into a semi-active state, enhancing CLEC-2 activation (Badolia *et al.*, 2017).

The theory that primary signalling events downstream of CLEC-2 take place in lipid rafts is controversial. Pollitt et al. showed that CLEC-2 translocated to lipid rafts upon ligand engagement and that translocation was essential for hemITAM phosphorylation, while Manne et al. reported that lipid rafts are not directly involved in CLEC-2 receptor signalling in platelets. In both studies, Methyl-β-Cyclodextran (MβCD) treated platelets were stimulated with low concentrations of rhodocytin. The difference in CLEC-2-mediated platelet aggregation could be attributed to the time points used to measure platelet aggregation – 5 minutes (Pollitt *et al.*, 2010a) or 10 minutes (Manne *et al.*, 2015). A recent study using LC-MS/MS proteomic analysis of lipid rafts isolated from platelets activated through CLEC-2, as well as from resting platelets, showed that CLEC-2 signalling events do not require lipid raft environment, although they found CLEC-2 in one out of four lipid raft-enriched samples (Izquierdo *et al.*, 2019).
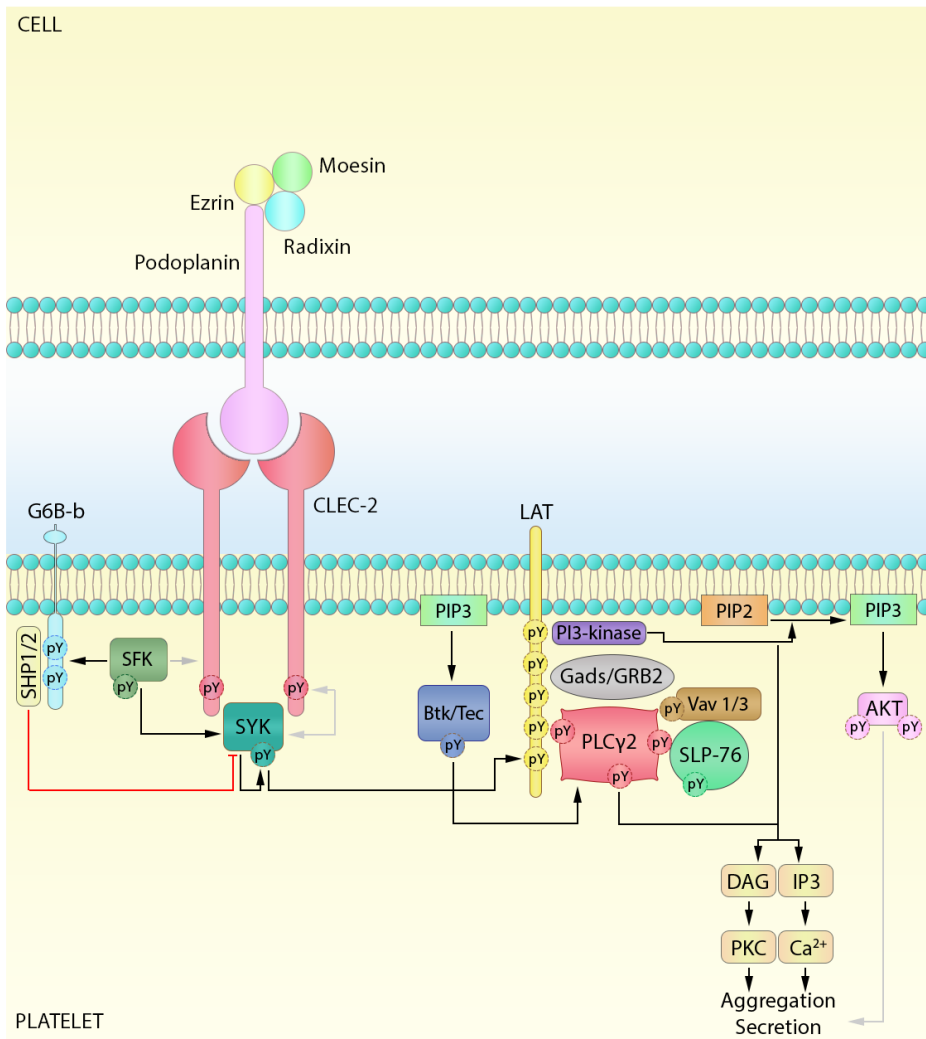
Figure 1.9. CLEC-2 signalling pathway.

CLEC-2 activation by podoplanin induces phosphorylation of the hem(ITAM),
allowing binding of Syk. Phosphorylation of CLEC-2 and Syk is mediated only
partially by Src family kinases (SFKs) but largely by Syk itself. Syk is responsible for
phosphorylating LAT, which recruits adaptor proteins SLP-76, Gads and Grb2. PI3K
becomes active and is recruited to the signalosome. It catalyses the production of PIP_3
from PIP_2, which recruits Btk and PLCγ2 where they interact with LAT in the
signalosome. Btk is phosphorylated by SFK's or Syk, and together phosphorylated Syk
and Btk mediate phosphorylation of PLCγ2 resulting in PKC activation and calcium
release.

1.7. Podoplanin

Podoplanin, also known as aggrus, T1α or gp36 in humans, OTS-8 in mice, E-11 antigen in rats and gp40 in canine cells, is a 36-43 kDa transmembrane sialomucin-like glycoprotein widely expressed on a variety of mammalian cells (Quintanilla *et al.*, 2019). It was named podoplanin due to its association with the transformation of arborized foot processes to flat feet (Latin, pes planus) in podocytes (Breiteneder-Geleff *et al.*, 1997). The structure of podoplanin is presented in section 1.5.2. and Figure 1.6B.

The intracellular domain of podoplanin binds to ezrin and moesin, which anchor podoplanin to the actin cytoskeleton. Ezrin, radixin and moesin belong to the ERM protein family that associates the actin cytoskeleton to the plasma membrane and is involved in cell polarity, adhesion, and migration. Podoplanin overexpression is associated with increased phosphorylation of ERM proteins (Martín-Villar *et al.*, 2006; Wicki *et al.*, 2006). ERM proteins are phosphorylate by a small Rho GTPase, leading to a conformational change that exposes binding sites to allow their association with integral membrane proteins and F-actin (Bretscher *et al.*, 2002). The podoplanin–ERM interaction is involved in promoting epithelial-mesenchymal transition (EMT) during embryonic development and cancer (Krishnan *et al.*, 2018).

Podoplanin associates with transmembrane domains of the tetraspanin cluster of differentiation 9 (CD9). It has been shown that binding of CD9 to the fibrosarcoma cell line HT1080 via podoplanin inhibits cell motility, its platelet aggregation ability and podoplanin-induced metastasis (Nakazawa *et al.*, 2008). Moreover, podoplanin associates with the hyaluronan receptor CD44. It has been demonstrated that CD44 and podoplanin expression is upregulated during EMT and advanced stages of tumour progression (Martín-Villar *et al.*, 2010).

Another two reported proteins which interact with podoplanin are galectin-8 and CCL21. Galectin-8 is highly expressed on lymphatic endothelial cells. It has been proposed that galecin-8 associates with podoplanin on lymphatic endothelium and promotes its association with the ECM (Cueni and Detmar, 2009). CCL21 is a lymphatic specific chemokine expressed on lymphatic endothelial cells and fibroblastic reticular cells. It has been demonstrated that CCL21 interacts with podoplanin with a high affinity and may be involved in the trafficking of dendritic cells to lymph nodes (Kerjaschki *et al.*, 2004; Acton *et al.*, 2012).

1.8. Physiological roles of the podoplanin-CLEC-2 signalling axis

Podoplanin, the endogenous ligand for CLEC-2, is expressed outside the blood vasculature, suggesting an unlikely role in thrombosis because there is no direct contact under physiological conditions. In addition, there is currently no evidence of humans deficient in CLEC-2. However, the role of the CLEC-2 in thrombosis has been demonstrated in the mouse models.

Treatment of mice with a rat monoclonal CLEC-2-specific antibody, INU1, has been used to remove CLEC-2 from the surface of platelets. Thrombus formation under high shear flow conditions showed that platelets can attach normally to collagen, however they do not form a stable aggregate. Additionally, INU1-treated mice displayed an increase in the tail bleeding time compared to control mice. Like in the *in vitro* thrombus formation assay, CLEC-2-deficient platelets also formed unstable thrombi after ferric chloride–induced mesenteric arterial injury (May *et al.*, 2009). Another study using antibody-mediated blockade of either CLEC-2, using INU1 antibody and GPVI, using JAQ1 antibody in mice, in contrary to May et al. demonstrated that these receptors can be depleted with high specificity from platelet surface *in vivo*, however no effect on tail bleeding time was observed. To analyse the data, Bender et al considered the size of the vessel, whereas it is unclear in work of May et al, what could make a difference in the results of these two research group. Additionally, mice deficient in both receptors in platelets completely inhibited thrombus formation, and the effect was greater than that seen in GPVI- or CLEC-2 single-depleted animal. These results were reproduced in genetically-depleted $Gp6^{-/-}$, $Clec-2^{fl/fl}$ and $Gp6^{-/-}/Clec-2^{fl/fl,\ Pf4-Cre}$ mice. Double-depleted mice showed markedly prolonged tail bleeding times as compared with control or single-deficient mice (Bender *et al.*, 2013). These findings showed that

CLEC-2 may have functions in haemostasis and occlusive thrombus formation, however the difference in the results of May et al. and Bender et al. is controversial.

Using antibodies to remove the receptor antigen from platelets may have some additional effects on thrombus formation. Suzuki-Inoue et al. generated CLEC-2-deficient mice and demonstrated under flow conditions a significant inhibition of thrombus formation in CLEC-2 chimeras, although the initial steps for thrombus formation, like platelet adhesion and spreading, remained intact. In addition, the authors shown no statistically significant change in tail bleeding time of CLEC-2 chimeras compared to wild type controls. The authors proposed that CLEC-2 may be a good candidate for an anti-platelet drug that inhibits pathological thrombus formation, but not physiological haemostasis (Suzuki-Inoue *et al.*, 2010). Similar results have been showed in another study using CLEC-2-deficient mice. There was no statistically significant difference in the tail bleeding times between WT and CLEC-2 deficient mice. However, in contrary to May et al, there was no difference in platelet aggregation on collagen when blood was flowed at similar shear (Hughes *et al.*, 2010).

1.9. Pathological roles of the podoplanin-CLEC-2 signalling axis

1.9.1. Deep venous thrombosis

Deep venous thrombosis is defined as the formation of blood clots in the deep veins. It mostly occurs in the lower extremities and is associated with pulmonary embolism. During hypoxia in the blood vessel, endothelial cells release Weibel-Palade bodies (WPBs) containing cytokines, which recruit platelets and leucocytes, resulting in thrombus development.

A deep venous thrombosis model of inferior vena cava (IVC) stenosis has been developed in anesthetized mice by separation of the IVC from the aorta, ligating it over a 30-gauge needle and removing the needle without causing endothelial injury. Partial flow restriction in the IVC mimics conditions created in human venous valves and results in the formation of a thrombus similar in structure to human thrombi. After 48 hours, the mice were culled, and thrombi developed in the IVC were taken for analysis. In CLEC-2-genetically deficient mice (Clec1b$^{fl/fl}$ Pf4^{Cre+}) it has been demonstrated that in the absence of CLEC-2 the thrombus formation is inhibited compared to WT controls. Depletion of CLEC-2 reduced platelet aggregation and leukocyte recruitment at the stenosed vessels. In addition, it has been demonstrated, using immunostaining and western blotting, that podoplanin is expressed in IVC walls below the endothelium and is upregulated following stenosis. Administration of anti-podoplanin antibody reduced the accumulation of platelets. These data suggest that both, CLEC-2 and podoplanin, play an important role in DVT (Payne *et al.*, 2017).

It has been reported that podoplanin expression was upregulated in the venous valves adjacent to a femoral vein thrombus from a patient who died with DVT, but not upregulated in the unaffected valves of the same vein, when stained with an anti-human

podoplanin antibody (NZ-1). These preliminary results suggest an important role of podoplanin in DVT, however, it still remains the question whether the upregulation of podoplanin is a cause or consequence of DVT (Nicolson *et al.*, 2020).

1.9.2. Blood lymphatic development

The interaction between CLEC-2 and podoplanin plays a role in the development of the lymphatic system. It was first indicated in mice deficient in the important proteins downstream of CLEC-2, such as Syk (Turner *et al.*, 1995), SLP-76 (Clements *et al.*, 1999) and PLCγ2 (Wang *et al.*, 2000). Embryos from these deficient mice showed a "non-separating" phenotype of the lymphatic-blood vascular characterised by abnormal blood-filled lymphatic vessels.

It has since been shown that CLEC-2 and Syk in platelets are critical to ensure lymphatic-blood vascular separation in embryos (Bertozzi *et al.*, 2010; Finney *et al.*, 2012; Hess *et al.*, 2014). This was achieved by conditional deletion of CLEC-2 and Syk in the megakaryocyte/platelet lineage. These mice had defects in lymphatic development. In contrast, conditional deletion of Syk in other hematopoietic lineages had no effect on viability and lymphatic development. These data suggest that CLEC-2 and Syk expression in megakaryocytes and platelets is required for normal lymphatic development (Finney *et al.*, 2012).

Furthermore, a knock-in mouse model expressing CLEC-2 with a point mutation (Y7A) in its hemITAM also had a blood-lymphatic mixing phenotype and lethality like that seen with CLEC-2 deficient mice. These data suggest the critical role for CLEC-2 hemITAM signalling in the prevention of blood lymphatic mixing (Haining *et al.*, 2017). To investigate whether the blood and lymphatic vascular remodelling may be required for blood filling, two challenge models in Pf4-Cre CLEC-2-deficient mice

were used. In the first model, mice were challenged with cutaneous reverse passive Arthus (rPA) reaction, which leads to a vascular response without inducing vessel growth or network remodelling. rpA-induced local skin inflammation did not lead to evidence of blood filling dermal lymphatics adjacent to, or within, the site of inflammation in a Pf4-Cre CLEC-2-deficient mice, neither in WT mice. However, in a melanoma tumour model used to induce of inflammation and vascular network remodelling and growth, it has been shown that tumorigenesis included by injection of B16F10 melanoma cells was significantly associated with blood-filled lymphatics of Pf4-Cre CLEC-2-deficient mice compared to WT mice. These results suggest that although in adult CLEC-2-deficient mice lymphatic blood filling does not occur during the expansion of lymphatic vessels in isolation, it can occur during the chronic concomitant remodelling of the blood and lymphatic vasculatures as seen in tumours (Haining *et al.*, 2021).

Mice lacking the glycosyltransferase T-synthase, which is crucial for O-glycosylation of the extracellular domain of podoplanin demonstrated incomplete separation of lymphatic vessel. This result suggests that O-glycosylation of podoplanin is important to lymphatic endothelial cell identity (Fu *et al.*, 2008). The phenotype observed in this KO mouse is likely due to the inability of unglycosylated podoplanin to interact with CLEC-2.

1.9.3. Septic thrombosis

Sepsis is defined as a systemic response to infection, leading to organ failure and death (Hotchkiss and Karl, 2003). It has been reported that platelets play a protective role in septic shock by inhibiting macrophage- dependent inflammation via the cyclooxygenase 1 signalling pathway. Reduction of platelet number to ~10% compared to controls in a sepsis mouse model by injection of an anti-GPIbα monoclonal antibody

showed no significant haemorrhage observed in the lungs and brains of thrombocytopenic mice. These data suggest that increased mortality from sepsis in thrombocytopenic mice may be due an exacerbated inflammatory response, rather than inflammatory haemorrhage. Moreover, transfusion of platelets reduced mortality in lipopolysaccharide (LPS)-induced endotoxemia and a bacterial infusion (Xiang *et al.*, 2013).

Podoplanin expression is upregulated during inflammation in different types of cells, including macrophages (Hou *et al.*, 2010). In a mouse model of systemic *Salmonella Typhimurium* infection, Hitchcock et al. showed upregulation of podoplanin expression on macrophage subsets and platelet activation in an infection-driven thrombosis in the liver. The bacteria in the liver leads to the accumulation of podoplanin-expressing macrophages and due the combination of bacteraemia, infection, inflammation and cell migration, there is a damage of the vascular endothelium, resulting in an increase of podoplanin-expressing macrophages leading to CLEC-2 activation and platelet aggregation. In addition, it has been shown that both, platelet specific depletion of CLEC-2 in mice and reducing the podoplanin-expressing cells (F4/80[+]) in liver using clodronate liposomes, reduced the thrombosis after infection (Hitchcock *et al.*, 2015).

In a mouse model of sepsis with genetically depleted CLEC-2 (CLEC2^{fl/fl}PF4[cre+]), it has been demonstrated that platelets limit the intensity of sepsis via CLEC-2 and this effect is independent of thrombosis. There was no difference in thrombus formation in kidney or liver vessels in the absence of platelet CLEC-2. In addition, in the absence of CLEC-2 there was a significant increase in organ damage, especially acute kidney injury, which is the first organ damaged during sepsis. A mouse with depleted podoplanin from the podoplanin-expressing kidney cells – glomerular podocytes, showed that the protective effect of CLEC-2 during sepsis is not associated with podoplanin on

podocytes. However, the protective effect of CLEC-2 has been shown in macrophages expressing podoplanin, which regulates TNF-α secretion. Adding anti-podoplanin antibody 8.1.1 to bone marrow derived macrophages treated with LPS reduced TNF-α secretion. Nevertheless, injection of 8.1.1 antibody into cecal ligation and puncture WT mice increased pro-inflammatory cytokines and chemokines but inhibited immune cell recruitment into the infected peritoneum. These data suggest that anti-podoplanin antibody may be a novel strategy to modulate the inflammatory reaction and immune cell infiltration dependent on podoplanin expression (Rayes *et al.*, 2017).

1.9.4. Cancer

Podoplanin is expressed in different types of cancer cells, including squamous cell carcinoma, melanoma, skin cancer, mesotheliomas, and cancer-associated fibroblasts (Schacht *et al.*, 2005; Shibahara *et al.*, 2006; Wicki and Christofori, 2007).

In a metastasis model using podoplanin-transfected CHO cells inoculated intravenously into lateral tail vein of mice, an increase in the number of pulmonary metastatic nodules was observed when compared with the control CHO cells. In addition, the *in vivo* interaction between podoplanin-expressing CHO cells and platelets demonstrated that podoplanin-expressing cells were arrested in the lung 30 minutes after injection, compared to the control cells. These data suggest that podoplanin induces platelet aggregation after injection of the cells, and that might help the cells to survive and form metastasis (Kunita *et al.*, 2007).

Moreover, anti-podoplanin antibody (P2-0) administration inhibited podoplanin-induced experimental lung metastasis in mice injected with podoplanin-transfected CHO cells. In addition, a murine/human chimeric P2-0 antibody maintained its

inhibitory activity in a same model, and additionally when endogenously expressing podoplanin cancer cells (HT1080) were used (Nakazawa *et al.*, 2011).

Takemoto et al. reported that platelet aggregation induced by bladder squamous cell carcinoma cell line UM-UC-5, which endogenously expresses podoplanin, promotes tumour-platelet aggregate formation and induces the EMT of tumour cells. That enhances the platelet release of transforming growth factor-β (TGF-β) and increases the invasiveness and metastatic spread of UM-UC-5 cells. In addition, mice treatment with a TGF-β neutralizing antibody (clone 1D11) suppressed a podoplanin-mediated metastasis *in vivo*, suggesting that podoplanin promotes metastasis in part by releasing TGF-β from platelets which is essential for EMT of tumour cells (Takemoto *et al.*, 2017).

A non-cytotoxic 5-nitrobenzoate small molecule 2CP binds to CLEC-2 with an affinity constant of 33.2 ± 1.9 μM. Incubation of 2CP with podoplanin-expressing cancer cells (C6/Lung cells or human osteosarcoma cell line HOS or MG63) inhibited platelet aggregation. Additionally, 2CP has been used in a mouse xenograft model to determine the effect on pulmonary metastases of C6/Lung cells. 2CP was injected into nude mice in the presence or absence of the anti-cancer agent cisplatin. 2CP alone was not effective in the metastasis model. However, the combination of 2CP with cisplatin decreased the number of metastatic foci more than using cisplatin alone, suggesting its role in the improvement of anti-cancer therapy (Chang *et al.*, 2015).

Treatment of mice with an anti-mouse CLEC-2 antibody, 2A2B10, has been used to remove CLEC-2 from the surface of platelets. By injecting podoplanin-expressing mouse B16F10 melanoma cells into the CLEC-2 depleted mice, it has been demonstrated that lung weights of mice were significantly decreased compared to the WT control. These data suggest that inhibition of the CLEC-2-podoplanin interaction

suppresses hematogenous metastasis. In addition, co-culturing podoplanin-expressing B16F10 cells with CLEC-2-deficient platelets, but not with WT platelets, decreased their proliferation, suggesting that platelets stimulate tumour cell proliferation via the CLEC-2–podoplanin interaction. However, the effect on proliferation was not observed *in vivo* in CLEC-2 depleted mice. The authors hypothesized that solid tumour cells and platelets may not interact directly *in vivo* as they do in co-culture. These results require a further studies (Shirai *et al.*, 2017).

1.10. Aims of the thesis

This project is a one of 15 PhD projects within the Targeting Platelet Adhesion Receptors in Thrombosis (TAPAS) consortium. The over-arching goal of the TAPAS consortium was to determine the molecular basis of platelet activation by the receptors GPVI and CLEC-2 and the role of ITAM receptors in haemostasis, thrombosis, and vascular integrity. Additionally, TAPAS was investigating the mechanism of Src and Syk-mediated phosphorylation of the conserved tyrosines in the YxxL sequences of the GPVI/FcRγ complex ITAM and CLEC-2 hemITAM, identifying new targets for therapeutic intervention and novel lead compounds, modelling the molecular events of receptor clustering, and the generating of novel transgenic mouse models to study mechanisms of platelet receptor signalling.

Known antiplatelet medications target crucial haemostasis platelet activation pathways that may increase the risk of major bleeding. GPVI and CLEC-2 are two platelet receptors important in a variety of disorders that involve arterial thrombosis and thrombi-inflammation. They are promising targets for novel antiplatelet drugs because they have minimal roles in haemostasis.

Many cell surface receptors and downstream signalling molecules coalesce into micron and submicron clusters, following the initiation of signalling cascades. CLEC-2 forms clusters following podoplanin engagement, however, the regulation and effects of this clustering on signalling molecule recruitment, distribution and signal transduction is poorly understood.

This project "Artificial lipid membranes to study the platelet CLEC-2-podoplanin interaction" has two hypotheses:

1. This project "Artificial lipid membranes to study the platelet CLEC-2-podoplanin interaction" has two hypotheses: Artificial lipid bilayers may help measure and study the molecular behaviour of signalling platelet receptor components in ways that cannot be achieved using intact platelets.

2. CLEC-2 may be a good target for novel anti-platelet drugs having therapeutic effects on platelet activation. Targeting CLEC-2, rather than podoplanin, may be a good strategy because it is relatively restricted in expression when compared to podoplanin which has a wider tissue distribution.

Aims:

1. Develop a semi-high throughput reconstituted artificial lipid membrane platform as an experimental approach to test and validate signal manipulation of CLEC-2 intracellular macromolecular assembly and regulation.

2. Optimise and perform a high-throughput screen to identify a small molecule inhibitor of the CLEC-2-podoplanin interaction.

3. Characterise the effect of identified small molecule inhibitors on human platelet function.

Chapter 2

Materials and methods

2.1. Materials

2.1.1. Molecular biology reagents

DH5α Competent Cells, Phusion High-Fidelity PCR Master Mix and GeneRuler 1 kb Plus DNA Ladder were purchased from Thermo Scientific. Agarose and Ampicillin sodium salt were purchased from Fisher BioReagents. SYBR® Safe DNA gel stain and Zeocin were purchased from Invitrogen. T7 Express Competent *Escherichia coli* cells, Gel Loading Dye Purple (6×) buffer, CutSmart, all restriction enzymes (HindIII, KpnI, PmeI and NotI) and Quick Ligation™ Kit were purchased from New England Biolabs. IPTG, GenElute™ Gel Extraction Kit, GenElute™ Plasmid Miniprep kit, GenElute™ Plasmid Maxiprep kit and LB Broth (Miller) were purchased from Sigma-Aldrich. Kanamycin sulphate was obtained from Gibco.

2.1.2. Vectors and plasmids

pSF-OXB20-COOH-EKT-His10, pSF-OXB20-NH2-TEV-His10 were purchased from Sigma-Aldrich. pSNAPf and pSNAP-tag® (T7)-2 were purchased from New England Biolabs.

pFuse-hPdpn-rFc encoding a dimeric form of human podoplanin extracellular domain fused to rabbit Fc and pFuse-hFc-CLEC2 encoding a dimeric form of human CLEC-2 extracellular domain fused to human Fc were gifts from the Watson Lab, University of Birmingham.

2.1.3. Primers

Primers were synthesised by Sigma-Aldrich. All primer sequences are listed in Table 2.1. Primers were designed using SnapGene (version 4.2.9).

Table 2.1. List of primers.

Name	Nucleotide sequence 5' – 3'
09CLEC2-HindIII-Fw	GAAAGCTTGGCGGCTCGATGCAGGATGAAGATG
10CLEC2-KpnI-Rv	AATTGGTACCGCCATCACACGCCACCAGGAG
11CLEC2-His-PmeI-Fw	TACGTTTAAACATGGCGGCGGCTCGATGCAG
12CLEC2-His-NotI-Rv	ATTCTGCGGCCGCCTAATGGTGATGGTGG

2.1.4. Cell culture reagents

Human dermal lymphatic endothelial cells (HDLEC), CD31 and PDPN positive and Endothelial Cell Growth Medium MV 2 were purchased from PromoCell. Dulbecco's Modified Eagle's Medium (DMEM), ultra-low IgG Fetal Bovine Serum and Penicillin/Streptomycin were purchased from Gibco. Fetal Bovine Serum, Dulbecco's Phosphate Buffered Saline (DPBS), Trypsin-EDTA solution, L-Glutamine solution and Poly-L-lysine solution were obtained from Sigma.

2.1.5. Protein purification and labelling reagents

HiTrap™ Protein A HP column was purchased from GE Healthcare. HisPur™ Ni-NTA resin, EZ-Link™ Sulfo-NHS-LC-Biotin, Slide-A-Lyzer™ MINI Dialysis Device, 10K MWCO, 0.1 mL and Slide-A-Lyzer™ Dialysis Cassettes, 10K MWCO, 3 mL, Pierce™ Protein Concentrator PES, 10K MWCO, 5-20 mL and SnakeSkin™ Dialysis Tubing, 10K MWCO, 22 mm were purchased from Thermo Scientific. Alexa Fluor® Protein Labelling Kit was purchased from Invitrogen. SNAP-Surface® Alexa Fluor® 488 was obtained from New England Biolabs.

2.1.6. Lipids

Synthetic 1,2,-dioleoyl-sn-glycero-3-phosphocholine (DOPC), 1,2,-dioleoyl-sn-glycero-3-phophoethanolamine-N-(cap-biotinyl)(sodium-salt) (Biotin-Cap-PE) and (1,2,-dioleoyl-sn-glycero-3-[(N-(5-amino-1-carboxypentyl)iminodiacetic acid)succinyl (nickel salt) (DGS-NTA) were purchased from Avanti® Polar Lipids, Inc.

2.1.7. Flow cytometry reagents

Streptavidin-coated Microspheres (5 μm diameter), Silica Beads (4.98 μm diameter), Quantum™ Alexa Fluor® 488 MESF, Quantum™ Simply Cellular® Mouse IgG, PE-Mouse IgG1 kappa Isotype Control and BD Phosflow Perm Buffer III were purchased from BD Biosciences. Calcein-AM and Flow Cytometry Size Calibration Kit were obtained from Invitrogen. Microplate 96-well, PS, V-bottom, clear were purchased from Grainer-Bio-One. Anti-Rat IgG was purchased from Sigma.

2.1.8. Agonists, proteins, and inhibitors

Collagen-related peptide (CRP-XL) was obtained from Professor Richard Farndale (University of Cambridge, UK). Rhodocytin was a kind gift from Dr Johannes Eble (University of Münster, Germany). Thrombin was purchased from Merck. Hematoporphyrin was obtained from MedChemExpress. Integrillin was purchased from GlaxoSmithKline. Indomethacin, apyrase, PRT-060318 and Fibrinogen were purchased from Sigma. Recombinant Human CLEC-2/CLEC1B Protein was purchased from R&D systems. Small molecule inhibitors (MAS1-9) were obtained from SPECS (www.specs.net).

2.1.9. Antibodies

The primary and secondary antibodies used in this thesis are listed in a Table 2.2 and Table 2.3 respectively.

Table 2.2. List of primary antibodies.

WB – western blot, IP – immunoprecipitation; IF – immunofluorescence.

Antibody	Species	Application and dilution	Source
Phospho-tyrosine (4G10)	Mouse	WB 1:1000	Millipore
Phospho-PLCγ2 (Y759)	Mouse	WB 1:300	R&D Systems
PLCγ2	Rabbit	WB 1:1000	Santa Cruz Biotechnology
Phospho-Src (Y419)	Rabbit	WB 1:1000	Invitrogen
Src	Rabbit	WB 1:1000	Invitrogen
Phospho-Syk (Y525+Y526)	Rabbit	WB 1:1000	Abcam
Syk (4D10)	Mouse	WB 1:1000	Santa Cruz Biotechnology
AYP1	Mouse	IP/5 μg	Dr Alice Pollitt
AYP2	Mouse	WB 1:1000	Dr Alice Pollitt
Podoplanin (D9D7)	Rabbit	WB 1:1000 IF 1:200	Cell Signalling Technology
Podoplanin (NZ-1)	Rat	IF 1:200	AngioBio
Podoplanin (NZ-1.3)	Rat	IF 1:200	Invitrogen
APC anti-human CD42b	Mouse	IF 1:400	BD Biosciences
FITC anti-human Fibrinogen	Rabbit	Flow 1:100	Dako
PE/Cy5 anti-human CD62P	Mouse	Flow 1:100	BD Biosciences
PE anti-human GPVI (HY101)	Mouse	Flow 2.5 μl/test	BD Biosciences
FITC anti-human Syk	Mouse	Flow 5μl/test	BD Biosciences
His-tag	Mouse	WB 1:5000	Proteintech
GAPDH	Rabbit	WB 1:5000	Abcam
SNAP-tag	Rabbit	WB 1:1000	New England Biolabs

Table 2.3. List of secondary antibodies.

WB – western blot; IF – immunofluorescence.

Antibody	Species	Application and dilution	Source
Alexa Fluor 647 conjugated anti-rabbit	Donkey	WB 1:4000	Invitrogen
Alexa Fluor 488 conjugated anti-mouse	Goat	WB 1:4000	Invitrogen
Alexa Fluor 488 conjugated anti-rat	Goat	IF 1:1000	Invitrogen
Anti-Rabbit IgG (H+L) HRP	Goat	WB 1:5000	Thermo Scientific
Anti-Mouse IgG (H+L) HRP	Goat	WB 1:5000	Thermo Scientific

2.1.10. Other relevant materials

Bovine Serum Albumin heat shock fraction, protease free, fatty acid free was purchased from Merck. Streptavidin, Streptavidin AlexaFluor405 conjugated and Streptavidin AlexaFluor488 conjugated were purchased from Invitrogen. AlphaScreen Histidine (Nickel Chelate) Detection Kit and AlphaScreen TruHits Kit were purchased from PerkinElmer. 1536-well White Polystyrene Not Treated Microplates (3725) were purchased from Corning. 96-well PS, half area, clear microplates and 96-well, PP, F-bottom, black microplates were purchased from Grainer-Bio-One. 96-well glass bottom microwell plates, black (MatriPlate) were purchased from Brooks Life Science System. Formalin solution, 10% neutral buffer, Hellmanex III and Octyl β-D-glucopyranoside were purchased from Sigma-Aldrich. Ni-NTA Biosensors were purchased from Sartorius. Immobilon-FL transfer membrane was obtained from Millipore. Spectra/Por® Dialysis Membrane MWCO: 12-14,000 was purchased from Spectrum Laboratories, Inc. Bradford reagent was purchased from VWR.

Unless stated, all other reagents were of chemical grade and obtained from Sigma Aldrich or Thermo Scientific.

2.2. Methods

All the experiment in this thesis have been performed by me, except the analysis of the high-throughput screening and hit selection. The high-throughput screening has been performed at the Pivot Park Screening Centre (https://www.ppscreeningcentre.com) during my 2-month secondment. The identified compounds have been validated firstly at the University of Santiago the Compostela during my research stay for one-year secondment, and then continued at the University of Reading. The molecular biology, protein purification and microscopy-based experiments were fully performed by me at the University of Reading.

2.2.1. Molecular biology methods

Molecular biology methods have been used to prepare the DNA construct of CLEC-2 intracellular domain fused with histidine- and SNAP-tag. Both features of the plasmid are important to reconstitute signalling pathway using SLBs.

2.2.1.1. Agarose gel electrophoresis

Agarose gel electrophoresis was carried out using 50 mL of 1-2% agarose in 1×Tris-acetate-EDTA (TAE) buffer (40 mM Tris-HCl, 20 mM acetic acid, 1 mM EDTA). To dissolve the agarose, the solution was heated in a microwave before addition of SYBR® Safe DNA gel stain at a 1:10.000 dilution and pouring into a gel mould. The gel was covered with 1×TAE buffer before loading the samples and GeneRuler 1 kb Plus DNA Ladder into the wells. The samples were prepared using Gel Loading Dye Purple (6×) buffer. The running conditions were 100V for 45 minutes or until good separation achieved.

2.2.1.2. Insert amplification – Polymerase chain reaction (PCR)

PCR amplification of insert DNA was carried out using Phusion High-Fidelity PCR Master Mix. Reaction mixture contained 25 µl 2×Phusion Master Mix, 2.5 µl of both forward and reverse primers (10 µM), 100 ng template DNA and ddH$_2$O to a final volume of 50 µl. Reaction conditions were 98°C for 30 s of initial denaturation, 30 cycles of: 98°C for 10 s of denaturation, 69°C for 20 s of annealing followed by 72°C for 20 s per kb of extension, with a final extension of 5 min at 72°C. The PCR mixture was resolved via agarose gel electrophoresis, resulting fragments excised and purified using a gel extraction kit.

2.2.1.3. Restriction enzyme digestion

Digestion of vectors and inserts was carried out using restriction enzymes and CutSmart buffer at 37°C for 1 hour or in case of double digestion overnight or overnight with the first restriction enzyme and then 5 hours with the second one. The total reaction volume was 20 µl: 1 µg of DNA, 2µl of 10×CutSmart buffer, 1 µl of each restriction enzyme, adjusted with ddH$_2$O to the final volume. Digestion mixtures were resolved via agarose gel electrophoresis, digested fragments excised from gel and purified using a gel extraction kit.

2.2.1.4. Ligation of vector and insert

For all ligation reactions a Quick Ligation™ Kit was used. The reaction was performed in a 20 µl final volume comprising of 10 µl Quick Ligase Reaction Buffer (2×), 9 µl vector DNA and insert DNA (vector-insert ratio 1:5), 1 µl Quick Ligase and Nuclease-free water to the final volume. The reaction was incubated for 10 minutes at 25°C.

Chilled on ice, 2-4 µl of ligation mixture was transformed into 50 µl DH5α chemically competent cells.

2.2.1.5. Transformation

2-4 µl ligation mix or plasmid DNA were added into 50 µl thawed on ice competent bacterial cells. The cells were gently mixed and incubated on ice for 30 minutes. Heat shock was performed at 42°C for 45 seconds and the tube with the cells immediately transferred on ice for 2 minutes. Then 700 µl of room temperature LB was added to the tube and incubated at 37°C for 60 minutes with vigorously shaking (250 rpm). The cells were spread into LB-Agar plates supplemented with 100 µg/ml ampicillin, 50 µg/mL kanamycin or 25 µg/ml zeocin and incubated overnight at 37°C.

2.2.1.6. Plasmid DNA isolation

A single bacterial colony was selected from the LB-Agar plate using a sterile pipette tip and used to inoculate 5 ml of LB supplemented with appropriate antibiotic (100 µg/ml ampicillin, 50 µg/ml kanamycin or 25 µg/ml zeocin) in a 15 ml Falcon tube and incubated at 37°C overnight with vigorously shaking (225 rpm). Plasmid DNA was purified using a plasmid miniprep kit.

2.2.2. Cell cultures

Human endothelial kidney (HEK) 293T cells were grown in DMEM supplemented with 10% FBS, 100 U/ml of penicillin, 100 µg/ml streptomycin and 2 mM L-Glutamine solution. Human Dermal Lymphatic Endothelial Cells (HDLEC) were grown in Endothelial Cell Growth Medium MV 2 (Ready-to-use) supplemented with SupplementMix (0.05 ml Fetal calf serum, 5 ng/ml epidermal growth factor (recombinant human), 10 ng/ml basic fibroblast growth factor (recombinant human), 20 ng/ml insulin-like growth factor (long R3 IGF-1), 0.5 ng/ml vascular endothelial growth

factor 165 (recombinant human), 1 μg/ml ascorbic acid and 0.2 μg/ml hydrocortisone), 100 U/ml of penicillin and 100 μg/ml streptomycin. The cells were grown in adherent cultures in 75 cm^2 flasks at 37°C and a CO_2 level of 5%.

2.2.3. Protein overexpression, purification, and quantification

2.2.3.1. Protein overexpression in bacterial system

A starter culture was prepared by selecting a single colony from the LB-Agar plate with transformed T7 Express Competent *Escherichia coli* bacteria using a sterile pipette tip, inoculating 50 ml of LB supplemented with appropriate antibiotic in a 250 ml flask and incubated at 37°C overnight with vigorously shaking (225 rpm). Next day, six 2 litres flasks with 500 ml of LB supplemented with appropriate antibiotic was inoculated with 1 ml of starter culture. Flasks were incubated at 37°C with shaking (180 rpm) until an OD_{600} of around 0.4-0.5 is reached. The cultures were then cooled on ice for 20 minutes. Bacteria were induced with Isopropyl β-D-1-thiogalactopyranoside (IPTG) at a final concentration of 0.1 mM and incubated overnight at 16°C with shaking (120 rpm). After overnight incubation the cultures were centrifuged at 10,000×g for 15 minutes at 4°C. Supernatant was decanted and the pellet was used for protein purification.

2.2.3.2. His-tagged protein purification from inclusion bodies

Prior protein purification, growth expression studies were performed. These were tested against different overexpression conditions: temperature (37˚C, 30˚C and 16 ˚C), IPTG concentration (0.1 mM and 0.4 mM), growth time after induction with IPTG (3 hours, 5 hours, overnight) and bacteria strain (T7 Express Competent *Escherichia coli,* One Shot BL21 (DE3) Chemically Competent *E. coli* and Lemo21(DE3) Competent *E. coli.* The bacteria pellets of different conditions were lysed and sonicated and the samples were resolved by SDS-PAGE and stained with Coomassie dye.

The pellet was re-suspended in 10 ml of BugBuster Protein Extraction Reagent. The suspension was gently shaken at room temperature for 30 min, subjected to 5 cycles of sonication (45 second each, 5 second ON, 1 second OFF, amplitude 30%) and centrifuged at 16,000×g for 20 minutes at 4°C. The inclusion body pellet was re-suspended in 10 ml of Solubilization buffer (20 mM Tris-HCl, 500 mM NaCl, 6M guanidine hydrochloride, 5 mM imidazole, 1 mM β-mercaptoethanol, pH 8.0), stirred for 1 hour at room temperature and centrifuged at 16,000×g for 20 minutes at 4°C. Supernatant was saved for purification and refolding steps.

A column was packed with 3 ml of HisPur Ni-NTA resin and equilibrated with 10 ml of distilled water and 20 ml of Solubilization buffer. To 10 ml of supernatant, 10 ml of solubilization buffer was added. Protein extract was loaded on the column, flow-through was collected and re-applied to the column to ensure maximise binding. Refolding of the bound protein was performed on the column, using an Urea gradient, by washing with 10 ml of Wash Buffer A (6M Urea, 20 mM Tris-HCl, 500 mM NaCl, 20 mM imidazole, 1 mM β-mercaptoethanol, pH 8.0), 10 ml of Wash Buffer B (4M Urea, 20 mM Tris-HCl, 500 mM NaCl, 20 mM imidazole, 1 mM β -mercaptoethanol, pH 8.0), 10 ml of Wash Buffer C (2M Urea, 20 mM Tris-HCl, 500 mM NaCl, 20 mM imidazole, 1 mM β -mercaptoethanol, pH 8.0) and 10 ml of Wash Buffer D (20 mM Tris-HCl, 500 mM NaCl, 20 mM imidazole, 1 mM β -mercaptoethanol, pH 8.0). Refolded recombinant protein was eluted using 30 ml of Elution Buffer (20 mM Tris-HCl, 500 mM NaCl, 500 mM imidazole, 1 mM β -mercaptoethanol, pH 8.0).

Fractions containing eluted protein were dialyzed 3 times for a minimum of two hours each against 1×PBS in SnakeSkin™ Dialysis Tubing (to remove the imidazole). Recombinant protein was concentrated to 2 ml using a Pierce™ Protein Concentrator 10K MWCO, aliquoted and stored at -80°C.

2.2.3.3. Protein overexpression in mammalian cells – transfection

For protein overexpression of hPodoplanin-Fc, a calcium phosphate method was used, as it was confirmed by transfection of the HEK293T cells with a GFP-containing plasmid using epifluorescence microscopy, that this method worked better for protein overexpression compared to the method using polyethylenimine (PEI). A plasmid pFuse-hPdpn-rFc was a gift from University of Birmingham. hPodoplanin was expressed as an Fc-fusion to increase avidity of the ligand interacting with the platelet CLEC-2 in artificial lipid membrane platform. Fc-fusion provides two binding sites, compared to one binding site in a monomeric form.

HEK293T cells were harvested and re-plated on six 150 mm × 25 mm cell culture dishes 24-48 hours before transfection, until the cells reached 70% confluency. Cell media was replaced with of 10% ultra-low IgG FBS containing media 1 hour before transfection. 1.08 ml of 2.5 M $CaCl_2$, 180 μg of plasmid (pFuse-hPdpn-rFc) and 9.260 ml of ultrapure H_2O were mixed and added drop wise to 10.8 ml of 2×HEPES buffered saline (140 mM NaCl, 1.5 mM Na_2HPO_4, 50 mM HEPES, 10mM KCl, 0,2% glucose, pH 7.2), with gently mixing. The mixture was incubated at room temperature for 30 minutes. 3.5 ml per plate of calcium phosphate-DNA particle complexes were added directly to the cells in a dropwise manner over the entire surface of culture medium. The cells were incubated at 37°C for 8 hours, before transfection media was replaced with fresh medium supplemented with ultra-low IgG FBS. Cells were then cultured under standard conditions for 5 days. After this time, the medium was collected, and the cells were fed with fresh low IgG medium and cultured for a further 3 days. To remove cellular debris the collected medium was centrifuged in 50 ml Falcon tubes at 1000×g for 10 minutes at room temperature, the supernatant was transferred to the new tubes and stored at 4˚C with addition of 0.05% sodium azide for protein purification.

2.2.3.4. Fc-Fusion protein purification from cell media

Fc-fusion protein was purified using ÄKTA™ pure system (GE/cytivia). A HiTrap™ Protein A HP (5 mL) column, which can yield highly purified Fc-containing proteins, was connected into the system and equilibrated with 10 column volumes (CVs) of PBS. The medium containing protein was loaded on the column using sample pump P9S and subsequently washed with 5 CVs of PBS. Recombinant protein was eluted using 15 CVs of 0.1 M glycine, pH 3.0. Each 1.5 mL fraction was collected using Fraction collector F9-C into a 96-well 2mL plate containing 200 µL of 1M Tris-HCl, pH 9.0 (neutralization buffer). A sample of each step of the purification process was collected for SDS-PAGE and analysed using Coomassie staining and western blotting in reduced and non-reduced conditions. Fractions containing recombinant protein were concentrated and dialysed against PBS.

2.2.3.5. Bradford assay

The protein concentration was quantified using Bradford Reagent. 5 µl of each BSA standards (0, 0.1, 0.2, 0.4, 0.8, 1.2, 1.6, 2.0 mg/ml) as well as protein samples with unknown protein concentrations was pipetted into the wells of a 96-well plate. 100 µl of Bradford Reagent was added to each well, mixed by pipetting and left for 5 minutes at room temperature. The absorbance was measured at 595 nm using a FlexStation 3 Reader. By plotting absorbance at 595 nm versus protein concentration, the standard curve was generated, and the unknown sample concentrations determined.

2.2.4. Protein labelling

2.2.4.1. Monobiotinylation of recombinant protein

Monobiotinylated hPodoplanin-Fc was prepared by incubating the protein with limiting concentrations of EZ-Link™ Sulfo-NHS-LC-Biotin. The protein was dissolved in PBS

at 0.5 mg/ml and aliquoted in 0.5 ml fractions. To determine the optimal concentration of Sulfo-NHS-LC-Biotin needed for mono-biotin labelling varying final concentrations of Sulfo-NHS-LC-Biotin from 50 µl/ml to 0.005 µl/ml in 1/10 dilutions was added into the protein aliquots. The reaction was incubated for 30 minutes at room temperature, and then dialyzed against PBS four times at 4°C to remove the excess biotin reagent. Monobiotinylation of the recombinant protein was confirmed using flow cytometry (Chapter 2.2.6.1.).

2.2.4.2. *In vitro* labelling of monobiotinylated protein

The monobiotinylated protein was labelled using an Alexa Fluor® Protein Labelling Kit. To 0.5 ml of 2 mg/ml monobiotinylated hPodoplanin-Fc, 50 µl of 1M Sodium Bicarbonate (pH 8.3) was added. The protein was transferred into a vial of reactive dye containing a magnetic stir bar and was stirred for 1 hour at room temperature in the dark. The column was filled with purification resin and left so excess buffer drained away. The reaction mixture was loaded onto the column and elution buffer (10mM potassium phosphate, 150 mM NaCl, pH 7.2, with 2mM sodium azide) was added. Two coloured bands, which represented the separation of labelled protein from unincorporated dye was observed. The first coloured band contained the labelled protein was collected.

The concentration and the labelling degree of monobiotinylated hPodoplanin-Fc were determined by measuring the absorbance of the conjugate solution at 280 nm and 494 nm using a NanoDrop2200. To calculate the protein concentration the following equation was used:

$$protein\ concentration\ [M] = \frac{[A_{280} - (A_{494} \times 0.11)]}{\varepsilon}$$

The molar extinction coefficient (ε) was estimated by knowing the number of tryptophan (W), tyrosine (Y) and cysteine (C) residues in the sequence of protein and calculated by using the following equation:

$$\varepsilon \, [cm^{-1}M^{-1}] = (nW \times 5500) + (nY \times 1490) + (nC \times 125)$$

The degree of labelling was calculated using following equation:

$$moles \; dye \; per \; mole \; protein = \frac{A_{494}}{71000 \times protein \; concentration}$$

where 71,000 $cm^{-1}M^{-1}$ is the approximate molar extinction coefficient of the Alexa Fluor® 488 dye at 494 nm.

2.2.4.3. *In vitro* labelling of SNAP-tagged protein

Recombinant protein in fusion with SNAP-tag and 10×Histidine tag was labelled using SNAP-Surface® Alexa Fluor® 488. To set up the reaction, the following components were mixed: 5 µl of 50 µM SNAP-tagged recombinant protein, 1 µl of 50 mM DTT, 2 µl of 250 µM SNAP-tag Alexa Fluor 488 Substrate, topped up with 1×PBS to a final volume of 50 µl. The reaction was incubated for 2 hours at 25°C in the dark and then at 37°C for 10 minutes. Labelled protein was dialysed against 1L of 1×PBS for 1 hour at room temperature in the dark using Slide-A-Lyzer™ MINI Dialysis Device. The protein sample was run on an SDS-PAGE gel and detected using a Typhoon FLA 9500. The sample was stored at -20°C with addition of 1mM DTT (final) in the dark.

2.2.5. Liposomes preparation

Three different compositions of liposomes were prepared: 25% DGS-NTA -75% DOPC; 2% Biotin-Cap-PE -98% DOPC; 100% DOPC. The selected ratio of lipids were based on previously reported literature ratios used for SLBs preparation (Dustin and Pollitt, 2018, Pollitt *et al.*, 2014). To 2ml of $CHCl_3$ in a glass test tube, the phospholipids

were added to a final concentration of 4 mM and the ChCl₃ evaporated under a nitrogen stream leaving a lipid film at the bottom of the test tube. The tubes were capped with parafilm squares and lyophilized for 90 minutes to remove any residual ChCl₃. After lyophilization, 2 ml of 2% Octyl-β-D-glucopyranoside were added and the mixture was sonicated to solubilize the lipids. Subsequently, the lipids were sterilized using a 0.22 μm filter. 100 μl of appropriate lipids were added to 900 μl of 2% Octyl β-D-glucopyranoside, to make a 0.4 mM working solution. Prepared liposomes were dialysed into degassed Tris-buffered saline (25 mM Tris-HCl, 150 mM NaCl, pH 8,0) using Spectra/Por Dialysis Membrane. The dialysis was performed 3 times, changing tubing to fresh buffer each time. After dialysis, liposomes were aliquoted into 1.5 ml Eppendorf tubes and stored at 4°C. To minimise exposure to oxygen, air was purged from the tubes using argon.

2.2.6. Flow cytometry

All flow cytometry experiments were performed using a BD Accuri C6 Plus system. To ensure that the signal was collected, and the noise was ignored, 20,000 on FSC-H threshold was used. Data was collected from 10,000 events for each gated cell sample.

2.2.6.1. Determination optimal concentration to monobiotinylate protein

2 μl of Streptavidin-coated Microspheres (5 μm diameter) per reaction were washed in Eppendorf tubes with reaction buffer (1% BSA, 0.02% Tween20 in PBS) by centrifugation at 7.500×g for 1 minute at room temperature, and then incubated with 2 μl of biotinylated protein in 50 μl of reaction buffer for 20 minutes at room temperature with agitation (to prevent the beads from settling in the bottom of the tube).

The beads were washed 2 times with reaction buffer by centrifugation at 7.500×g for 1 minute at room temperature. The beads were incubated with a 1:100 dilution (10 μg/ml

final) of Streptavidin Alexa Fluor 488 and with a 1:100 dilution of podoplanin (D9D7) Rabbit mAb in 50 µl of reaction buffer and incubated for 20 minutes with agitation. The beads were washed 2 times with reaction buffer by centrifugation at 7.500×g for 1 minute at room temperature, and then incubated with 1:500 dilution of Alexa Fluor 647 donkey anti-rabbit IgG in 50 µl of reaction buffer for 20 minutes with agitation. The beads were washed 3 times with reaction by centrifugation at 7.500×g for 1 minute at room temperature and analysed by flow cytometry. The optimal biotin labelling to result in monobiotinylation of the recombinant protein was the concentration at which staining was detected in the FL4 (675/25 BP) channel, but not in the in the FL1 (530/30 BP) channel. It suggests that there are no more biotin molecules on the protein surface than one, occupied by streptavidin beads and that protein is incorporated into the beads by biotin because it is recognised by the anti-specific antibody, giving a fluorescence signal.

2.2.6.2. Quantification of the protein density deposited on the bilayer

2.5 µl of 4.98 µm silica beads were transferred into an Eppendorf tube, washed once with 150 µl of FACS buffer (1% BSA, 10 mM HEPES, 0.02% sodium azide in PBS) and centrifuged at 600×g for 2 minutes. Supernatant was removed, 5 µl of liposomes were added and incubated with the beads for 20 minutes at room temperature. The beads were washed 3 times with FACS buffer by centrifugation at 600×g for 2 minutes. 150 µl of Blocking buffer (5 mg/ml heat denatured BSA in PBS) was added, and the beads were incubated for 20 minutes at room temperature. The beads were washed 3 times as above, then 50 µl of 10 µg/ml Streptavidin was added and incubated for 20 minutes at room temperature. The washing step was repeated as above, then 50 µl of 10 µg/ml Fc-tagged fluorescently labelled recombinant protein was added and incubated for 20 minutes at room temperature. The beads were washed 3 times as above, then

resuspended in 150 μl of FACS buffer and transferred to flow cytometry tubes containing 300 μl of FACS buffer. At the same time the calibration beads (Quantum™ Alexa Fluor® 488 MESF) were prepared following the protocol attached by supplier. The samples were read using flow cytometry (Accuri CSampler Plus).

For NTA-lipids the protocol was similar except the buffers: Blocking Buffer (5 mg/ml BSA in 10 mM Tris-HCl pH 8.0 with addition of 100 μM NiCl$_2$), FACS buffer (1% BSA, 10 mM HEPES, 0.02% sodium azide in 10 mM Tris-HCl pH 8.0) and the time of incubation beads with His-tagged fluorescently-labelled recombinant protein was 1 hour.

The median fluorescence of calibration beads was used to generate a standard curve by plotting the number of Alexa Fluor 488 molecules on the x axis against median fluorescence intensity (MFI) on the y axis. A linear regression was fitted to the standard curve and equation was displayed. Bead saturation was confirmed by a high R^2 value close to 1. Using the equation, the number of fluorescent dye molecules associated with the bilayer coated bead was determined. To calculate the density of protein molecules tethered to the bilayers, the equation below was used.

$$density\ molecules/\mu m^2 = \frac{sample\ MFI/\ (fluorescent\ dye : protein\ ratio)}{bead\ surface\ area}$$

where fluorescent dye:protein ratio was estimated during labelling of monobiotinylated hPodoplanin-Fc; and bead surface area was calculated using the equation $4\pi r^2$ and is equal to 77.87 μm^2 for 4.98 μm diameter beads.

2.2.6.3. Quantification of intracellular protein copy number

8×10^6 human washed platelets (20 μl of platelets at 4×10^8/ml) was suspended in 180 μl 1×HBS buffer (20 mM HEPES, 150 mM NaCl, pH 7.0) and fixed with an equal volume

of 4% Paraformaldehyde for 10 minutes at room temperature. Platelets were washed three times with 2 ml of 1×HBS buffer by centrifugation for 15 minutes at 500×g. Platelets were permeabilized by incubation with 50 µl of BD Phosflow Perm Buffer III for 30 minutes on ice. Following three washes with 2 ml 1×PBS buffer, platelets were incubated with a saturating concentration of FITC Mouse Anti-Human Syk (5 µl of 200 µg/ml, clone 4D10) or 5 µl of FITC with PE- Mouse IgG1 kappa Isotype Control in 45 µl of PBS for 20 minutes at room temperature. 450 µl of 1×PBS was added, and the mixture was transferred into a FACS tube. At the same time the calibration beads (Quantum™ Simply Cellular® Mouse IgG) were prepared following the protocol attached by supplier. All samples were read using flow cytometry. The sample analysis and determination of the copy number of intracellular proteins in platelets was the same as for surface proteins.

2.2.6.4. Estimation of HDLECs size

200 µl of 5×10^5 HDLEC or 5 µl of different size of microspheres (1 µm, 2 µm, 4 µm, 6 µm, 10 µm and 15 µm-diameter) from Flow Cytometry Size Calibration Kit were transferred into 96-well plate, washed once with PBS and then read using flow cytometry. The beads and the cells were gated using side scatter (SSC-A) and forward scatter (FSC-H) measuring cell granularity and cell size, respectively. The median in FSC-H was estimated using BD Accuri C6 plus software. A standard curve was generated by plotting sizes of beads on x axis against median in FSC-H scatter A linear regression was fitted to the standard curve and equation was displayed. The size of HDLECs was calculated from the equation.

2.2.6.5. Quantification of podoplanin density in HDLECs

1×10^6/ml of HDLECs suspended in 45 µl of PBS were incubated with a saturating concentration of PE-conjugated anti-human podoplanin antibody NZ-1.3, starting from 5 µl of antibody per test. The samples were incubated for 20 minutes at room temperature in dark. At the same time the calibration beads (Quantum™ Simply Cellular® Rat IgG) were prepared following the protocol attached by supplier, using the same antibody as to stain HDLECs. To remove unbound antibody, the samples were washed 3 times with PBS. All samples were read using flow cytometry. As a control against non-specific antibody binding, platelets were incubated with PE- Rat IgG2a kappa Isotype Control.

The median fluorescence of calibration beads was used to generate a standard curve by plotting antibody binding capacity on the x axis against MFI on the y axis. A linear regression was fitted to the standard curve and equation was displayed. Bead saturation was confirmed by a high R^2 value close to 1. Using the HDLEC diameter and the podoplanin copy number, the surface density of podoplanin was determined.

2.2.7. Supported lipid bilayer formation

2.2.7.1. Formation of SLB in FCS2 chamber

Liposomes (2% Biotinyl-Cap-PE, 98% DOPC) were deposited on a glass coverslip cleaned by piranha solution (a mixture of 35 ml 18M concentrated sulfuric acid and 15 ml of 30% (w/v) hydrogen peroxide) as single 1 µl droplets, assembled in Bioptechs FCS2 chamber and incubated for 20 minutes at room temperature. Formed SLB were washed using 5 ml of PBS delivered into the chamber using a three-way stopcock, afterwards blocked with 1 ml of blocking buffer (5 mg/ml heat denatured fatty acid free bovine serum albumin in PBS solution) and incubated 20 minutes at room temperature.

Unbound blocking buffer was removed by passing 5 ml of PBS through the chamber. 1 ml of 10 µg/ml streptavidin (Invitrogen) was added into the chamber and incubated for 20 minutes at room temperature in the dark. Unbound streptavidin was removed by passing 5 ml of PBS through the chamber. Then 1 ml of 10 µg/ml of biotinylated and fluorescently labelled recombinant protein was added into the chamber, incubated 20 minutes at room temperature in the dark. Unbound protein was removed by passing 5 ml of PBS through the chamber. The chamber was ready for microscopy analysis.

For NTA-lipids the protocol was similar except the Blocking Buffer (5 mg/ml BSA in 10 mM Tris-HCl pH 8.0 with addition of 100 µM $NiCl_2$), there was no step with Streptavidin and the SLB were incubated with His-tagged fluorescently-labelled recombinant protein for 30 minutes.

2.2.7.2. Formation of SLB in 96-well glass bottom plate

Supported lipid bilayers were formed in 96-well glass bottom plates. Each well of the plate was washed with 200 µl of 5% Hellmanex III solution at 50°C overnight, followed by washing 10 times with 250 µl distilled water. Afterwards, the wells were cleaned 3 times with 5M NaOH for 30 minutes at 50°C and again washed with water. The plate was dried by centrifugation upside down at 500×g for 2 minutes. 5 µl of liposomes was then deposited in each well and allowed to form SLB for 30 minutes at room temperature. After 30 minutes, wells containing liposomes were washed 3 times with PBS and then blocked with 200 µl blocking buffer (5 mg/ml heat denatured bovine serum albumin in PBS solution) for 20 minutes at room temperature, to block the surface and minimise non-specific protein adsorption. 200 µl of 10 µg/ml streptavidin was added to the well, incubated for 20 minutes at room temperature and washed 3 times with PBS. Then 200 µl of 10 µg/ml biotinylated and fluorescently labelled

recombinant protein was added, incubated for 20 minutes at room temperature in the dark and washed again 3 times with PBS. 100 μl of PBS was added to the wells and the plate was ready for microscopy analysis.

2.2.8. Microscopy

2.2.8.1. Fluorescent and DIC microscopy

Microscope slides from platelet spreading assays on immobilized agonists or HDLECs were imaged using an Eclipse Ti2 Inverted Microscope with HP Plan Apo VC 100xH objective and Camera Nikon DS-Qi2. DIC and epifluorescence pictures were taken with a frame size of 2424x2424 pixels (0.07 μm/px). Platelet spreading analysis was performed manually by counting the number of platelets in the field of view or, to determine the platelet surface area, by drawing the platelets and measuring them using the measure function in ImageJ (Fiji, version 1.53c).

2.2.8.2. Fluorescence recovery after photobleaching (FRAP)

Bilayer mobility was confirmed using fluorescence recovery after photobleaching (FRAP). Experiments were performed with a Plan apo λ 60x Oil emersion objective on a Nikon Eclipse Ti inverted microscope using Nikon A1plus camera. During the FRAP experiment, the FCS2 chamber or 96-well plate was kept at 37°C. The fluorescence within the region of interest was photobleached for 2-15 seconds (depending on the experiment) at 100% intensity with a 488 nm Argon ion laser. Before and after bleaching, confocal image series were recorded at 5 sec time intervals at low laser intensity. Simultaneously, a reference ROI of the same size was measured for each time point. Confocal images series were recorded with a frame size of 1024x1024 pixels (0.03 μm/px).

2.2.8.3. Total internal reflection fluorescence (TIRF) microscopy

To the prepared FCS2 chamber (or glass-bottom 96-well plate) with CAP-Biotin-PE SLB and biotinylated and fluorescently labelled hPodoplanin-Fc, 1 ml (or 200 µl) of human washed platelets at 10^7 per ml were added. The chamber (or plate) was imaged with a Nikon TIRF system mounted on a Ti-E stand, using an Apo TIRF 100x 1.49 Oil DIC N2 objective. Images series were recorded with a frame size of 512x512 pixels (0.16 µm/px).

2.2.9. High-throughput screening (HTS)

The high-throughput screen was performed by me with the support of Dr Jan van Groningen. during my 2-month secondment in the Pivot Park Screening Centre in the Netherlands. The characterization of true hits and dose-response studies were performed at University of Santiago de Compostela.

2.2.9.1. HTS using AlphaScreen

The high-throughput screen with the Pivot Park Screening Centre library (18,476 compounds, Prestwick Chemical Library and SPECS) was carried out using Amplified Luminescent Proximity Homogeneous Assay (AlphaScreen™). The Prestwick Chemical Library is composed of 1520 FDA-approved & EMA-approved drugs. It was selected due it's chemical and pharmacological diversity since the compounds in this library have been addressed to more than 600 targets. The SPECS library is composed of a variety of novel small molecules, which have not been described previously. The assay was performed using monobiotinylated human Podoplanin-rFc and a commercial recombinant human CLEC-2/CLEC1B with Histidine tag. Firstly, 10 nl of 2 mM compounds (dissolved in 100% DMSO) were added into 1536-well plates using Echo®

555 acoustic liquid dispenser, whereas into columns 1-8 was added 10 nl of 100% DMSO. Secondly, 0.5 µl of reaction buffer (0.1% BSA in PBS) was added to all the wells using Certus Flex liquid dispenser, except column 5 and 6, where 0.5 µl of 160 µM Hematoporphyrin was added as a positive control of inhibition. Podoplanin and CLEC-2 were then diluted using reaction buffer to concentrations of 100 nM and 400 nM respectively and added together at a 1:1 ratio (1 µl each) to all wells, except column 1, 2, 7, 8, where 2 µl of reaction buffer was added. Following a 30 minutes incubation of the proteins with the compounds at room temperature, 0.75 µl of 133 µg/ml nickel-chelate (Ni-NTA) acceptor beads were added into all wells and incubated for 1 hour at room temperature in the dark. Then, 0.75 µl of 133 µg/ml of streptavidin donor beads were added and incubated for another 1 hour at room temperature in the dark. The final volume of the reaction was 4 µl and the concentration of individual components was 5 µM of compounds, 20 µM of Hematoporphyrin, 25 nM of podoplanin, 100 nM of CLEC-2, 25 µg/ml of nickel-chelate acceptor and streptavidin donor beads. Following an incubation with the donor beads, the fluorescence intensity at 520/620 nm (ex/em) was subsequently read using an Envision multi-label plate reader (Perkin-Elmer). The data was analysed by Dr Jan van Groningen and the resulting list of the hits was sent via e-mail.

2.2.9.2. Characterising the true hits

To confirm the inhibitory effect of compounds on protein-protein interactions, compounds identified through the high-throughput screen were analysed again using the AlphaScreen™ assay. Additionally, to identify any false-positive hits, an AlphaScreen™ TruHits™ assay was performed. Each compound identified using high-throughput screen was dispensed again into a 1536-well plate in the same concentration as before and then diluted with the assay buffer to a final volume of 0.75 µl. The kit

components, Biotinylated Acceptor beads and Streptavidin-Donor beads, were premixed in the assay buffer to final concentrations of 6.25 µg/ml and 12.5 µg/ml respectively and incubated for 30 minutes at room temperature in the dark. 3.25 µl of premixed beads was added to each well with compounds and incubated for another 10 minutes. Following an incubation, the fluorescence intensity at 520/620 nm (ex/em) was subsequently read using an Envision multi-label plate reader (Perkin-Elmer). Compounds with a fluorescent signal lower than the control wells with DMSO by more than two standard deviations were identified as false positives.

2.2.9.3. Dose-response curve

To generate a dose-response curve of lead compounds which inhibit the hPodoplanin-hCLEC-2 interaction, the optimised AlphaScreen assay from above was performed. A total of ten serial dilutions ranging from 160 µM to 0.3125 µM (final concentrations in the well) of the lead compounds were prepared in reaction buffer from a 10 mM stock dissolved in 100% DMSO and run on the AlphaScreen assay. Additionally, a total of ten serial dilutions of DMSO, corresponding to the final concentration of DMSO in each compound point (ranging from 1.6% to 0.003125% (v/v)) were run to control for the impact of DMSO on the AlphaScreen signal. Percentage inhibition was calculated for each concentration of compound and plotted against the logarithm of the concentration. The compounds were tested in duplicate at each concentration and the assay was repeated three times. The obtained data was analysed and fitted using GraphPad Prism 7.04.

2.2.9.4. HTS data analysis

The signal to background ratio (S/B) was determined by dividing the mean of maximum fluorescent signal (DMSO with proteins) by the mean of minimum

fluorescent signal (signal inhibition by Hematoporphyrin) to determinate fluorescence change in the assay. The Z' factor was calculated using the mean and standard deviation (sd) of the fluorescence of the maximum fluorescent signal (max, DMSO with protein) and the minimum of fluorescent signal (min, signal inhibited by Hematoporphyrin) using the following equation:

$$Z' = 1 - \frac{3sd\ of\ \max + 3sd\ of\ \min}{|mean\ of\ \max - mean\ of\ \min|}$$

The Z' value higher than 0.5 describes an ideal assay.

2.2.10. Platelets

2.2.10.1. Platelet Rich Plasma (PRP) preparation

Whole blood was obtained from healthy volunteers who had not taken any medication affecting platelet function in the previous 10 days using methodology approved by the University of Reading Research Ethics Committee. Whole blood was collected in a 4.5 mL or 9 mL vacutainers containing 3.2% sodium citrate. The blood was transferred into sterile round base tubes (4.9 ml tube, LP4) and PRP was obtained by centrifugation the tubes at 200×g for 20 min at room temperature. PRP (the upper layer after centrifugation) was removed gently to the falcon tube and rested for 30 minutes prior to the experiments.

2.2.10.2. Human washed platelets preparation

Whole blood was collected in a 4.5 mL or 9 mL vacutainers containing 3.2% sodium citrate. 10% tube volume of acid-citrate-dextrose (ACD; 85 mM sodium citrate, 71 mM citric acid and 110 mM glucose) was added into the blood and gently mixed. The blood was transferred into sterile round base tubes (4.9 ml tube, LP4) and PRP was obtained by centrifugation the tubes at 200×g for 20 min at room temperature. The top layer

(PRP) was collected into the falcon tube, 0.36 µl per every 1 ml of PRP of 0.25 µg/ml Prostacyclin (PGI$_2$, solubilized in ethanol) was added and platelets were pelleted by centrifugation at 1000×g for 10 minutes at 20 ºC. The pellet was re-suspended in 1 ml of warmed Tyrode's buffer (134 mM NaCl, 2.9 mM KCl, 0.34 mM Na$_2$HPO$_4$, 12 mM NaHCO$_3$, 20 mM HEPES, 1 mM MgCl$_2$ and 5 mM glucose, pH 7.3) and 150 µl of ACD and then 3 ml of ACD was added and the mixture was topped up with Tyrode's buffer to 28 ml. The number of platelets was determined using a Sysmex Automated Hematology Analyzer or a Z1 Coulter Particle Counter (Beckman Coulter), 10 µl of 0.25 µg/ml PGI$_2$ was added and then platelets were pelleted by centrifugation at 1000×g for 10 minutes at 20 ºC. The pellet was re-suspended to the appropriate cell density using Tyrode's buffer. Platelets were rested for 30 minutes to recover before being used for experiments.

2.2.10.3. Light transmission aggregometry (LTA)

LTA was preformed using an aggregometer AggRAM (Helena Biosciences) in a final volume of 250 µl. 215 µl of washed platelets at concentration 4×10^8/ml were added into a AggRAM Cuvette with a stirring bar inside and incubated for 5 minutes with 10 µl of inhibitor or 0.3% (v/v) DMSO final. Under stirring conditions (1200 rpm at 37˚C), platelets were then stimulated with 25 µl of agonist: CRP-XL (0.3 or 3 µg/ml final), rhodocytin (30 or 100 nM final), or thrombin (0.05 U/ml final). Light transmission was monitored for 5 minutes. Tyrode's buffer was used as a blank (100% of aggregation).

2.2.10.4. Plate-based aggregometry (PBA)

40 µl of washed platelets (4×10^8/ml) were loaded into 96-well half area plates and incubated with 5 µl of inhibitor or DMSO (0.3% (v/v) final) for 5 minutes before the addition of 5 µl of CRP-XL (3 µg/ml final), rhodocytin (200 nM final) or thrombin

(0.05 U/ml final). A plate was shaken BioShake iQ (Q Instruments) at 1200 rpm and 37°C for 5 minutes for CRP-XL and thrombin, and 10 minutes for rhodocytin. The absorbance was measured at 405 nm using a FlexStation 3 Reader Platelet.

2.2.10.5. Spreading assay

Single glass coverslips (⌀ 13 mm) were placed in each well of a 24-well plate, coated with 300 µl of 10 µg/ml hPodoplanin-rFc, 300 nM rhodocytin, 3 µg/ml CRP-XL or 100 µg/ml fibrinogen and incubated overnight at 4°C. The coverslips were washed 3 times with 1×PBS, then blocked with 5 mg/ml heat denatured BSA for 1 hour at room temperature and washed again. 300 µl of washed platelets at 2×10^7/ml, pre-treated with inhibitor or 0.3 % (v/v) DMSO final for 5 minutes, were added and incubated for 45 minutes at 37°C. Non adherent platelets were removed by washing 3 times with 1×PBS and coverslips were fixed with 300 µl of Formalin Solution, 10% neutral buffered for 10 minutes, washed 3 times with 1×PBS, and permeabilized with 300 µl of 0.1% (v/v) Triton-X100 for another 10 minutes. The coverslips were washed 3 times with 1×PBS, stained with 100 µl Alexa Fluor 647 Phalloidin (1:100 dilution) and incubated for 50 minutes at room temperature in the dark. The coverslips were washed 3 times with 1×PBS, then 3 times with distilled water and mounted on 75 mm × 25 mm microscope slides using Hydromount™. Prepared slides were analysed using epifluorescence microscopy method described in section 2.2.8.1.

2.2.10.6. Flow cytometry of platelets

In a V-bottom 96-well plate, 5 µl of PRP or washed platelets (4×10^8/ml) were incubated with 5 µl of 10x concentrated inhibitor or DMSO, 1 µl PE/Cy5 anti-human CD62P antibody and FITC anti-human Fibrinogen antibody for PRP (or 100 µg/ml Alexa Fluor 488 Fibrinogen final for washed platelets) in a final volume of 45 µl. Then 5 µl of 10x

concentrated agonist was added and the plate was incubated for 20 minutes in the dark. To stop the reaction, the samples were fixed with 150 µl 0.2% formyl saline. Negative controls for antibodies were set by using appropriate isotype controls: EDTA for fibrinogen binding and PE- Mouse IgG1 kappa Isotype Control for P-selectin exposure. Samples were analysed using a BD Accuri C6 Plus flow cytometer. A gate was applied around platelets population using side scatter (SSC) and forward scatter (FSC) measuring cell granularity and cell size, respectively, and data was collected from 10,000 events for each sample.

2.2.10.7. Platelet viability assay

200 µl of washed platelets (2.5×10^6/ml) were incubated with the inhibitor or 0.3% (v/v) DMSO final for 10 minutes at 37°C. For the positive control, which affects platelet viability, Triton X-100 (0.01% (v/v) final) was used. After 10 minutes, 1 µl of 0.1 mg/ml Calcein-AM was added to the samples and incubated for 20 minutes at 37°C in the dark. Samples were analysed using a BD Accuri C6 Plus flow cytometer in the FL1 (530/30 BP) channel. Data was collected from 10,000 events for each gated platelet sample.

2.2.10.8. Platelet signalling study

270 µl of washed platelets (8×10^8/ml) were pre-treated with 9 µM Integrillin (for platelets stimulated with rhodocytin) or 9 µM Integrillin, 2 U/mL of apyrase and 10 µM of indomethacin (for platelets stimulated with CRP-XL). Then, platelets were incubated with 10 µl of inhibitor or DMSO (0.3% (v/v) final) for 5 minutes. Samples were stimulated with Tyrode's buffer (resting), 1 µg/ml CRP-XL or 100 nM rhodocytin under stirring conditions (1200 rpm at 37°C) using an aggregometer. The reaction was stopped after 90 seconds (for CRP-XL) or 5 minutes (for rhodocytin) by adding the

same volume of ice-cold 2x Lysis buffer (0.3 M sodium chloride; 20 mM Tris; 2 mM EGTA; 2 mM EDTA; 2% (v/v) NP-40; 10 µg/mL aprotinin; 1 µg/mL pepstatin; 10 µg/mL leupeptin; 400 µg/mL AEBFS; 5 mM sodium orthovanadate; pH 7.5) and then incubated for 30 minutes on ice. To remove insoluble debris, samples were centrifuged at 15,000×g for 15 min at 4˚C. Samples for SDS-PAGE were prepared by adding 10 µl of 6X sample buffer (12% (w/v) Sodium Dodecyl Sulphate (SDS), 30% (v/v) glycerol, 0.15M Tris-HCl (pH 6.8), 0.001% (w/v) Brilliant Blue R, 30% (v/v) β-mercaptoethanol), into 50 µl of lysed platelets. Samples were heated at 95°C for 5 minutes and separated using SDS-PAGE.

2.2.10.9. Platelet spreading assay on HDLECs

Single glass coverslip (⌀ 13 mm) was sterilised with 70% (v/v) ethanol and placed in each well of a 24-well plate. $1×10^5$ of HDLECs were harvested in each well and cultured until 90-100 % confluency. On the day of the experiment, cell media was removed, and the cells were washed three times with DPBS, before adding 300 µl of washed platelets at $2×10^7$/ml, pre-treated with inhibitor or 0.3 % (v/v) DMSO final for 5 minutes. Cells with platelets were incubated for 45 minutes at 37˚C. Non adherent platelets were removed by washing 3 times with DPBS and coverslips were fixed with 300 µl of Formalin Solution, 10% neutral buffered for 10 minutes, washed 3 times with 1×PBS, and permeabilized with 300 µl of 0.1% (v/v) Triton-X100 for another 10 minutes. The coverslips were washed 3 times with DPBS, stained with anti-podoplanin (NZ-1) and APC conjugated anti-human CD42b antibodies. The excess of the antibodies was removed by washing 3 times with DPBS. Afterwards, coverslips were incubated with Alexa Fluor 488 conjugated anti-rat antibody, as a secondary antibody to stain anti-podoplanin (NZ-1). The coverslips were washed 3 times with DPBS, then 3 times with distilled water and mounted on 75 mm × 25 mm microscope slides using

Hydromount™. Prepared slides were analysed using epifluorescence microscopy method described in section 2.2.8.1.

2.2.10.10. Bio-Layer Interferometry (BLI)

The interaction between human CLEC-2 and MAS9 was measured using Bio-Layer Interferometry using an Octet K2 (ForteBio). The interaction analysis was performed at 37°C in PBS buffer with 0.02% (v/v) Tween-20 (PBS/Tween20). CLEC-2, containing his-tag was immobilized on Ni-NTA biosensors for 600 s. The 96-well plate was filled with 200 µl of sample or buffer per well and agitated at $1000 \times g$. The loaded biosensors were washed in a buffer for 180 s and transferred into the wells containing MAS9 at concentrations 100, 70, 50, 30, 10 and 1 µM in PBS/Tween20 respectively. The association was monitored for 40 s and dissociation for 240 s. As a negative control 1% (v/v) of DMSO final was used. Kinetic parameters (k_a and k_d) and affinities (K_D) were calculated from a non-linear global fit of the data between CLEC-2 and MAS9 using the Octet Data Analysis HT 11.1 software.

2.2.10.11. Molecular docking

For docking studies, the crystal structure of human CLEC-2 (2C6U) from RCSB Protein Data Bank (PDB) was used. 2C6U is the only available crystal structure for human CLEC-2 alone. Before commencing a docking, the protein structure was subjected to preparation using Protein Preparation Wizard in Maestro Schrödinger (Release 2020-4). During preparation, the missing hydrogens were added, the ionization states at pH 7.0 ± 2.0 were generated by Epik and water molecules were removed beyond 5 Å from het groups (non-standard residues). The addition of missing hydrogens is required to perform docking studies, as these are required for the energy function and because macromolecular structures do not contain hydrogen atoms in their

corresponding PDB files. In addition, H-bond assignment was optimised using PROPKA (pH 7.0) and the structure was minimised using OPLS4 (Optimised Potentials of Liquid Simulations) force field. OPLS4 is the latest version of the of the force field in Maestro Schrödinger. It takes into consideration the bond stretching, angle bending, torsions and non-bonds. Compared to the previous version (OPLS3e), it has improvements including more accurate modelling of sulphur and charged groups. The 2D structure of MAS9 was converted to 3D structure using Ligprep module in Maestro Schrödinger and then minimised using OPLS4 force field.

MAS9 was docked using GLIDE (Grid-based Ligand Docking with Energetic) module in Maestro Schrödinger (Release 2020-4) using standard precision (SP) mode by enabling flexible ligand sampling for the docking procedure. SP includes terms for hydrophobic interactions, hydrogen bonds of charged and neutral types, metal interactions, a rotational bond penalty (for conformational entropy), coulombic and van der Waals terms, and considers water molecule presence. The grid was generated by centralising it between selected residues: Arg107, Arg118, Arg152, Arg157 (common binding sites on CLEC-2 structure for podoplanin and rhodocytin, known from the crystal structures 3WSR and 3WWK) with a side length of 5 Å. The best confirmations for MAS9 were ranked based on their GLIDE docking scores that represent binding energies.

2.2.11. Protein biochemistry

2.2.11.1. SDS-PAGE

Protein separation was performed by SDS-PAGE using 10% polyacrylamide gels and 1×Running buffer (25 mM Tris-HCl, 192 mM glycine, 0,1% SDS). Precision Plus Protein™ Dual Color Standards were run alongside the samples. Electrophoresis was run

at a constant voltage of 80V for the first 20 minutes and then at 120V until the dye front reaches the bottom of the gel. Separated proteins were electro-transferred onto a PVDF membrane or stained by Coomassie Brilliant Blue Dye.

2.2.11.2. Coomassie Brilliant Blue staining

Coomassie staining was performed by incubation of the polyacrylamide gel with a Staining solution (0.1% Coomassie Brilliant Blue R-250, 50% methanol and 10% glacial acetic acid) for 1 hour with constant shaking. Afterwards, the gel was destained using Destaining solution (40% methanol and 10% glacial acetic acid), replacing the solution several times until the background of the gel was clear.

2.2.11.3. Western blot

The Western Blot was performed using a Trans-Blot$^®$ Turbo$^{™}$ Blotting System (Bio-Rad), transferring proteins from a polyacrylamide gel into polyvinylidene difluoride (PVDF) membrane by traditional semi-dry method at 25V for 40 min. Membranes were then blocked with 5% (w/v) bovine serum albumin (BSA) and 0.1% (w/v) sodium azide in Tris-buffered Saline (200 mM Tris base, 1.37 M NaCl, pH 7.6) containing 0.1% (v/v) Tween-20 (TBS-T) for 1 hour. The blocked membrane was then incubated with primary antibodies in 5% (w/v) BSA TBS-T for 1 hour at room temperature or overnight at 4°C. Afterwards, the membrane was washed 3 times for 5 minutes with TBS-T, incubated with fluorescent-labelled secondary antibodies for 1 hour at room temperature in the dark and again washed 3 times for 5 minutes with TBS-T. The proteins were visualised using a Typhoon FLA 9500.

2.2.12. Data analysis

The flow cytometry analysis was performed using BD Accuri C6 plus (population gates, median estimation). The fluorescent recovery after photobleaching time was estimated using NIS-Elements package. The microscope pictures were analysed using Fiji (Image J based) software. The calculations were performed using Microsoft Excel or GraphPad Prism 7.04. Most experiments were performed in at least three repetitions.

Statistical analysis was performed using GraphPad Prism 7.04 by using one-way ANOVA with a multiple comparison between each column with a control column, corrected with Dunnett or Sidak post-test. The level of significance of p values is as follows, ns $p \geq 0.05$ – not significant; *p between 0.01 and 0.05 – significant; ** p between 0.001 and 0.01 - very significant; *** p between 0.0001 to 0.001 – extremely significant; and **** $p < 0.0001$ – extremely significant.

Chapter 3

Artificial lipid bilayer to study platelet receptor clustering

3.1. Introduction

Receptors may be distributed at the cell surface in different ways, as multiple versions of the same receptor or as groups of different receptors. Receptor clustering plays an important role in a signal transduction. It possibly triggers a cell response by the recruitment of other receptors and signalling molecules, following the initiation of signalling cascades, signal transduction and termination. When receptors are packed together, signal-enhancing phenomena can occur, such as ligand receptor switching, or improved ligand-receptor and receptor-effector encounter probabilities (Caré and Soula, 2013). However, the effect of clustering on receptor-ligand binding dynamics and afterwards cell response is poorly understood.

There are many different methods to study receptor clustering. One of them, which has been widely used with B-cells and T-cells, is incorporating an appropriate receptor or ligand into a SLB. This method provides an access to study the molecular dynamic of cluster formation. More importantly, it is compatible with TIRF microscopy which selectively illuminate the fluorophores close to the coverslip, showing the events occurring in a plasma membrane.

There are many examples of studies using SLB platforms combined with TIRF microscopy to investigate receptor clustering. Su et al. reconstituted biochemical reactions of T-cell receptor intracellular signalling on SLBs. Using TIRF microscopy they visualized clustering of LAT and its binding partners. Additionally, they reconstituted the signalling pathway from CD3ζ/TCR phosphorylation to actin polymerization using signalling components mobilised on the SLB or in solution (Su *et al.*, 2016). Lin et al. developed a SLB platform to study the formation and maturation of phagocytic Fcγ-receptor signalling complexes in macrophages. They demonstrated using TIRF microscopy that incorporation of IgG into SLB can activates Fcγ-receptor

on macrophages and forms microclusters at the surface. Additionally, Syk-mCitrine-expressing murine bone marrow derived macrophages dropped onto IgG-coated SLB recruited Syk to Fcγ-IgG microclusters (Lin *et al.*, 2016). Ketchum et al. used a TIRF microscopy to study B-cell receptor clustering of B cells using a mobile ligand incorporated into SLBs. They showed that ligand mobility modulates B-cell spreading dynamics, formation of the receptor clusters, actin organization and signalling activation (Ketchum *et al.*, 2014).

There is no evidence of self-dimerization of CLEC-2 based on the crystal structure (Nagae *et al.*, 2014a). Hughes et al. demonstrated that Syk activation by CLEC-2 is mediated by the cross-linking two CLEC-2 receptors through binding of its tandem SH2 domains to the conserved YxxL motif in each receptor. Additionally, they showed using electron microscopy that CLEC-2 is present as a dimer in resting platelets and converts to larger complexes upon activation (Hughes *et al.*, 2010).

The interaction between CLEC-2 and its endogenous ligand podoplanin, may play a crucial role in a receptor clustering. Pollitt et al. proposed a model of CLEC-2-mediated clustering of podoplanin (Figure 3.1). The proposed model assumes that interaction of CLEC-2 with podoplanin enhances platelet adhesion to lymphatic endothelial cells (LECs) through CLEC-2-mediated clustering involving Syk. This mechanism may possibly lead to clustering of podoplanin on LECs.

Pollitt et al. investigated CLEC-2-podoplanin clustering using mouse CLEC-2 and mouse podoplanin. TIRF microscopy showed that on contact with SLBs, platelets formed microclusters, which migrated to the centre of the platelet, forming a single bright cluster. Clustering of mouse podoplanin is likely a consequence of the interaction with mouse CLEC-2 in platelets with the podoplanin ligand tethered to the SLB. Additionally, a Förster resonance energy transfer (FRET) between mobile podoplanin

on bilayer showed that podoplanin molecules are within 10 nm distance one from another and form a tight cluster, which is not seen in the presence of Src or Syk inhibitors. These data suggest a role of CLEC-2 signalling in co-clustering of CLEC-2 and podoplanin. However, it has not been confirmed that the same is seen with human platelets.

Platelet clustering may be important in a CLEC-2-mediated signal transduction; however, this process is poorly understood. The studies of platelet clustering may help to answer the questions of why the clustering is important in platelets, how multivalent interactions drive and regulate this process, what is the minimum unit to induce CLEC-2-podoplanin clustering and what determines the biochemical properties of platelet signalling. Additionally, it may help to understand the role of novel antiplatelet drugs showing how the molecules downstream CLEC-2 signalling pathway behave, what molecules are important in the formed cluster and does the process of platelet clustering is reversible and how the declustering of the already formed cluster may influence a signalling cascade.
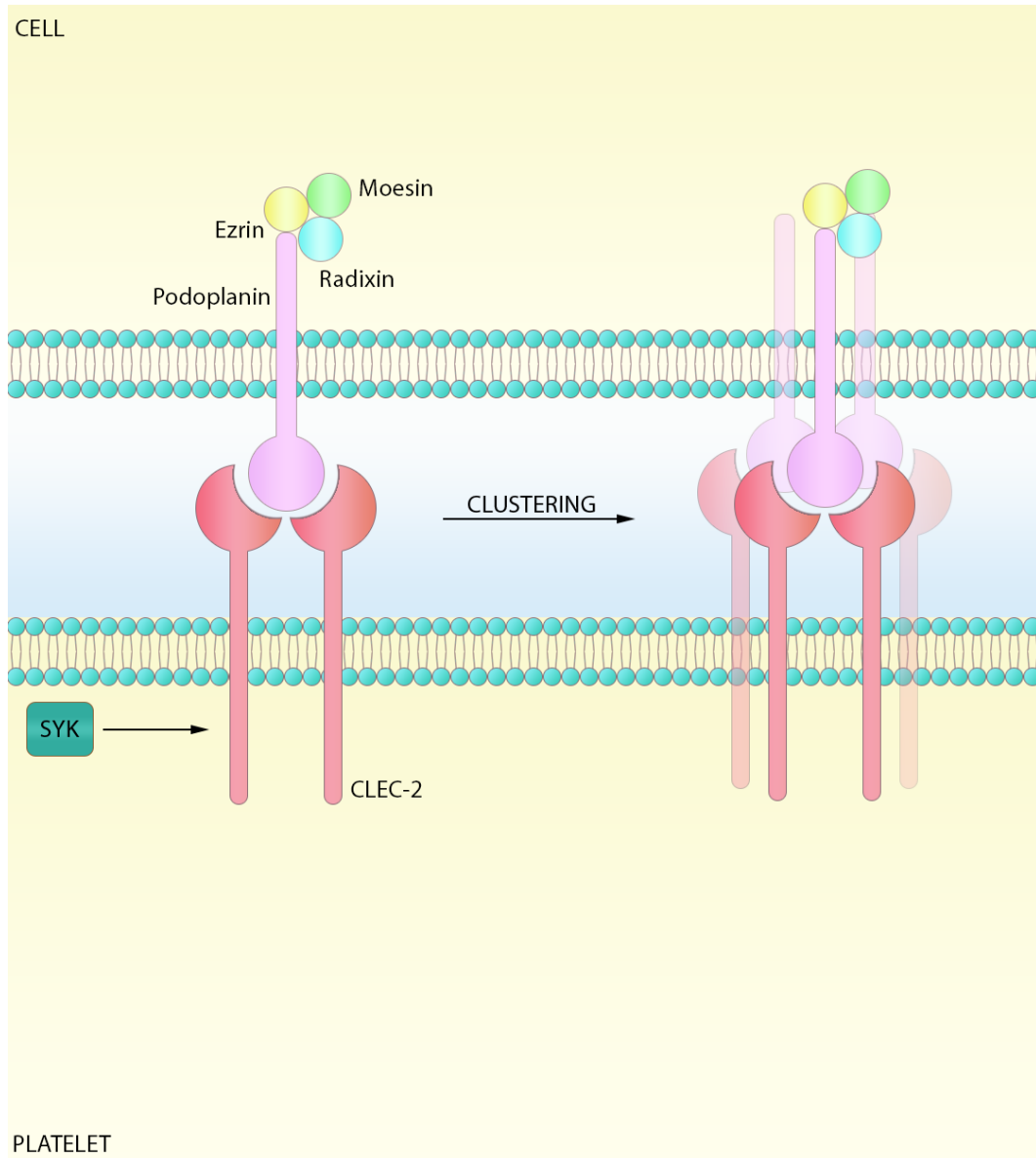
Figure 3.1. Model of CLEC-2-mediated clustering of podoplanin.

Model suggests that the binding of CLEC-2 to podoplanin enhances platelet adhesion to lymphatic endothelial cells through CLEC-2-mediated clustering involving Syk. This mechanism may possibly lead to clustering of podoplanin on LECs.

3.1.1. Lipid membranes and lipid rafts

The lipid membrane is a structure that separates the cell contents from the external environment. In 1972, Seymour Singer and Garth Nicolson proposed a model of the cell membrane structure, called the fluidic mosaic model, which has been described as "protein icebergs floating in a sea of lipids" (Singer and Nicolson, 1972). Based on a series of further studies, it has been shown that lipids and proteins are not uniformly distributed in the membrane but are organized into characteristic domains. These discoveries contributed to the concept of the membrane rafts (van Meer *et al.*, 1987; Graeve *et al.*, 1988).

The bilayer is composed of three different types of lipids: phospholipids, glycolipids, and cholesterol (Feizi, 1985). Phospholipids, including phosphatidylcholine (PC), phosphatidylethanolamine (PE), phosphatidylinositol (PI), phosphatidylserine (PS) and cardiolipin are the main groups of lipids within the bilayer. These molecules have a phosphate-containing hydrophilic head and two, saturated or unsaturated, hydrocarbon tails, connected to a glycerol via ester bonds. The length of the tails has the effect on cell membrane fluidity (van Meer *et al.*, 2008). Another class of lipids, glycosphingolipids, differs from phospholipids in that they have a carbohydrate in their head. They are predominantly distributed in the outer leaflet of the membrane with the carbohydrate exposed to the extracellular space (Patel and Balaji, 2011). Cholesterol, the third group of lipids within the bilayer, has a different structure from phospholipids and glycolipids. It contains a planar steroid ring and a non-polar hydrocarbon tail. Cholesterol plays a role in a membrane stability and fluidity. Increased the number of cholesterol molecules within the bilayer decreases fluidity and permeability of the membrane. Interaction of cholesterol with the other lipids is essential for lipid raft formation in the cell membrane (Crocke, 1998).

Lipid rafts are defined as small, heterogenous and highly dynamic membrane domains, rich in cholesterol and sphingolipids (Pike, 2006). These domains contain a variety of proteins, such as glycosylphosphatidylinositol (GPI) anchor proteins, caveolins, flotillins, signalling proteins, GPCR proteins, myristylated and palmitoylated proteins (Simons and Toomre, 2000). The presence of lipid rafts influences the dynamics and polarization of the cell membrane, for example, in the process of cell migration and adhesion. Additionally, lipid rafts are involved in other processes, such as actin polymerization, phagocytosis, membrane fusion, intracellular transport, and signal transduction (Hancock, 2006; Lingwood and Simons, 2010).

3.1.2. Supported lipid bilayers

The importance of lipid membranes initiated the development of a membrane model – supported lipid bilayers (SLBs), also known as artificial lipid bilayers. It was firstly described by Tamm and McConnel in early 1980s and since then, SLBs have been widely used as a model to study the cell membrane and membrane associated proteins. The main application of supported lipid bilayer is to mimic the eukaryotic cell membrane, including its cellular lipid composition and components. It has been used in many studies of the dynamics, multivalent ligand-receptor interactions, membrane structure and electrochemical properties of membranes (Reimhult *et al.*, 2010).

The first step of supported lipid bilayer formation is the preparation of the liposomes. Liposomes are defined as small artificial phospholipid vesicles of spherical shape composed of one or more lipid bilayers enclosing an aqueous space. There are several methods to prepare liposomes. The one used in this thesis is based on the preparation of a lipid film in a glass tube by drying the lipids under a slow stream of nitrogen to remove the organic solvent. This is followed by rehydration in a non-ionic detergent, sonication, and dialysis against desired buffer. It is important to use during the liposome

preparation inert gas (nitrogen/argon) to prevent lipid oxidation, which can change the physical and chemical properties of the liposomes and interfere with lipid-protein interactions (Seltzer and Gregoriadis, 1988).

The next step is the formation of a glass supported lipid bilayer. Upon the contact of liposomes with a clean glass substrate, they initially absorb into the surface, then become deflated and start to rupture forming a continuous phospholipid bilayer covering the entire surface (Richter *et al*., 2006). This process is illustrated in Figure 3.2.
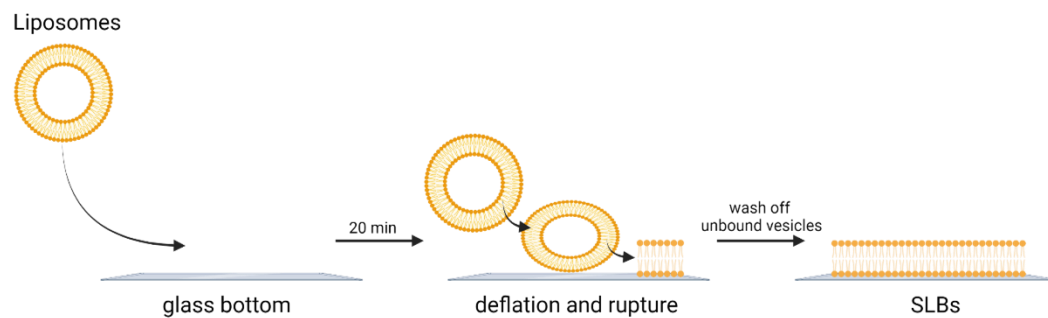
Figure 3.2. Strategy for supported lipid bilayer formation on the glass surface. Liposomes upon the contact with a clean glass substrate initially absorb into the surface, then become deflated and start to rupture forming a continuous phospholipid bilayer covering the entire surface.

The concept of SLB has been used to study the immunological synapse formed by B, T, and natural killer cells (Fooksman *et al.*, 2010), and recently, to study platelet receptors (Dustin and Pollitt, 2018). Examples of SLBs application to study immunological synapse and platelet receptors are described in detail in section 3.2.

Compared to ligands immobilised directly onto a glass surface, supported lipid bilayers have many advantages. It offers a distinct advantage in their lateral fluidity, providing the possibility for proteins to move within the bilayer (Yu *et al.*, 2011). Combined with advanced imaging methods, the mobility and distribution of receptors can be followed. It allows receptor clustering to be imaged on the cell membrane prior to signalling (Garcia-Parajo *et al.*, 2014). In many cases, especially for surface receptors, clusters are actively transported within the membrane (Mossman *et al.*, 2005; Hartman *et al.*, 2009), which demonstrates the importance of receptor lateral transport, which can be achieved using SLBs. This cannot be achieved when the receptor is immobilised on the glass surface.

Another advantage of SLB is the possibility of tethering multiple different proteins to the surface of the bilayer. There are several ways to bind proteins into SLBs to make them laterally mobile. The first strategy is using Ni^{2+}-chelating phospholipids to which proteins with a histidine tag can be attached to the SLB. The histidine tag can be different lengths (6-10 histidine residues), be placed on the C- or N-terminus of the protein, and the binding to the liposomes is noncovalent. Another strategy is using biotinylated lipids, which enables biotinylated proteins to be tethered to the SLBs using an avidin/streptavidin bridge. Recombinant proteins can be biotinylated randomly using N-Hydroxysulfosuccinimide (NHS) esters or the biotin targeting to specific regions using a BirA or Avi-tag sequence. In both strategies, the proteins can be expressed in bacteria, insect cells or mammalian cells. The last strategy is using proteins with one or two GPI anchors. These proteins must be expressed in mammalian cells in order to have the GPI anchor added (Dustin *et al.*, 2007). The composition of the lipids can be estimated depending on the experiment. The most established lipids to prepare SLB are shown in figure 3.3.

In addition, SLBs offer several experimental advantages. The 2D geometry of the bilayer on a glass substrate allows the quantitative analysis of receptor oligomerization and diffusion using fluorescent recovery after photobleaching (FRAP), fluorescence correlation spectroscopy (FCS) and the fluorescent imaging of tagged proteins or lipids (Tamm and McConnell, 1985).

Artificial lipid bilayers provide an opportunity to study cell receptors, including the platelet receptor CLEC-2 and its ligand, podoplanin. The development of a reconstituted artificial lipid membrane platform can be used as an experimental approach to test and validate signal manipulation of intracellular and extracellular macromolecular assembly and regulation. The reconstitution of signalling pathways from purified components may allow the mechanism and functional consequences of platelet receptors microclusters to be investigated. That can be achieved using microscopy techniques, such as Total Internal Reflection Fluorescence (TIRF) microscopy and Stochastic Optical Reconstruction Microscopy (STORM) imaging.
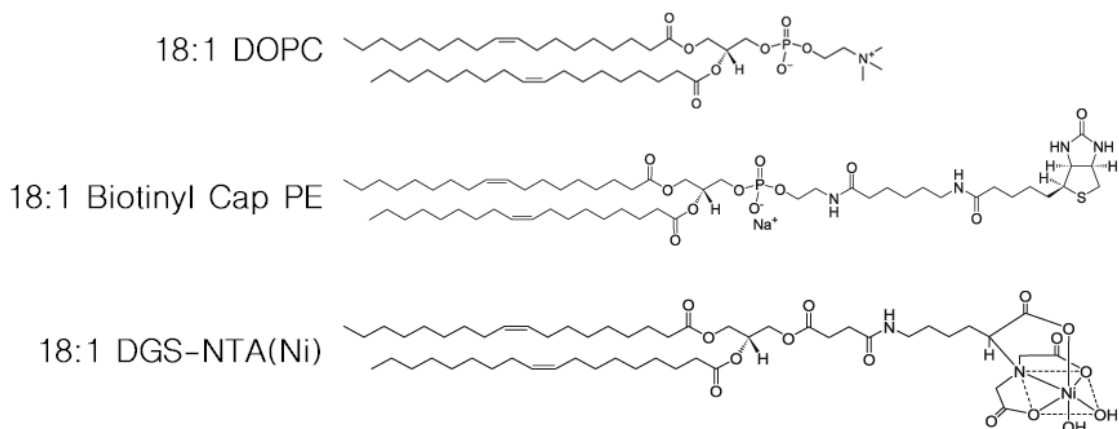
Figure 3.3. The most common lipids used in SLB preparation.

3.1.3. Fluorescence recovery after photobleaching (FRAP)

Fluorescent recovery after photobleaching (FRAP) is a microscopy-based method, firstly described in the 1970s as a technique to measure cellular membrane diffusion (Liebman and Entine, 1974; Poo and Cone, 1974). It was used to study protein mobility in the living cells by measuring fluorescent recovery after bleaching in a region of interest (Axelrod *et al.*, 1976). Nowadays, FRAP is widely used for studying diffusion, transport, interactions of biological molecules and molecular dynamics within living cells or cell models, such as SLBs.

FRAP allows the lateral mobility of fluorescent molecules to be determined and to check the diffusion of molecules and movement or recycling of cell components. To perform FRAP the protein must be tagged with a fluorophore. The method is based on the irreversible bleaching of fluorescent molecules localised to a region of interest (ROI) and the measurement of the fluorescent recovery time compared to a non-bleached reference ROI.

The first step of a FRAP experiment is the definition of the ROIs: stimulation, background, and reference; and the four phases: pre-bleach, bleach, post-bleach, and recovery (Ishikawa-Ankerhold *et al.*, 2014).

1. Pre-bleach is the initial step, when the fluorescent intensity is recorded in ROIs using low illumination conditions.

2. Bleach is the step, where ROI named 'stimulation' is bleached by a high intensity focused laser beam. This causes irreversible depletion of fluorescent molecules in that region.

3. Post-bleach is the monitoring of the bleached ROI.

4. Recovery is the final step when bleached (not-fluorescent) molecules exchange with unbleached (fluorescent) molecules, to recover the dark area over time to achieve full recovery.

The schematic principle of FRAP technique is shown in Figure 3.4.
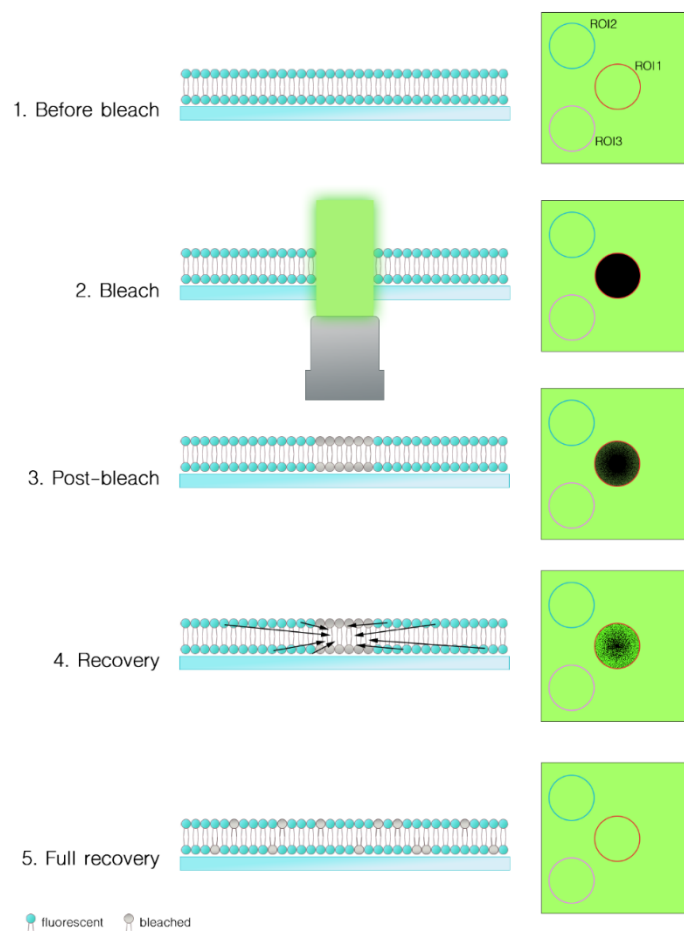
Figure 3.4. FRAP principle.

FRAP experiment includes a definition of the ROIs and the four phases: pre-bleach (1), bleach (2), post-bleach (3) and recovery (4-5). Before the bleach, the fluorescent proteins are uniformly distributed within a bilayer and the equilibrium is immediately lost after the bleach. The fluorescence intensity recovers due to the moving of the fluorescent proteins within the bilayer into the ROI.

The data analysis of a FRAP experiment is based on the fluorescent intensity is recorded over time in ROI1 (stimulation), ROI2 (reference) and ROI3 (background) and requires correction and normalisation. For the SLBs a ROI3 is not required since the fluorescence is uniformly distributed through the surface and there is no background. After this step, the normalised data (fluorescent intensity) versus time (s) can be plotted to obtain the FRAP curve and determine the mobile and immobile fractions. A schematic curve is shown in Figure 3.5.

FRAP enables lateral mobility of tethered proteins into SLBs to be determined.
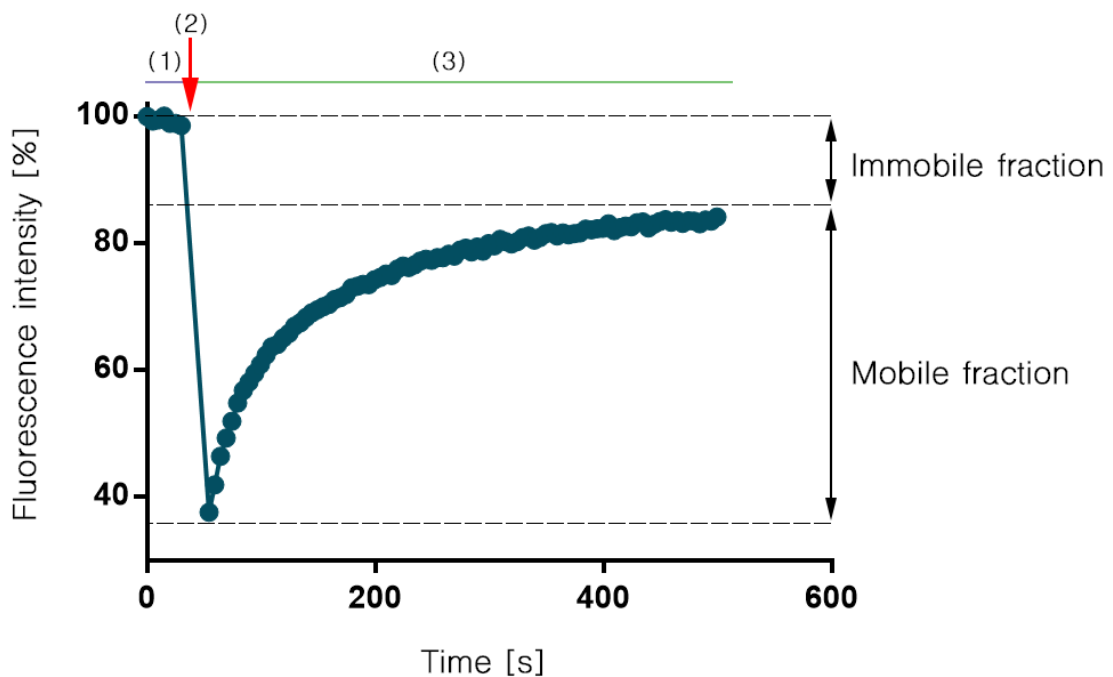
Figure 3.5. Example FRAP curve.

The fluorescence signal is recorded before bleaching of the ROI (1), just after bleaching (2) and during recovery (3). The information, including the mobile and immobile fractions, recovery rate and the half time of equilibrium ($t_{1/2}$) can be estimated using a curve.

3.1.4. Total internal reflection fluorescence (TIRF) microscopy

Total internal reflection fluorescence microscopy is a method where the fluorophores close to the coverslip (within ~ 100 nm) are selectively illuminated, showing events occurring in close proximity to the plasma membrane. This method allows high-contrast images of fluorophores near the plasma membrane to be obtained. (Mattheyses *et al.*, 2010) .

In TIRF microscopy, in contrast to fluorescent microscopy, a laser is directed into the surface at a critical angle. That forms an evanescent wave, which can illuminate the sample less than 100 nm from the solid surface. This technique is based on the index of refraction of two materials: a sample (N_2) and the coverslip (N_1). The light reaches an interface when N_2 has a lower index of refraction than N_1. For the glass coverslip N_1=1.518, while for the aqueous medium N_2=1.33. The critical angle (θ_C) can be determined by Snell's law:

$$\theta_c = sin^{-1}\frac{N_2}{N_1}$$

where N_2 – lower refraction index; and N_1 – higher refraction index (Ambrose, 1956; Axelrod, 1981).

The principle of TIRF is shown in a Figure 3.6.
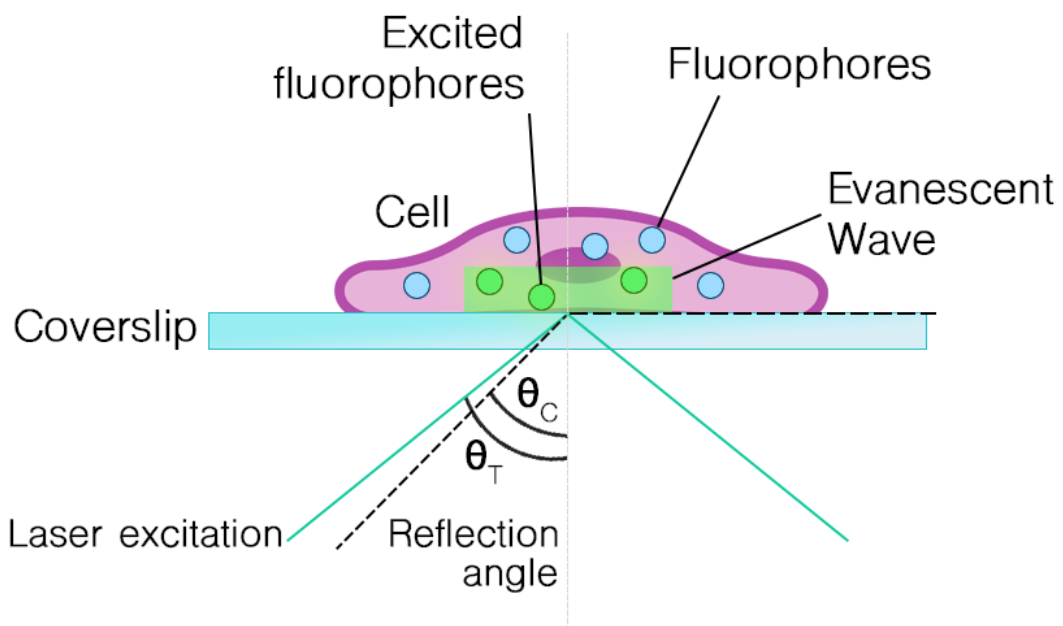
Figure 3.6. The principle of TIRF microscopy.

In TIRFM laser is directed into the surface at a critical angle. As the light is reflected away, an evanescent field is formed which refracts into the sample, illuminating within 100 nm of the coverslip. The critical angle (θ_C) is described by Snell's law. θ_C = angle of the incident beam in respect to the normal interface; θ_T = the refracted beam angle within the lower index medium.

3.2. Aims

The aim of this chapter is:

- To reconstitute CLEC-2 platelet signalling, using an intracellular domain of CLEC-2 and SLBs to investigate what determinates the biochemical properties of platelet signalling and how intracellular multivalent interactions of the molecules downstream CLEC-2, e.g., Syk, Lyn or actin, drive cluster formation (Figure 3.7A).

- To develop the SLB platform to study platelet CLEC-2-mediated signalling, focusing on the interaction between human CLEC-2 and human podoplanin (Figure 3.7B).
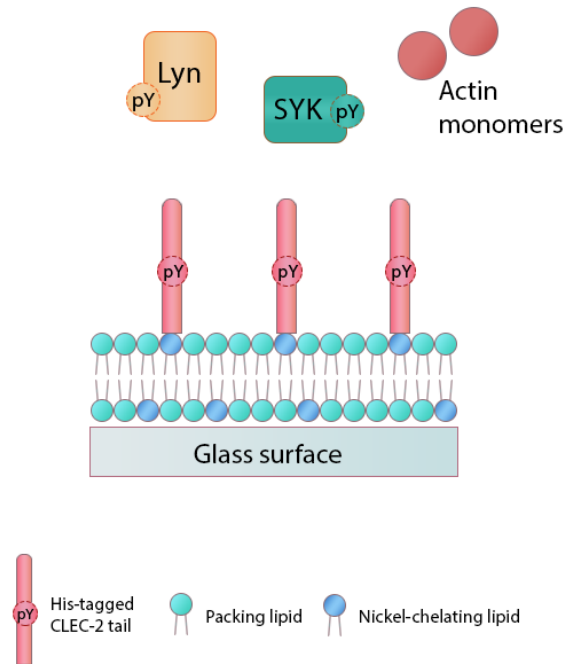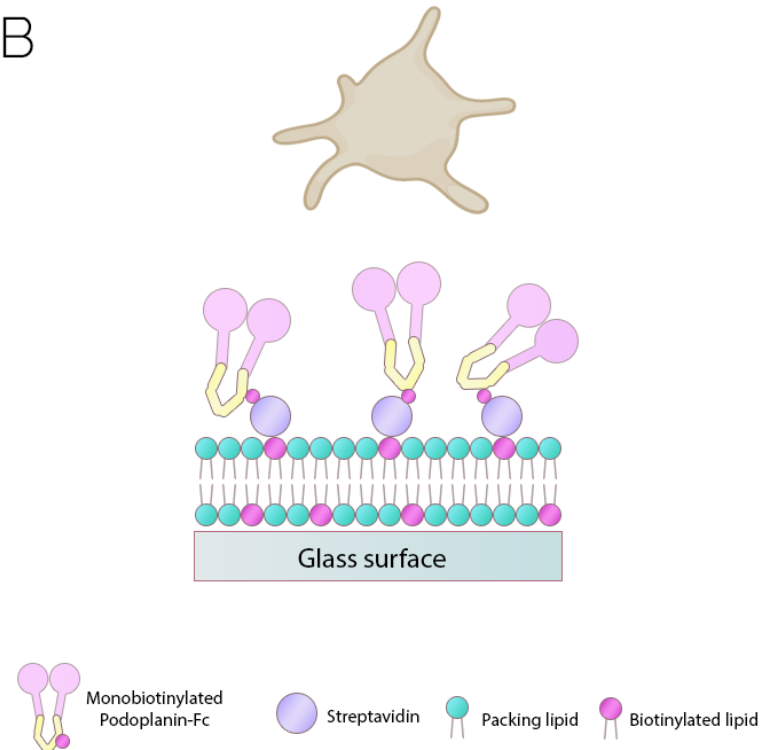
Figure 3.7. Schematic for supported lipid bilayer platform to study CLEC-2 clustering.

A) Intracellular domain of CLEC-2 incorporated via a His-tag into SLB containing nickel-chelating lipids formed on a glass surface and interacting with signalling molecules Lyn, Syk or actin. B) Monobiotinylated Podoplanin-Fc incorporated into SLB containing biotinylated lipids via a streptavidin bridge, which forms clusters by the interaction with human platelets.

3.3. Results

3.3.1. Development of an artificial lipid membrane platform to investigate intracellular protein assembly and clustering

3.3.1.1. Molecular cloning of the intracellular tail of CLEC-2

Traditional restriction cloning is one method to prepare DNA constructs with a gene of interest. The procedure involves preparing both DNA fragments to be cloned – insert (amplified frequently by PCR) and a self-replicating DNA vector by cutting with two unique restriction enzymes that flank the target DNA sequence and are also present in the multiple cloning sites of the vector. By using two different restriction endonucleases, two non-compatible ends are generated which allow the insert to be cloned to the vector using a DNA ligase, prior to bacterial transformation.

The insert of the intracellular domain of human CLEC-2 (aa 1-33) was cloned in frame into pSF-OXB20-NH2-TEV-His10 containing a 10×His-tag downstream of the multiple cloning sites using HindIII and KpnI. The amplified insert of the intracellular domain is presented in Figure 3.8. The band size of the PCR product, as expected, was 128 bp. The band corresponding to the size of the insert was excised and purified from the agarose gel. Digested and ligated insert and vector were transformed into DH5α cells and colonies were grown on LB-agar supplemented with kanamycin for minipreps. The sequence of a plasmid containing the correct insert was confirmed by Sanger sequencing.

Generated vector was used as a template to subclone the his-tagged domain into pSNAP-tag® (T7)-2. This vector encodes a self-labelling SNAP-tag protein, which can be covalently tagged with a suitable ligand, such as a fluorescent dye, and an IPTG inducible T7 promotor, which allows expression of the protein in a bacteria strain

containing a T7 polymerase. The SNAP-tag was fused in frame to the N-terminus of hCLEC-2 intracellular domain (using PmeI and NotI restriction sites). The strategy of cloning was the same as for previous plasmid, except the antibiotic used, which was ampicillin. The sequence of the plasmid containing the correct insert was confirmed by Sanger sequencing. The maps of generated plasmids are presented in Appendix 1.
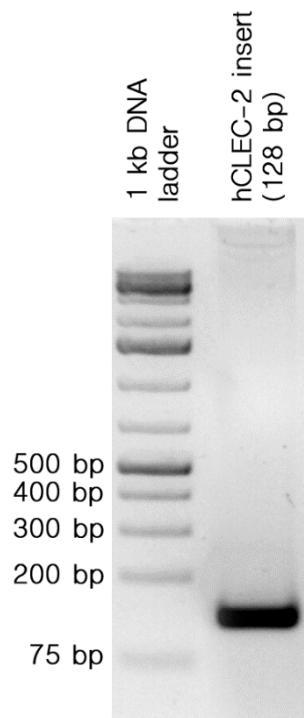
Figure 3.8. Polymerase chain reaction gel of hCLEC-2 tail (128 bp). cDNA encoding the intracellular domain of hCLEC-2 was extracted from their original vector and new restriction sites were introduced by PCR. Following PCR, the DNA fragment was separated on a 2% agarose gel alongside a 1kb plus DNA ladder. The predicted product size was observed, confirming the success of the PCR.

3.3.1.2. Expression and purification of the intracellular domain of CLEC-2

To overexpress the intracellular domain of hCLEC-2 (aa 1-33) in fusion with a C-terminal 10x histidine tag and N-terminal SNAP tag, the plasmid pMAS-SNAP-T7-hCLEC-2-H10 was transformed into T7 Express Competent *Escherichia coli* cells, containing T7 RNA Polymerase in the *lac* operon. This allows the bacteria to produce protein using the plasmid under the control of an IPTG inducible T7 promotor. The bacterial samples before and after induction with IPTG were run on SDS-PAGE and analysed by Coomassie staining. In Figure 3.9, a strong band at around 30 kDa can be seen in the bacterial lysate after induction (lane 2, +IPTG). This is the expected protein size known from amino acid sequence (~30 kDa), whereas we cannot see any over-expression in the sample before induction (lane 1, -IPTG).
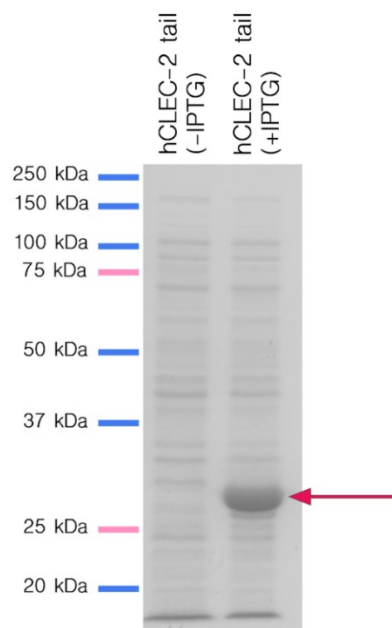
Figure 3.9. Overexpression of the hCLEC-2 intracellular domain in *E. coli*. Coomassie staining of 10% polyacrylamide gel – bacteria lysates before (lane 1) and after (lane 2) induction with IPTG. The red arrow points to the overexpressed hCLEC-2 intracellular domain.

His-tagged protein purification was performed using in-column refolding approach, which permitted the purification of the protein from inclusion bodies by, firstly, denaturing the protein to an unfolded form with a high concentration of guanidinium chloride, and secondly, refolding the protein using a urea gradient with decreasing urea concentrations. hCLEC-2-H10-SNAP was eluted from the Ni-NTA column with a buffer containing 500 mM imidazole, dialysed to remove imidazole from the buffer, and the protein concentration was measured using Bradford assay. The samples of washing and eluting steps were resolved by SDS-PAGE and stained with Coomassie dye (Figure 3.10A). Lanes 1-4 represent unbound proteins washed out from the Ni-NTA resin in the urea gradient. The elution fractions (lane 5-7) represent purified hCLEC-2 tail (dashed line rectangle). There is an additional band around 70 kDa, which represents another protein. To separate these two proteins, an additional purification step is required. The elution fraction was also analysed using western blot. As expected, using anti-His tag and anti-SNAP tag antibody, the band of purified hCLEC-2 tail was observed around 30 kDa (Figure 3.10B), whereas the 70 kDa band was not detected (not shown).

The protein was labelled with SNAP-Surface® Alexa Fluor® 488 which is a photostable green fluorescent substrate used to label SNAP-tag® fusion proteins. Labelled protein was run on an SDS-PAGE gel and the protein was detected using a fluorescent gel scanner (Figure 3.10C). The protein band migrated at the same position as the recombinant protein detected by western blot, around 30 kDa.
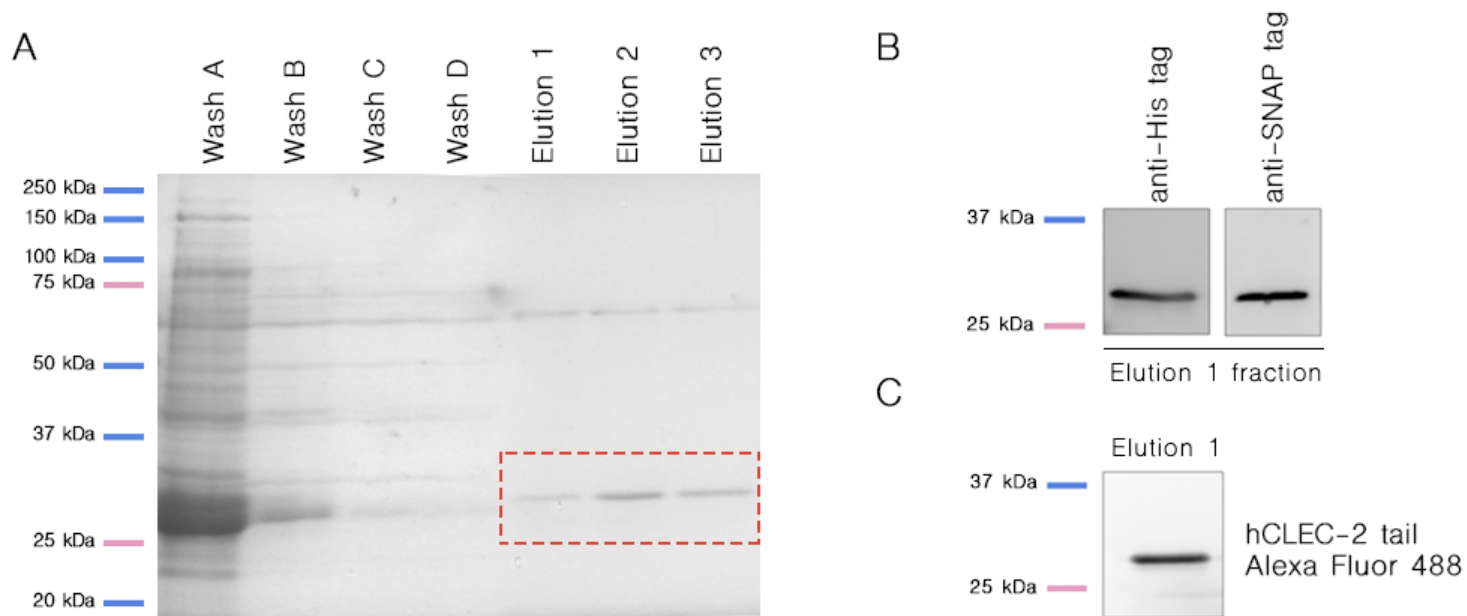
Figure 3.10. Purification of hCLEC-2 intracellular domain from inclusion bodies.

A. Coomassie staining of SDS-PAGE gel – bacteria lysates from wash and elution steps of the protein purification. Dashed line rectangle shows the size range of CLEC-2 tail. B. Western blot analysis of Elution 1 fraction using anti-His tag antibody (lane 1) or anti-SNAP tag antibody (lane 2). C. SDS-PAGE analysis of the recombinant hCLEC-2 intracellular domain (Elution 1 fraction) labelled with SNAP-Surface® Alexa Fluor® 488 via the SNAP tag resolved using denaturing conditions. The gel was imaged using a Typhoon FLA 9500 with a LD488 laser.

3.3.1.3. hCLEC-2 intracellular domain binds into SLB-coated silica beads

To confirm that the recombinant hCLEC-2 intracellular domain molecules incorporate into the upper leaflet of the supported lipid bilayer, flow cytometry was performed. Supported lipid bilayers were formed on silica beads using DOPC:DGS-NTA liposomes in ratio 75:25. The selected ratio of lipids is based on previously reported literature (Dustin *et al.*, 2007, Dustin and Pollitt, 2018). The SLB-coated beads were incubated with recombinant hCLEC-2. To monitor the binding of the protein to the SLB-coated beads, anti-SNAP tag primary antibodies with Alexa Fluor™ 488 conjugated secondary antibodies were used. Figure 3.11A shows that the recombinant protein containing the hCLEC-2 intracellular tail can tether to the beads coated with the nickel chelating lipids (DOPC:Ni-NTA) and not to control beads coated only with the packing lipid (DOPC). In addition, the median fluorescence intensity in the FL1 channel is significantly higher for DOPC-Ni-NTA compared to the DOPC control (Figure 3.11B). The interaction of the hCLEC-2 tail to the SLBs was confirmed also by directly labelling the recombinant protein with SNAP-Surface® Alexa Fluor® 488. Figure 3.11C shows that the labelled hCLEC-2 intracellular tail can tether to the beads coated with the nickel chelating lipids (DOPC:Ni-NTA) and not to control beads coated only with the packing lipid (DOPC). The same shows comparison of the median fluorescence intensity in FL1 channel (Figure 3.11D).
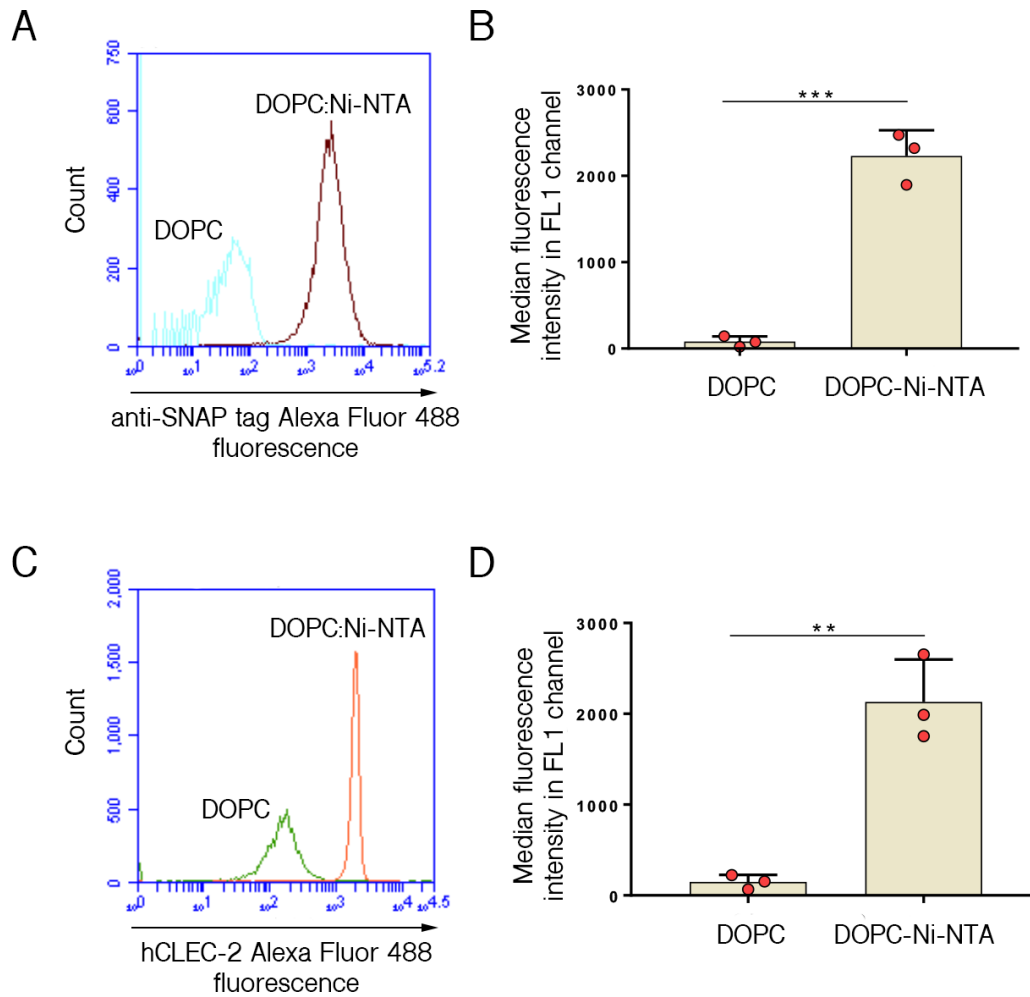
Figure 3.11. Flow cytometry analysis of binding hCLEC-2 intracellular domain into SLB-coated silica beads.

DOPC:Ni-NTA (ratio 75:25) or DOPC (100%) supported lipid bilayer formed on silica beads were incubated with the intracellular domain of hCLEC-2, primary anti-SNAP tag antibodies and secondary Alexa Fluor™ 488 conjugated antibodies (A,B) or with Alexa Fluor® 488 labelled hCLEC-2 intracellular domain (C,D) and analysed by flow cytometry. Count is referred to as the number of events identified in a selected fluorescence channel. Statistical significance was calculated using one-way ANOVA with Dunnett's post-test. Data are shown as mean ± SD and are representative of three experiments. **$p \leq .01$, ***$p \leq .001$.

3.3.1.4. Determination of intracellular Syk in human platelets

The knowledge of the protein copy number in platelets allows an appropriate protein concentration to be chosen to mimic a physiologically relevant concentration when used with the SLBs. One of the molecule downstream CLEC-2-mediated activation is Syk.

Syk copy number was determined by comparing antibody labelled human platelets to antibody labelled calibration beads with known antigen binding capacities. The median fluorescence intensity of platelets stained with saturating concentrations or anti-Syk (4D10) (Figure 3.12A) were compared to beads of known antigen binding capacity, labelled with the same antibodies, which were used to generate a calibration curve (Figure 3.12B). Using this, human platelets were determined to have 5192 ± 1055 of intracellular Syk.
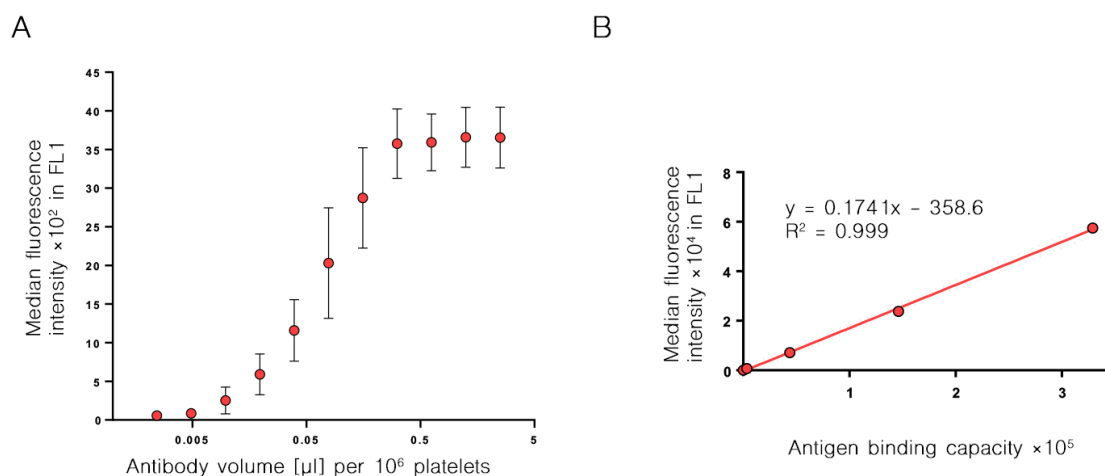
Figure 3.12. Determination of copy number of Syk in human platelets.

Saturating concentrations of anti-Syk antibody (A) were used to label human platelets. Using the median fluorescent intensity of the beads, a standard curve was generated (B) and the copy number of the protein was determined. Data are shown as mean $\pm$ SD and are representative of three experiments.

3.3.1.5. The human CLEC-2 intracellular domain is not mobile when tethered to a supported lipid bilayer

To study the mobility of supported lipid bilayers containing the human CLEC-2 intracellular tail, FRAP was used. This method has been described in a Chapter 3.1.3. Supported lipid bilayers were formed using liposomes consisting of nickel-chelating lipids (DGS-NTA) and DOPC in ratio 25:75 on a glass coverslip cleaned by piranha solution (a mixture of concentrated sulfuric acid and hydrogen peroxide). Fluorescently labelled human CLEC-2 intracellular domain at a concentration of 10 µg/ml was added into the chamber and its mobility was assessed by FRAP. The microscope images before (1), immediately after (2) and 9 minutes 10 seconds after photo-bleaching are presented in Figure 3.13A. The fluorescence intensity was measured every 5 seconds. Following bleaching, the fluorescent intensity of the ROI decreased from 100% to 20 % and during the recovery time showed no significant increase (Figure 3.13B). No fluorescence recovery was observed when compared to a non-bleached reference ROI. This indicates the immobile fraction is almost 100%. Without mobility, the model of human CLEC-2 intracellular domain tethered to a SLB was not taken forward for further characterisation.
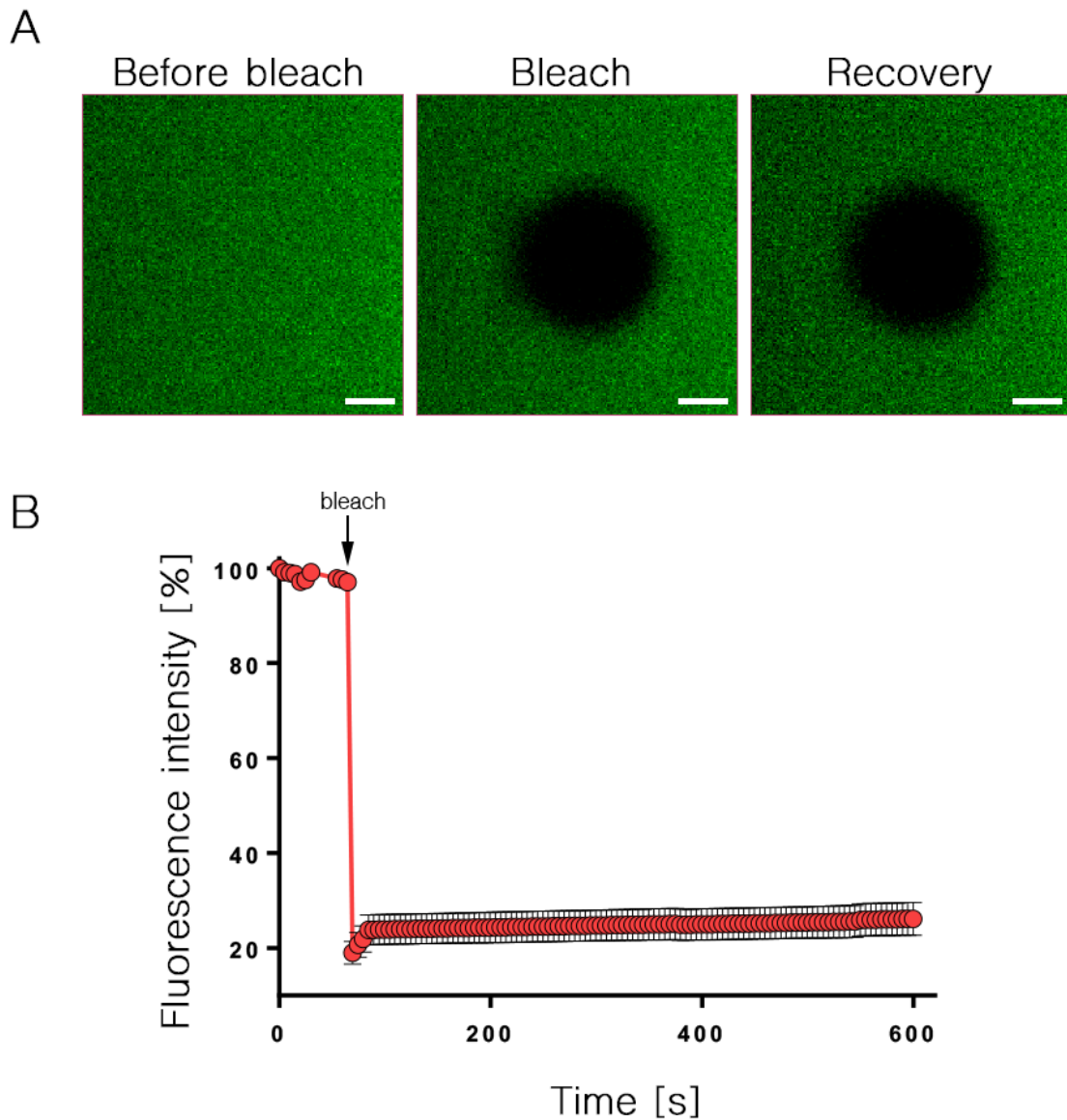
Figure 3.13. Lateral mobility within a supported lipid bilayer containing the hCLEC-2 intracellular domain.

Representative images of the bilayer before bleach (1), immediately post-bleach (2), and 9 minutes 10 seconds after bleach (3). Scale bar 10 μm. B. Fluorescent intensity kinetics over time; the fluorescence intensity was measured every 5 seconds. The graph presents mobile and immobile fraction of the protein in bilayer. Data are shown as mean ± SD and are representative of 3 independent experiments.

3.3.2. Development of an artificial lipid membrane platform to investigate platelet-cell interactions

3.3.2.1. Expression and purification of the extracellular domain of human podoplanin

To purify the extracellular domain of human podoplanin in fusion with rabbit Fc, the plasmid pFuse-hPdpn-rFc was transfected into HEK293T cells. This cell line is derived from the HEK293 cell line and expresses the SV40 large T antigen, which binds to SV40 enhancers of expression vectors increasing protein production. Additionally, mammalian cell lines can produce proteins with their post-translational modifications (e.g. glycosylation, phosphorylation) (Durocher and Butler, 2009). The transfection method (calcium phosphate transfection) used for protein production is based on the formation of a calcium phosphate-DNA precipitates that adheres to the cell surface, allowing the DNA to enter into the cell by endocytosis (Kingston *et al.*, 1999). Overexpressed human podoplanin-Fc will be secreted into the media. The IgG-Fc-fusion tag is widely used in recombinant protein expression and production as it allows the purification of proteins using protein A or protein G affinity chromatography. Due to the nature of the antibody IgG-Fc, Fc-tagged proteins are expressed as homodimer. hPodoplanin was expressed as an Fc-fusion to increase avidity of the ligand interacting with the platelet CLEC-2 in artificial lipid membrane platform. Fc-fusion provides two binding sites, compared to one binding site in a monomeric form.

The media containing the expressed protein were applied to a protein A column. The column was washed to remove unbound protein and protein bound to the column was eluted using a low pH elution buffer. Samples from each purification step as well as elution samples in reducing (which will show the monomeric form of the protein) and

non-reducing (which will show the oligomeric form of the protein, in this case dimeric) conditions were run on SDS-PAGE and analysed using Coomassie staining or western blot. Figure 3.14A shows each step of the protein purification process for hPodoplanin-Fc. Lane 'Flow through' represents the fraction collected after loading the protein extract from the column. The strong band around 50-70 kDa corresponds to the size of BSA, a major component of FBS. Non-reduced conditions of the SDS-PAGE represents the dimer of the protein in the 'Elution' fractions, whereas reduced conditions represent the monomeric form of the protein. The band around 50 kDa in non-reduced elution fractions may represent non-glycosylated version of human podoplanin. The presence of dimeric and monomeric forms of both proteins were confirmed using western blot analysis, showing the difference in protein size (Figure 3.14B), where the specific antibody against the podoplanin was used. Many bands on the blots may represent different forms of podoplanin: dimeric glycosylated, dimeric-non-glycosylated, monomeric-glycosylated, and monomeric-non-glycosylated. Another explanation would be that anti-podoplanin antibody is not specific. Because of numerous glycosylation sites in the sequences of hPodoplanin-Fc (Kato *et al.*, 2003; Kaneko *et al.*, 2007), the protein size presented on SDS-PAGE cannot be precisely predicted. The size of the protein from the amino acid sequence is 48.53 kDa.
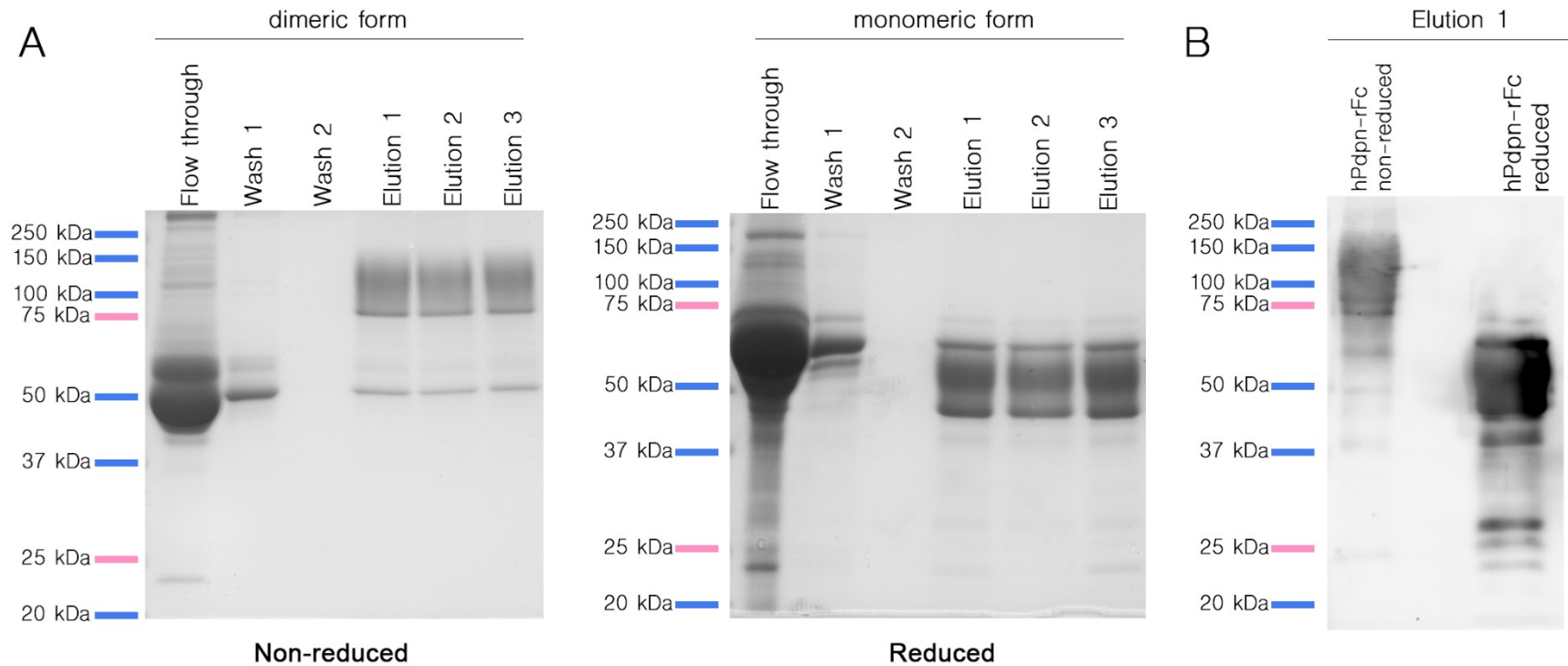
Figure 3.14. hPodoplanin-Fc purification.

Coomassie staining of SDS-PAGE gel – fractions of purification of hPodoplanin-Fc (A). The gels were run in non-reduced and reduced

conditions. The band around 50 kDa in non-reduced elution fractions may represents non-glycosylated version of human podoplanin.

Additionally, western blot analysis for hPodoplanin-Fc (B) under non-reduced (lane 1) and reduced (lane 2) conditions was performed.

3.3.2.2. Platelets spread on immobilized podoplanin

To determine if the purified hPodoplanin-Fc is functional and able to support platelet adhesion, a platelet spreading assay was performed. This approach is based on the immobilization of adhesive proteins to a glass surface followed by the imaging of platelet adhesion and spreading using microscopy (Aslan *et al.*, 2011). hPodoplanin-Fc treated glass coverslips were incubated with human washed platelets for 45 minutes at 37°C, fixed with paraformaldehyde, permeabilized with a low concentration of Triton-X100, stained with Phalloidin Alexa Fluor 488 and mounted onto microscope slides. Phalloidin is a peptide that is used for staining actin filaments (also known as F-actin). It binds to all variants of actin filaments in many different species of animals and plants, including human platelets. The negative controls were prepared at the same time – coverslips covered with BSA (to confirm that there is no unspecific binding between the platelet and the glass) or rabbit IgG (to confirm that the interaction was not mediated via the Fc domain of the recombinant protein). Prepared slides for each condition were visualised by epifluorescent microscopy and the number of platelets adhered and spread platelet area were determined.

Washed platelets adhere to and spread on immobilised hPodoplanin-Fc coated onto a glass coverslip (Figure 3.15A). The average number of platelets for hPodoplanin-Fc was 2.46 ± 0.4 platelets $\times 10^{-3}$ per μm^2, whereas for BSA and Rabbit IgG the numbers of platelets were lower than 0.1×10^3 per μm^2 (Figure 3.15B). Additionally, the average platelet area on immobilized hPodoplanin-Fc was 41 ± 6 μm^2, whereas for BSA and Rabbit IgG 9 ± 2 μm^2 and 13 ± 4 μm^2 respectively (Figure 3.15C).
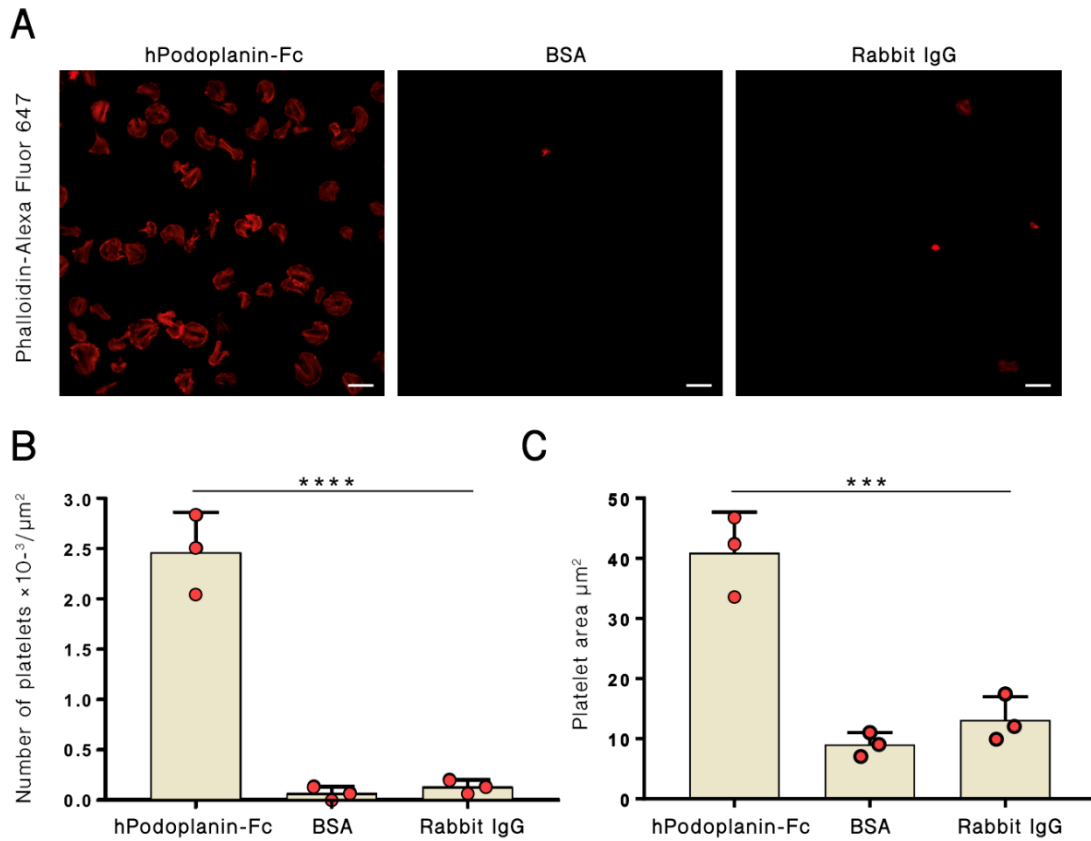
Figure 3.15. Platelets adhere to and spread on immobilised hPodoplanin-Fc.

Washed platelets (2×10^7/ml) were allowed to interact with immobilised podoplanin, BSA or rabbit IgG on a glass coverslip. A) Bound platelets were fixed, permeabilized, stained with Phalloidin Alexa Fluor 647, and imaged using epifluorescent microscopy. The representative fields of view are shown. Scale bar – 10 μm. B) The number of platelets per field of view and C) the average platelet area were determined. Statistical significance was calculated using a one-way ANOVA with Dunnett's post-test. Data are shown as mean ± SD and are representative of three independent experiments. ***$p \leq$ .001, ****$p \leq$ .0001.

3.3.2.3. Determination of how much human podoplanin is deposited on the artificial bilayer and HDLECs

3.3.2.3.1. Monobiotinylation of human Podoplanin-Fc

Biotinylation is a process of attaching biotin to proteins and other molecules. The advantage of this approach is that biotin binds to streptavidin and avidin with high affinity and these interactions are used for many laboratory methods. Protein may be site-specific biotinylated using a BriA substrate, if the target protein possesses a specific peptide tag (AviTag); or randomly biotinylated, using amine-reactive reagents (Gautier and Hinner, 2015). Using random biotinylation, the protein may be monobiotinylated, where one molecule of biotin is attached to one molecule of protein, or multi-biotinylated, where several molecules of biotin bind to one molecule of protein. To estimate the degree of protein biotinylation, flow cytometry can be used (Figure 3.16).

For effective monobiotinylation of hPodoplanin-Fc, the concentration of Sulfo-NHS-LC-Biotin had to be optimised. Concentrations from 50 µg/ml to 0.005 µg/ml of Sulfo-NHS-LC-Biotin were tested. The biotinylated protein with different degrees of biotin labelling was immobilized as a ligand on to streptavidin-coated beads and incubated with Streptavidin-Alexa Fluor 488 conjugated (to label free biotin) for the signal in FL1 channel and anti-podoplanin rabbit antibodies with Alexa Fluor 647 donkey anti-rabbit IgG (to label the recombinant protein) for the signal in the FL4 channel. Flow cytometry analysis showed that in the FL1 channel there is no fluorescent signal at concentrations 0.005 µg/ml, 0.05 µg/ml, and 0.5 µg/ml, whereas it appears for concentrations 5 µg/ml and 50 µg/ml (Figure 3.17). For FL4 channel, the fluorescent signal is observed in a range 0.05-50 µg/ml, whereas for 0.005 µg/ml is not. The

majority of monobiotinylated hPodoplanin-Fc occurs when 0.05-0.5 µg/ml of biotin is used.
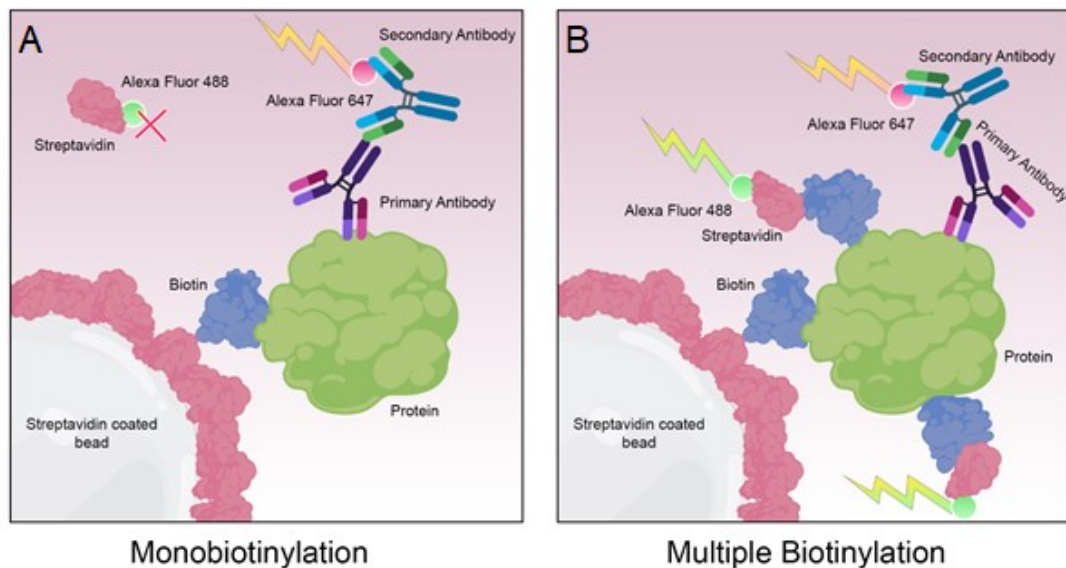
Figure 3.16. Protein mono- and multiple biotinylation.

A. Protein is monobiotinylated. Biotin-binding site is occupied by streptavidin occurring on a bead surface. There are no more available biotin-binding sites on the surface of the protein, so Alexa Fluor 488 Streptavidin cannot bind and the signal in the FL1 channel is undetectable. At the same time, the protein specific primary antibody binds to the protein, Alexa Fluor 647 labelled secondary antibody binds to primary antibody and emits fluorescence in channel FL4. B. Protein is multi-biotinylated and has several biotin-binding sites. One of them binds to the streptavidin-coated bead. To another site, Alexa Fluor 488 Streptavidin binds and emits fluorescence in the FL1 channel. Additionally, the protein specific primary antibody binds to the protein, Alexa Fluor 647 labelled secondary antibody binds to the primary antibody and emits the fluorescence in channel FL4.
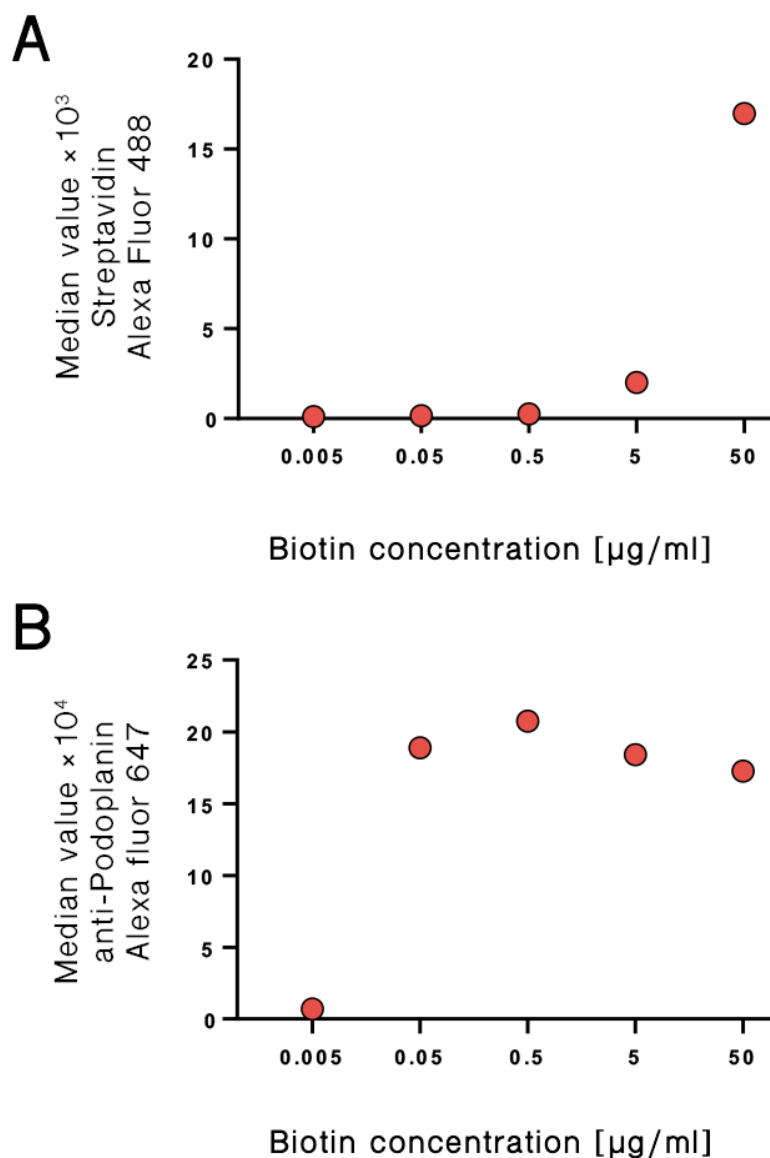
Figure 3.17. Optimisation of the monobiotinylation of human Podoplanin-Fc.

Flow cytometry analysis of different concentrations of Sulfo-NHS-LC-Biotin used to monobiotinylate hPodoplanin-Fc. Labelled protein was immobilized on to streptavidin beads and incubated with streptavidin conjugated with Alexa Fluor 488 and anti-podoplanin primary antibodies with Alexa Fluor 647 secondary antibodies. Curves represent the median values in FL1, identifying the presence of free biotin (A) and in FL4 channel, identifying the presence of recombinant hPodoplanin on the beads (B). The optimal concentration of biotin to monobiotinylation the protein is in range of 0.05-0.5 μg/ml of biotin. The results are representative of one experiment.

3.3.2.3.2. Flow cytometry analysis of human Podoplanin-Fc incorporated into different ratios of the lipids within SLB

hPodoplanin-Fc was successfully labelled using an Alexa Fluor 488 Protein Labelling Kit. The concentration of labelled protein was estimated by measuring the absorbance of the conjugate solution at 280 nm and 494 nm. The molar extinction coefficient of hPodoplanin-Fc was calculated from the amino acid sequence of the protein and was 36160 $cm^{-1}M^{-1}$. Knowing this factor, the concentration was estimated as 13.02 μM (0.83 mg/ml) and the degree of labelling as 1.43 moles of dye per mole protein.

To estimate the density of recombinant hPodoplanin-Fc molecules incorporated into the upper leaflet of the bilayer, flow cytometry was used. Different ratios of DOPC:CAP-Biotin-PE liposomes were used to form the SLBs on 4.98 μm diameter silica beads. Using a streptavidin bridge, a labelled hPodoplanin-Fc was attached to bilayer. The ligand copy number was determined by comparing the hPodoplanin-coated beads to calibration beads with known numbers of molecules of equivalent soluble fluorochrome. The median values of Alexa Fluor 488 fluorescence of hPodoplanin (Figure 3.18A) were compared to calibration beads (Figure 3.18B), using a generated calibration curve (Figure 3.18C). Using these, SLBs with the ratio of 98:2 DOPC:CAP-Biotin-PE lipids have 1,084 ± 54 of hPodoplanin molecules/μm^2; 99:1 have 537 ± 105 molecules/μm^2, and 99.5:0.5 have 140 ± 34 molecules/μm^2 (Figure 3.18D). These numbers were estimated including estimated before the degree of labelling (1.43 moles of dye per mole protein). The ratio of lipids within the bilayer were selected based on previously reported literature (Pollitt *et al.*, 2014).
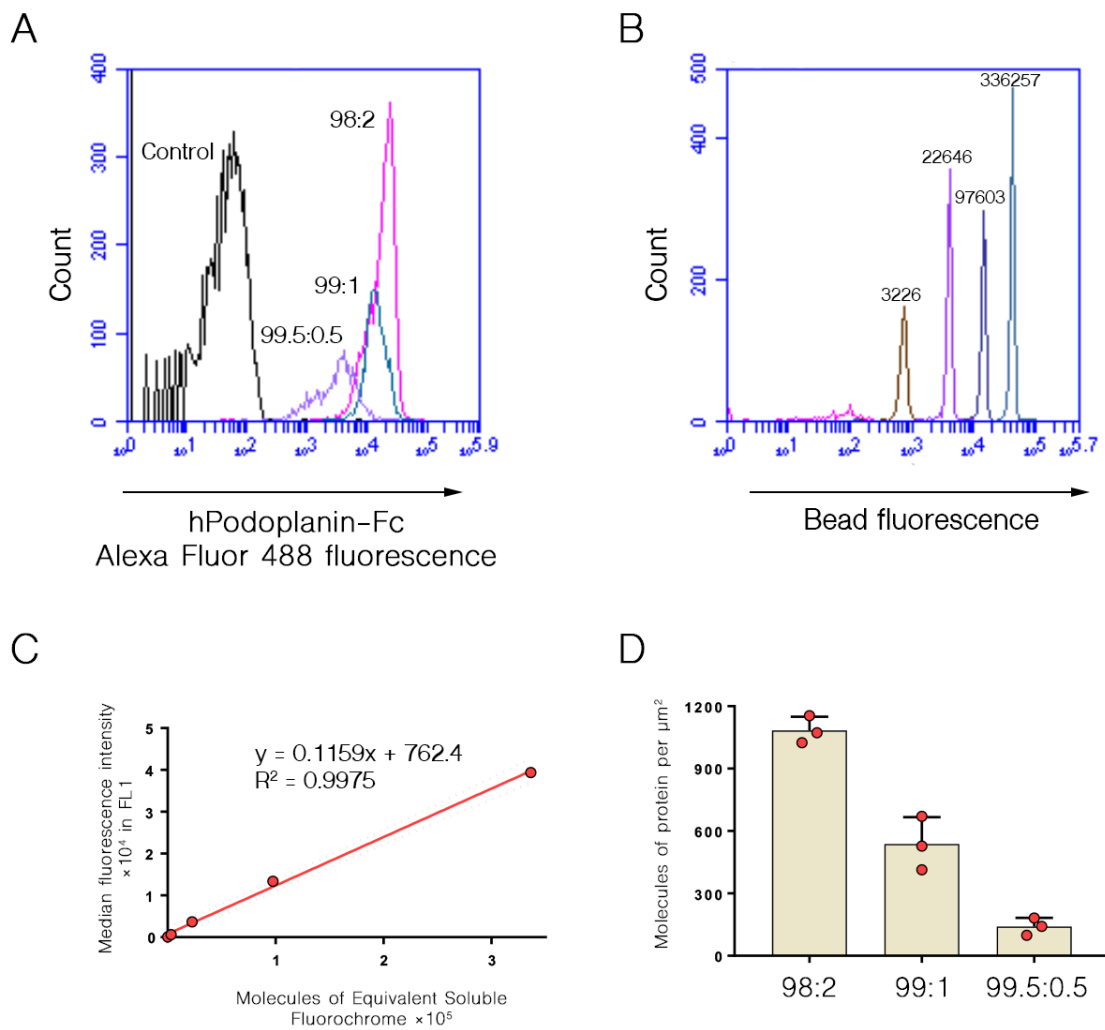
Figure 3.18. Quantification of how much hPodoplanin-Fc is incorporated into the bilayer.

Flow cytometry analysis of hPodoplanin-Fc attached into silica beads, coated with different ratios of DOPC:CAP-Biotin-PE liposomes or DOPC control using a streptavidin bridge (A); compared to beads with known number of molecules of equivalent soluble fluorochrome (B). The median fluorescent intensity (MFI) of the beads was used to construct a standard curve (C), which allowed the number of molecules of hPodoplanin-Fc per μm^2 deposited into the bilayer to be calculated (D). Count is referred to as the number of events identified in a selected fluorescence channel. Data are shown as mean $\pm$ SD and are representative of three independent experiments.

3.3.2.3.3. Determination of the size of HDLECs and copy number of podoplanin in HDLECs

To mimic a physiologically relevant density of recombinant podoplanin in the SLB platform, the surface area of cells and the density of podoplanin molecules at the cell surface are required. The cell surface area of HDLECs is not known. To determinate the size of HDLECs, two approaches were used: differential interference contrast (DIC) microscopy and flow cytometry.

5×10^5 HDLEC in suspension were added into 6-well plate and then imaged on a Ti2 microscope using differential phase contrast. ImageJ was used to analyse the diameter of ten randomly selected cells (Figure 3.19A). The average diameter of the cell was estimated as 19.29 μm. Using the cell radius, the average cell surface area was estimated as 1168 μm^2.

The second approach was to estimate the cell surface area of HDLECs using flow cytometry. Beads with a known diameter (1 μm, 2 μm, 4 μm, 6 μm, 10 μm and 15 μm-diameter) were run on flow cytometer, alongside 5×10^5 HDLECs. Using the median values in the forward scatter (FSC-H) channel of the standard beads (Figure 3.19B), a calibration curve was generated (Figure 3.19C). From the equation of the line, the diameter of the cells was calculated as 23.59 ± 1.84 μm. Using the cell radius, cell surface area was estimated as 1747 μm^2.
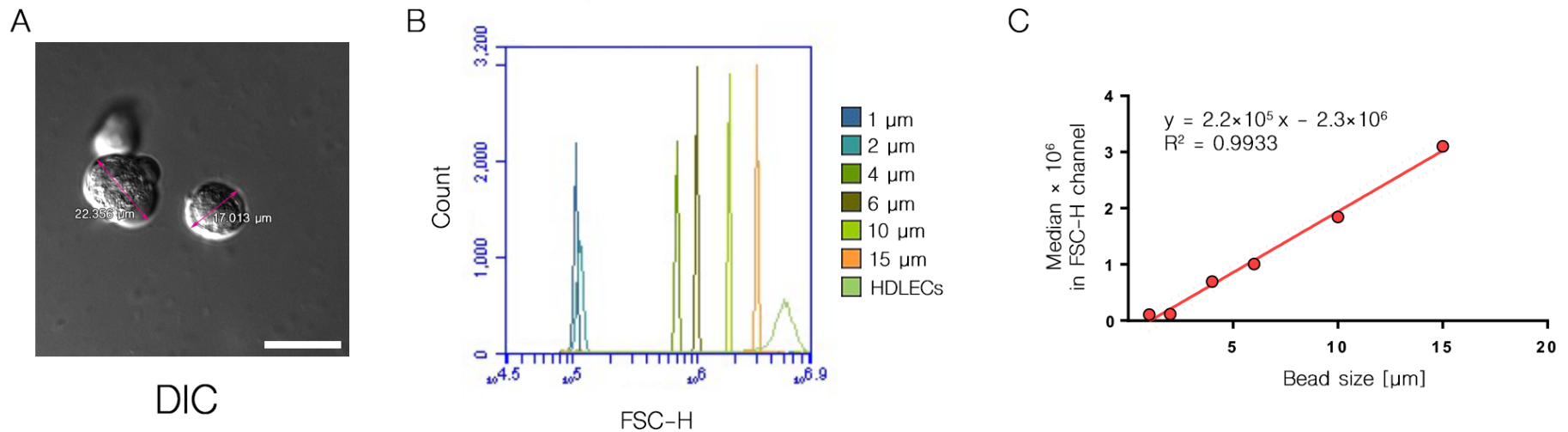
Figure 3.19. Size determination of human dermal lymphatic endothelial cells size.

HDLECs diameter was estimated using differential interference contrast microscopy (A, Scale bar – 20 μm); or flow cytometry by comparing beads of known size (B) with the signal from HDLECs. The median fluorescent intensity of the beads was used to construct a standard curve (C) and estimate the diameter of the cells. Count is referred to as the number of events identified in a selected fluorescence channel. Data are representative of three independent experiments.

To estimate the density of podoplanin molecules expressed at the surface of HDLECs, flow cytometry was used. HDLECs were incubated with saturating concentration of PE-conjugated anti-human podoplanin antibody NZ 1.3 (Figure 3.20A) and the median fluorescent intensity was compared with calibration beads of known antigen binding capacity. Using a calibration curve and the estimated cell size, the copy number of podoplanin in HDLECs was estimated as 1395.8 ± 439 podoplanin molecules per μm^2 (cell size determined by flow cytometry) or 2067.9 ± 656 podoplanin molecules per μm^2 (cell size determined by microscopy).
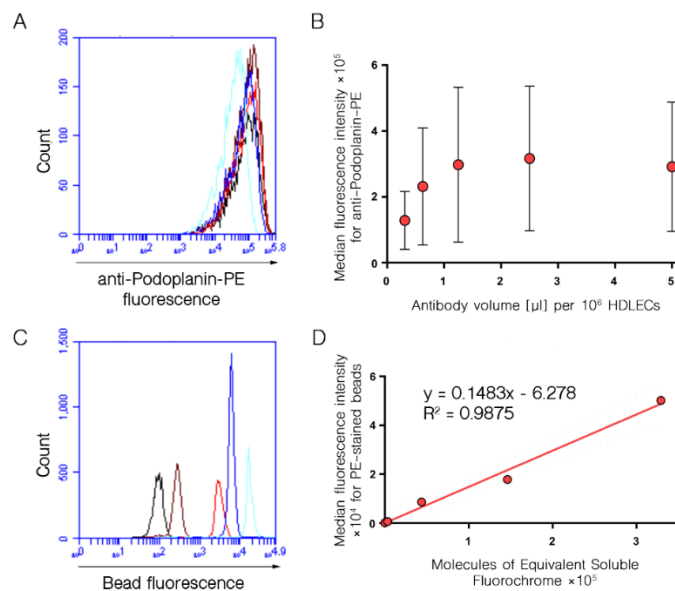
Figure 3.20. Determination of copy number of human podoplanin in HDLECs. Representative traces of chosen anti-podoplanin antibody (A) and beads of known antigen binding capacity (C). Saturating concentration of anti-podoplanin antibody (B) was used to label cells and beads of known antigen binding capacity (C). The median fluorescent intensity of the beads was used to construct a standard curve (D) and estimate podoplanin copy number in HDLECs. Count is referred to as the number of events identified in a selected fluorescence channel. Data are shown as mean $\pm$ SD and are representative of three independent experiments.

3.3.2.4. Human Podoplanin-Fc is mobile within a supported lipid bilayer in a FCS2 chamber

FRAP was performed to study the mobility of supported lipid bilayers in a FCS2 imaging chamber. To achieve this, supported lipid bilayers were formed using liposomes consisting of CAP-Biotin-PE and DOPC at a ratio of 2:98 on a glass coverslip cleaned by piranha solution. Selected lipid ratio corresponds to the similar number of hPodoplanin-Fc on SLB, when compared with the podoplanin copy number in the HDLECs (estimated in previous chapters). Afterwards, Streptavidin being a molecular bridge between biotinylated lipids was added into the chamber, followed by the Alexa Fluor® 488 labelled and monobiotinylated hPodoplanin-Fc extracellular domain. The mobility of the bilayer with tethered recombinant hPodoplanin was determined using FRAP. The microscope images 30 s before (1), just after (2) and 9 minutes 25 s after photo-bleaching are presented in Figure 3.21A. The fluorescence intensity in the ROI was measured every 5 seconds. As presented in Figure 3.21B, the intensity of fluorescence recovers from around 30% up to 82% within 9 minutes 25 s. This suggests that the bilayer from three independent experiments is highly mobile with a mobile fraction of almost 82 ± 3.4 %. High mobility of SLB will allow to follow a hPodoplanin cluster formation using TIRF microscopy, due the fact that protein tethered into SLB can freely migrate within the bilayer.
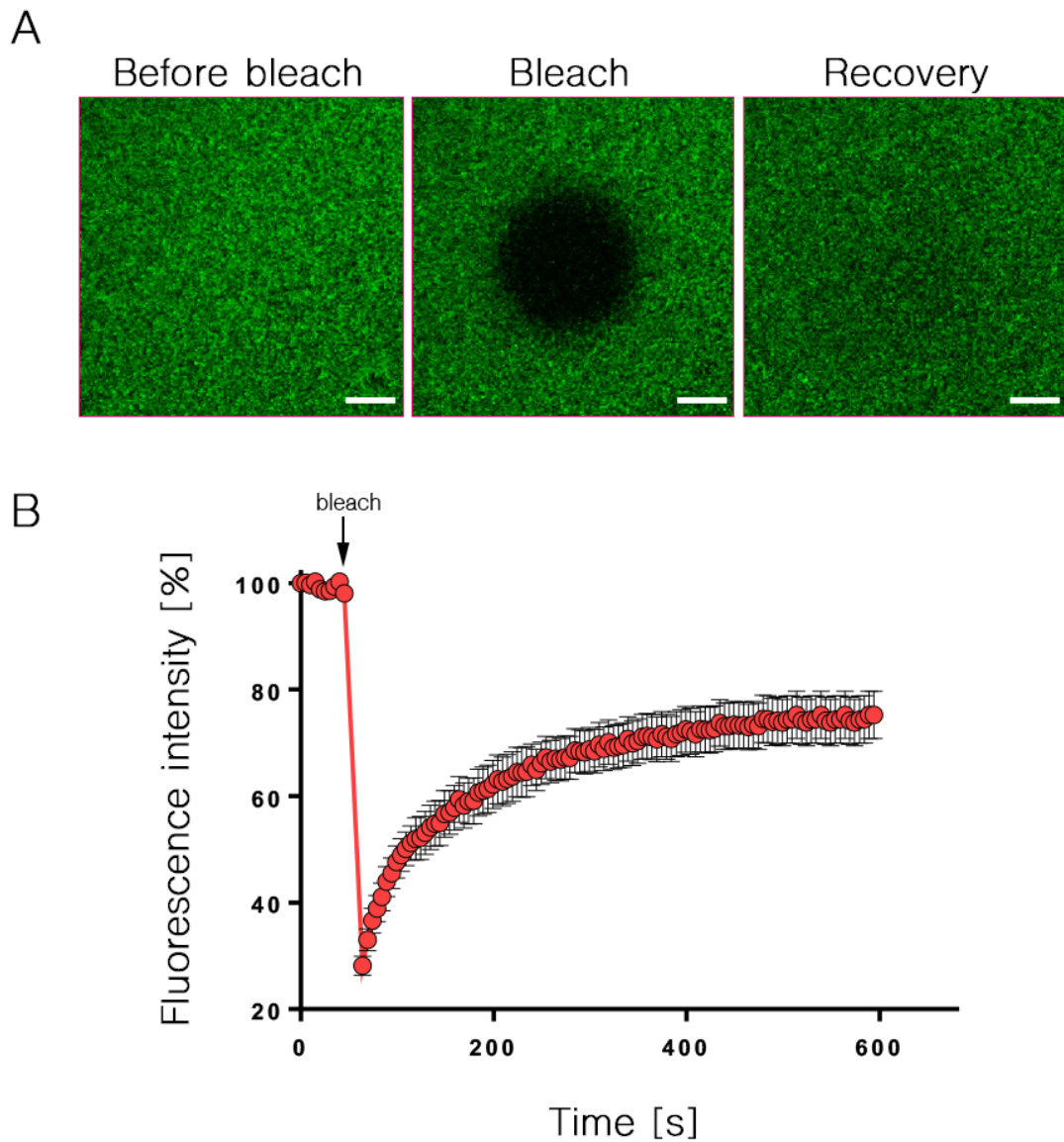
Figure 3.21. Lateral mobility within supported lipid bilayer containing hPodoplanin-Fc extracellular domain assembled in the FCS2 chamber.

A. Representative fluorescent images of the bilayer at three different time points: before bleach (30 s), immediately post-bleach, and 9 minutes 25 s after bleach. Scale bar – 10 µm. B. Fluorescent intensity kinetics in time; the fluorescence intensity was measured every 5 seconds. The graph presents mobile and immobile fraction of the protein within the bilayer. Data are shown as mean ± SD and are representative of 3 independent experiments.

3.3.2.5. Platelets cluster human Podoplanin-Fc presented on a glass-supported artificial lipid membrane

To investigate the dynamics of platelet-mediated clustering of hPodoplanin-Fc, live cell imaging was performed. This was achieved by monitoring the interaction of washed platelets pre-treated with IV.3 mAb (which inhibits ligand binding to $Fc\gamma RIIA$ and blocks $Fc\gamma RIIA$ function) with labelled Alexa Fluor® 488 hPodoplanin-Fc tethered to a supported lipid bilayer (CAP-Biotin-PE and DOPC in ratio 2:98) assembled in a FCS2 chamber using TIRF microscopy.

As soon as the platelet contacts the membrane, the accumulation of hPodoplanin-Fc under the platelet can be detected. Figure 3.22. shows that initially small clusters form and that these migrate to form a single bright central cluster within 10 minutes. Additionally, DIC imaging shows that the cluster forms under the platelet.
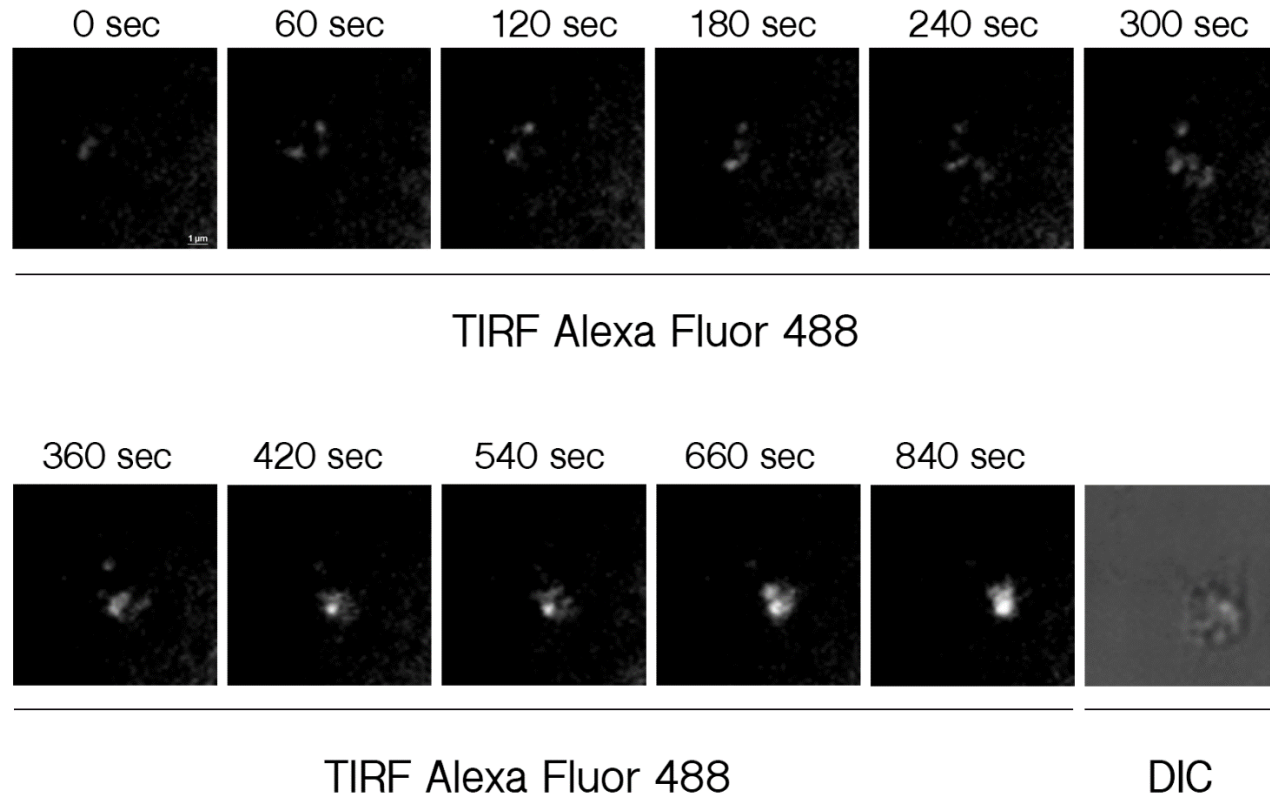
Figure 3.22. Platelets cluster hPodoplanin presented on a glass-supported artificial lipid membrane.

Washed human platelets, pre-treated with IV.3 mAb, were allowed to interact with labelled hPodoplanin presented on a supported lipid membrane and imaged using TIRF microscopy. The location of the platelet is shown using DIC microscopy. Scale bar – 1 μm. The results are representative of 3 independent experiments.

3.3.2.6. Human Podoplanin-Fc is mobile and forms clusters on a 96-well glass-supported artificial lipid membrane

Due to limitations of the FCS chamber (the need to do one experiment at a time and high volumes of reagents used), the approach was optimised in a higher-throughput format – 96-well glass bottom plates. To study the mobility of supported lipid bilayers assembled in a 96-well plate, FRAP was performed. To achieve this, supported lipid bilayers were formed using liposomes consisting of CAP-Biotin-PE and DOPC in a ratio 2:98 assembled in wells of a 96-well glass bottom plate cleaned thoroughly with alkaline cleaning concentrate and high concentrations of sodium hydroxide. Afterwards, Streptavidin was added into the wells, followed by the Alexa Fluor 488 labelled and monobiotinylated hPodoplanin-Fc extracellular domain. Mobility of the SLBs in each well of the plate was tested by FRAP. The microscope pictures 30 s before (1), just after (2) and 9 minutes 25 s after photo-bleaching are presented in Figure 3.23A. The fluorescence intensity was measured every 5 seconds. Figure 3.23B shows that the intensity of fluorescence recovers in a similar manner to the recovery seen with SLBs assembled in a FSC2 chamber, from around 30% up to 90% within the 9 minutes 25 s. This suggests that the bilayer from three independent experiments is highly mobile with a mobile fraction of almost $90 \pm 4.8\%$.

To investigate a platelet-mediated clustering of hPodoplanin-Fc, TIRF microscopy analysis was used. This was achieved by monitoring the interaction of washed platelets with labelled Alexa Fluor® 488 hPodoplanin-Fc tethered to a supported lipid bilayer (CAP-Biotin-PE and DOPC in ratio 2:98) after a fixed time of 25 minutes in a 96-well plate.

Similarly to the FCS2 chamber, the accumulation of hPodoplanin-Fc under the platelet was detected upon the contact of the platelet with the bilayer (Figure 3.24), suggesting the interaction of hPodoplanin with platelet CLEC-2.
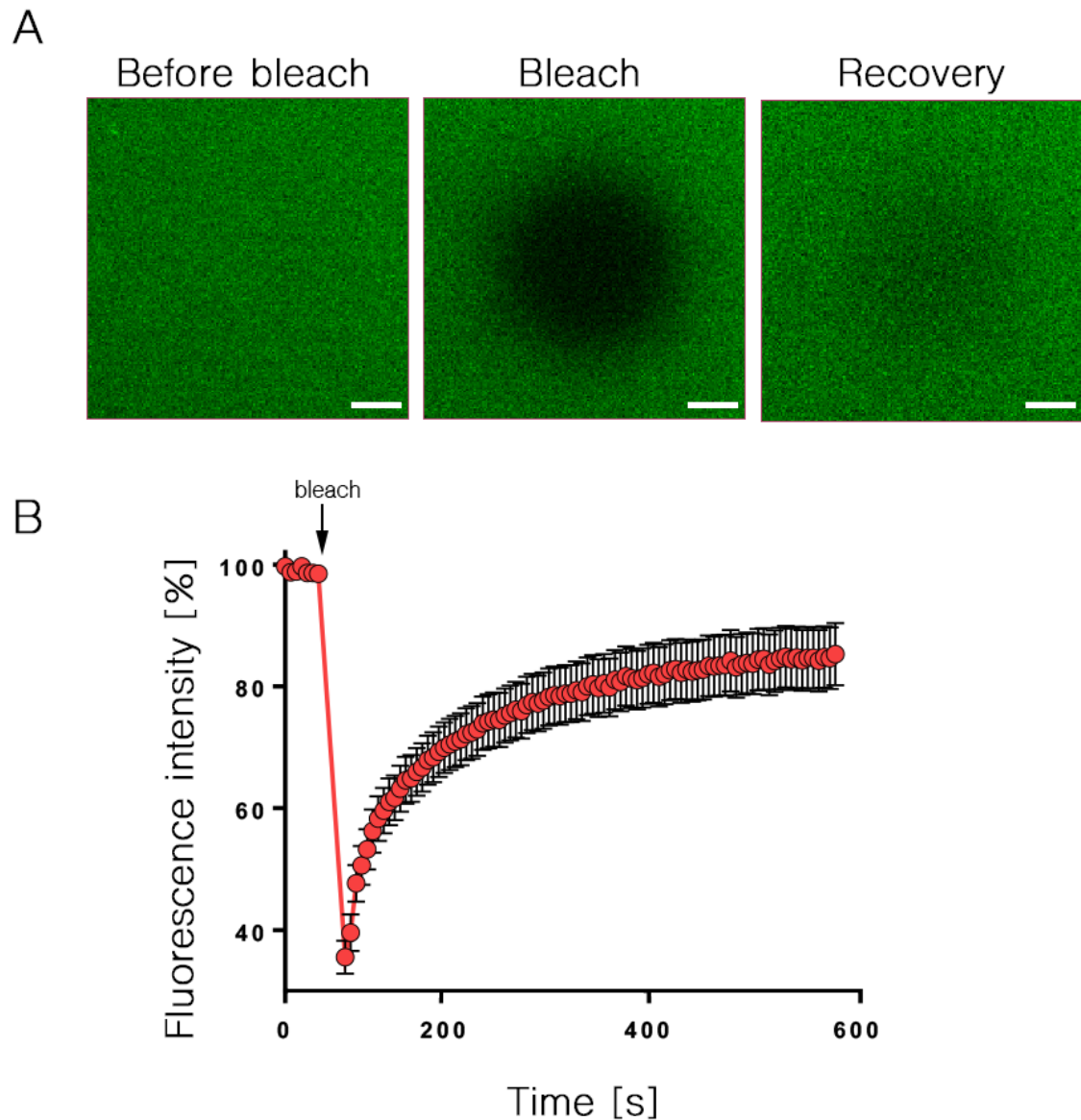
Figure 3.23. Lateral mobility within supported lipid bilayer of hPodoplanin-Fc extracellular domain in a 96-well plate.

A. Microscope images of SLB containing Alexa Fluor 488 labelled hPodoplanin-Fc at three different time points: before bleach (30 s), immediately post-bleach, and 9 minutes 25 s after bleach. Scale bar – 10 μm. B. Fluorescent intensity kinetics over

time. The graph presents mobile and immobile fraction of the protein within the bilayer. Data are shown as mean ± SD and are representative of 3 independent experiments.
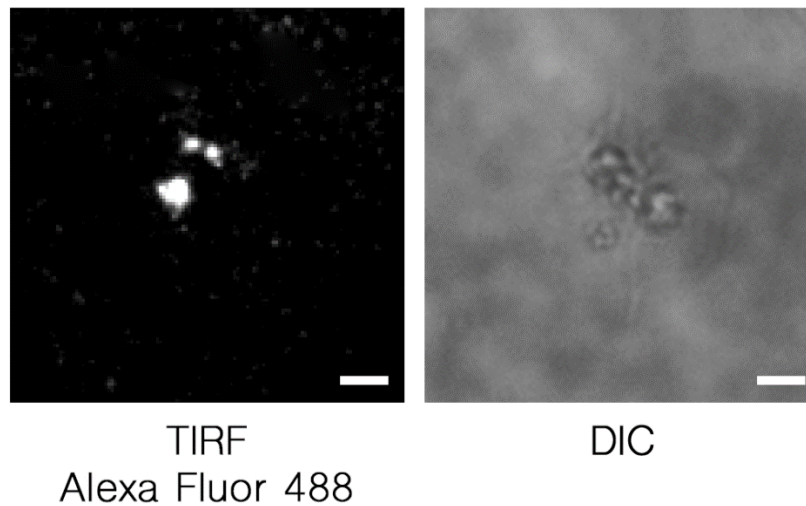
Figure 3.24. Platelets cluster hPodoplanin presented on a 96-well glass-supported artificial lipid membrane.

Washed human platelets were allowed to interact for 25 minutes with labelled hPodoplanin presented on a supported lipid membrane and imaged using TIRF microscopy. The location of the platelet is shown using DIC microscopy. Scale bar – 2 μm. The results are representative of 3 independent experiments.

3.4. Discussion

3.4.1. Reconstitution of the CLEC-2 signalling pathway

This chapter begins to develop a reconstituted artificial lipid membrane to investigate intracellular platelet receptor signalling and clustering. Firstly, the plasmid containing the sequence for the intracellular domain for CLEC-2 was generated and the proteins overexpressed and purified from *E. coli*. Secondly, recombinant protein was introduced into the supported lipid bilayer and their incorporation and mobility into SLBs analysed via flow cytometry and FRAP.

Plasmid containing the human CLEC-2 intracellular domain containing 10×Histidine-tag (for protein purification using Ni-NTA agarose and to tethering of proteins into SLBs) and SNAP-tag (for irreversible covalent labelling of the protein using a synthetic probe) has been successfully generated. Firstly, the gene of the domain was amplified via PCR and the size of the product was confirmed on an agarose gel (Figure 3.8). The expected size of the gene fragment (128 bp) was obtained and ligated into the vector with a histidine tag. Secondly, the generated plasmid was used to amplify the genes fused with histidine tag and subcloned into the vector containing a SNAP tag.

His- and SNAP-tagged hCLEC-2 intracellular domain was successfully overexpressed in *E. coli* (Figure 3.9) and purified from inclusion bodies on a Ni-NTA column. The Coomassie stained gel (Figure 3.10A) shows two different sizes bands in the elution fractions, 30 kDa – the expected size of the protein; and an additional one at around 70 kDa. The larger band is probably one of the commonly co-purified proteins separated using Ni-NTA resin, Hsp70 prokaryotic homologue DnaK (Robichon *et al.,* 2011). To separate the protein from the target recombinant protein, an additional purification step, such as size-exclusion chromatography is needed. Western blot analysis using anti-His

tag and anti-SNAP tag antibodies (Figure 3.10B), as well as direct protein labelling (Figure 3.10C) confirmed that the purified 30kDa protein is the hCLEC-2 tail fused to His- and SNAP-tags.

Recombinant protein containing the hCLEC-2 intracellular domain fused to His- and SNAP-tags interacts with SLBs containing nickel chelating lipids. Flow cytometry analysis of SLBs formed on silica beads with the hCLEC-2 tail with specific antibodies, as well as a labelled version of the protein shows that compared to a negative control, the recombinant protein can interact with SLBs (Figure 3.11).

Additionally, the copy numbers of intracellular Syk in human platelets were determined. There are available proteomic datasets with the estimation of absolute numbers of proteins in platelets (Burkhart *et al.*, 2012), however this data can be confirmed using flow cytometry. Comparing proteomic data with flow cytometry data, the copy number human Syk was similar (4600 (proteomic) vs 5192 ± 1055 (flow cytometry) molecules per platelet). To conclude, flow cytometry-based method may be used to validate the available proteomics data.

The mobility of SLBs composed of DOPC:DGS-NTA (in ratio 75:25) containing hCLEC-2 tails was tested using FRAP. No lateral mobility of the labelled hCLEC-2 tail was seen, with the mobile fraction almost equal to zero (Figure 3.13). This method requires optimisation by changing the composition or ratio of lipids within the SLB or changing the protein concentration used in the chamber. Indeed, Su et al. have found that bilayers containing 5% DGS-NTA or more tend to become less fluid (Su *et al.*, 2017). The high percentage of DGS-NTA used here may be responsible for the lack of mobility. Another reason for lack of mobility could be incorrectly folded protein after the purification from inclusion bodies. Circular dichroism could be used to check the folding of the refolded recombinant protein; however, it has not been done.

Alternatively, another method of protein incorporation into the SLBs, such as biotin-mediated via streptavidin bridge, could be used. As a future perspective, the model can be minimised into the 96-well format.

3.4.2. Development of SLBs to study CLEC-2-mediated clustering of Podoplanin

The results in this chapter show the development of a reconstituted artificial lipid membrane to investigate human podoplanin clustering by human platelets. Firstly, a dimeric form of the human podoplanin extracellular domain in fusion with rabbit Fc was overexpressed in mammalian cells and purified using affinity chromatography. Secondly, the functionality of the protein was tested using a platelet adhesion and spreading assay. Thirdly, the number of hPodoplanin molecules within SLBs of different lipid compositions was estimated using flow cytometry and compared with the density of hPodoplanin on the HDLECs surface. Finally, the mobility of hPodoplanin within the supported lipid bilayer was confirmed using FRAP and clustering mediated by human platelets monitored using TIRFM.

An Fc-tagged dimer of hPodoplanin was successfully overexpressed in mammalian cells and purified on a Protein A column. The Coomassie stained gel (Figure 3.14A) showed the different sized bands in non-reduced or reduced conditions. This confirms that hPodoplanin-Fc is a dimer as expected. Additionally, the western blot analysis (Figure 3.14B) confirmed that specific antibodies against hPodoplanin detects this protein.

The functionality of the hPodoplanin-Fc was confirmed using a platelet spreading assay and epifluorescent microscopy. The microscope images (Figure 3.15A) confirmed that platelets adhere to and spread on hPodoplanin-Fc-coated coverslips whereas on the

BSA- and rabbit IgG-coated coverslips, few or no platelets were found (Figure 3.15B). Additionally, the average platelet area on immobilized hPodoplanin-Fc shows that platelets are fully spread, whereas no spreading is seen on immobilised controls BSA and rabbit IgG (Figure 3.15C). This provides evidence that the expressed hPodoplanin-Fc protein is functional, and that the interaction between the platelets and the hPodoplanin-Fc protein is not due to the Fc domain or non-specific interactions with the BSA-coated glass.

Protein biotinylation is a key step, due to the high affinity of biotin to streptavidin, to attach the recombinant podoplanin via a streptavidin bridge into supported lipid bilayer containing biotinylated lipids. It is important to monobiotinylate the protein to have only one biotin-binding site, which will be occupied by streptavidin. The optimal concentration to monobiotinylate the hPodoplanin-Fc, where a signal in the FL4 channel (presence of hPodoplanin) was detected, and no signal in the FL1 channel (no detection of a second biotin), was estimated in range of 0.05 to 0.5 µg/ml of biotin (Figure 3.17). For the further experiments, 0.5 µg/ml was used. Followingly, biotinylated hPodoplanin-Fc was labelled with Alexa Fluor 488 and the concentration was estimated as 13.02 µM (0.83 mg/ml). Protein prepared this way allowed the number of recombinant hPodoplanin-Fc molecules incorporated into the upper leaflet of the bilayer to be estimated using flow cytometry. The number of molecules differed between the samples with decreasing ratio of the CAP-Biotin-PE lipids within supported lipid bilayer. As expected, comparing to the highest concentration of CAP-Biotin-PE lipids (2%), decreasing the concentration 2 times (1%) and 4 times (0.5%) resulted in a decrease the number of molecules 2 times and 4 times respectively (Figure 3.18). The hPodoplanin-Fc incorporated into SLBs with 2% of biotinylated lipids (1,084 ± 54 molecules/µm^2) reflects the number of podoplanin molecules endogenously

expressed on the surface of the HDLECs (1395.8 ± 439 molecules/μm^2). This allows the model to be most reminiscent of the natural biological situation.

Ketchum et al. showed that mobile ligand incorporated into SLB enabled BCR clusters on A20 lymphoma B cells to move further and merge more efficiently than immobile ligand and this difference was associated with differences in actin remodelling. These results suggest that ligand mobility is an important parameter for cell signalling and clustering (Ketchum *et al.*, 2014). The mobility of prepared supported lipid bilayers composed of DOPC:CAP-Biotin-PE liposomes was tested using FRAP. FRAP is a powerful technique to investigate the lateral mobility of lipids and proteins in artificial lipid membranes. In the model presented here, the biotinylated hPodoplanin-Fc molecules will bind to the biotinylated lipids via a streptavidin bridge. The FRAP experiment has been performed in an FCS2 chamber. The result shows that the mobile fraction is equal to 82% (Figure 3.21). That means the lipids coupled to the hPodoplanin-Fc protein molecules are largely free to migrate within the supported bilayer and mimic the biological environment of proteins in a membrane (Khan *et al.*, 2013; Shilts and Naumann, 2018)

Many membrane receptors need to form clusters to initiate signalling. It is characteristic of ITAM/hemITAM containing receptors. Large central cluster formation may enhance the intracellular signal, decrease molecule diffusion, and exclude negative regulators like CD45 in T-cell receptor (Davis and van der Merwe, 2011). The clustering of podoplanin by platelets is similar to the T-cell receptor and has been investigated using mouse platelets with mouse podoplanin. It has been showen that mCLEC-2 mediated signalling by SFKs and Syk plays an important role in the formation of large mPodoplanin clusters in a mPodoplanin-containing SLB and in a cell membrane (Pollitt *et al.*, 2014). The TIRF experiment showed that when a human platelet comes into

contact with labelled hPodoplanin-Fc mobilised on a supported lipid bilayer, a central bright cluster of hPodoplanin forms (Figure 3.22). Clustering of hPodoplanin is likely a consequence of the interaction with hCLEC-2 in platelets, as it has been shown by Pollitt et al. with mouse platelets with mouse podoplanin. This interaction could be further investigated using inhibitors which disrupt the interaction between hCLEC-2 and hPodoplanin to show that the mechanism of clustering is conserved between mouse and human platelets.

Similar experiments were performed in a 96-well glass bottom plate. Usage of 96-well plate may help to perform more experiments with different conditions at the same time and use a smaller volume of liposomes and proteins. Additionally, optimisation of the assay in a 96-well plate format gives the opportunity to use it as a high-throughput platform to identify novel protein-protein interaction inhibitors.

The FRAP analysis of the SLBs in the 96-well plate indicates that the mobile fraction is almost 90% (Figure 3.23). This value is similar to the mobility of the SLBs obtained in the FCS2 chamber. This result shows that the 96-well plate may be use for further experiments and has incredible potential to perform multiple experiments simultaneously. Moreover, the TIRF experiment showed that supported lipid bilayer tethered hPodoplanin-Fc clusters in contact with human platelets (Figure 3.24). The developed platform is a 96-well high-throughput format that gives more possibilities than the platform formed in FCS2 chamber. It can be used to study novel inhibitors of CLEC-2-mediated signalling, focusing on a primary event – platelet activation by podoplanin, and testing different conditions at a selected time point in the fixed samples.

3.5. Conclusions

The artificial lipid membrane model provides an opportunity to study extracellular receptor and ligand clustering. Reconstitution of signalling pathways may be a powerful tool to understand the interactions, localisations and dynamics of signalling components. The recombinant signalling pathway components reconstituted into the artificial lipid membrane may enable the dynamics of macromolecular assemblies and molecular behaviour of signalling proteins to be studied in ways that cannot be achieved using intact platelets. Additionally, platforms for the CLEC-2 receptor may help to determine what regulates cluster size and density, understand how intracellular multivalent interactions drive cluster formation and to investigate how small molecule inhibitors affect receptor clustering.

Purification of signalling pathway components and optimisation of the artificial lipid membrane platform are key steps to achieve the aims of this thesis. Application of supported lipid platforms may be further used for many purposes, for example as a high-throughput screening platform, to identify the novel inhibitors, and to study the interactions and dynamics between signalling pathway components and the inhibitors using advanced microscopy.

Although the intracellular platform for human CLEC-2 proved to be immobile, the information in this thesis gives the good starting point to continue this process. A platform for human CLEC-2-mediated human podoplanin clustering gives the possibility to study further platelet receptor ligand clustering and may be used as a platform to test novel inhibitors of the CLEC-2-podoplanin interaction.

Chapter 4

Identification of small-molecule inhibitor of the CLEC-2-podoplanin interaction

4.1. Introduction

HTS is a process which allows large libraries of compounds to be tested against a particular biological target or system. The target identified in this thesis is an interaction between human CLEC-2 and human podoplanin. CLEC-2, by interaction with its endogenous ligand podoplanin, plays a major role in thrombo-inflammation, which has been shown in mouse models of deep venous thrombosis and *Salmonella* infection (Thomas and Storey, 2015; Rayes *et al.*, 2017). Additionally, CLEC-2-podoplanin interaction is important in arterial thrombosis, blood lymphatic development and cancer (Harbi *et al.*, 2021). That is why CLEC-2 may be a promising target for long-term prevention of pathologies such as arterial thrombosis, deep venous thrombosis, sepsis, and cancer, with a decreased bleeding risk relative to current therapies. The known small molecule inhibitors of CLEC-2-podoplanin interaction have its low potency, toxicity, and lack of oral availability. That is why they cannot be pursed for clinical development and there is still a need to look for new inhibitors.

There are only two known small molecule inhibitors of the CLEC-2-podoplain interaction. The first one, Cobalt-hematoporphyrin (Co-HP) is a member of porphyrins family and has been developed by changing vinyl groups at C2 and C4 of protoporphyrin IX (H2-PP) and adding a cobalt, to generate a stable complex with the nitrogen molecule in the centre of pyrrole ring (Figure 4.7A). It was identified in a modified sandwich enzyme-linked immunosorbent assay (ELISA)-based HTS by screening 6770 compounds at concentrations of 10 μg/ml. Computational molecular docking studies showed that Co-HP may bind to CLEC-2 Asn120, Asn210 and Lys211. The interaction between Co-HP and CLEC-2 has been confirmed by generating CLEC-2 mutants. Asn120-Ala and Lys211-Ala mutants lost the ability to bind podoplanin-expressing cells, suggesting that Asn120 and Lys211 may be required for podoplanin

binding. Additionally, Co-HP inhibited rhodocytin-induced human and mouse platelet aggregation, but not when stimulated with CRP and thrombin (Tsukiji *et al.*, 2018).

Another small molecule inhibitor of CLEC-2-podoplanin interaction is 2CP, a derivative of 4-O-benzoyl-3-methoxy-beta-nitrostyrene (BMNS) (Figure 4.7B). Computational molecular docking studies showed that 2CP may bind to CLEC-2 Arg107, Arg118 and Aar157, which are key residues for rhodocytin and podoplanin binding (Nagae *et al.*, 2014a). 2CP inhibited podoplanin-induced human platelet aggregation, but not when stimulated with thrombin, collagen, or ADP. Surprisingly, 2CP did not inhibited rhodocytin-induced human platelet aggregation, which may be explained by the difference in the binding affinity constant of CLEC-2 to podoplanin or rhodocytin, which has been estimated as 24.5 µM and 1 µM, respectively (Watson *et al.*, 2007; Christou *et al.*, 2008). The binding affinity constant of 2CP to CLEC-2 was estimated as 33.2 ± 1.9 µM. Chang et al. suggest that the lack of inhibitory effect on rhodocytin-induced platelet aggregation using 2CP is due to its low affinity for CLEC-2 when compared with rhodocytin (Chang *et al.*, 2015).
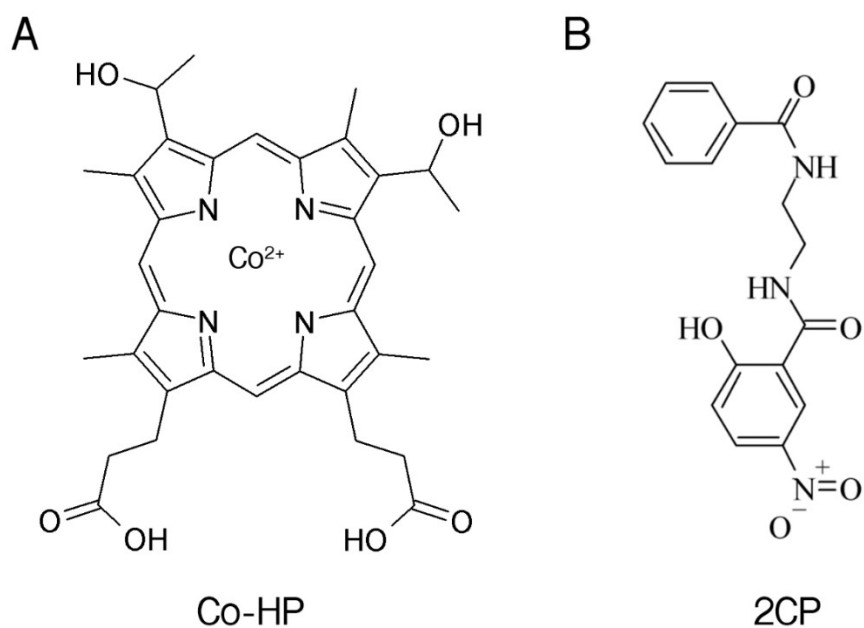
Figure 4.1. Cobalt-hematoporphyrin and 2CP structures.

Cobalt-hematoporphyrin, Co-HP (A) is a member of porphyrins family and has been developed by changing vinyl groups at C2 and C4 of protoporphyrin IX (H2-PP) and adding a cobalt, to generate a stable complex with the nitrogen molecule in the centre of pyrrole ring. 2CP (B) is a derivative of 4-O-benzoyl-3-methoxy-beta-nitrostyrene (BMNS).

4.1.1. High-throughput screening

High-throughput screening (HTS) is a technique used in the drug discovery process, mainly in the pharmaceutical industry but also in an academic environment (Frearson and Collie, 2009). It is based on the identification of a biological target involved in a pathway of interest or disease and screening against it, using a large number of compounds (modulators and inhibitors). The identified compounds become potential drugs, called leads (Sundberg, 2000).

HTS can be used in parallel with computational technique, called virtual high-throughput screening (vHTS). It uses *in silico* collection of compounds and is based on checking the binding affinity of the target with the compounds (Shoichet, 2006). The screened compounds are ranked using a scoring function, which computes the complementarity of the target with the compound (Bajorath, 2002).

The idea underlying HTS is the screening of as many compounds as possible in the shortest time, therefore the format of the assay must be miniaturised. Typical formats for HTS are 96-well, 384-well or 1536-well plates with the final volume of 100-200 μl, 30-100 μl and 2.5-10 μl respectively (Mayr and Bojanic, 2009). Using 1536-well format it is possible to screen more than 100,000 compounds per day. It is then called ultra-HTS (uHTS) (Hertzberg and Pope, 2000).

HTS is divided into several stages: target identification, assay development and validation, data analysis, hits identification and lead selection. The stages of HTS are presented in Figure 4.2.
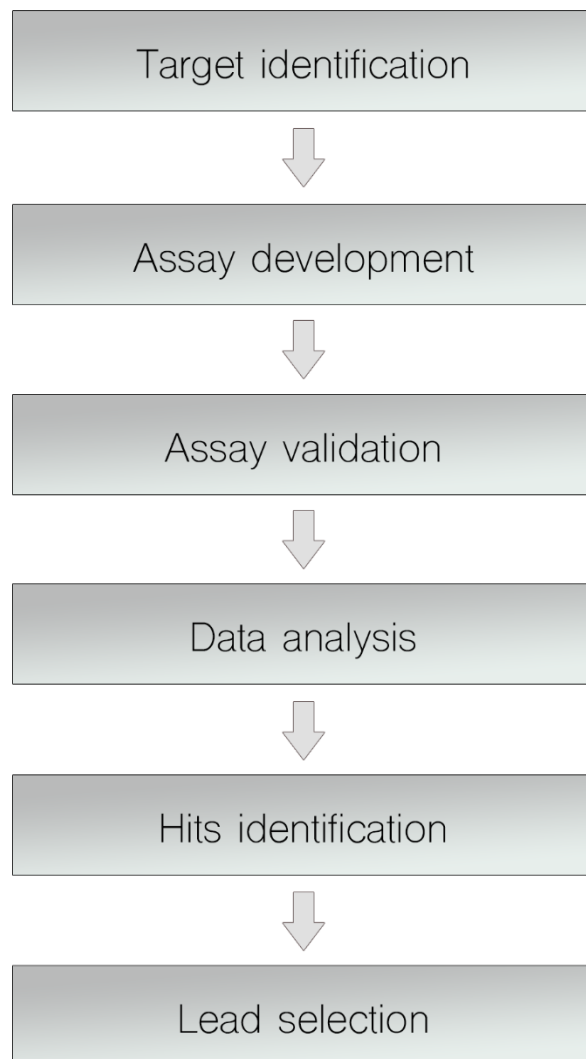
Figure 4.2. Stages of HTS.

There are 6 different stages in the HTS process: target identification, assay development, assay validation, data analysis, hits identification and lead selection. All these steps lead to the identification of compounds, which may have inhibitory or modulatory effect on the identified target.

4.1.1.1. Target identification and assay development

The first step of the HTS is target identification. There are a few important considerations for selecting a therapeutic target for HTS: relevance (how important it is in a disease or signalling pathway), chemical tractability (whether the target can interact with small molecules) and screen ability (possibility to develop a screening assay for the target) (Gashaw *et al.*, 2012).

After target identification, the next step is assay development to perform HTS. There are two different types of assays: biochemical and cell-based assays. Biochemical assays look for compounds that interact with recombinant targets in an artificial environment, whereas cell-based assays provide more physiological target environment.

Most of the biochemical assays in HTS are performed in a 'mix and read' format on high-density microtiter plates (384 or 1536 wells). The assays are based on optical measurements, looking at changes in absorbance, fluorescence, or luminescence (Macarron and Hertzberg, 2009). The most widely used are the fluorescence methods, which give very high sensitivity and allow for format miniaturisation with the use of very small volumes. It is important to avoid the short excitation wavelengths (below 400 nm) because many of small molecules can interfere by exciting this wavelength itself (Eggeling *et al.*, 2003). The most popular fluorescence method in HTS is fluorescence resonance energy transfer (FRET), however other biochemical methods are also widely used, such as amplified luminescence proximity homogenous assay (AlphaScreen), scintillation proximity assay (SPA) or homogenous time resolved fluorescence assay (HTRF). In this thesis, the AlphaScreen has been used to identify small molecule inhibitors of the CLEC-2-podoplanin interaction and the principle of this method has been described in detail in section 4.1.2.

The main advantage of biochemical assays is that the effect of inhibition/modulation is specific to the target, not to other molecules of the pathway or by alternative mechanisms. However, there are also some disadvantages. Protein production can be time-consuming, and some target proteins cannot be purified. Additionally, the activity of small molecules in biochemical assays may not always translate to the cellular context, due to requirements for cellular cofactors, membrane permeability, cytotoxicity, or off-target effects (An and Tolliday, 2010).

Another group of HTS assays are cell-based assays. They did not exist until the development of a fluorescent imaging plate reader (FLIPR) in mid-1990s, which has been designed to measure intracellular calcium mobilization in real time. Nowadays, FLIPR is compatible with 384-well and 1536-well microplate formats. Other cell-based methods include reporter gene assays (Beck et al. 2005; X. Li et al. 2007) and phenotypic assays for cellular processes (e.g., cytokinesis and cell migration) (Eggert *et al.*, 2004; Yarrow *et al.*, 2005).

Cell-based assays provide many advantages. The main advantage is that the compounds are tested in a physiological environment. In addition, it allows for the selection of compounds that can cross the cell membrane and give an indication about cytotoxicity at an early stage of the lead selection process. Nevertheless, there is also a major disadvantage, the possibility that compounds have no selectivity to the desired target (An and Tolliday, 2010).

4.1.1.2. Assay validation

To validate HTS assay, the statistical parameters need to be calculated. In 1999, Zhang et al. described a simple statistical parameter to evaluate and validate HTS assays (Zhang *et al.*, 1999). There are two statistical expressions to validate HTS quality: signal-to-background (S/B) ratio and signal-to-noise (S/N) ratio. S/B ratio is a ratio of the mean signal level to the mean background level and is described by equation:

$$S/B = \frac{mean\ signal}{mean\ background}$$

However, the S/B ratio is inadequate as it does not contain any information about data variation. The S/N ratio is an indication of the degree of confidence that signal value is different enough from the background noise, to be real. The S/N ratio is a better parameter than the S/B ratio because it considers the variation in the background. It is described by equation:

$$S/N = \frac{mean\ signal - mean\ background}{sd\ of\ background}$$

Neither S/B ratio nor S/N ratio take into account both, the variability in the sample and the background signal, and the signal dynamic range. That is why the most important statistical parameter to validate the HTS is the Z-prime factor (Z'), which describes the assay's robustness. This parameter is calculated using both, the mean and standard deviation of the samples and is described by equation below:

$$Z' = 1 - \frac{3sd\ of\ \max + 3sd\ of\ min}{|mean\ of\ max - mean\ of\ min|}$$

It is important to measure the separation of the positive and negative populations (Figure 4.3). The data variation is defined as the 3 standard deviations (3sd) of the mean of positive and negative control, which has 99.73% confidence limit. A signal window

(defined as a separation band) is defined as a difference between the sample means and describes the dynamic range of the screen.

An excellent assay has a small data variability and a large dynamic range. A Z' value greater than 0.5 is considered as an excellent assay. Assays which achieved Z' values below 0.5 are considered as marginal and require optimisation. The Z' values corresponding to the quality of the HTS assay have been presented in Table 4.1.

The quality of an assay can differ from how the samples and the compounds are dispensed (manually or robotically). The robotic dispensation gives less chance of pipetting error. It is common to use two columns per plate for the controls, one each for positive and negative controls. Additionally, this helps to calculate the exact Z'-factor, because it requires large data sets to improve accuracy.
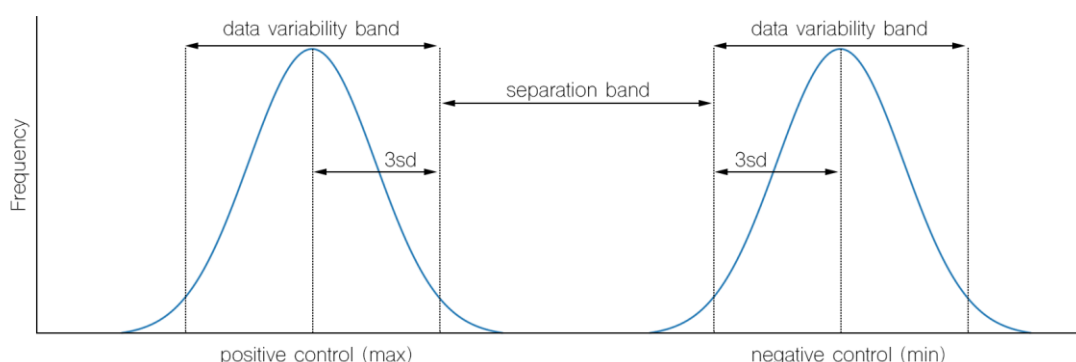
Figure 4.3. The Gaussian distribution of the data variation band and separation band observed in a typical HTS assay.

The variability of the assay is described as 3sd (standard deviations), whereas the assay dynamics as a separation band (difference of the means of positive and negative control). The highest Z' will be achieved when the separation band is large, and the standard deviation is small.

152

Table 4.1. Categorization of the HTS quality by the Z'-factor.

Z'-factor value	Structure of assay	Related to screening
1	sd = 0 (no variation)	An ideal assay
$1 > Z' \geq 0.5$	separation band is large	An excellent assay
$0.5 > Z' > 0$	separation band is small	A marginal assay
≤ 0	no separation band	Screening impossible

4.1.1.3. Hits identification and lead selection

After the validation of the primary screen, there are a few additional steps to select the best leads. These steps have been presented in the Figure 4.4 below:
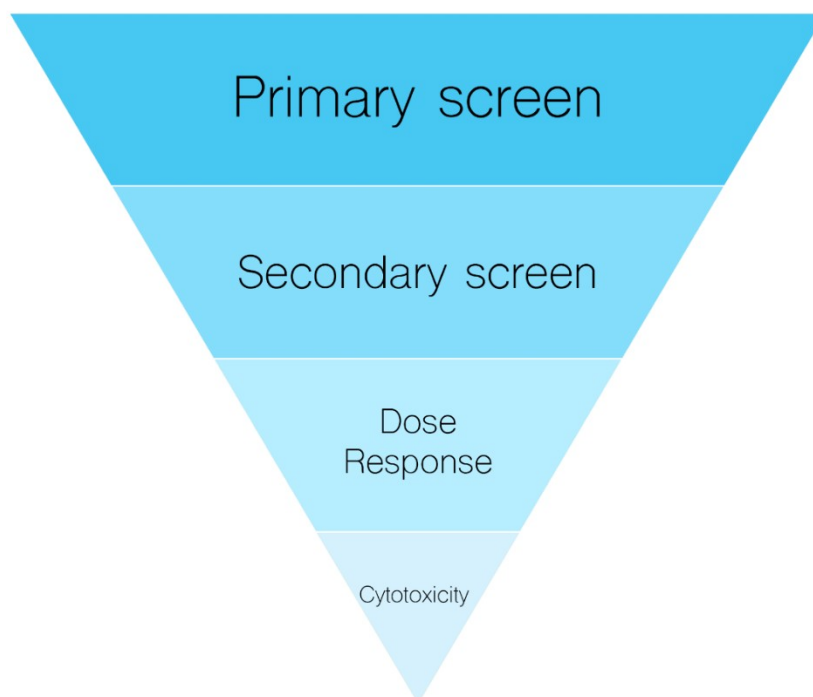
Figure 4.4. Lead selection stages from the primary screen to the cytotoxicity assay. In primary screening, the compound library is used to identify hit compounds. Then, the hit compounds are tested in a secondary screen to remove false negatives, followed by a dose-response study and a cytotoxicity assay.

Compounds identified as hits in the primary screen should be screened again, in the same way as before. This step allows compounds which showed a false positive effect on the performed assay to be discarded and confirms compounds which can be considered as true hits (Macarron and Hertzberg, 2009). In addition, many established assays, e.g., AlphaScreen, provide a special TruHits kit to identify false positive

compounds interfering with the assay. It includes singlet oxygen quenchers, colour quenchers, light scattering, and biotin mimetics.

After the secondary screen, to confirm the effect of the compounds, the next step is to prepare a dose-response curve, using a range of concentrations of the compounds (typically between 100 µM to 1 nM) in order to calculate IC_{50}, which is defined as a concentration of the compound required for 50% inhibition (Parham *et al.*, 2009). The dose-response curve is generated by using the same assay used for the primary screen and gives a starting point for compound evaluation in biological assays.

The last step of lead compound selection is a cytotoxicity assay. This allows lead compounds to be tested on human cells to check their off-target toxicity (Hamid *et al.*, 2004). In this thesis, to study if the compound is toxic to cells, Calcein-AM has been used with human washed platelets. Calcein-AM is a permeant non-fluorescent dye that indicates cellular health. When it enters the cells, it is converted by esterases present in the healthy and live cells into Calcein resulting in green fluorescence after excitation. If the compound is toxic for cells, the Calcein-AM is not converted, and the fluorescence is not observed (Gillissen *et al.*, 2016). The schematic principle of a viability assay using Calcein-AM is shown in Figure 4.5.
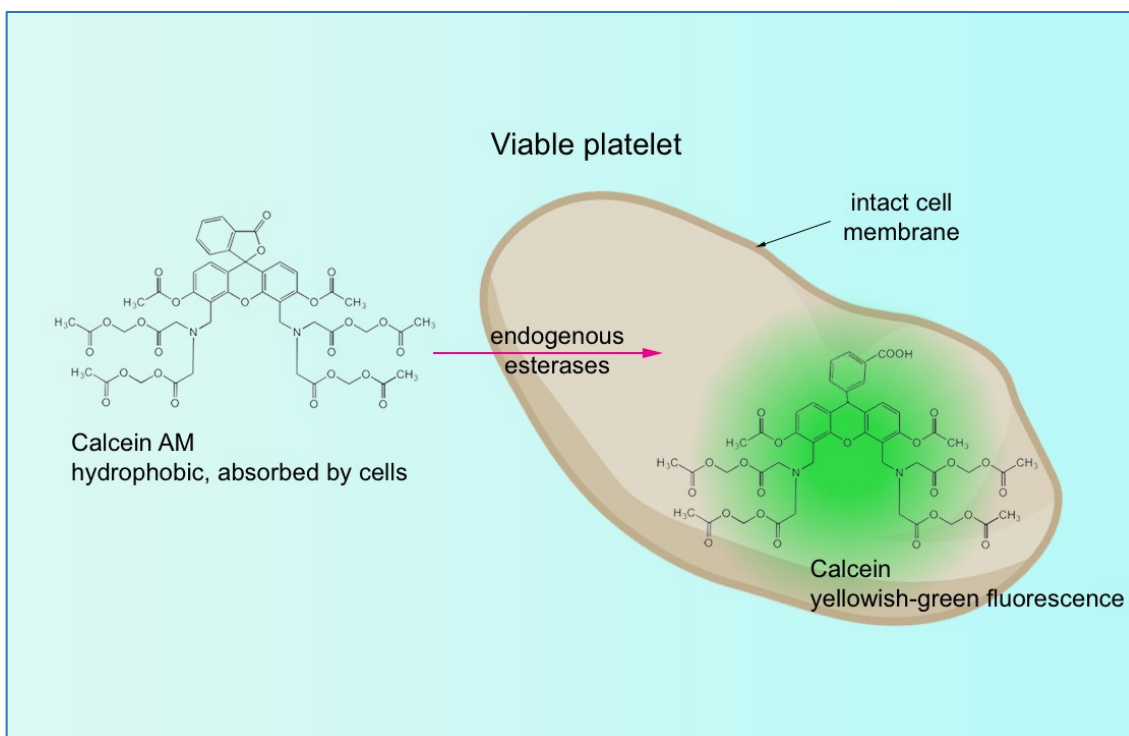
Figure 4.5. Cell-viability assay principle using Calcein-AM.

When Calcein-AM enters the cells, it is converted into Calcein by endogenous esterases present in live cells. Following excitation, the Calcein produces a green fluorescence. If the compound is toxic to the cells, there is no Calcein-AM conversion into Calcein, and no fluorescence is produced.

The last consideration in lead compound selection is described by Lipinski's 'rule of 5'. The rule determines if a compound with pharmacological or biological activity has properties to be an orally active drug in human. The rule of five states that an orally active drug has a molecular weight <500 Da, a partition coefficient (LogP) <5, a number of H-bond donors <5 and a number of H-bond acceptors <10. These criteria are commonly used to estimate druglikeness that relies on the physiochemical analysis of the approved drugs. The identified compounds which match these criteria should be considered as lead compounds (Lipinski *et al.*, 1997).

4.1.2. AlphaScreen

The Amplified Luminescent Proximity Homogeneous Assay Screen is a non-radioactive, homogeneous proximity approach to study biomolecular interactions. It has been developed to identify small molecule compounds for biological targets using a high-throughput screening assay of compound libraries. The AlphaScreen assay is based on the proximity of donor beads and acceptor beads, conjugated with a recognition site of an analyte of interest, such as peptide, protein, or antibody of interest. The donor beads contain a photosensitizer phthalocyanine, which converts ambient oxygen into a singlet form of O_2, following illumination at 680 nm. The acceptor beads contain a chemical dye, thioxene, which interact with a singlet oxygen. If the acceptor beads are in close proximity (< 200 nm) to donor beads, the energy of singlet oxygen is transferred to thioxene, and a fluorescent signal between 520–620 nm is generated (Peppard *et al.*, 2003). The lifetime of singlet oxygen is relatively short (~4 μsec) and can diffuse approximately 200 nm in solution, hence, in the absence of acceptor beads in proximity to donor beads, singlet oxygen converts to the ground state and no signal is produced. The principle of AlphaScreen, basing on the example of the assay performed in this thesis, is presented in Figure 4.6.

AlphaScreen has many advantages, such as high sensitivity, low background, high S/B ratios, miniaturisation into 1536-well plate, cost effective, optimal versatility in assay design and can identify low affinity to high affinity interactions. However, AlphaScreen also has several disadvantages. The assay is sensitive to intense light or long exposure to ambient light. That is why it is important to protect beads from light by using light levels of less than 100 Lux or to use green filters. In addition, all incubations should be performed in the dark. Another disadvantage is that experiment can be limited to a single read because of photo bleaching of donor beads. Additionally, AlphaScreen is

not compatible with all plate readers, this is why it may be more limited than other luminescent technologies (Eglen *et al.*, 2008).
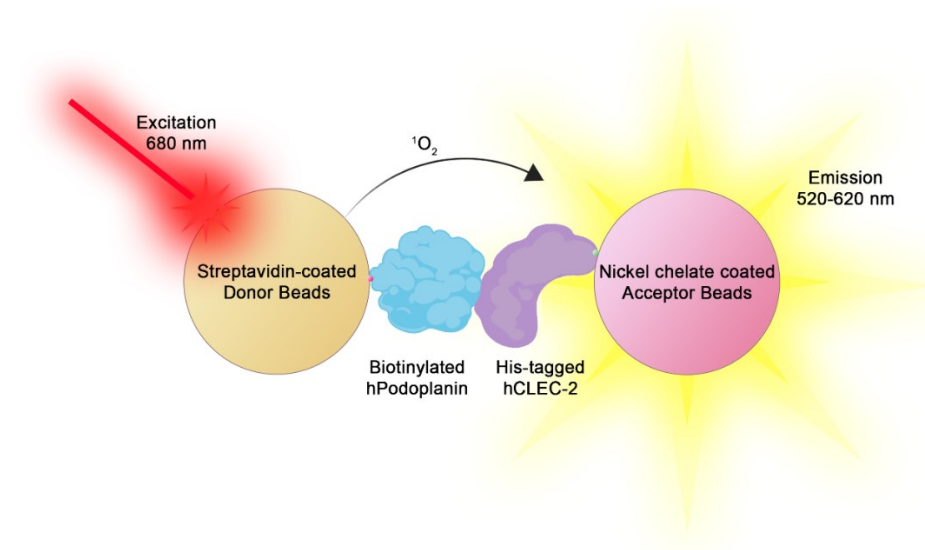
Figure 4.6. AlphaScreen principle.

Binding of biotinylated hPodoplanin to his-tagged hCLEC-2 brings streptavidin-coated donor and nickel chelate-coated acceptor beads into close proximity. Upon illumination of donor beads at 680 nm, an ambient oxygen is converted to an excited O_2 form (singlet oxygen), which leads to energy transfer to the acceptor beads, and a fluorescent signal between 520–620 nm is produced.

During optimisation of receptor-ligand concentrations for AlphaScreen, there is an observed phenomenon called the 'hooking effect'. It is a common effect in many detection assays involving saturable reagents used to capture specific molecules. In contrast to saturations curves, the curves characteristic for the hooking effect are often bell-shaped, as signal increases with increasing target molecule concentration up to a peak after which they become inhibitory to the signal production. This effect is illustrated in Figure 4.7.
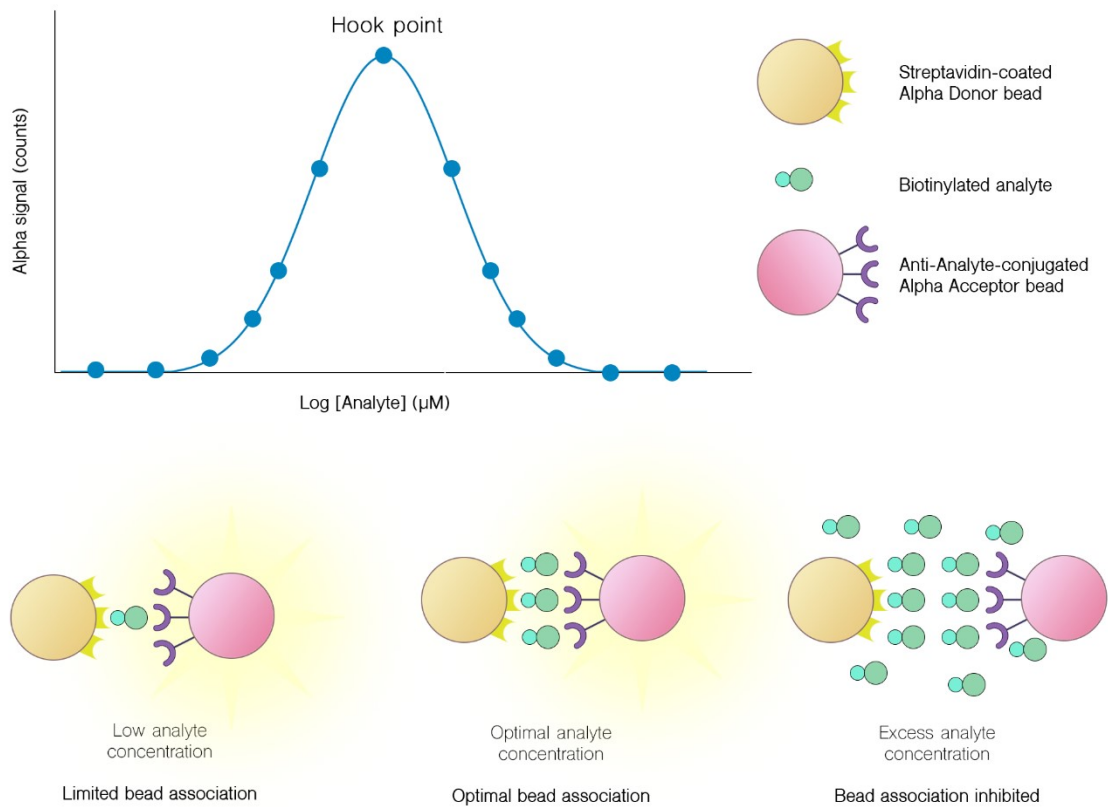
Figure 4.7. Hooking effect.

Over a range of target molecule concentrations, there is a point when the Alpha signal starts to drop. This point is called the hook point. Below the hook point, donor and acceptor molecules are becoming saturated and the signal increases. At the hook point, both molecules are fully saturated and achieve maximum signal. Above the hook point, an excess of molecules oversaturates the beads and become inhibitory to signal production.

The AlphaScreen assay provides an AlphaScreen™ TruHits™ kit to identify compounds which interfere with the assay and results in false positives. These compounds include singlet oxygen quenchers, colour quenchers, light scattering compounds and biotin mimetics. The TruHits kit contains streptavidin donor beads and biotinylated acceptor beads, which bind directly to each other. For the identification of compounds which interfere with the assay, hit compounds are incubate with beads that have been premixed. Examples of singlet oxygen quenchers include azide, ascorbate, and some transition metal ions such as Zn^{2+}, Cu^{2+}, Fe^{2+} and Fe^{3+}. Colour quenchers may absorb either the light at 680 nm, used to excite the donor beads, or the light between 520-620 nm emitted by the acceptor beads. These compounds are usually blue/green or blue, e.g., malachite green and dextran blue. Interference by light scattering compounds may be produced by insoluble compound aggregates, diffracting light at the excitation and/or emission wavelengths. The mechanism to identify biotin mimetics is different. Here, hit compounds are first incubated with streptavidin donor beads. Any compounds which possess biotin-like binding properties bind to the streptavidin and prevent the pairing of the donor and acceptor beads, resulting in a reduced Alpha signal (Baell and Holloway, 2010).

4.2. Aims

CLEC-2 is a good target for novel anti-platelet drugs having therapeutic effects on arterial/venous thrombosis and cancer, that is why the aims of this chapter are:

- To design, develop and optimise a biochemical assay using recombinant CLEC-2 and podoplanin which may be used in a high-throughput screen.

- To perform a primary high-throughput screen with the Pivot Park Screening Centre library to identify novel small molecule inhibitors which disrupt the CLEC-2-podoplanin interaction.

- To perform a secondary screen with the detection of false positives, dose-response study, and cytotoxicity assay to determinate whether any of the compounds identified in the HTS are suitable for lead development.

The first two aims were the focus of the work during 2-month secondment in the Pivot Park Screening Centre in the Netherlands. The last aim was focused on during 1-year visit at University of Santiago de Compostela in Spain.

4.3. Results

4.3.1. Optimisation of the AlphaScreen assay using recombinant CLEC-2 and podoplanin

4.3.1.1. CLEC-2 and podoplanin concentrations selection

Prior to the HTS assay, the interaction of hCLEC-2 with hPodoplanin was established in the AlphaScreen™ assay by using a monobiotinylated human Podoplanin-rFc (used previously in section 3.3.2.1) which binds to Streptavidin conjugated donor beads or Protein A acceptor beads and a commercial recombinant human CLEC-2 fused with a Histidine tag which binds to nickel-chelate donor or acceptor beads.

Firstly, a range of concentrations between 0.3-600 nM of recombinant human CLEC-2 and human podoplanin was tested with different combinations of beads: streptavidin donor beads plus nickel chelate acceptor beads or nickel chelate donor beads plus protein A acceptor beads in a 1536-well format.

In the first combination of the beads (streptavidin donor beads plus nickel chelate acceptor beads) the range of the concentration where a high Alpha screen signal was observed was between 100-600 nM of CLEC-2 and 1-100 nM of podoplanin (Figure 4.8A). In the second combination of the beads (nickel chelate donor beads plus protein A acceptor beads) the range of concentrations with the highest Alpha signal was between 300-600 nM of CLEC-2 and 1-30 nM of podoplanin (Figure 4.8C). In both cases a characteristic phenomenon for the AlphaScreen assay, called 'hooking effect', was observed where too high concentration of the proteins may have inhibitory effect for the signal production, whereas too low concentration may be not enough to produce any signal (Figure 4.8 B and D).
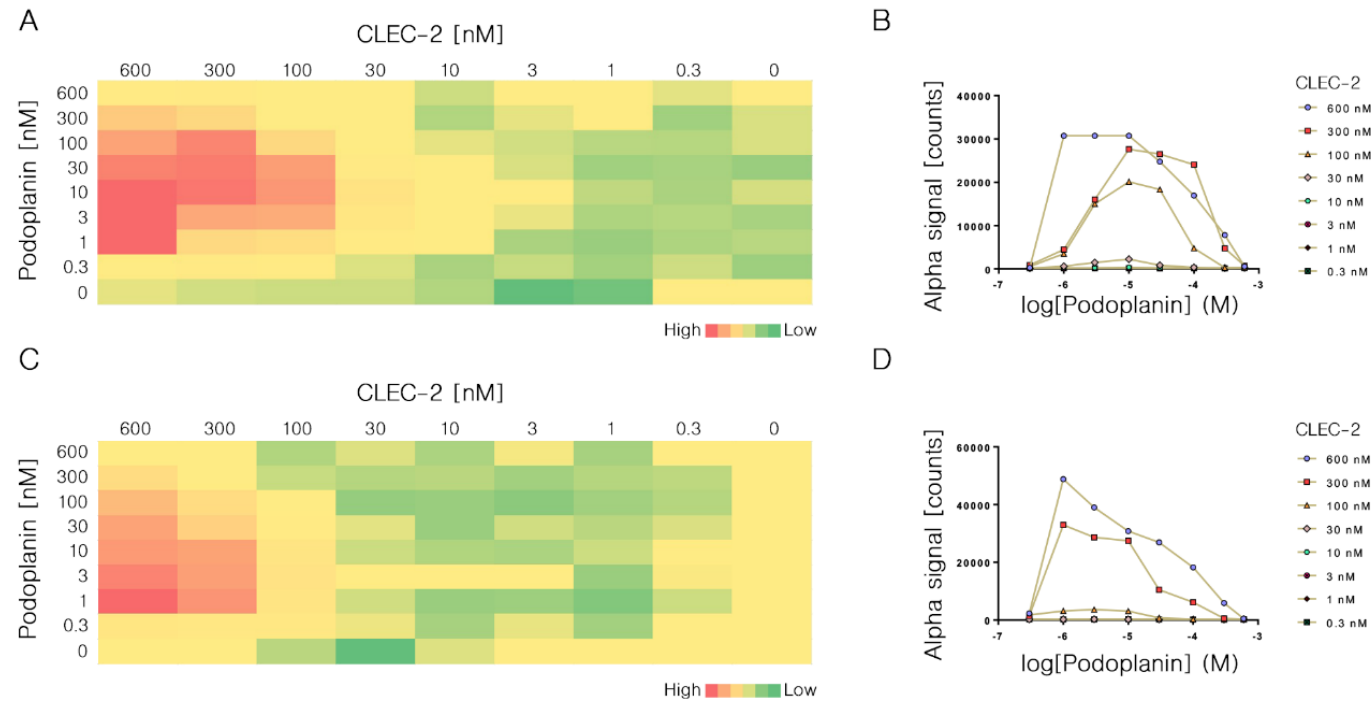
Figure 4.8. Optimisation of the concentration of human CLEC-2 and human podoplanin for an AlphaScreen assay.

The range of concentrations (0.3-600 nM) of recombinant human CLEC-2 and human podoplanin were tested in two bead configurations:

streptavidin donor beads plus nickel chelate acceptor (A, B) and nickel chelate donor beads plus protein A acceptor beads (C,D). The signals

from the wells are represented by a heat map, with red representing the highest signal and green the lowest (A, C), or by the saturation curves (B,

D). The results are representative of 1 experiment.

Knowing the optimal range of concentrations for human CLEC-2 and human podoplanin, the next step was to test a narrower range of concentrations for both proteins. Additionally, this has been done only for the first combination of the beads as it required less of the commercial recombinant CLEC-2.

Briefly, the range of concentrations for human CLEC-2 (25-300 nM) and podoplanin (5-30 nM) was tested again using streptavidin donor beads and nickel chelate acceptor beads. The optimal concentration for CLEC-2 was in the range of 100-300 nM, whereas for podoplanin was in the range of 15-30 nM (Figure 4.9). To balance the available recombinant material against Alpha signal strength, a 100 nM of human CLEC-2 and 25 nM of human podoplanin was taken forward for the primary HTS.
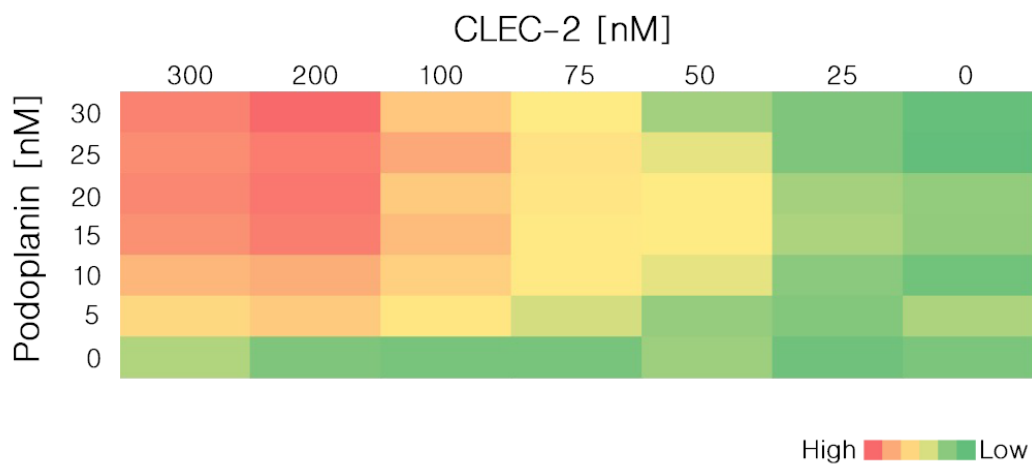
Figure 4.9. Representative results to determine the optimal concentration of hCLEC-2 and hPodoplanin for a primary AlphaScreen assay.

A range of concentrations of both proteins were tested in a 1536-well plate. The signals from the wells are represented by a heat map, with red representing the highest signal and green the lowest. The result is representative of 1 experiment.

4.3.1.2. Identifying a positive control which inhibits Alpha signal production.

Identification of a positive control of inhibition is crucial for HTS. Having established optimal concentrations of human CLEC-2 and podoplanin, the next step was to find an inhibitor which disrupts the interaction of these two proteins in the AlphaScreen assay. Two potential inhibitors were used: AYP1, which is a mouse monoclonal antibody specific to the human CLEC-2 (Gitz *et al.*, 2014), and cobalt hematoporphyrin, which has been identified as a small molecule inhibitor of the CLEC-2-podoplanin interaction (Tsukiji *et al.*, 2018).

A range of AYP1 concentrations (0.78-25 µg/ml) and Co-HP (0.5-20 µM) were incubated for 30 minutes with the optimised concentrations of human CLEC-2 (100 nM) and human podoplanin (25 nM) using the combination of streptavidin donor beads and nickel chelate acceptor beads. Figure 4.10A shows that AYP1 inhibits CLEC-2-podoplanin interaction dose dependently, achieving inhibition more than 80%, when incubated with at least 12.5 µg/ml of AYP1. Similarly to AYP1, Co-HP inhibited the interaction dose-dependently, achieving almost 80% of inhibition when 20 µM of Co-HP was used. For the further assays, 20 µM of Co-HP was selected as a positive control of inhibition.
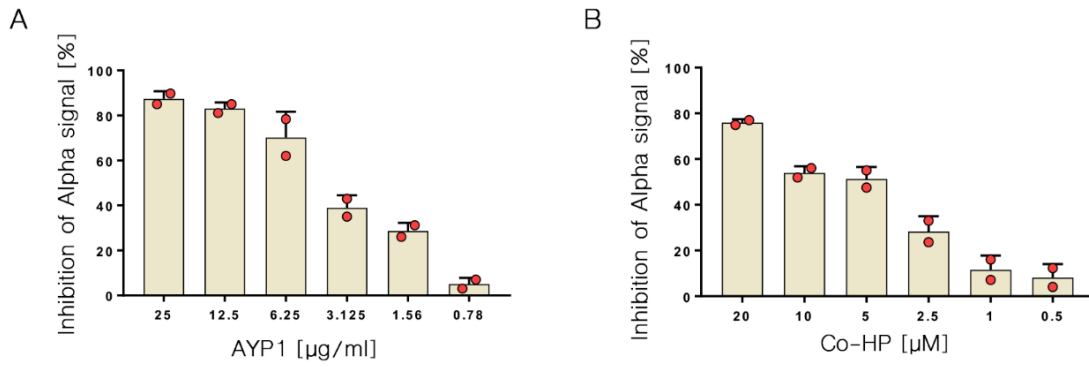
Figure 4.10. AYP1 and Co-HP inhibit the interaction between CLEC-2 and podoplanin.

A range of AYP1 (A) and Co-HP (B) concentrations were tested in an established AlphaScreen assay to determine their inhibition of the CLEC-2-podolanin interaction. Data are shown as mean ± SD and are representative of two independent experiments.

4.3.2. Primary high-throughput screening with the compound library

Following optimisation, the next step of the HTS process was to check the Z'-factor in two columns of 1536-well plate to investigate the separation band and data variation between control wells. The Z' was higher than 0.5, that is why the screen could be performed (data not shown). Next, the primary screen against the human CLEC-2-podoplanin interaction has been performed. The primary screen was carried out under the optimised conditions (100 nM of human CLEC-2 and 25 nM of human podoplanin) in 1536-well plates. As a positive control, a known inhibitor, 20 µM Co-HP was used. The screen was performed with a Pivot Park Screening Centre library of 18,476 small molecule compounds (Prestwick set and SPECS libraries) at concentration of 5 µM. The Prestwick Chemical Library is composed of 1520 FDA-approved & EMA-approved drugs. It was selected due it's chemical and pharmacological diversity since the compounds in this library have been addressed to more than 600 targets. The SPECS library is composed of a variety of novel small molecules, which have not been described before.

During the screen, all plates showed an S/B of 8.49 or higher and the Z' values above 0.58, therefore all plates were validated. A representative heat map of one of the screening plates is shown in Figure 4.11.

14 from 18,476 of compounds showed inhibition rates higher than 50% at 5 µM. 5 of them (Table 4.2) came from a Prestwick Chemical Library, which contains FDA- and EMA-approved drugs, whereas the other 9 compounds (Table 4.3) are novel small molecules. These novel compounds were named MAS 1 to 9.

Compounds identified using a Pivot Park Screening Centre library were further investigated. Biotin was excluded because it binds directly to the streptavidin donor

beads so does not disrupt the CLEC-2-podoplanin interaction and represents a false positive. Mitoxantrone is identified in most screening assays, inhibiting most biological interactions. This compound has three characteristic aromatic rings which are also found in Anthralin and Clofazimine. This suggests that they may have a false-positive inhibition effect. Lorglumide sodium salt has a region similar to biotin, which may affect the Alpha signal.

For the secondary screen, only 9 of the novel small molecules were taken forward.
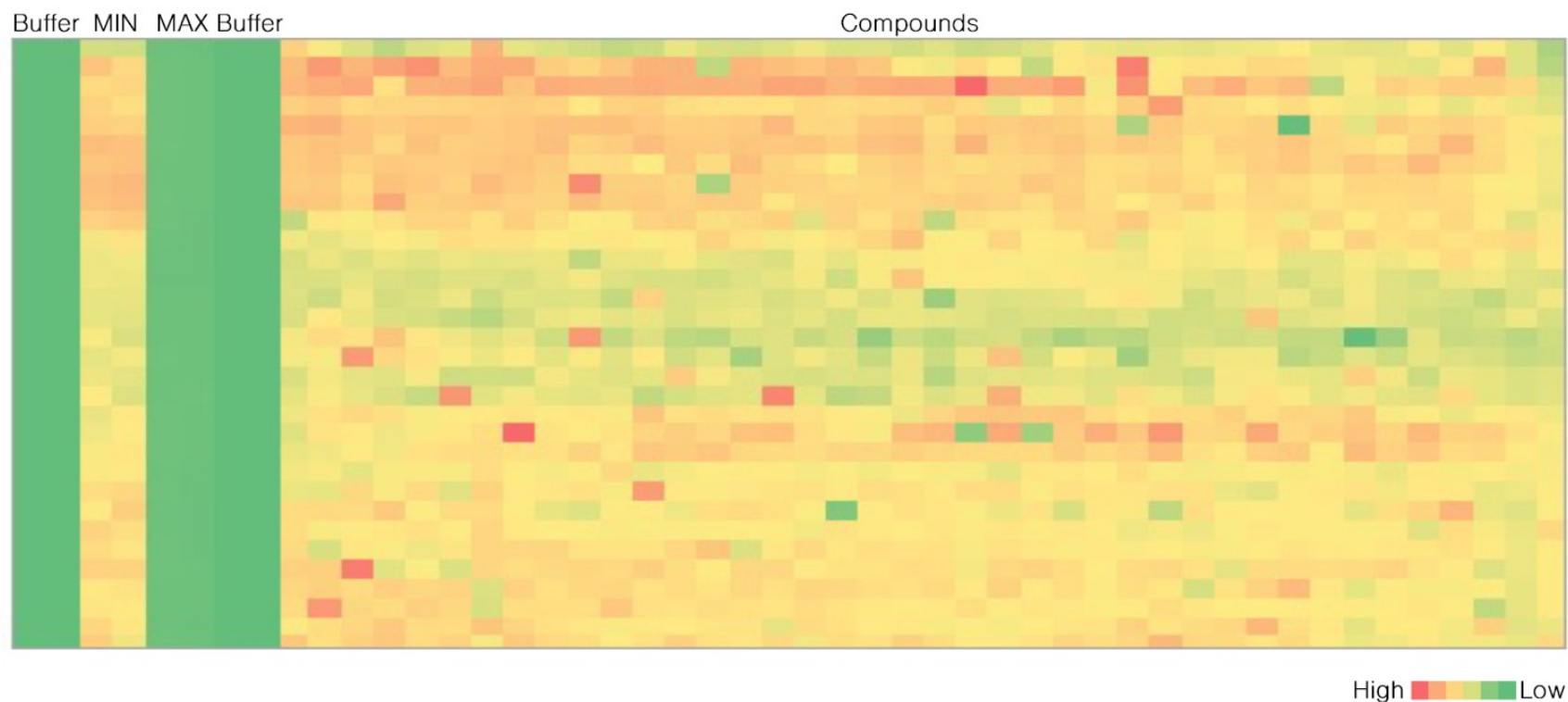
Figure 4.11. Representative 1536-well plate heat map of performed AlphaScreen using Pivot Park Screening Centre library.

Wells named Buffer (n=128, column 1, 2, 7 and 8) describe background control wells with Reaction Buffer and DMSO only. Min (n=64, column 3 and 4) describes wells with the minimum inhibition effect, where the signal came from incubation of CLEC-2 with podoplanin and 0.25% DMSO. Max (n=64, column 5 and 6) describes wells with the maximum inhibition effect, showing inhibition of CLEC-2-podoplanin interaction

using 20 µM Co-HP. Rest of the wells (named Compounds; n=1280, columns 9-48) show the effect of different compounds from PPSC library on CLEC-2-podoplanin interaction. The signals from the wells are represented by a heat map, with red representing the highest signal and green the lowest. The greater the green signal the greater the inhibitory effect. The results are representative of one plate from 18 plates used to perform a screen,

Table 4.2. List of commercially known compounds obtained from high-throughput screening with the Pivot Park Screening Centre library.
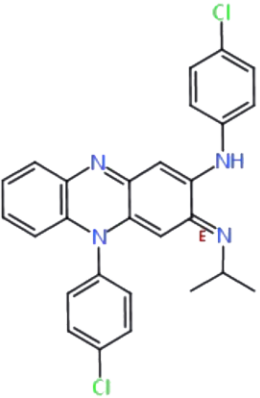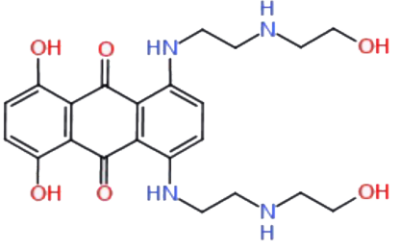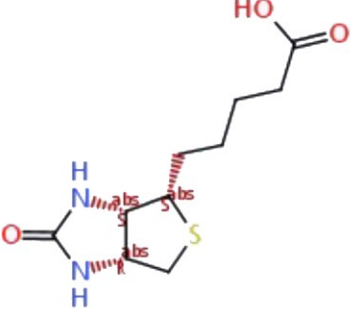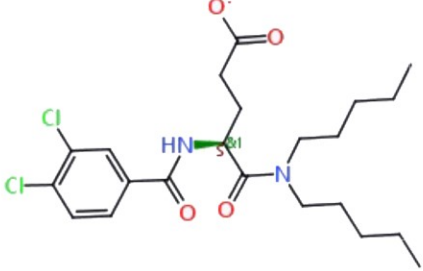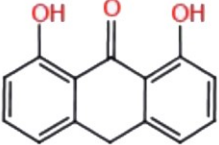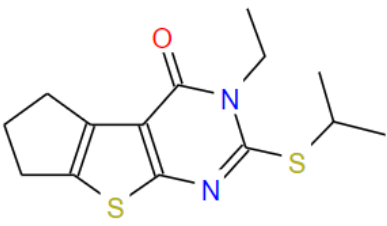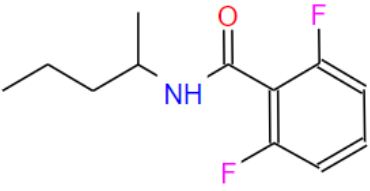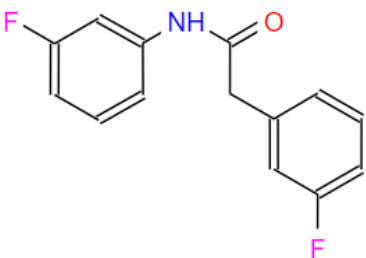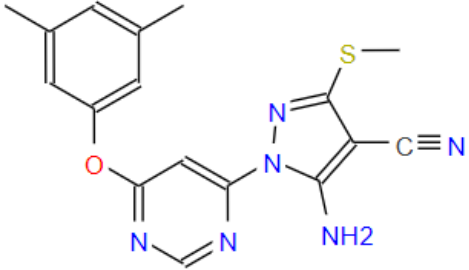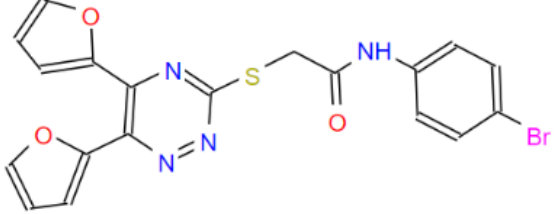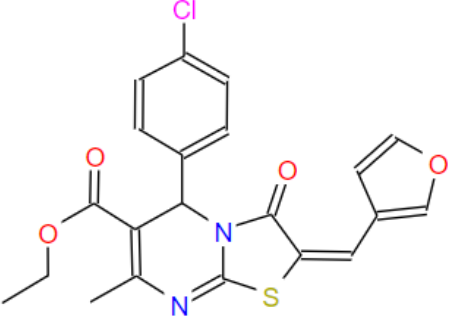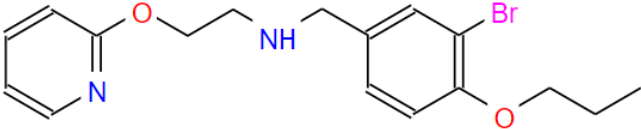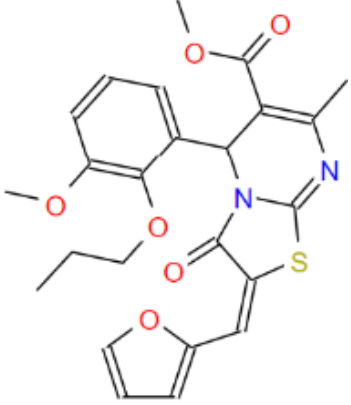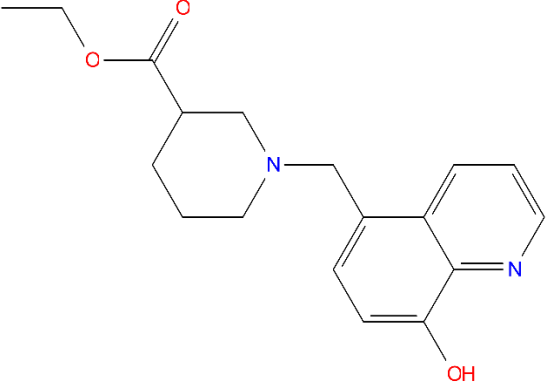
Name	Structure	Inhibition effect [%]
Clofazimine		84
Mitoxantrone dihydrochloride		86
Biotin		104
Lorglumide sodium salt		78
Anthralin		105

Table 4.3. List of novel small-molecule compounds obtained from high-throughput screening with the Pivot Park Screening Centre library.

Name	Structure	Inhibition effect [%]
MAS1		89
MAS2		74
MAS3		91
MAS4		80
MAS5		75

MAS6		64
MAS7		105
MAS8		57
MAS9		92

4.3.3. Lead selection

4.3.3.1. Secondary screening with the identified hits

To confirm the inhibitory effect of the identified compounds, 9 of them (MAS1-9) were run on a re-test of the primary assay at 10 µM and 20 µM. Only two compounds, MAS4 and MAS9, passed a re-test showing a significant inhibitory effect (60.8% at 10 µM and 83.0% at 20 µM for MAS4 and 59.6% at 10 µM and 80.9% at 20 µM for MAS9) on the human CLEC-2 to human podoplanin interaction (Table 4.4).

Table 4.4. Re-test of the primary screening assay for MAS1-9 indicating the percent of inhibition on CLEC-2-podoplanin interaction (N=1)

Compound name	Compound concentration	Inhibition [%]
MAS1	10 µM	0
	20 µM	5.8
MAS2	10 µM	0
	20 µM	0
MAS3	10 µM	0
	20 µM	0
MAS4	10 µM	60.8
	20 µM	83.0
MAS5	10 µM	0
	20 µM	0
MAS6	10 µM	14.7
	20 µM	28
MAS7	10 µM	0
	20 µM	0
MAS8	10 µM	20.9
	20 µM	33.9
MAS9	10 µM	59.6
	20 µM	80.9

4.3.2.2. Identifying false-positive hits

The next step was to identify compounds which interfere with AlphaScreen assay. This was achieved using an AlphaScreen TruHits assay (described in section 4.1.2). The compounds have been tested at 5 μM concentration.

To identify singlet oxygen quenchers, colour quenchers, or light scattering agents, streptavidin donor beads and biotinylated acceptor beads were pre-incubated together prior to the addition of the compounds to the assay wells. A drop in signal is an indication that compound interferes with the assay. A signal lower than the average of the control wells by more than two standard deviations indicates an interfering compound. For the control (100%), the standard deviation is 6.3%. Therefore, a signal lower than 87.4% indicates false-positive compound. Compounds, MAS5, MAS6 and MAS8, give signals of 82.3%, 70.0% and 1.9% respectively, suggesting that these compounds interfere with the Alpha signal leading to false positives. The rest of the compounds do not interfere with Alpha signal (Table 4.5).

To identify biotin mimetics, streptavidin donor beads were pre-incubated with the compounds, prior to adding the biotinylated acceptor beads. Biotin mimetic compounds will bind to the streptavidin and generate a signal lose. A signal lower than the average of control wells by more than two standard deviations indicates a biotin mimetic. MAS4 and MAS9, the two compounds which passed the secondary screen, where tested for being biotin mimetics. Both pass the test, suggesting that they are not biotin mimetics (Table 4.6).

Table 4.5. AlphaScreen™ TruHits™ assay for MAS1-9 indicating the compounds which interfere with AlphaScreen assay.

	MAS1	MAS2	MAS3	MAS4	MAS5	MAS6	MAS7	MAS8	MAS9	Control
Signal [%]	103.9	97.1	114.8	92.5	82.3	70.0	96.7	1.9	98.1	100
Standard deviation [%]	-	-	-	-	-	-	-			6.3

A signal lower than 87.4% indicates a false-positive compound which interferes with the Alpha signal. These are highlighted in orange.

Compounds which do not interfere with the signal are highlighted in green.

Table 4.6. AlphaScreen™ TruHits™ assay for MAS4 and MAS9 indicating the biotin mimetics.

	MAS4	MAS9	Control
Signal [%]	105.6	79.9	100
Standard deviation [%]	-	-	11.3

A signal lower than 77.4% indicates a false-positive compound which interferes with the Alpha signal. Compounds which do not interfere with

the signal are highlighted in green.

4.3.3.2. Dose-response curve

One of the last steps of a high-throughput screen is a dose-response study, which involves testing the identified compounds using an AlphaScreen assay over a range of concentrations. This allows the determination of an IC_{50} value, which is the concentration of the compound that inhibits 50% of the Alpha signal.

For the test, MAS4 and MAS9 with variable concentrations ranging from 160 µM to 0.3125 µM were incubated with biotinylated human podoplanin and his-tagged human CLEC-2, followed by the subsequent addition of acceptor and donor beads and the IC_{50} values determination (Figure 4.12). The data generated from the graph showed that an IC_{50} value for MAS4 was 5.354 µM, whereas for MAS9 was 4.508 µM.
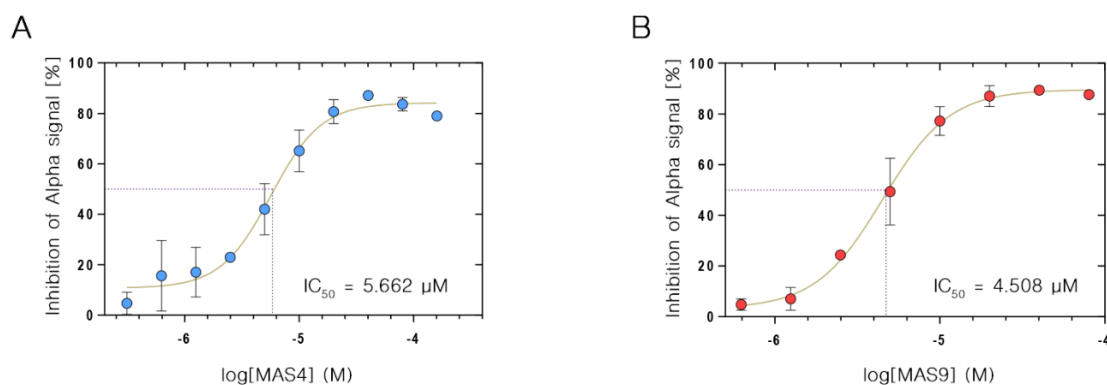
Figure 4.12. Dose-response curves for MAS4 and MAS9 generated from AlphaScreen assay at different concentration.

A range of concentrations (160 µM-0.3125 µM) of MAS4 (A) or MAS9 (B) were tested in an AlphaScreen assay to determinate their IC_{50} values. Data are shown as mean ± SD and are representative of three independent experiments.

4.3.3.3. Cytotoxicity assay

Only MAS9 was taken forward as MAS4 precipitated in different types of buffers at different pH. To evaluate the potential toxicity of the identified compound on platelets, a cell viability flow cytometry assay based on Calcein-AM labelling was performed. For this, the platelets were incubated in the presence of MAS9 at the different concentrations (5-30 µM) or their diluent (DMSO 0.3% (v/v)). As a positive control, a low concentration of Triton X-100 was used. The percentage of non-viable cells was calculated as the percentage of negative events for the Calcein-AM labelling in Q1, registered by flow cytometer (Figure 4.13).

MAS9 in a range 5-30 µM, as well as DMSO control did not affect platelet viability, whereas Triton X-100 killed the whole population of platelets.
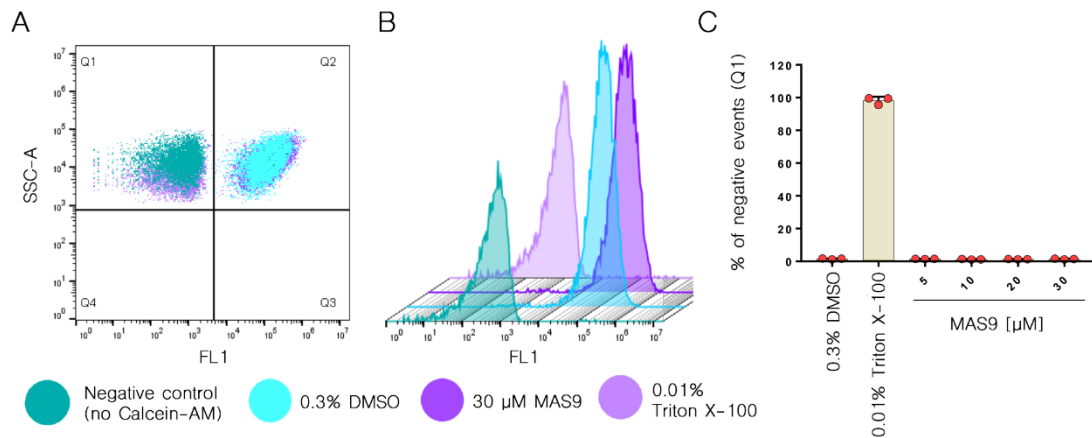
Figure 4.13. Platelet viability after treatment with MAS9 at a range of concentrations.

(A) Representative flow cytometry graph of SSC/FL-1 dot plot. The positive platelet population for Calcein-AM is in Q2. Triton-X100 acts as a positive control of cytotoxicity. (B) Representative histogram, showing the number of events with corresponding fluorescence in channel FL-1. (C) Percentage of non-viable platelets after treatment with MAS9, DMSO and Triton X-100. Data are shown as mean ± SD and are representative of three independent experiments.

4.4. Discussion

This aim of this chapter was to perform a high-throughput screen using a Pivot Park Screening Centre library to find novel small molecule inhibitors of the CLEC-2-podoplanin interaction. Firstly, the AlphaScreen assay was developed and optimised using recombinant human CLEC-2 and podoplanin. Secondly, a positive control of inhibition of the Alpha signal was identified. Thirdly, a HTS was performed using 18,476 small molecules. Finally, a secondary screen, false-positive hits identification and cytotoxicity assay were performed, and one novel small molecule (MAS9) was identified as a starting point of the lead selection. The structure of this compound may require further development.

The AlphaScreen assay was developed using recombinant human CLEC-2 fused with a histidine tag and monobiotinylated human podoplanin-rFc. Figure 4.8. shows that over a range of concentrations between 0.3 and 600 nM for both proteins, the hooking effect, a phenomenon seen in AlphaScreen assays, can be observed. This phenomenon is not limited only to AlphaScreen assay and has also been observed in many sandwich immunoassays (Hoofnagle and Wener, 2009; Rey *et al.*, 2017; Ross *et al.*, 2020).

Based on the results from the first experiment, a narrower range of concentrations (25-300 nM for CLEC-2 and 5-30 nM for podoplanin) were selected and tested again in the AlphaScreen assay. The optimal concentrations for use in the primary HTS were identified as 100 nM for human CLEC-2 and 25 nM for human podoplanin (Figure 4.9). A higher Alpha signal was observed when 200 nM and 300 nM of CLEC-2 were used, however, the amount of recombinant CLEC-2 was limited. Nevertheless, 100 nM of CLEC-2 achieved a sufficient Alpha signal to be used in the screen, and this concentration allowed more compounds to be tested in a primary screen.

As a positive control of inhibition for the interaction between CLEC-2 and podoplanin in the AlphaScreen assay, two molecules were considered: a small molecule identified by Tsukiji et al. – cobalt-hematoporphyrin, and monoclonal antibody to human CLEC-2 – AYP1. Tsukiji et al. showed that a 1.53 µM concentration of Co-HP completely inhibits rhodocytin-induced human and mouse platelet aggregation (Tsukiji *et al.*, 2018). Additionally, Watanabe et al. demonstrated in a pull-down-based inhibitory compound screening system for the interaction between human CLEC-2 and podoplanin, that Co-HP inhibits the interaction of 70% at 20 µM (Watanabe *et al.*, 2019). Regarding AYP1, it has been shown that AYP1 blocks platelet activation stimulated by rhodocytin and podoplanin (Gitz *et al.*, 2014). In this study, a range of concentrations of Co-HP and AYP1 have been tested in the AlphaScreen assay to see whether these molecules can inhibit the production of Alpha signal, indicating inhibition of the CLEC-2 and podoplanin interaction. Figure 4.10. shows that Co-HP (0.5-20 µM) and AYP1 (0.78-25 µg/ml) dose-dependently inhibit production of Alpha signal. As a positive control in the primary AlphaScreen, a Co-HP at a concentration of 20 µM was selected.

A primary screen was performed using 18,476 small molecule inhibitors from a Pivot Park Screening Centre library at concentrations of 5 µM, using the optimised AlphaScreen assay in a 1536-well plate format. The most important parameter to validate the screening is a Z', which takes into account the data variation and the dynamic range of the screen. An excellent assay is considered when Z' $\geq$ 0.5 (Zhang *et al.*, 1999). During the screen all plates showed Z' values above 0.58, therefore all plates were validated (Figure 4.11). From 18,476 compounds, 14 of them showed inhibition rates higher than 50%. That gives a 0.075% hit rate, which is typical from experimental HTS, with hit rates most often ranging between 0.01% and 0.14% (Zhu *et al.*, 2013).

The identified compounds belong to the two groups: FDA- and EMA-approved drugs (Table 4.2) and novel small molecules (Table 4.3).

For the secondary screen only 9 of the 14 compounds were taken forward. These 9 compounds have been named as MAS1-MAS9. The 5 compounds from the Prestwick Chemical Library were discarded due to their chemical structure being similar to biotin or they had a characteristic structure which inhibits most biological interactions and appear as a hit in most HTS experiments (David *et al.*, 2019). MAS1-9 were run on re-test at 10 µM and 20 µM. Only MAS4 and MAS9 showed a significant inhibition effect, and these two compounds were further characterised.

In parallel to the secondary screening, an AlphaScreen TruHits assay was used to identify compounds which interfere with the AlphaScreen assay. This assay allows to identify singlet oxygen quenchers, colour quenchers, light scattering compounds and biotin mimetics. Neither MAS4 nor MAS9 were identified as false positive compounds (Table 4.5 and Table 4.6).

A dose response study allowed the IC_{50} values for MAS4 and MAS9 to be determined. These values were 5.354 µM and 4.508 µM, respectively (Figure 4.12). The IC_{50} values give a starting point for compound evaluation in biological assays.

During the preparation of working solutions of MAS4, it was noticed that the compound precipitated in different types of buffers at different pH (data not shown). It is common that many small molecules can form aggregates which interfere with protein-protein interactions and give a false positive inhibition effect. It has been demonstrated by McGovern et al., who showed that 35 from 45 tested diverse screening hits were inhibited the signal in β-lactamase assay, due the formation of 30-400 nm diameter particles, which can be detected using dynamic light scattering and

transmission electron microscopy (McGovern *et al.*, 2002). As MAS4 precipitated in a range of different buffers, it was discarded from the hits list.

The cytotoxicity study showed that MAS9 is not toxic for platelets up to 30 μM. Taking all results together, MAS9 is a promising small molecule inhibitor of the human CLEC-2-podoplanin interaction, which is not toxic for platelets. However, the effect of this compound on receptor selectivity and platelet function must be characterised.

4.5. Conclusions

HTS gives an opportunity to find novel inhibitors of the identified target molecules. The work described in this chapter involved a development and optimisation of an AlphaScreen assay that was suitable for high-throughput screening to identify inhibitors of the human CLEC-2 podoplanin interaction. It was performed using recombinant human CLEC-2 and human podoplanin in 1536-well plates. The developed assay was used to screen a total of 18,476 small molecules from the Pivot Park Screening Centre library. 14 identified compounds were subjected to further experimentation. One of the small molecules, MAS9, passed a secondary screen and has been identified as a positive lead hit with no platelet cytotoxicity (Figure 4.14).

MAS9 may be a promising inhibitor of the human CLEC-2-podoplanin interaction having therapeutic effects on diseases, including cancer. The compound has been further characterised in biological assays described in the next chapter.
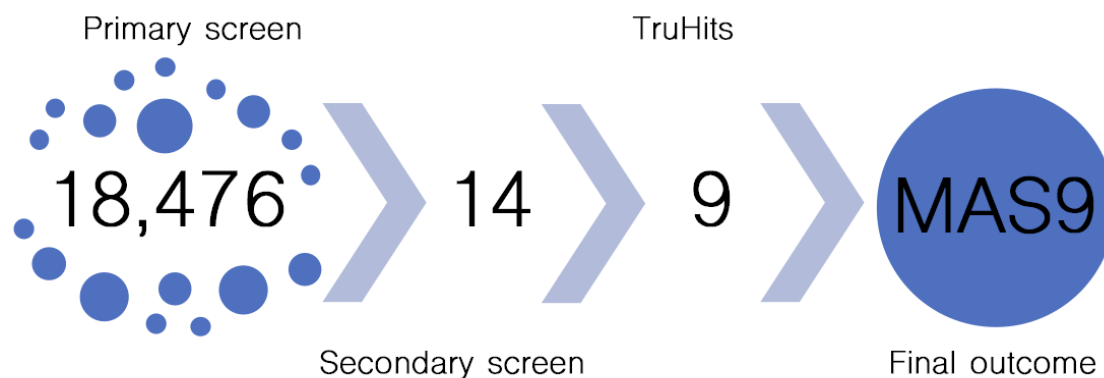
Figure 4.14. A CLEC-2-podoplanin small molecule inhibitor identification process outcome.

HTS was performed using 18,476 small molecules. A secondary screen, false-positive hits identification and cytotoxicity assays resulted in identification of one novel small molecule, MAS9.

Chapter 5

Characterisation of MAS9, a novel

small molecule inhibitor of the human

CLEC-2-podoplanin interaction.

5.1. Introduction

MAS9 has been identified in a HTS as a potential small molecule inhibitor of the CLEC-2-podoplanin interaction. The chemical name of MAS9 is ethyl 1-[(8-hydroxy-5-quinolinyl)methyl]-3-piperidinecarboxylate. It fulfils the criteria of a drug-like compound described by Lipinski's 'rule of 5'. It has a molecular weight less than 500 Da – it is 314.38 Da; a partition coefficient (logP) less than 5 – it is 2.73; less than five H-bond donors – it has 1; and less than 10 H-bond acceptors – it has 4. Additionally, the cytotoxicity studies performed in the previous chapter showed that MAS9 is not toxic for platelets up to 30 µM. The MAS9 structure and its chemical properties are shown in Figure 5.1.

There are only two known small molecule inhibitors of CLEC-2-podoplanin interaction: 2CP and Co-HP. They have been previously described in section 4.2. CLEC-2 is a good target for novel anti-platelet drugs having therapeutic effects on arterial/venous thrombosis and cancer. MAS9 may have therapeutic potential but needs further characterisation in platelet-based assays.

This chapter presents the characterisation of MAS9, a small molecule inhibitor of the human CLEC-2-podoplanin interaction identified in a high-throughput screen. The characterisation process includes molecular docking, bio-layer interferometry and platelet-based assays.

Formula:	C18 H22 N2 O3
Weight:	314.38 Da
Name:	ethyl 1-[(8-hydroxy-5-quinolinyl) methyl]-3-piperidinecarboxylate
SMILES:	CCOC(=O)C1CCCN(C1)Cc2ccc(O)c3ncccc23
LogP:	2.73
LogS:	-2.24
tPSA:	62.66 Å^2
H-acceptors:	4
H-donors:	1
Rotatable bonds:	5
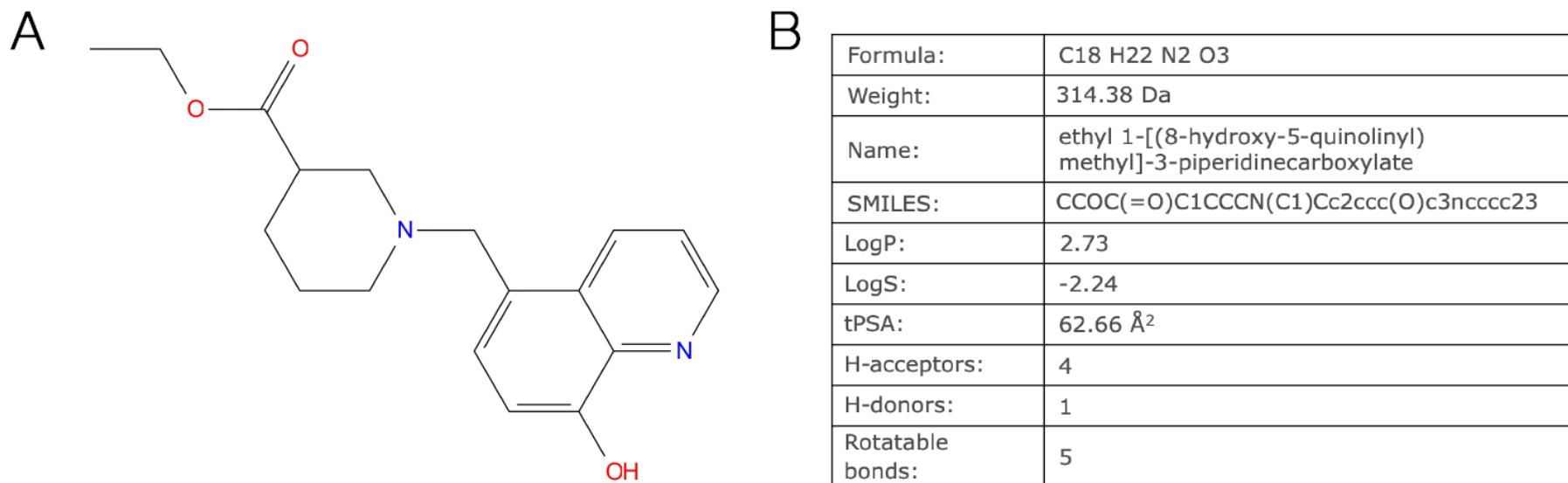
Figure 5.1. MAS9 – identified small molecule inhibitor of the human CLEC-2-podoplanin interaction.

(A) Structure of MAS9. (B) Detailed table of the MAS9 structure. logP (octanol-water partition coefficient) gives an indication of whether a compound can enter a cell or not; LogS is a water solubility; tPSA (topological polar surface area) is measured in square Angström (Å^2), which is a useful parameter for the prediction of drug transport properties; H-acceptors and H-donors are parameters which indicate whether a compound can bind to a receptor site in a biomolecule.

5.1.1. Molecular docking

Molecular docking is a computational method to predict the preferential binding mode (position, conformation, and orientation) of a small molecule ligand within the binding site of the biological target (Mobley and Dill, 2009). To perform a docking study, a high-resolution X-ray, NMR, or homology-modelled structure with known or predicted binding sites is required. To this day (accessed on 20-09-2021), the RCSB Protein Data Bank provides 182,176 biological macromolecular structures. Molecular docking is based on the fitting of a ligand into binding sites of the target by combining and optimising electrostatic, hydrophobic, and steric complementarity and estimating the free energy of the binding using a scoring function (Diller and Merz, 2001). There are few main classes of scoring function: force-field based, clustering and entropy-based, knowledge-based, empirical, and consensus-based (Elokely and Doerksen, 2013).

In this work, Maestro (Schrödinger) was used to perform the molecular docking. It is centred on grid-based ligand docking with energetics (Glide) which uses a hierarchical filter to search for the possible interactions between the ligand and a target receptor. There are four steps to perform docking with Glide: protein preparation, grid generation, ligand preparation and ligand docking.

Protein preparation is the most important step to ensure that the crystal structure of the protein is refined correctly to optimise docking results. It can be done by a Protein Preparation Wizard that optimises hydrogen bonds, adds missing hydrogen atoms, removes steric clashes within the structure, corrects any metal ionisation states and removes water molecules (Schrödinger, 2015).

Grid generation requires some knowledge about the active site of the receptor, or it can be identified by Schrödinger's SiteMap, a function which allows one or more regions

on the receptor to be determined as potential ligand binding site. A grid is represented by two boxes, which designate the active site or ligand binding site. The first box is formed based on the distances from the site point to the receptor surface, whereas the second one is assigned based on the distance from the ligand centre. During the docking process, the ligand conformations will be fitted within the generated grid.

The next step is ligand preparation. During this step, the ligand is prepared by generating possible tautomers and different protonation states, and finally minimised in the field of the receptor using a standard molecular mechanics energy function (OPLS4 force field) in conjunction with a distance-dependent dielectric model.

The last step is ligand docking, where the prepared ligand is docked in different conformations to the target receptor using the previously generated grid. As a result, the different ligand-receptor poses will be generated and scored using a force-field-based scoring function. The force-field parameters consider the contribution of electrostatic potential, van der Waals interactions and solvation effects, and help to simulate the geometry and interactions between the receptor and ligand. The minimised poses of ligand are scored using Schrödinger's GlideScore function (Friesner *et al.*, 2006) and it is described by the equation:

$$GScore = 0.05 \times vdW + 0.15 \times Coul + Lipo + HBond + Metal$$
$$+ Rewards + RotB + Site$$

where vdW is van der Waals energy, Coul – Coulomb energy; Lipo – lipophilic (hydrophobic grid potential); HBond – hydrogen bonding; Metal – metal binding; Rewards – rewards and penalties for various features, such as buried polar groups,

hydrophobic enclosure, correlated hydrogen bonds, amide twists, and so on; RotB -

Penalty for freezing rotatable bonds; Site - Polar interactions in the active site.

5.1.1. Bio-Layer Interferometry

Bio-layer interferometry (BLI) is a label-free technology to study analyte-ligand interactions. It analyses the interference pattern of white light reflected from two surfaces: protein immobilized onto a biosensor tip, and the internal reference layer. It allows the real time detection in a shift in the interference pattern caused by the analyte kept in solution binding to the ligand immobilized onto the biosensor tip. Biosensors are coated with covalently or non-covalently linked biological molecules, such as streptavidin, Ni-NTA, protein A/G, antibodies etc. That allows the measurement in real time the binding specificity, rates of association and dissociation, and finally analyte-ligand affinity and kinetics (Kumaraswamy and Tobias, 2015).

The BLI instrumentation system allows rapid sample analysis of the assay by enabling it to be performed in 96- or 384-well formats and can process up to 8 or 16 samples at the same time, respectively. The instrument used in this thesis was an Octet K2 system (ForteBio Inc.), which detects protein-protein and protein-small molecules interactions, with molecules of at least 150 Da in size. This system allows 2 assays to be performed in parallel in a 96-well format with a final sample volume of 180-220 μl per well. The deck can be heated up to 40˚C with the orbital flow capacity of 400-1500 rpm to adequately mix the analyte samples. Biosensor tips are supplied in an 8×12 format tray, which can be directly placed into an instrument stage. The Octet K2 system allows the analysis of kinetics in a range of 10^1 to 10^7 $M^{-1} s^{-1}$ for association rates (k_a), 10^{-6} to 10^{-1} s^{-1} for dissociation rates (k_d) and 10^{-3} to 10^{-11} M for affinities constant (K_D).

The volume of sample or buffer used for each well of 96-well plate for Octet system is usually 200 μl. Biosensors tips must be pre-hydrated in a buffer for 1 hour before use. The experiment can be designed using the Data Acquisition software prior to starting the experiment. The experiment starts from the immobilization (loading) of a ligand

molecule, such as protein or antibody, on to the surface of the biosensor. Next, the ligand-loaded biosensors are moved into a solution containing the analyte (e.g., protein, antibody, or small molecule) and the analyte association to the ligand is measured. Finally, the biosensors are moved into the wells containing buffer, and the dissociation of the analyte from the ligand is measured. The biosensor regeneration step is optional and depends on the biosensors used in the experiment. The measurements of ligand-loading, the association and dissociation of the analyte are plotted in real time on a graph. The schematic principle of BLI technique is shown in Figure 5.2.

Binding association and dissociation rate constants (k_a and k_d) and the affinity constant (K_D) are determined by fitting the association and dissociation curves using mathematical equations.

$$A + B \underset{k_d}{\overset{k_a}{\rightleftharpoons}} AB$$
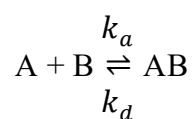
where A represents the ligand, and B is the analyte.

This equation describes a 1:1 binding model, where one ligand molecule interacts with one analyte molecule. The complex AB is formed during the association step and is described as a function of the association constant (k_a), which is expressed in $M^{-1}s^{-1}$. When the biosensor is moved into the well containing buffer, the complex dissociates back to A+B. The dissociation constant (k_d) describes the fraction of complexes decaying per second and is expressed in s^{-1}. The affinity constant (K_D) measures how tightly a ligand binds to its analyte and is described as the ratio of the on-rate and off-rate and is represented in molar units (M):

$$K_D = \frac{[A] \times [B]}{[AB]} = \frac{k_d}{k_a}$$

To calculate the kinetic parameters (k_a and K_D), the concentration of analyte must be known. A k_d is concentration-independent and can be calculated without knowing how much analyte is present.
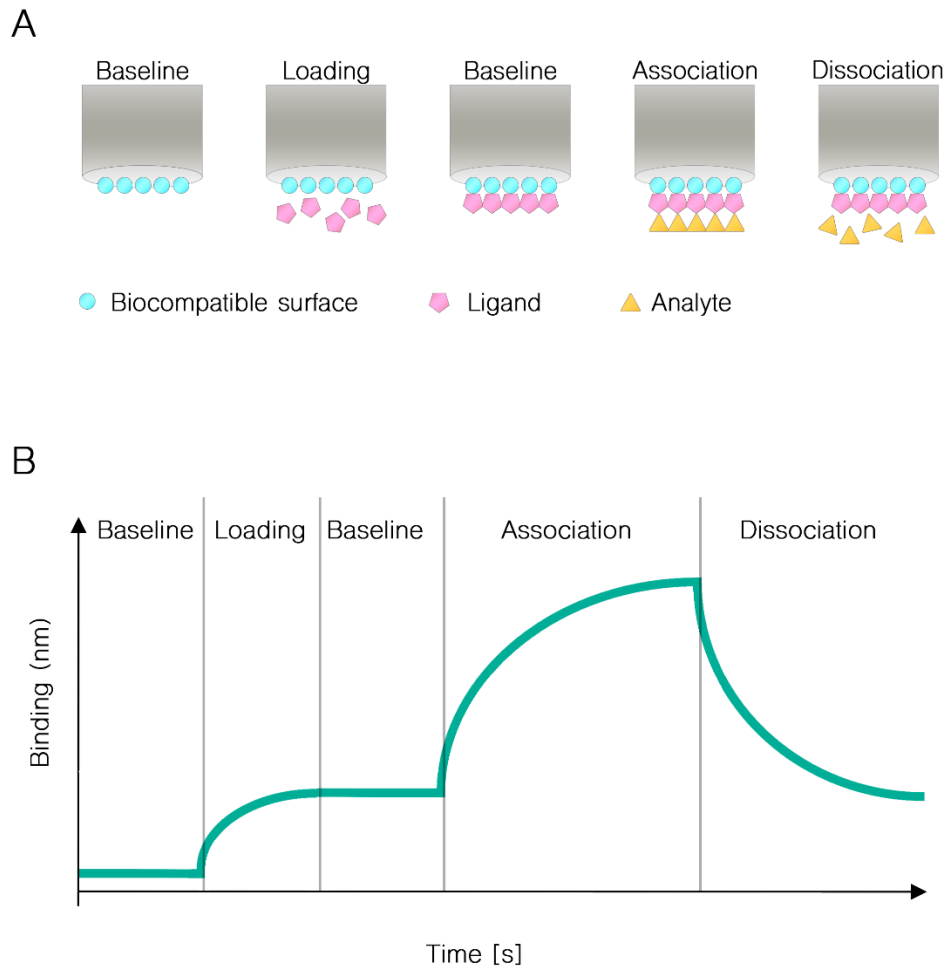
Figure 5.2. Binding kinetic experiment using BLI biosensors.

(A) A ligand is immobilized on the biocompatible surface. After a baseline step, analyte binding starts the association step, followed by a dissociation step in buffer. (B) A typical trace graph showing all steps of the experiment: baseline, loading, association, and dissociation.

5.2. Aims

The aim of this chapter is:

- To predict the preferential binding mode of MAS9 to human CLEC-2.

- To determine the affinity constant of the CLEC-2-MAS9 interaction.

- To investigate the role of MAS9 in CLEC-2-dependent platelet aggregation, activation, adhesion and spreading.

- To investigate the role of MAS9 in CLEC-2-dependent fibrinogen binding and P-selectin exposure.

- To determine the selectivity of MAS9 to CLEC-2 over other platelet receptors, including GPVI, PAR1 and PAR4.

- To use the HDLECs to investigate the role of MAS9 on the platelet adhesion to cells.

5.3. Results

5.3.1. MAS9 binds to CLEC-2 in *in silico* docking

Molecular directed docking has been described in section 5.1.1 and was used to predict the preferential binding mode of MAS9 within the binding sites of the CLEC-2 structure. The software used for this purpose was Maestro Schrödinger (Release 2020-4).

The crystal structure of human CLEC-2 (2C6U) was taken from the RCSB Protein Bank and was subjected to preparation using Protein Preparation Wizard to optimise hydrogen bonds, add missing hydrogen atoms, remove steric clashes within the structure and remove water molecules. The grid was generated by centring it between the common binding sites for podoplanin and rhodocytin with a side length of 5 Å. The MAS9 structure was converted to a 3D structure using the Ligprep module and minimised using a selected force field. The docking was performed using the GLIDE module and the best MAS9 conformations were ranked based on their GLIDE docking scores.

The predicted interaction between CLEC-2 and MAS9 has been shown in Figure 5.3. Computational molecular docking studies showed that MAS9 binds to Arg107, Arg152, Thr153 and Arg157 by hydrogen bonds and creates a noncovalent interaction, called 'Pi-Pi stacking' between an aromatic ring of MAS9 with His154 of CLEC-2 (Figure 5.4). A predicted glide score for this docking pose was -3.576 kcal/mol. The other binding modes (with the lower glide score) showed that MAS9 binds to Arg107 and Arg152 or Arg107 and Arg157 (data not shown). This data suggest that Arg107 is important for MAS9 binding to CLEC-2.

The modelling suggests that MAS9 may bind to 3 of the 4 common binding sites for podoplanin and rhodocytin (Arg107, Arg152, Arg157), one additional site for podoplanin (Thr153) and may interact via Pi-Pi-stacking interaction with one site, which is important for podoplanin binding (His154).

To validate the docking result, the known inhibitor of CLEC-2-podoplanin interaction, 2CP, was used. Chang et al, showed in the molecular docking studies, using Discovery Studio 4.0, that 2CP interacts with residues Asn105, Arg107, Phe116, Arg118 and Arg157 of CLEC-2, which mostly match with the binding sites for podoplanin and rhodocytin (Chang *et al.*, 2015), The molecular docking experiment using Maestro Schrödinger, was performed in the same way as for MAS9. The results showed that 2CP may bind to Arg107, Phe116, Arg118 and Arg152 by hydrogen bonds (Appendix, Figure 8.3), with a glide score of -4.138 kcal/mol. Compared to the results obtained by Chang et al., three residues (Arg107, Phe116 and Arg118) are the same. The difference between the results may be due to the use of different software and parameters selected (not mentioned by authors in the paper).
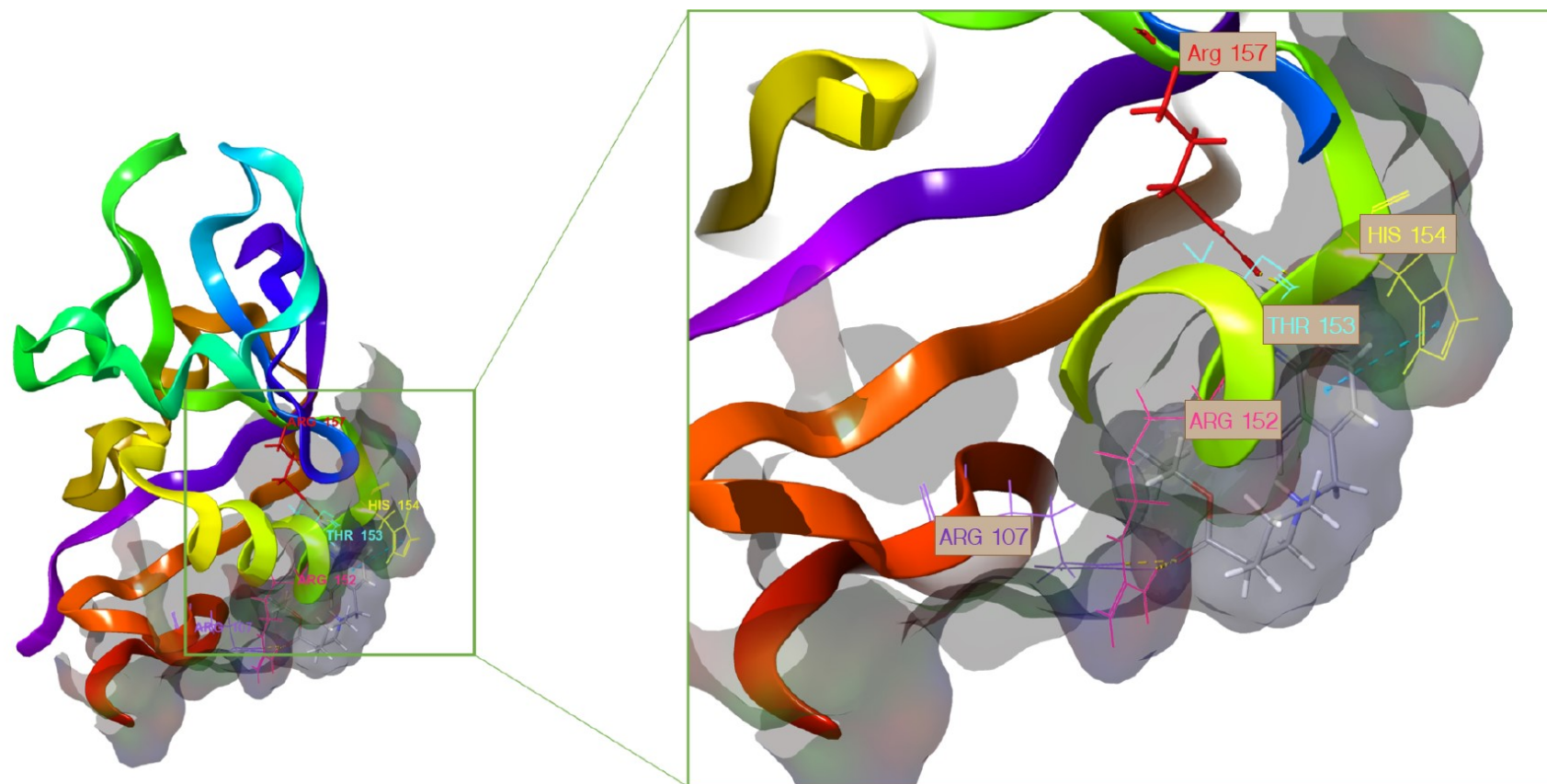
Figure 5.3. 3D visualisation of the binding of MAS9 to the human CLEC-2 structure.

The amino acid residues of CLEC-2 involved in MAS9 binding have been highlighted. Yellow dotted lines represent H-bond, and the blue

dotted lines represent a pi-pi stacking interaction.
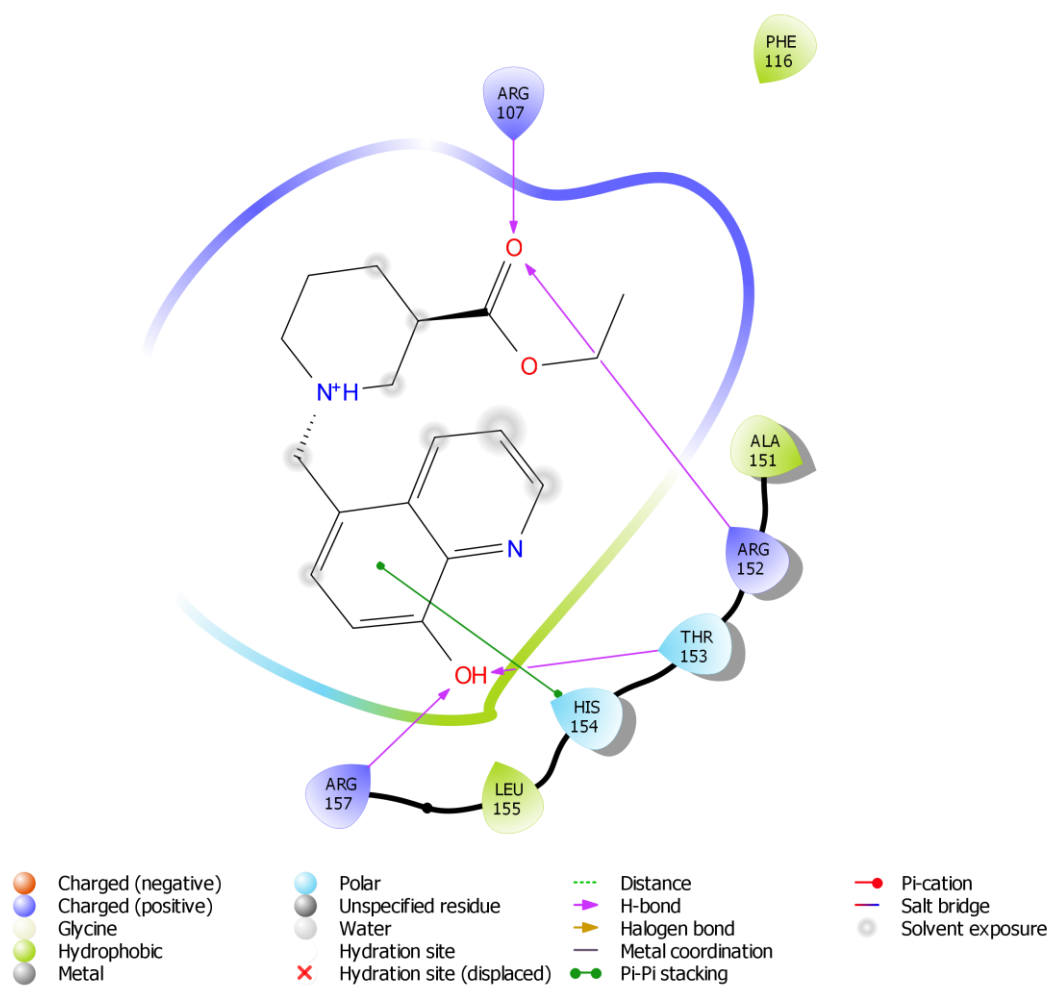
Figure 5.4. 2D diagram of MAS9 binding to CLEC-2.

Interactions of CLEC-2 and MAS9 are shown. MAS9 is shown as stick diagram. H-bonds between the receptor and ligands are shown as purple lines. Pi-Pi stacking interaction is shown as a green line.

5.3.2. Direct interaction of MAS9 with human CLEC-2

The affinity constant of the CLEC-2-MAS9 interaction has been determined using bio-layer interferometry. This approach has been described in section 5.1.2.

2.5 μg/ml recombinant human CLEC-2 containing his-tag was immobilized on Ni-NTA biosensors. Following the loading and baseline steps, the sensors were transferred into wells containing a range of MAS9 concentrations (100, 70, 50, 30, 10 and 1 μM). The association was monitored for 40 s and dissociation for 240 s. Kinetic parameters (k_a and k_d) and affinities (K_D) were calculated from a non-linear global fit of the data between CLEC-2 and MAS9 using the Octet software.

The estimated K_D of the human CLEC-2-MAS9 interaction has been determined as 7.79 $\pm$ 3.5 μM from three independent experiments (Figure 5.5). MAS9 binding to human CLEC-2 was characterised by kinetic rate association (k_a) and dissociation (k_d) constants of $k_a = 2.24 \pm 0.4 \times 10^3$ mol^{-1} s^{-1} and $k_d = 1.62 \pm 0.4 \times 10^{-2}$ s^{-1}.

These data confirm that MAS9 can bind to human CLEC-2 with micromolar affinity constant. However, this data needs to be further validated by using other small molecules (2CP, Co-HP) or CLEC-2 ligands (podoplanin, rhodocytin, hemin) in BLI experiment.
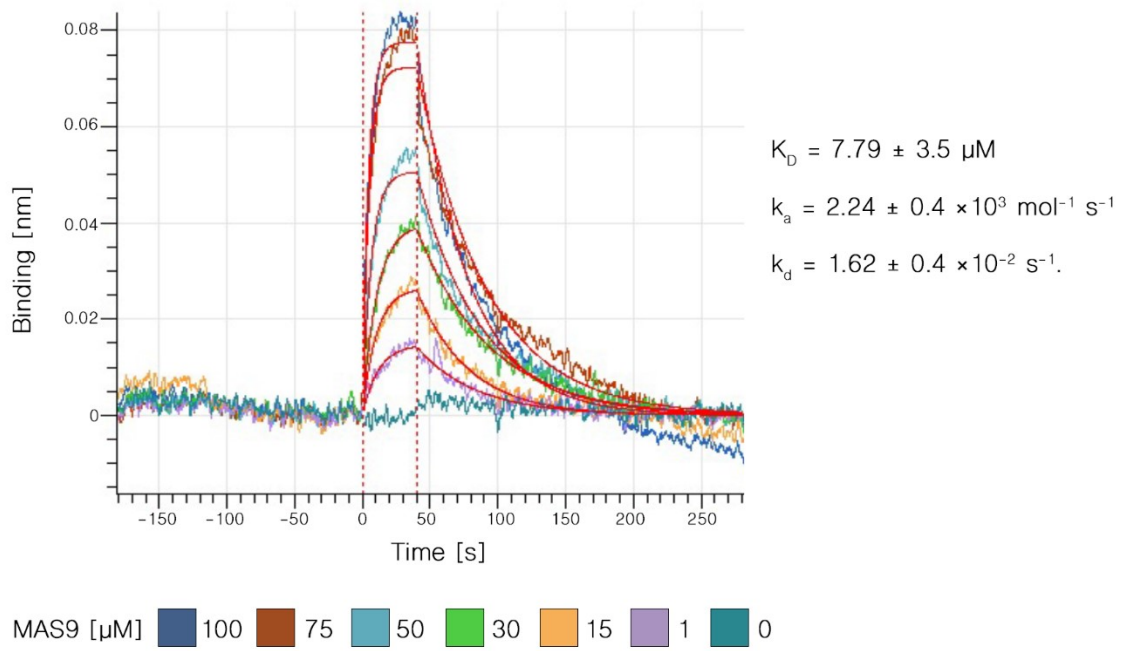
Figure 5.5. Determination of the equilibrium dissociation constant (K_D) of the interaction of CLEC-2 with MAS9.

Association was followed for 40 s in order to reach equilibrium. Afterwards, the protein-bound biosensor was incubated for 240 s in buffer to measure dissociation. The red lines represent curves fitted using the 1:1 binding model. The estimated K_D, k_a and k_d are presented on the graph as mean $\pm$ SD and are representative of three independent experiments.

5.3.3. MAS9 inhibits CLEC-2-mediated platelet aggregation when stimulated with low dose of rhodocytin

Light Transmission Aggregometry (LTA) is a basic method to test platelet function. In LTA, WPs are stirred at 37°C within a cuvette located between a light source and a detector. Then, when the agonist (e.g., CRP-XL, rhodocytin, thrombin or hemin) is added, platelet aggregation leads to increased light transmission (O'Brien, 1961; Born, 1962).

To study the effect of MAS9 on CLEC-2-mediated aggregation, washed platelets (4×10^8/ml) were pre-incubated with different concentrations of MAS9 (10 μM, 20 μM and 30 μM) or vehicle control (0.3% (v/v) DMSO) for 10 minutes before stimulation with 100 nM or 30 nM of rhodocytin. After stimulation, the aggregation was monitored for 5 minutes. Additionally, to investigate whether MAS9 is selective for CLEC-2-mediated aggregation, washed platelets pre-treated with MAS9 were stimulated with 3 μg/ml or 0.3 μg/ml CRP-XL (GPVI receptor agonist) or 0.05 U/ml thrombin (PAR1 and PAR4 receptors agonist).

20 μM and 30 μM of MAS9 significantly inhibited platelet aggregation stimulated with 30 nM rhodocytin (Figure 5.6A). Aggregation was reduced to $22 \pm 6\%$ for platelets pre-incubated with 20 μM MAS9 and to 10 ± 6 % for platelets pre-incubated with 30 μM MAS9, compared to 77 ± 10 % of the vehicle control (Fig 5.6B). However, when a higher concentration of the same agonist (100 nM rhodocytin) was used, MAS9 had no inhibitory effect on platelet aggregation (Figure 5.6C).

Additionally, MAS9 had no inhibitory effect when platelets were stimulated with CRP-XL or thrombin. MAS9 did not inhibit aggregation stimulated with high (3 μg/ml,

Figure 5.7A) or low (0.3 µg/ml, Figure 5.7B) concentrations of CRP-XL, or a low dose

(0.1 U/ml, Figure 5.7C) of thrombin.

These data suggest that MAS9 is selective to CLEC-2 receptor, but not to GPVI

receptor nor PAR1 and PAR4.
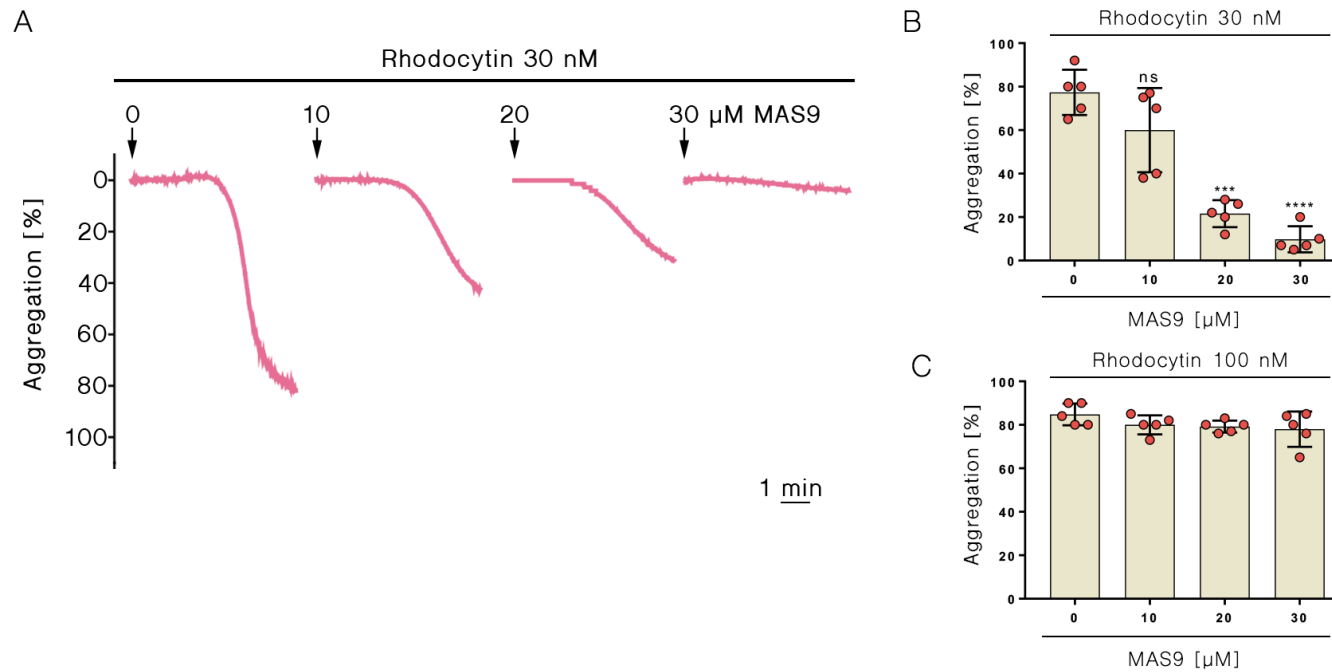
Figure 5.6. MAS9 inhibits platelet aggregation stimulated with a low dose of rhodocytin, but not at a high dose.

Washed platelets (4×10^8 /ml) were incubated with MAS9 (10 µM, 20 µM or 30 µM) or vehicle control (0.3 % (v/v) DMSO) for five minutes before being stimulated with 30 nM (A, B) or 100 nM (C) rhodocytin and the aggregation was monitored using LTA. Representative traces for platelets stimulated with 30 nM rhodocytin (A) and quantified aggregation values for human washed platelets stimulated with 30 nM rhodocytin (B) or 100 nM rhodocytin (C) have been shown. Statistical significance was calculated using one-way ANOVA with Dunnett's post-test. Data are shown as mean ± SD and are representative of five experiments. *p ≤ .05 **p ≤ .01, ***p ≤ .001, ****p ≤ .0001.
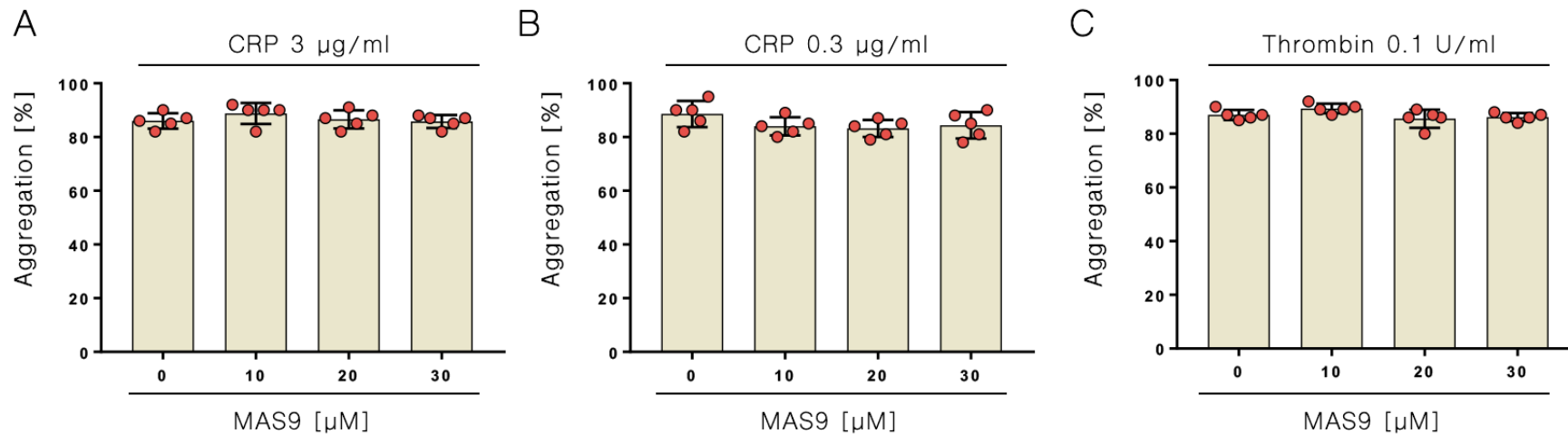
Figure 5.7. MAS9 has no inhibitory effect on platelet aggregation stimulated with CRP-XL or thrombin.

Washed platelets (4×10^8 /ml) were incubated with MAS9 (10 μM, 20 μM or 30 μM) or vehicle control (0.3 % (v/v) DMSO) for five minutes before being stimulated with 3 μg/ml CRP-XL (A), 0.3 μg/ml CRP-XL (B) or 0.1 U/ml thrombin (C). Quantified aggregation values for human washed platelets have been shown. Statistical significance was calculated using one-way ANOVA with Dunnett's post-test. Data are shown as mean ± SD and are representative of five experiments. *$p \leq .05$ **$p \leq .01$, ***$p \leq .001$, ****$p \leq .0001$.

5.3.4. The effect of MAS9 on CLEC-2-mediated platelet aggregation using plate-based aggregometry

An alternative approach to LTA is plate-based aggregometry (PBA). PBA is performed in a 96-well plate format. This format has several advantages, such as the possibility to process many samples with different conditions at the same time and a reduction of the blood volume used to prepare PRP or washed platelets. However, PBA measures a % of aggregation as an end point assay unlike standard LTA which is in real time. The percent of aggregation is calculated based on the absorbance of PPP (or buffer) and PRP (or WPs) controls. For PRP the readings of absorbance are performed between 575 and 650 nm, whereas for WPs at 405 nm (Fratantoni *et al.*, 1990; Chan *et al.*, 2018).

To examine the effect and selectivity of MAS9 on CLEC-2-mediated platelet aggregation, washed platelets (4×10^8/ml) were loaded into 96-well plate and incubated with different doses of MAS9 (10 µM, 20 µM and 30 µM) or vehicle control (0.3% (v/v) DMSO) for 5 minutes before stimulation with 200 nM rhodocytin, 3 µg/ml CRP-XL or 0.05 U/ml thrombin. The plate was shaken for 5 minutes for samples stimulated with CRP-XL or thrombin, and 10 minutes for rhodocytin and the absorbance at 405 nm was immediately measured. The longer time point for rhodocytin takes into account the lag period observed before the onset of aggregation seen with CLEC-2 ligands (Suzuki-Inoue *et al.*, 2007).

20 µM of MAS9 significantly ($p < 0.1$), but not completely inhibited a platelet aggregation when stimulated with 200 nM rhodocytin, however, lower (10 µM) and higher (30 µM) doses of MAS9 had no inhibitory effect (Figure 5.8A). Additionally, MAS9 showed no significant inhibitory effect, when platelets were stimulated with 3 µg/ml CRP-XL (Figure 5.8B) or 0.05 U/ml thrombin (5.8C). The inhibition was

compared with Syk inhibitor PRT-060318, which fully inhibited aggregation, when stimulated with rhodocytin and CRP, but not thrombin (data not shown).

The plate-based aggregation data cannot firmly reveal that MAS9 has an inhibitory effect on CLEC-2-mediated platelet aggregation, however it has no effect on GPVI, PAR1 and PAR4 receptors.
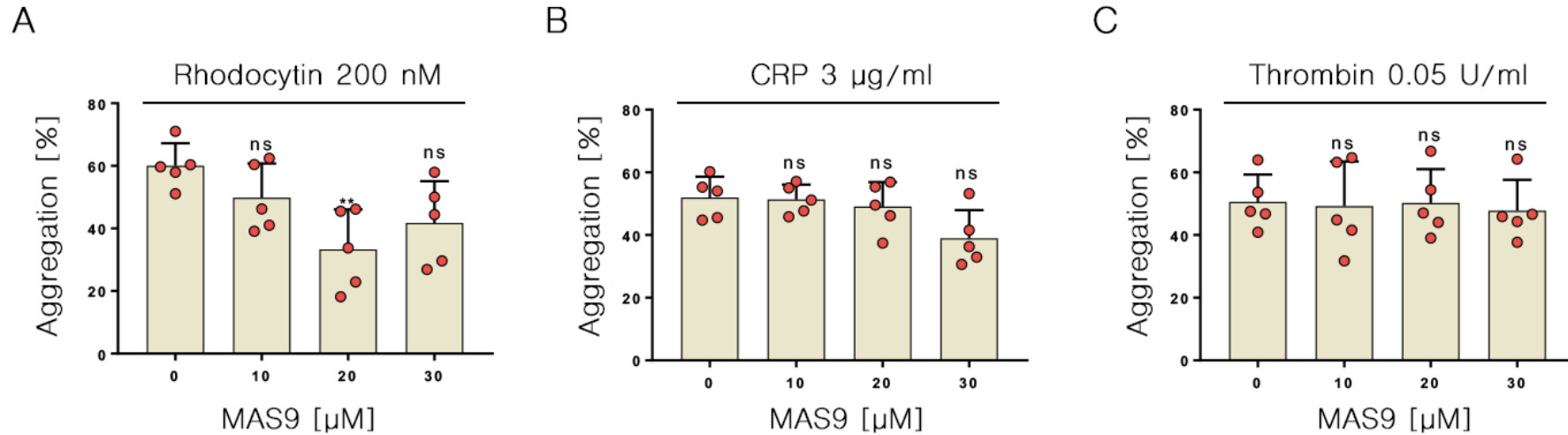
Figure 5.8. MAS9 significantly inhibits a CLEC-2-mediated plate-based aggregation only at 20 µM concentration.

Washed platelets (4×10^8 /ml) were incubated with MAS9 (10 µM, 20 µM or 30 µM) or vehicle (0.3 % (v/v) DMSO) for five minutes before being stimulated with 200 nM rhodocytin for 10 minutes (A) or stimulated with 3 µg/ml CRP-XL (B) or 0.05 U/ml thrombin (C) for 5 minutes. Statistical significance was calculated using one-way ANOVA with Dunnett's post-test. Data are shown as mean ± SD and are representative of five experiments. **$p \leq .01$.

5.3.5. MAS9 selectively inhibits phosphorylation downstream of CLEC-2, but not GPVI

CLEC-2 and GPVI have similar signalling pathway. Platelet activation by CLEC-2 or GPVI agonists leads to Src kinase-dependent phosphorylation of (hem)ITAM, which provides a binding site for the SH2 domains of Syk, leading to a series of auto- and trans-phosphorylations of Syk and initiation of a signalling cascade that activates and phosphorylates PLCγ2 (Pasquet *et al.*, 1999).

Therefore, protein phosphorylation studies were conducted to study the effect of MAS9 on the phosphorylation profile of specific phospho-proteins (pSrc, pSyk and pPLCγ2) downstream CLEC-2. Additionally, to investigate the selectivity of MAS9 into CLEC-2, GPVI-mediated protein phosphorylation was investigated alongside.

All activations were performed after the addition of 9 μM integrillin, to avoid platelet aggregation and activation of the $\alpha_{IIb}\beta_3$ integrin signalling cascade. Additionally, for GPVI activation, 2 U/ml apyrase (which inhibits platelet stimulation by ADP and T_XA_2) and 10 μM indomethacin (which inhibits cyclooxygenase 1 and thus the synthesis of T_XA_2) were added to the platelet suspension. Apyrase and indomethacin were omitted from CLEC-2 stimulated samples as CLEC-2 requires the presence of secondary mediators to reinforce its signalling pathway (Pollitt *et al.*, 2010b; Badolia *et al.*, 2017; Izquierdo *et al.*, 2020).

Washed platelets (8×10^8/ml) were pre-treated with MAS9 (20 μM or 30 μM) or vehicle control (0.3% (v/v) DMSO) for 5 minutes before stimulation under stirring conditions with 100 nM rhodocytin or 1 μg/ml CRP-XL. The reaction was stopped after 90 seconds (for CRP-XL) or 5 minutes (for rhodocytin). The time points used to assess phosphorylation, where the significant levels of phosphorylation were obtained were

consistent with previous literature (Mazet *et al.*, 2015; Izquierdo *et al.*, 2020). The samples were separated by SDS-PAGE and transferred to a PDVF membrane using western blotting.

Total cell phosphorylation was assessed using an anti-phosphotyrosine antibody, 4G10 (Figure 5.9A). 100 nM rhodocytin leads to an increase in tyrosine phosphorylation which is reduced in sample treated with 30 μM MAS9. A partial reduction is seen with 20 μM MAS9 when compared to the vehicle control (Figure 5.9A, lanes 2-4). No significant differences were revealed in the pTyr profile, in the samples stimulated with 1 μg/ml CRP (Figure 5.9A, lanes 6-8).

In samples stimulated with 100 nM rhodocytin the phosphorylation of PLCγ2 (Y759), Syk (Y525-526) and Src (Y419) were inhibited by 30 μM of MAS9, and less by 20 μM of MAS9 when compared to the vehicle control (Figure 5.9B). MAS9 did not alter the phosphorylation of these proteins when platelets were stimulated with 1 μg/ml CRP.

Quantification of the western blot bands of PLCγ2 (Y759), Syk (Y525-526), Src (Y419) was made by normalising the band intensity against the GAPDH loading control. In samples stimulated with 100 nM rhodocytin, 30 μM and 20 μM MAS9 significantly inhibited the phosphorylation of Src, Syk and PLCγ2 when compared to the vehicle control (Figure 5.10).

Taken together, these results suggest that MAS9 is selective to the CLEC-2 receptor, and not to GPVI. MAS9 inhibits CLEC-2-mediated phosphorylation of PLCγ2, Syk and Src.
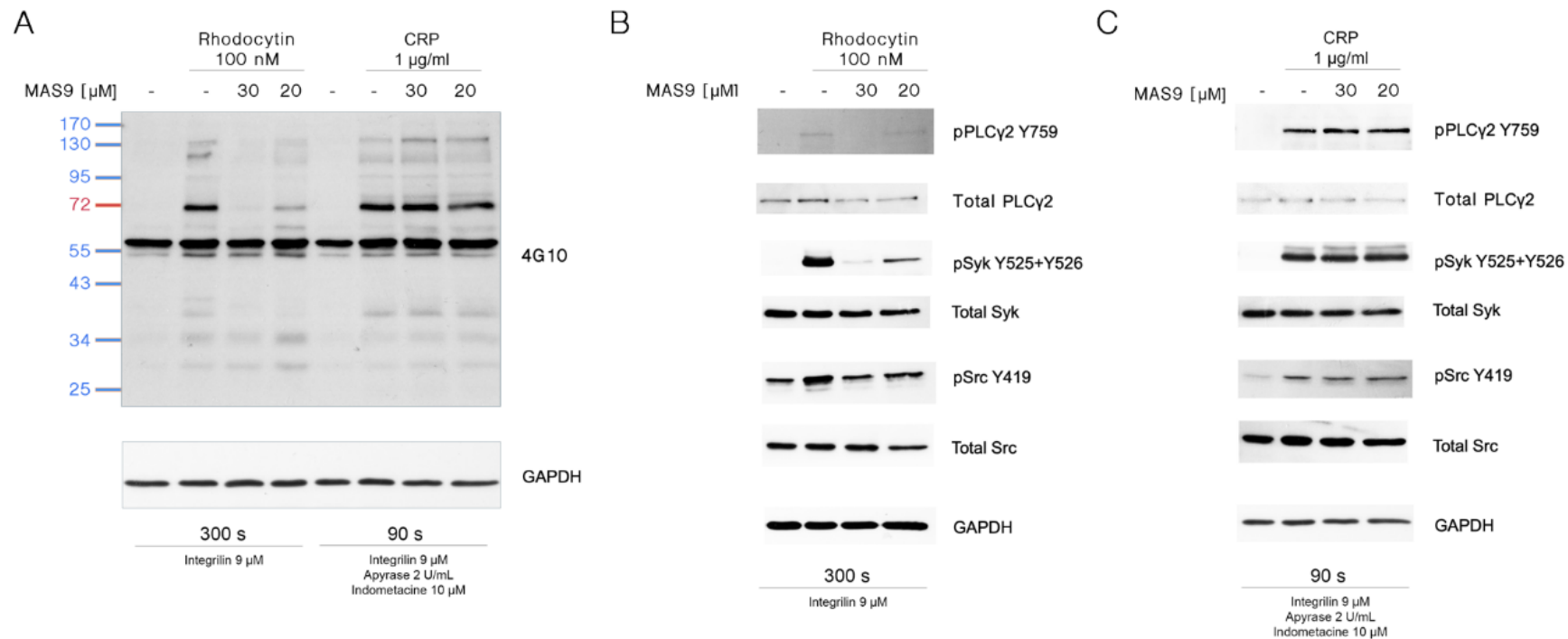
Figure 5.9. MAS9 selectively inhibits tyrosine signalling downstream of CLEC-2 and not GPVI.

Washed platelets (8×10^8 /ml) were pre-treated with different concentrations of MAS9 for 10 min before stimulation with 100 nM rhodocytin or 1 µg/ml CRP. Stimulations were stopped with addition of lysis buffer and the whole-cell lysates were separated by SDS-PAGE and analysed by western blotting for (A) pTyr (4G10), (B, C) pPLCγ2 (Y759), pSyk (Y525-526), pSrc (Y419) and total PLCγ2, Syk and Src, with a GAPDH loading control. Representative blot from 3 independent experiments.
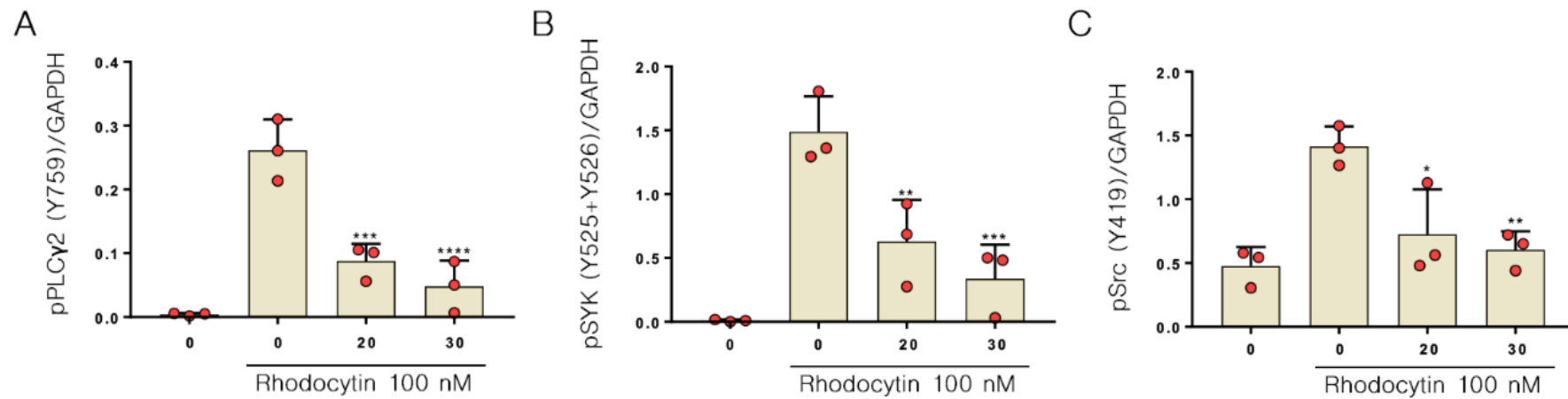
Figure 5.10. Quantification of the bands from western blot analysis of platelets lysates stimulated with 100 nM rhodocytin.

Densitometry graphs, representing tyrosine phosphorylation levels of (A) pPLCγ2 (Y759), (B) pSyk (Y525-526) and (C) pSrc (Y419) normalised against the GAPDH loading control. Statistical significance was calculated using one-way ANOVA with Dunnett's post-test. Data are shown as mean ± SD and are representative of three independent experiments. *p ≤ .05 **p ≤ .01, ***p ≤ .001, ****p ≤ .0001.

5.3.6. MAS9 inhibits fibrinogen binding and P-selectin exposure in washed platelets, but not in PRP

The integrin $\alpha_{IIb}\beta_3$ plays an important role in platelet signalling. Due to platelet activation by different agonists, the integrin $\alpha_{IIb}\beta_3$ changes its confirmation from a low-affinity to a high-affinity state for its ligand, fibrinogen. This process is called "inside-out" signalling (Hato *et al.*, 1998). Fibrinogen binding promotes "outside-in" signalling, which initiates different processes in platelets, including aggregation, spreading and clot retraction (Springer *et al.*, 2008). The fibrinogen binding to integrin $\alpha_{IIb}\beta_3$ in activated platelets can be measured using flow cytometry, which allows to estimate of the extent of integrin $\alpha_{IIb}\beta_3$ molecules in the active confirmation at the platelet surface.

Platelet α-granules contain biologically important molecules that contribute to platelet regulation and thrombus formation. They include a transmembrane receptor P-selectin (CD62P). During platelet activation, P-selectin can be rapidly translocated to the platelet surface during the release of α-granules (Koedam *et al.*, 1992). This makes P-selectin a good marker of platelet activation and α-granule release. Like fibrinogen binding, P-selectin exposure on the platelet surface can also be measured using flow cytometry.

Rhodocytin- and CRP-XL-mediated fibrinogen binding and P-selectin exposure was measured using flow cytometry in the presence and absence of MAS9. Washed platelets (4×10^8/ml) were incubated with different doses of MAS9 (10 μM, 20 μM and 30 μM) or vehicle control (0.3% (v/v) DMSO) for 5 minutes in the presence of Alexa Fluor 488 Fibrinogen and PE/Cy5 anti-human P-selectin (CD62P) antibody. Prior to flow cytometry analysis, platelets were stimulated with 100 nM rhodocytin or 3 μg/ml CRP-XL and incubated for 20 minutes in the dark. After the incubation, the reaction was

terminated by fixing the samples with 0.2% formyl saline and the samples were measured using a BD Accuri C6 Plus flow cytometer. A gate was applied around platelets population and data was collected from 10,000 events for each sample.

MAS9, only at the highest concentration (30 µM), significantly inhibited $\alpha_{IIb}\beta_3$ activation (Figure 5.11A) and granule secretion (Figure 5.11B) downstream of CLEC-2. The lower doses (10 µM and 20 µM) had no effect on fibrinogen binding and P-selectin exposure. Unexpectedly, MAS9 dose-dependently inhibited $\alpha_{IIb}\beta_3$ activation when platelets were stimulated with CRP-XL (Figure 5.11C), however it had no effect on granule secretion (5.11D).

These results show that MAS9 at a high dose has an inhibitory effect on $\alpha_{IIb}\beta_3$ activation and granule secretion downstream of CLEC-2. It also suggests that MAS9 may have an effect on $\alpha_{IIb}\beta_3$ activation or function since fibrinogen binding was also inhibited downstream GPVI.

Similar experiments were performed using PRP. However, a FITC anti-human Fibrinogen antibody was used rather than Alexa Fluor 488 Fibrinogen since fibrinogen is present in a plasma. MAS9 had no inhibitory effect on $\alpha_{IIb}\beta_3$ activation and granule secretion when stimulated with either, rhodocytin (Figure 5.12A and B) or CRP-XL (Figure 5.12C and D). This suggests that MAS9 may be not bioavailable due the presence of plasma proteins in the PRP.
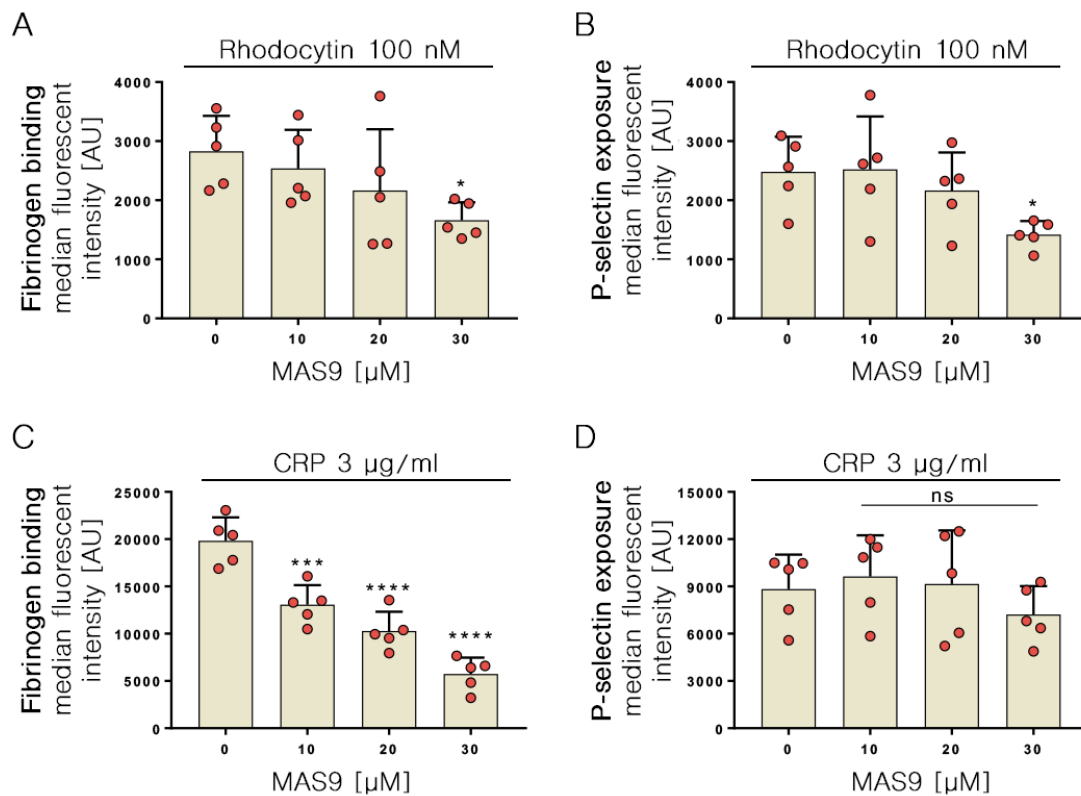
Figure 5.11. MAS9 at a high dose inhibits fibrinogen binding and P-selectin exposure downstream of CLEC-2, and dose-dependently inhibits fibrinogen binding downstream of GPVI.

Washed platelets (4×10^8 /ml) were incubated with MAS9 (10 μM, 20 μM or 30 μM) or vehicle control (0.3 % (v/v) DMSO) with the addition of Alexa Fluor 488 Fibrinogen to measure fibrinogen binding (A, C), and PE/Cy5 anti-human CD62P antibody to measure P-selectin exposure (B, D). Samples were stimulated with 100 nM rhodocytin (A, B) or 3 μg/ml CRP-XL (C, D) for 20 minutes, before the flow cytometric analysis. The median fluorescence intensity was plotted against the inhibitor concentration and analysed using a one-way ANOVA with Dunnett's post-test. Data are shown as mean ± SD and are representative of five independent experiments. *$p \leq .05$ **$p \leq .01$, ***$p \leq .001$, ****$p \leq .0001$.
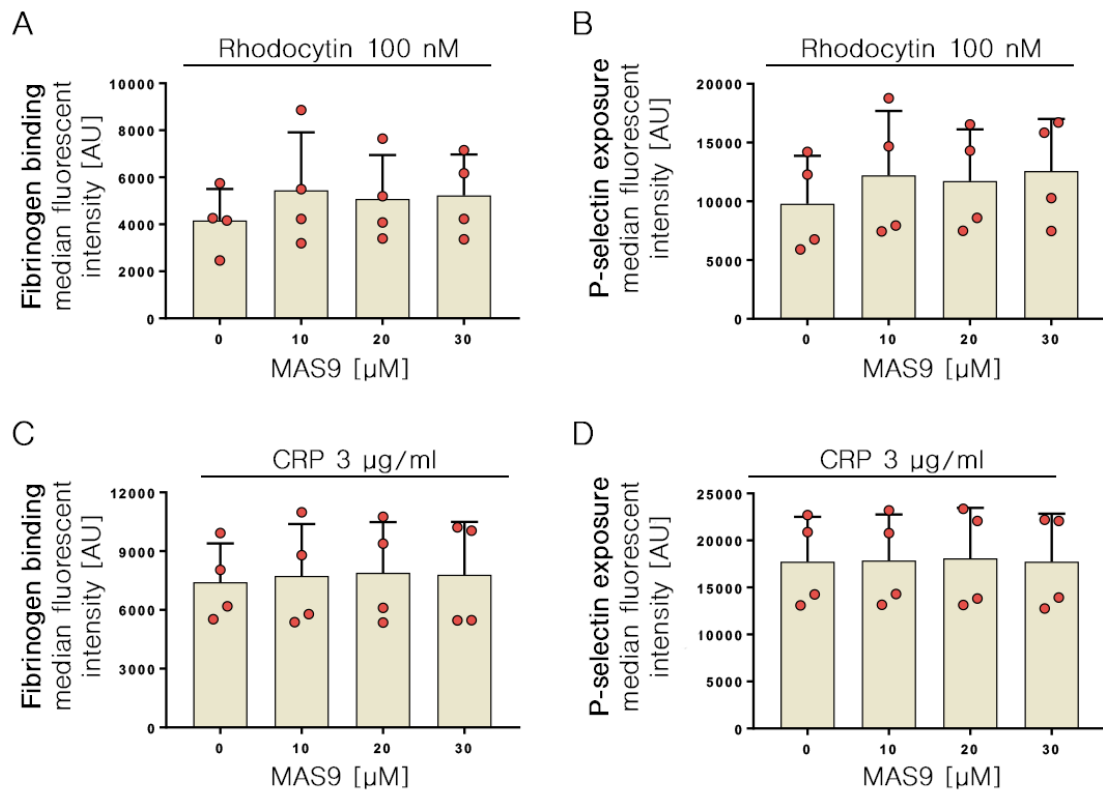
Figure 5.12. MAS9 has no inhibitory effect on fibrinogen binding and P-selectin exposure downstream of CLEC-2 and GPVI in PRP.

PRP was incubated with MAS9 (10 µM, 20 µM or 30 µM) or vehicle control (0.3 % (v/v) DMSO) with the addition of a FITC anti-human Fibrinogen antibody to measure fibrinogen binding (A, C) and PE/Cy5 anti-human CD62P antibody to measure P-selectin exposure (B, D). Samples were stimulated with 100 nM rhodocytin (A, B) or 3 µg/ml CRP-XL (C, D) for 20 minutes, before the flow cytometric analysis. The median fluorescence intensity was plotted against the inhibitor concentration and analysed using a one-way ANOVA with Dunnett's post-test. Data are shown as mean ± SD and are representative of four independent experiments.

5.3.7. MAS9 inhibits CLEC-2-mediated platelet spreading and adhesion

The experiments described above were performed using soluble ligands. However, the endogenous ligand for CLEC-2, podoplanin, is normally exposed on the surface of a cell rather than in a soluble form. To determine if MAS9 inhibits the interaction of platelets to immobilised ligands, a platelet spreading assay was performed.

To test whether MAS9 has an inhibitory effect on platelet spreading via CLEC-2-mediated activation, glass coverslips were coated with rhodocytin (300 nM) and human podoplanin-rFc (10 μg/ml) overnight, then blocked with BSA for 1 hour to prevent non-specific binding of the platelets to the glass surface. Washed platelets (2×10^7 /ml) were incubated with different doses of MAS9 (10 μM, 20 μM and 30 μM) or vehicle control (0.3% (v/v) DMSO) for 5 minutes, then plated on the agonist-coated coverslips. Unbound platelets were removed after 45 minutes incubation at 37°C by washing with PBS. Next, the samples were fixed using paraformaldehyde, permeabilized with a low concentration of Triton-X100, stained with Phalloidin Alexa Fluor 647 and mounted onto microscope slides. The slides were imaged on a Nikon Ti2 microscope using epifluorescent microscopy. For each sample, ten images were taken from random locations on each slide. Analysis was performed using ImageJ to count the number of adhered platelets and the spread platelet surface area.

Representative images of platelet adhesion and spreading on rhodocytin-coated coverslips in presence or absence of MAS9 are presented in Figure 5.13A. Platelet incubation with MAS9 dose-dependently inhibited the number of platelets adhered to rhodocytin (Figure 5.13B), with the average numbers of 2.58 ± 0.3, 2.06 ± 0.3, 1.34 ± 0.2 and $0.92 \pm 0.1 \times 10^{-3}$ platelets/μm^2 for vehicle control and platelets treated with 10 μM, 20 μM and 30 μM of MAS9, respectively. Additionally, MAS9 inhibited platelet spreading on rhodocytin (Figure 5.13C), showing an approximate 58% decrease in

platelet spreading in the presence of MAS9 when compared to the vehicle treated platelets (39.3 ± 3.6 μm^2 for the vehicle control compared to 16.5 ± 2.6 μm^2 for platelets incubated with 30 μM MAS9).

The same effect was observed when platelets were incubated with MAS9 and plated on to podoplanin-coated coverslips (Figure 5.13D). MAS9 dose-dependently inhibited number of platelets adhered to podoplanin (Figure 5.13E), with the average numbers of 2.52 ± 0.3, 1.55 ± 0.5, 1.36 ± 0.2 and $1.10 \pm 0.2 \times 10^{-3}$ platelets/μm^2 for the vehicle control and platelets treated with 10 μM, 20 μM and 30 μM of MAS9, respectively. Additionally, MAS9 inhibited platelet spreading on podoplanin (Figure 5.13F), showing an approximate 67% decrease in platelet spreading in the presence of MAS9 when compared to the vehicle treated platelets (40.3 ± 5.6 μm^2 for the vehicle control compared to 13.3 ± 2.4 μm^2 for platelets incubated with 30 μM MAS9).

To study the selectivity of MAS9 for CLEC-2, the spreading assay was performed for other platelet receptors; GPVI and $\alpha_{IIb}\beta_3$. The glass coverslips were coated with 3 $\mu g/ml$ CRP-XL (for GPVI) or 100 $\mu g/ml$ fibrinogen (for $\alpha_{IIb}\beta_3$). The protocol was the same as described above.

Representative images of platelet adhesion and spreading on CRP-XL- and fibrinogen-coated coverslips in presence or absence of MAS9 are presented in Figure 5.14A and D. Preincubating the platelets with MAS9 did not inhibit the number of platelets adhered to both agonists, CRP-XL and fibrinogen (Figure 5.14B and E), when compared to their vehicle controls. However, MAS9 significantly and dose-dependently inhibited platelet spreading, showing an approximate 61% decrease in CRP-XL mediated spreading when compared to vehicle control (41.8 ± 1.8 μm^2 for the vehicle control compared to 16.3 ± 0.6 μm^2 for platelets incubated with 30 μM MAS9) and an approximate 55% decrease in fibrinogen mediated platelet spreading (39.7 ± 2.5 μm^2 for the vehicle control

compared to 18.0 ± 2.6 μm^2 for platelets incubated with 30 μM MAS9) (Figure 5.14C and F).

Taken together, these data indicate that MAS9 inhibits CLEC-2-mediated platelet spreading by inhibiting the interaction of CLEC-2 with its ligands. However, inhibition of platelet spreading, but not adhesion, on CRP and fibrinogen suggest that MAS9 may have additional effects. This may be by a biological relevant mechanism, such as cross-talk between receptors in mediating spreading or by a non-specific effect.
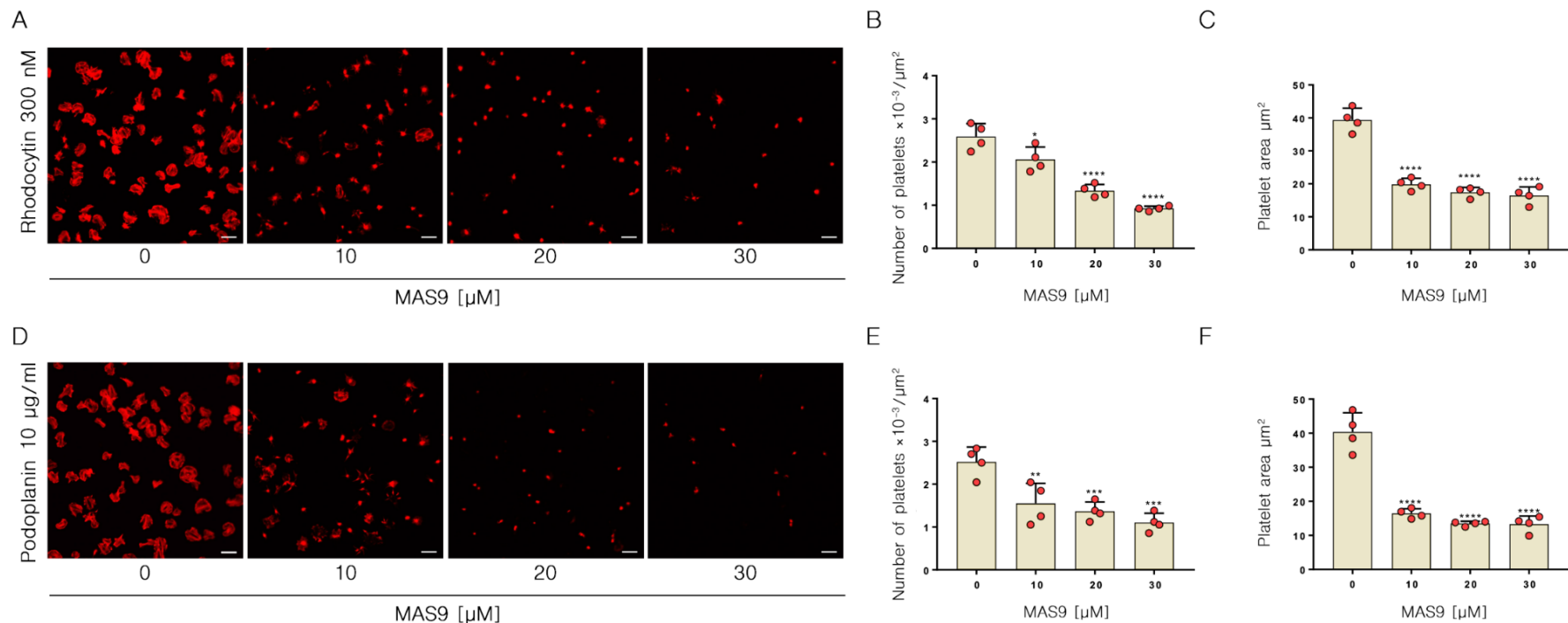
Figure 5.13. MAS9 inhibits platelet adhesion and spreading on rhodocytin and podoplanin.

Washed platelets (2×10^7 /ml) were incubated with MAS9 (10 μM, 20 μM or 30 μM) or vehicle control (0.3 % (v/v) DMSO) for five minutes

before being plated on to rhodocytin-(300 nM) or podoplanin-(10 μg/ml) coated coverslips. The platelets were incubated for 45 min at 37°C,

then permeabilized, fixed, stained with Phalloidin Alexa Fluor 647 and mounted onto microscope slides. The samples were visualised with a

Nikon TiE2 microscope with a 100x objective. Scale bar – 10 μm. Representative images of platelet adhesion and spreading on (A) rhodocytin

and (D) podoplanin are shown. Analysis was performed using ImageJ to count the number of platelets (B, E) and to determine the spread surface area (C, F). Statistical significance was calculated using a one-way ANOVA with Dunnett's post-test. Data are shown as mean ± SD and are representative of four independent experiments. $*p \leq .05$ $**p \leq .01$, $***p \leq .001$, $****p \leq .0001$.
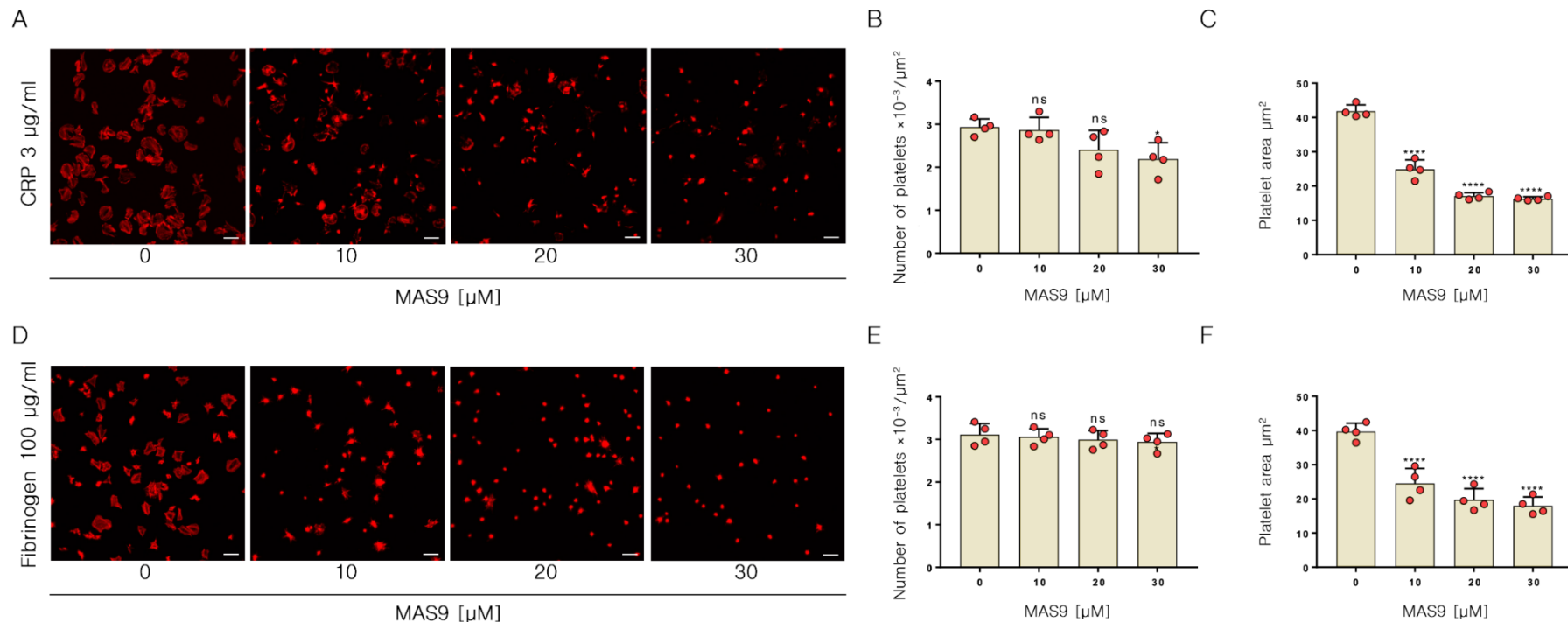
Figure 5.14. MAS9 inhibits platelet spreading on CRP-XL and fibrinogen, but not adhesion.

Washed platelets (2×10^7 /ml) were incubated with MAS9 (10 μM, 20 μM or 30 μM) or vehicle (0.3 % (v/v) DMSO) for five minutes before being plated on to CRP-(3 μg/ml) or fibrinogen-(100 μg/ml) coated coverslips. The platelets were incubated for 45 min at 37°C, then permeabilized, fixed, stained with Phalloidin Alexa Fluor 647 and mounted onto microscope slides. The samples were visualised with a Nikon TiE2 microscope with a 100x objective. Scale bar – 10 μm. Representative images of platelet adhesion and spreading on (A) CRP and (D)

fibrinogen are shown. Analysis was performed using ImageJ to count the number of platelets (B, E) and to determine the spread surface area (C, F). Statistical significance was calculated using a one-way ANOVA with Dunnett's post-test. Data are shown as mean ± SD and are representative of four independent experiments. $*p \leq .05$ $**p \leq .01$, $***p \leq .001$, $****p \leq .0001$.

5.3.8. MAS9 inhibits platelet spreading on human dermal lymphatic endothelial cells.

Lymphatic endothelial cells express the endogenous CLEC-2 ligand, podoplanin. To determine how MAS9 affects the interaction of platelets to podoplanin expressed at the surface of a cell, Human Dermal Lymphatic Endothelial cells were used. It has been shown that HDLECs can induce mouse platelet aggregation and that mouse platelets can adhere and spread on the monolayer of HDLECs in a CLEC-2 dependent manner (Borgognone *et al.*, 2014). Additionally, it has been shown that HDLECs can support human and mouse platelet adhesion and aggregation at venous shear rates (50-150 s^{-1}) (Navarro-Núñez *et al.*, 2015).

Most of the previous experiments investigating the effect of MAS9 on CLEC-2-mediated platelet activation were carried out using rhodocytin. However, MAS9 was first identified as an inhibitor of the CLEC-2-podoplanin interaction. Therefore, HDLECs, which endogenously express podoplanin, were used to investigate the effect MAS9 on platelet adhesion to the cells. Washed platelets (2×10^7 /ml) were incubated with different doses of MAS9 (10 µM, 20 µM and 30 µM) or vehicle control (0.3% (v/v) DMSO) for 5 minutes, then plated on to coverslips coated with a monolayer of HDLECs. Unbound platelets were removed after 45 minutes incubation at 37°C by washing with PBS. Next, the samples were fixed using paraformaldehyde, permeabilized with a low concentration of Triton-X100, stained with anti-podoplanin antibodies (NZ-1, to stain the cells) and APC-conjugated anti-human CD42b antibodies (to stain platelets) and mounted onto microscope slides. The slides were imaged on a Nikon TiE2 microscope using epifluorescent microscopy. For each sample, five images were taken from random locations on each slide. Analysis was performed using ImageJ to count the number of adhered platelets on the HDLECs.

Representative images of platelets adhered to a HDLECs monolayer in presence or absence of MAS9 are presented in Figure 5.15A. MAS9 at concentrations of 20 μM and 30 μM significantly inhibited platelet adhesion to HDLECs (2.6 ± 0.6 and 1.7 ± 0.5 $\times 10^{-3}$ platelets/μm^2 in the presence of 20 μM and 30 μM of MAS9 respectively, compared to $4.1 \pm 1.0 \times 10^{-3}$ platelets/μm^2 for the vehicle control) (Figure 5.15B). It can be observed that platelets predominantly localise to the periphery of the cells. Interestingly, in the podoplanin-stained images (Figure 5.15A, first row) green spots are observed, suggesting the localised accumulation of podoplanin. The merged images of podoplanin and CD42b staining (Fig 5.15A, third row) suggest that the accumulation of podoplanin coincides with the presence of a platelets.

To investigate the accumulation of podoplanin by platelets, Z-stack images were taken using a Nikon A1R confocal microscope (Figure 5.16). The Z projection shows that podoplanin accumulates at the interface of the platelet and the surface of the monolayer of HDLEC cells (Figure 5.16, top panel). The accumulation of podoplanin under the platelet is lost in the presence of 30 μM MAS9 (Figure 5.16, bottom panel).

These data suggest that MAS9 can inhibit the interaction of physiologically expressed CLEC-2 and podoplanin by showing the inhibition of platelet adhesion to HDLECs and the inhibition of accumulation of membrane associated podoplanin by platelets.
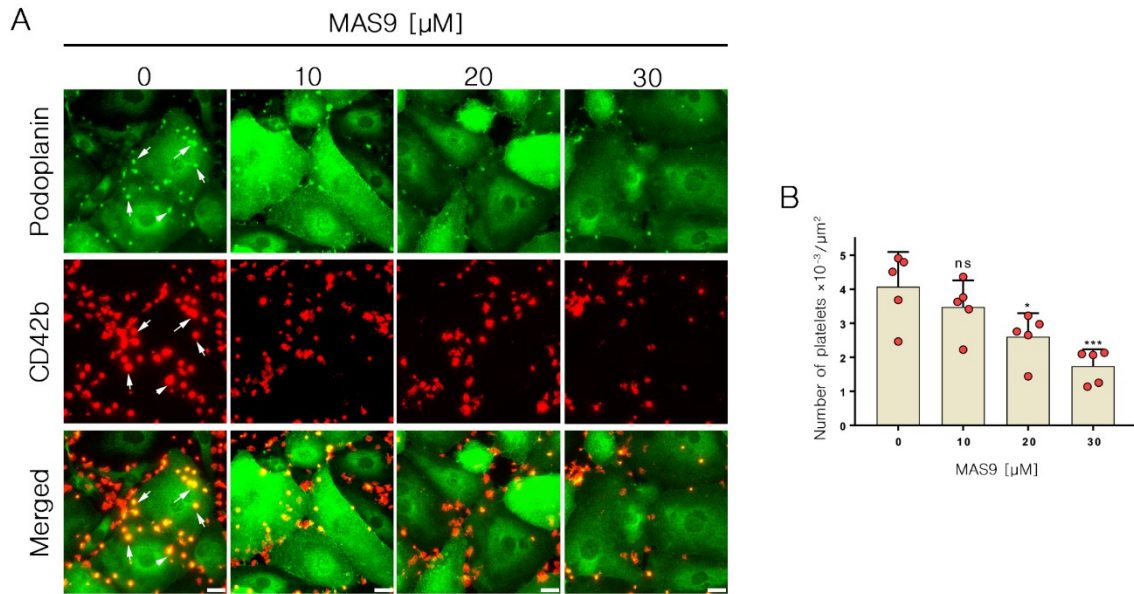
Figure 5.15. MAS9 inhibits the platelet adhesion on HDLECs-coated coverslips.
Washed platelets (2×10^7 /ml) were incubated with MAS9 (10 µM, 20 µM or 30 µM) or vehicle control (0.3 % (v/v) DMSO) for five minutes before being plated on HDLECs-coated coverslips. The platelets were incubated for 45 min at 37°C, then permeabilized, fixed, stained with anti-podoplanin and anti-human CD42b antibodies and mounted onto microscope slides. The samples were visualised with a Nikon TiE2 microscope with a 100x objective. Scale bar – 10 µm. Representative images of platelet adhesion on HDLECs are shown (A). Accumulation of podoplanin has been pointed using white arrows. Analysis was performed using ImageJ to count the number of platelets (B). Statistical significance was calculated using a one-way ANOVA with Dunnett's post-test. Data are shown as mean ± SD and are representative of five independent experiments. *p ≤ .5, ***p ≤ .001.
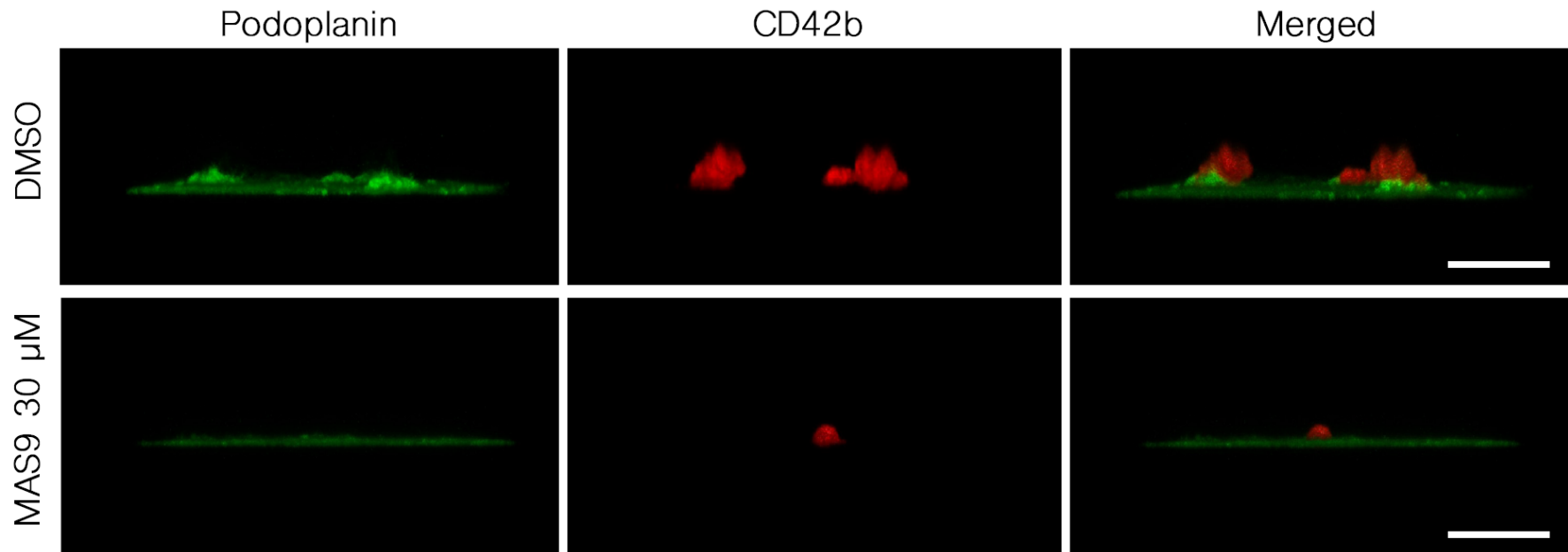
Figure 5.16. Podoplanin from HDLECs accumulates under the platelets.

Washed platelets ($2×10^7$ /ml) were incubated with MAS9 (30 µM) or vehicle (0.3 % (v/v) DMSO) for five minutes before being plated on HDLECs-coated coverslips. The platelets were incubated for 45 min 37°C, then permeabilized, fixed, stained with anti-podoplanin and anti-human CD42b antibodies and mounted onto microscope slides. The Z-stack images were taken with a Nikon A1R confocal microscope using Plan Apo λ 100x Oil objective. Scale bar 10 µm. Representative Z projections have been shown.

5.4. Discussion

This chapter presents the characterisation of MAS9 – a small molecule inhibitor of the human CLEC-2-podoplanin interaction identified in a high-throughput screen. Firstly, molecular docking was performed to identify the preferential binding mode of MAS9 to CLEC-2. Secondly, the affinity constant of the CLEC-2-MAS9 interaction was determined using bio-layer interferometry. Thirdly, MAS9 was tested in different platelet-based functional assays, to determine if it can inhibit platelet aggregation, activation, adhesion and spreading in a CLEC-2-dependent manner. Finally, human dermal lymphatic endothelial cells, which endogenously express the CLEC-2 ligand podoplanin have been used to investigate the effect of MAS9 on platelet adhesion to cells. The result summary of the washed platelet-based experiment has been presented in Table 5.1

The known common binding sites to induce CLEC-2 activation by podoplanin and rhodocytin, based on their crystal structures (PDB: 3WSR for podoplanin and 3WWK for rhodocytin), are four arginine residues: Arg107, Arg118, Arg152, Arg157. The additional binding sites for podoplanin are Tyr153 and His154, and for sialylated O-glycan of podoplanin are Asn105, His119 and Tyr129 *(Watson et al., 2008; Nagae et al.*, 2014a). Additionally, the molecular docking predictions of known small molecule inhibitors of the CLEC-2-podoplanin interaction suggest that 2CP interacts with residues Asn105, Arg107, Phe116, Arg118 and Arg157 of CLEC-2, which mostly match with the binding sites for podoplanin and rhodocytin (Chang *et al.*, 2015), whereas the identified binding sites for Co-HP were Asn120, Asn210 and Lys211, suggesting that inhibition is mediated by an allosteric mechanism (Tsukiji *et al.*, 2018).

Computational molecular docking studies identified that MAS9 binds by hydrogen bonds to Arg107, Arg152, Thr153 and Arg157 of CLEC-2. Additionally, it creates a Pi-

Pi-stacking interaction with His154 of CLEC-2. These results imply that MAS9 can interact with key amino acid residues involved in podoplanin- and rhodocytin-CLEC-2 binding. Hence, MAS9 is likely to integrate into the same binding pocket or spatial location of podoplanin and rhodocytin, interfering with their binding to CLEC-2.

Bio-layer interferometry showed that MAS9 binds directly to CLEC-2. The calculated binding affinity constant was 7.79 ± 3.5 μM (Figure 5.5). Compared to the affinity constant of known CLEC-2 ligands, the K_D for MAS9 is higher than the K_D for podoplanin (24.5 μM) (Christou *et al.*, 2008), however it is lower than the K_D estimated for rhodocytin (1 μM) (Watson *et al.*, 2007) and hemin (less than 1 μM) (Bourne *et al.*, 2021; Oishi *et al.*, 2021). Compared to other small molecules, MAS9 has a greater K_D than 2CP (33.2 μM) (Chang *et al.*, 2015). The K_D of Co-HP for CLEC-2 could not be determined as it did not dissociate during a surface plasmon resonance experiment. The authors of this study suggested that the avidity of Co-HP for CLEC-2 is strong and may be in range of 10-100 pM (Tsukiji *et al.*, 2018). Taken together, the bio-layer interferometry data presented here suggests that MAS9 is more potent than 2CP and may be important in disrupting the interaction of CLEC-2 with its physiological ligand, podoplanin.

MAS9 at concentrations of 20 μM and 30 μM significantly inhibited washed platelet aggregation stimulated with a low-dose of rhodocytin (30 nM) in LTA, however, when a higher concentration of rhodocytin (100 nM) was used, there was no inhibitory effect of MAS9 (Figure 5.6). This may be related to the difference in affinity for rhodocytin and MAS9 to CLEC-2. Affinity describes how strongly a single ligand molecule binds to the receptor. The binding affinity constant for MAS9 was estimated to be 7.79 ± 3.5 μM, whereas the affinity constant of rhodocytin is 1 μM. When molecules compete for the CLEC-2 binding sites, the molecule with the higher affinity wins.

An alternative explanation can be the difference in the avidity of the ligand for the receptor. Rhodocytin is a tetrameric protein containing two α and two β subunits, linked covalently with a disulphide bond. Both subunits multimerise and lead to CLEC-2 clustering (Clemetson, 2010) and this increases the avidity of rhodocytin for CLEC-2 compared to the interaction of a single molecule of MAS9 to CLEC-2. These possibilities may explain why the inhibitory effect of MAS9 on platelet aggregation was only observed at low concentration of rhodocytin.

Additionally, MAS9 displayed a selectivity for CLEC-2 over the other platelet receptors, GPVI, PAR1 and PAR4. MAS9 did not alter platelet aggregation stimulated with high or low doses of CRP-XL nor with low dose of thrombin in an LTA assay (Figure 5.7). These data suggest that MAS9 inhibits CLEC-2-mediated platelet aggregation, and the inhibitory effect is specific for CLEC-2. This is also found with other reported small molecule inhibitor of the CLEC-2-podoplanin interaction. Co-HP at concentration greater than 1.14 μM fully inhibited human platelet aggregation stimulated with 5 nM rhodocytin and did not inhibit collagen- and thrombin-induced platelet aggregation. However, when a higher dose of rhodocytin (10 nM) was used to stimulate platelet aggregation, the inhibitory effect of Co-HP was weaker when compared with 5 nM rhodocytin (Tsukiji *et al.*, 2018). In this study, platelet aggregation was not induced by 5 nM or 10 nM rhodocytin and it may reflect differences in rhodocytin potency which is purified from snake venom (data not shown) (Chung *et al.*, 1999).

2CP, another small molecule inhibitor, did not inhibit rhodocytin-induced platelet aggregation when 2 μg/ml (65 nM equivalent) rhodocytin was used. However, human platelet aggregation stimulated with 8 μg/ml podoplanin was suppressed when 20 μM 2CP was used (Chang *et al.*, 2015). In this study, human platelet aggregation by

recombinant podoplanin did not induce platelet aggregation in the LTA assay. The reason why human podoplanin may be readily induce platelet aggregation may be due the low affinity of human podoplanin for human CLEC-2 (Christou *et al.*, 2008). An alternative method to induce podoplanin-mediated platelet aggregation is by human podoplanin-expressing CHO cells, which at 1×10^6 cells/mL can stimulate platelet aggregation (Pollitt *et al.*, 2010b; Tsukiji *et al.*, 2018).

To investigate further the impact of MAS9 on agonist-induced platelet aggregation, an alternative approach, plate-based aggregometry, was used. This method allows the % of platelet aggregation to be measured for all conditions at once as an end point assay. In this assay, only the middle concentration of MAS9 (20 μM) showed a significant inhibition of platelet aggregation induced by rhodocytin (Figure 5.8), however this was only a partial inhibition, when compared to Syk inhibition with PRT-060318. Additionally, there was no inhibitory effect of MAS9 on aggregation induced by CRP-XL and thrombin. These data suggest that MAS9 may partially inhibit CLEC-2-mediated aggregation, with selectivity of CLEC-2 over other receptors, such as GPVI- and PAR1/4-mediated aggregation. PBA is widely use with PRP, rather than with WPs. That may be a reason why the MAS9 inhibitory effect is not completely clear, and this method requires more optimisation when used with rhodocytin.

The signalling pathways of ITAM (GPVI) and hemITAM (CLEC-2) receptors are similar. Platelet activation via the ligands for CLEC-2 and GPVI leads to the downstream phosphorylation of different proteins including Src, Syk and PLCγ2. The phosphorylation studies were conducted in the presence of integrillin, to avoid a platelet aggregation and activation through $\alpha_{IIb}\beta_3$. Additionally, for the GPVI activation studies, apyrase, which inhibits platelet stimulation by ADP and T_XA_2 and indomethacin, which inhibits cyclooxygenase 1 and thus the synthesis of T_XA_2 were added. These two

inhibitors were not added to the CLEC-2 stimulated platelets because CLEC-2 requires secondary mediators to reinforce the signalling pathway (Pollitt *et al.*, 2010b; Badolia *et al.*, 2017; Izquierdo *et al.*, 2020).

MAS9 suppressed the phosphorylation of the rhodocytin-induced phospho-Tyr profile (Figure 5.9A) and specific phosphoproteins: PLCγ2 (Y759), Syk (Y525-526) and Src (Y419) (Figure 5.9B) at concentration 30 μM, and partially at 20 μM. No inhibitory effect was seen downstream of CRP-XL. These data suggest that MAS9 selectively inhibits the phosphorylation downstream CLEC-2 and does not inhibit phosphorylation downstream of GPVI.

In a flow cytometry experiment, MAS9 inhibited fibrinogen binding and α-granule secretion downstream of CLEC-2. The effect was observed only at the highest concentration of MAS9 (30 μM), when stimulated with 100 nM rhodocytin (Figure 5.11A and B). Interestingly, MAS9 inhibited fibrinogen binding but not α-granule secretion downstream of GPVI. The effect was observed in a dose-dependent manner (Figure 5.11C). These data suggest there might be a cross-talk between integrins and ITAM-bearing receptors. The functional relationship between $\alpha_{IIb}\beta_3$ and FcγRIIa has been demonstrated in a platelet spreading experiment. IV.3 Fabs (which inhibit ligand binding to FcγRIIA and block FcγRIIA function), inhibited platelet spreading, but not adhesion, on immobilized fibrinogen (Boylan *et al.*, 2008). These data suggest that there is a relationship between ITAM-bearing receptors (FcγRIIa) with integrins ($\alpha_{IIb}\beta_3$), that links "outside-in" integrin-mediated signalling to shared components with ITAM-mediated signalling.

While MAS9 inhibits CLEC-2-mediated platelet responses in washed platelets it has no effect when used with PRP (Figure 5.12). This suggests that it is not bioavailable due the presence of the plasma proteins in PRP. To overcome this problem, the structure of

MAS9 should be chemically improved, or another way to deliver MAS9 into the target should be found.

The initial characterisation of MAS9 was performed with soluble agonists. However, this is not representative of CLEC-2 ligands such as podoplanin which is found at the surface of cells. To model a ligand presented on a surface, different agonists were cross-linked on a glass surface. The first two agonists, rhodocytin and podoplanin, were used to investigate the role of MAS9 on platelet adhesion and spreading. There is no evidence in the literature about the ability of human platelets to spread on rhodocytin. Here, it has been shown that platelets adhere to and spread on coverslips coated with a high concentration of rhodocytin (300 nM). Additionally, Pollitt et al, demonstrated that platelets can adhere and spread on mouse podoplanin-Fc at a concentration of 10 μg/ml . The adhesion and spreading on human podoplanin-Fc have been demonstrated in this thesis, in section 3.3.2.2, using the same concentration as the mouse protein (10 μg/ml) (Pollitt *et al.*, 2014). MAS9 inhibited platelet adhesion and spreading in a dose-dependent manner on both surfaces, rhodocytin and podoplanin (Figure 5.13). To test the selectivity of MAS9 for the CLEC-2 receptor, other agonists (CRP-XL and fibrinogen) were tested in a spreading assay. For both, MAS9 did not inhibit platelet adhesion, however it significantly and dose-dependently inhibited platelet spreading (Figure 5.14). The inhibition of spreading may be biologically relevant and may be due to crosstalk between receptors. Crosstalk between platelet receptors has been reported in the literature particularly between (hem)ITAM receptors and integrins. For example, Boylan et al. demonstrated that platelet spreading on fibrinogen can be inhibited by using antibodies against FcγRIIA. Additionally, they showed that the cytoplasmic domain of the integrin β3 subunit is required for phosphorylation of FcγRIIA (Boylan *et al.*, 2008). Moreover, Zhi et al. demonstrated that transgenic FcγRIIA-positive murine

platelets had increased spreading on fibrinogen, as well as tyrosine phosphorylation of Syk and PLCγ2 compared to the murine WT control platelets. Additionally, murine platelets expressing FcγRIIA retracted a fibrin clot faster and increased thrombus formation and fibrin deposition in electrolytically injured femoral veins (Zhi *et al.*, 2013). The other reason could be a non-specific action of MAS9 on a component of platelet spreading which is independent of receptor activation. These data demonstrate an important role of MAS9 in the inhibition of CLEC-2-mediated platelet adhesion and spreading. However, a question regarding the observed inhibition of spreading but not adhesion of platelets to other agonists, such as CRP-XL and fibrinogen in the presence of MAS9 remains.

Human dermal lymphatic endothelial cells endogenously express human podoplanin. It has been demonstrated that HDLECs can induce mouse and human platelet aggregation, adhesion and spreading (Borgognone *et al.*, 2014; Navarro-Núñez *et al.*, 2015). Here, MAS9 dose-dependently inhibited platelet adhesion to HDLECs, when compared to a vehicle control (Figure 5.15). Intriguing, in images of vehicle control and low concentration of MAS9-treated samples green spots can be observed where platelets are located. It shows that podoplanin accumulates at sites of contact between platelets and the HDLECs. These data suggest that endogenous human podoplanin is being clustered by platelets. Additionally, visualisation of mouse podoplanin accumulation mediated by mouse CLEC-2 signalling has been demonstrated by Pollitt, et al. TIRF microscopy, showing that mobile mouse podoplanin incorporated into a SLB on contract with the mouse platelet membrane forms microclusters of podoplanin, which migrate to the centre of the platelets forming a single bright cluster. Moreover, FRET analysis of AcGFPmPodoplanin-expressing HEK293T cells incubated with mouse platelets demonstrated a significant difference in fluorescent lifetime compared to control,

suggesting that platelets can initiate podoplanin clustering, similarly to SLBs (Pollitt *et al.*, 2014). In addition, the section 3.3.2.5. of this thesis showed that human podoplanin forms the clusters withing SLB in contact with the human platelets, suggesting a common mechanism between human and mouse.

The accumulation of podoplanin at the platelet cell interface was further investigated by confocal microscopy. Analysis of Z-stack projections demonstrated that the podoplanin is localised at the interface between platelets and HDLEC surface. The accumulation of podoplanin is inhibited by MAS9. This suggests that MAS9 may inhibit the human CLEC-2-podoplanin interaction, however lack of podoplanin accumulation could be the effect of platelet binding inhibition. The formation of a podoplanin cluster at the interface between platelets and HDLECs shares many similarities to the immunological synapse seen between B-cell antigen with primary B cells (Nowosad and Tolar, 2017). This raises the questions about the role of CLEC-2-podoplanin clustering.

Table 5.1. The result summary of the washed platelet-based experiment.

Assay	Platelet concentration	Agonist	Agonist concentration	MAS9 effect		
				10 µM	20 µM	30 µM
Light Transmission Aggregometry	4×10^8 /ml	Rhodocytin	100 nM	-	-	-
			30 nM	-	↓	↓
		CRP-XL	3 µg/ml	-	-	-
			0.3 µg/ml	-	-	-
		Thrombin	0.1 U/ml	-	-	-
Plate-based aggregometry	4×10^8 /ml	Rhodocytin	200 nM	-	↓	-
		CRP-XL	3 µg/ml	-	-	-
		Thrombin	0.05 U/ml	-	-	-
Phosphorylation studies	8×10^8 /ml	Rhodocytin	100 nM	N/A	↓	↓
		CRP-XL	1 µg/ml	N/A	-	-
Fibrinogen binding	4×10^8 /ml	Rhodocytin	100 nM	-	-	↓
		CRP-XL	3 µg/ml	↓	↓	↓
P-selectin exposure	4×10^8 /ml	Rhodocytin	100 nM	-	-	↓
		CRP-XL	3 µg/ml	-	-	-
Platelet adhesion	2×10^7 /ml	Podoplanin	10 µg/ml	↓	↓	↓
		Rhodocytin	300 nM	↓	↓	↓
		CRP-XL	3 µg/ml	-	-	↓
		Fibrinogen	100 µg/ml	-	-	-
Platelet spreading	2×10^7 /ml	Podoplanin	10 µg/ml	↓	↓	↓
		Rhodocytin	300 nM	↓	↓	↓
		CRP-XL	3 µg/ml	↓	↓	↓
		Fibrinogen	100 µg/ml	↓	↓	↓
Platelet adhesion	2×10^7 /ml	Podoplanin in HDLECs	-	-	↓	↓

'↓' (inhibition), '-' (no effect), N/A (not applicable)

5.5. Conclusions

In this chapter MAS9 has been characterised using a variety of different approaches. Firstly, molecular docking studies showed that MAS9 may bind to the CLEC-2 structure in the similar way to podoplanin and rhodocytin. The information about the potential binding sites gives the possibility to understand how MAS9 inhibits the interaction of CLEC-2 with its ligands. Moreover, it has been demonstrated using bio-layer interferometry that MAS9 can bind to CLEC-2 with a binding affinity constant of 7.79 ± 3.5 μM. This affinity constant is greater than the affinity constant of the human CLEC-2-podoplanin interaction, which makes MAS9 a physiologically interesting small molecule inhibitor of this interaction.

In platelet-based assays, it has been demonstrated that MAS9 can inhibit CLEC-2-mediated platelet aggregation, activation, adhesion and spreading, α-granule secretion, and fibrinogen binding. However, these assays used washed platelets in the absence of plasma proteins. Flow cytometry experiments using PRP suggest that MAS9 may be not bioavailable and requires chemical modification to upgrade the structure to make it more potent in plasma. Additionally, MAS9 inhibited the platelet adhesion to HDLECs, which endogenously express podoplanin. It was the only experiment, next to the platelet spreading on the immobilized podoplanin, which showed the potential inhibitory effect of MAS9 for the CLEC-2-podoplanin interaction.

Finally, MAS9 seems to be selective to the CLEC-2 receptor in most of the platelet-based assays, however it also had an inhibitory effect on fibrinogen binding when platelets were stimulated with a GPVI agonist, and it also inhibited platelet spreading but not adhesion to immobilized GPVI and $\alpha_{IIb}\beta_3$ agonists. These results suggest that there might be a cross-talk between ITAM receptors with the integrins. However, this

may not be in itself an issue for anti-platelet actions, although this needs to be tested *in vivo* to establish no major effects on, for example, integrin function elsewhere.

6. General discussion and future directions

This study was focused on platelet receptor CLEC-2 and its interaction with podoplanin. This interaction is involved in many pathological roles, including deep venous thrombosis, blood lymphatic development, septic thrombosis, and cancer. The current antiplatelets therapies may affect other platelet activation pathways that are crucial for haemostasis and may increase the risk of major bleeding. Furthermore, there is also a problem of inadequate efficacy as some patients treated with these drugs may still suffer recurrent thrombosis. Therefore, targeting the CLEC-2-podoplanin interaction, which has a minimal role in haemostasis, can have a therapeutical potential.

In this thesis, the CLEC-2-podoplanin interaction has been investigated in two different ways. Firstly, a semi-high-throughput artificial lipid membrane platform has been developed as an experimental approach to investigate CLEC-2-mediated clustering of its endogenous ligand, podoplanin. Secondly, a high-throughput screen was optimised to identify a small molecule inhibitor of the CLEC-2-podoplanin interaction. The effect of an identified small molecule (MAS9) on human platelet function has been further characterised.

6.1. Development of the artificial lipid membrane platforms

The artificial lipid membrane model provides an opportunity to study the molecular behaviour of platelet receptor signalling components in ways that cannot be achieved using intact platelets. Su et al. biochemically reconstituted a 12-component signalling pathway using an artificial lipid membrane model, beginning with T-cell receptor activation, and ending with actin assembly (Su *et al.*, 2016). Moreover, Pollitt et al. demonstrated that recombinant mouse podoplanin tethered to the supported lipid bilayer formed microsclusters, which migrated to the centre of the mouse platelet, forming a

single bright cluster (Pollitt *et al.*, 2014). Based on the literature, the first aim of this thesis was to develop two semi-high-throughput artificial lipid membrane platforms. The first one, similarly to the reconstituted model of T-cell ITAM signalling pathway established by Su et al., was based on the reconstitution of the intracellular CLEC-2 pathway, beginning with CLEC-2 hemITAM activation, and ending with LAT phosphorylation. The second platform, similarly to the model described by Pollitt et al., was based on the reconstitution of human CLEC-2-mediated activation by tethering human podoplanin into supported lipid bilayer.

To develop the model of the intracellular CLEC-2 pathway, a plasmid containing human CLEC-2 intracellular domain containing histidine- and SNAP-tags has been generated. It has been used to overexpress the protein in *Escherichia coli*. Even though the overexpressed protein formed inclusion bodies, it has been successfully purified using a column-based protein refolding method. The binding of the CLEC-2 intracellular domain to the supported lipid bilayer was firstly confirmed using flow cytometry. The SLBs were formed on silica beads, following incubation with the intracellular domain of CLEC-2, which had been fluorescently labelled through SNAP-tag or not labelled, but recognised by an anti-specific antibody. CLEC-2 tethered to the Ni-NTA-SLBs, compared to a negative control showed the interaction of the recombinant protein with the SLBs. Afterwards, the copy number of Syk, one of the molecules involved in a signalling pathway downstream CLEC-2, was determined in washed platelets using flow cytometry. The copy number was similar to the estimation of absolute numbers of Syk molecules reported in human platelets using a proteomic approach (Burkhart *et al.*, 2012). The knowledge of the protein copy number in platelets allows an appropriate protein concentration to be chosen to mimic a physiologically relevant concentration when used with the SLBs. Finally, the mobility of SLBs

composed of DOPC:DGS-NTA tethered with histidine-tagged fluorescently-labelled CLEC-2 intracellular domain prepared in a FCS2 chamber was tested using a fluorescent recovery after photobleaching approach. However, no lateral mobility of the CLEC-2 withing SLBs was seen. There could be many possibilities of mobility failure. One of the options could be the high lipid ratio within the SLBs. Indeed, Su et al. have found that bilayers containing 5% DGS-NTA or more tend to become less fluid (*Su et al.*, 2017). Another reason for lack of mobility could be incorrectly folded protein after the purification from inclusion bodies. Circular dichroism could be used to check the folding of the refolded recombinant protein. Alternatively, another method of protein incorporation into the SLBs, such as biotin-mediated via streptavidin bridge, could be used. If the lateral mobility of the bilayer could be improved, the next step would be the minimisation of the assay into a 96-well format. Several examples of SLB formation on glass bottom 96-well plates have been reported, including the study mentioned before performed by Su et al. (Taylor *et al.*, 2017; Valvo *et al.*, 2017). Development of this platform gives many perspectives to understand the interactions, localisations, and dynamics of signalling components. It could be used to determine what regulates cluster size and density, understand how intracellular multivalent interactions drive cluster formation and to investigate how small molecule inhibitors affect receptor clustering. Finally, it could be used to study the inhibitory effect of known or novel inhibitors for CLEC-2, focusing on single interactions downstream the pathway. Despite an unachieved goal of the development an intracellular platform, the results in this thesis can be used as a starting point to continue the development process.

The development of a model of human CLEC-2-mediated activation by its endogenous ligand podoplanin began from overexpression of the human podoplanin extracellular domain in fusion with rabbit Fc in mammalian cells. Overexpression in a mammalian

system was required due the fact that podoplanin is highly glycosylated and the glycosylation is needed for its interaction with CLEC-2 (Kato *et al.*, 2003; Kaneko *et al.*, 2007). Podoplanin was purified using a protein A column and confirmed using western blot analysis. Its functionality was demonstrated by the ability for platelets to spread on immobilized purified podoplanin on a glass coverslip. In this SLB model, the podoplanin molecules were tethered to the SLBs via streptavidin bridge. The recombinant podoplanin was monobiotinylated and labelled with a fluorescent dye. The number of podoplanin molecules incorporated into the upper leaflet of the bilayer composed of DOPC:CAP-Biotin-PE lipids was estimated using flow cytometry. This number was compared with the estimated copy number of podoplanin expressed endogenously in human dermal lymphatic endothelial cells. The number of podoplanin molecules incorporated into SLB was similar to the number of podoplanin molecules in cells, which allows the model to be reminiscent of the natural biological conditions. SLBs composed of DOPC:CAP-Biotin-PE lipids have been formed in a FCS2 chamber and the mobility of podoplanin molecules within the bilayer was confirmed. In contrast to the model of the intracellular CLEC-2 pathway, the podoplanin mobility was high. Afterwards, podoplanin clustering caused by platelets was investigated using total internal reflection fluorescence microscopy. Similarly to the observation of Pollitt et al. using mouse podoplanin, when human platelets came into contact with labelled podoplanin mobilised on a supported lipid bilayer a central bright cluster of podoplanin was formed. Clustering of human podoplanin is likely a consequence of the interaction with human CLEC-2 in platelets, as it has been showed with mouse platelets with mouse podoplanin. The platform was then minimised into a 96-well format, the mobility of podoplanin confirm using FRAP and the cluster formation observed using TIRF microscopy. The developed platform has the potential to enable CLEC-2-

mediated clustering to be investigated. It can be used to estimate the minimum unit required to induce CLEC-2-mediated extracellular clustering. Additionally, the platform gives the opportunity to study what regulates cluster size and density, and what regulates podoplanin clustering. Finally, the platform can be used to study novel inhibitors of CLEC-2-mediated signalling, focusing on a primary event – platelet activation by podoplanin.

6.2. HTS and MAS9 characterisation

Recently, there has been a growing interest in the study of small molecules that can inhibit the interaction between CLEC-2 and podoplanin. Over the past few years, two small molecules have been identified as potential inhibitors of the CLEC-2-podoplanin interaction, having a therapeutic potential (Chang *et al.*, 2015; Tsukiji *et al.*, 2018).

The second aim of this thesis was to optimise and perform a high-throughput screen to identify small molecule inhibitors of the CLEC-2-podoplanin interaction. This was achieved during a 2-month secondment to the Pivot Park Screening Centre in the Netherlands. The biochemical assay, called AlphaScreen, was developed using recombinant human CLEC-2 fused with a histidine tag and monobiotinylated human podoplanin-rFc. The optimal protein concentrations were estimated, and this allowed the identification of a positive control for the assay. There were two considered control molecules, which inhibit the CLEC-2-podoplanin interaction: a small molecule Co-HP (Tsukiji *et al.*, 2018) and anti-CLEC-2 antibody AYP1 (Gitz *et al.*, 2014). Since both compounds inhibited the Alpha signal in a similar manner, the small molecule Co-HP was taken forward as the positive control of inhibition. A high-throughput screen was performed using 18,476 small molecule inhibitors from a Pivot Park Screening Centre library at concentrations of 5 μM in a high throughput volume of 4 μl in a 1536-well

plate format. All of the platelets were validated based on the Z' parameter. A hit rate for this screening was estimated as 0.075%, which is typical from experimental HTS, with hit rates most often ranging between 0.01% and 0.14% (Zhu *et al.*, 2013).

14 compounds were identified as potential inhibitors. 5 of these compounds were excluded before the secondary screen due their chemical structure. From the 9 compounds run in the secondary screen, only two, MAS4 and MAS9, showed a significant inhibition effect. These two compounds were further characterised. They were confirmed as true hits using an AlphaScreen TruHits assay. However, during the preparation of MAS4 working solutions it was noticed that the compound precipitated in different buffers and at different pH. The only compound remaining, MAS9, was confirmed to have no toxic effects on platelets up to 30 µM. MAS9 was taken forward as a lead compound for further characterisation in platelet-based assays.

The final aim of this thesis was to characterise the effect of identified small molecule inhibitors identified in HTS on human platelet function. Ethyl 1-[(8- hydroxy- 5- quinolinyl) methyl]- 3-piperidinecarboxylate (MAS9) is a 314 Da small molecule identified in an AlphaScreen-based HTS by screening 18,476 compounds. MAS9 fulfils the criteria of a drug-like compound described by Lipinski's 'rule of 5' and is not toxic for platelets up to 30 µM. The molecular docking study demonstrated that MAS9 binds to CLEC-2 in a similar way to podoplanin and rhodocytin.. Further investigation using recombinant CLEC-2 showed that MAS9 can bind to CLEC-2 with an affinity constant of 7.79 ± 3.5 µM. To compare, the affinity constant of podoplanin has been estimated as 24.5 µM. It suggests that MAS9 may be a good CLEC-2-podoplanin inhibitor, since it has a higher K_D than podoplanin.

In platelet-based assays using rhodocytin and recombinant podoplanin, it was demonstrated that MAS9 selectively inhibits CLEC-2-mediated platelet aggregation, activation, adhesion, spreading, α-granule secretion, and fibrinogen binding at concentrations of 30 µM. As further experiments, a novel ligand for CLEC-2, hemin could be used in the same assays. This would provide further evidence that MAS9 inhibits CLEC-2-mediated activation.

MAS9 also inhibited the interaction of platelets with cells that endogenously express podoplanin. It inhibited platelet adhesion to HDLECs. It was observed that platelets accumulate podoplanin at the surface of HDLECs. The physiological consequence of this accumulation is unknown. But is reminiscent of immunological synapse formed between anti-Igκ and B-cells, detected using plasma membrane sheets (Nowosad and Tolar, 2017).

This assay, alongside platelet spreading on immobilized podoplanin, showed the potential inhibitory effect of MAS9 for the CLEC-2-podoplanin interaction. However, these assays used washed platelets in the absence of plasma proteins. Flow cytometry experiments using PRP suggest that MAS9 may be not bioavailable. However, this needs further confirmation with additional PRP- and whole blood-based platelet assays. The medicinal chemistry could be used to make chemical modifications to be more bioavailable.

In most of the assays used to characterise MAS9, the small molecule was selective to the CLEC-2-mediated response. However, it also presented an inhibitory effect on fibrinogen binding when platelets were stimulated with a GPVI agonist, and it also inhibited platelet spreading but not adhesion to immobilized GPVI and the $\alpha_{IIb}\beta_3$ ligands. It is unclear if these results represent a non-specific action of MAS9 or are a

consequence of a biologically relevant effect. There might be a cross-talk between hemITAM receptors and the integrin, as seen between FcγRIIA and $\alpha_{IIb}\beta_3$ (Boylan *et al.*, 2008; Zhi *et al.*, 2013). However, this hypothesis must be further investigated.

An additional experiment to determine the specificity of MAS9 to other platelet receptors could be achieved using bio-layer interferometry, for example to GPVI or another platelet receptor. This would require the production of recombinant protein with appropriate post-translational modifications. This experiment would confirm the selectivity of MAS9 into CLEC-2.

6.3. Conclusions

To conclude, this study provides the opportunity to take full advantage of the supported lipid bilayer model to understand CLEC-2-mediated signalling and clustering. In addition, since CLEC-2 is a good target for novel anti-platelet drugs having therapeutic effects on arterial/venous thrombosis and cancer, MAS9 may be a good tool to explore therapeutic potential. This work provides a framework for future research focused on the CLEC-2-podoplanin interaction and novel drug identification and development.

7. References

Acton, S. E. *et al.* (2012) 'Podoplanin-Rich Stromal Networks Induce Dendritic Cell Motility via Activation of the C-type Lectin Receptor CLEC-2', *Immunity*, 37(2), pp. 276–289.

Aibibula, M., Naseem, K. M. and Sturmey, R. G. (2018) 'Glucose metabolism and metabolic flexibility in blood platelets', *Journal of Thrombosis and Haemostasis*, 16(11), pp. 2300–2314.

Alshehri, O. M. *et al.* (2015) 'Activation of glycoprotein VI (GPVI) and C-type lectin-like receptor-2 (CLEC-2) underlies platelet activation by diesel exhaust particles and other charged/hydrophobic ligands', *Biochemical Journal*, 468(3), pp. 459–473.

Alshehri, O. M. *et al.* (2015) 'Fibrin activates GPVI in human and mouse platelets', *Blood*, 126(13), pp. 1601–1608.

Ambrose, E. J. (1956) 'A Surface Contact Microscope for the study of Cell Movements', *Nature*, 178(1053), p. 1194.

An, W. F. and Tolliday, N. (2010) 'Cell-based assays for high-throughput screening', *Molecular Biotechnology*, 45(2), pp. 180–186.

Andrews, R. K. *et al.* (2002) 'Interaction of calmodulin with the cytoplasmic domain of platelet glycoprotein VI', *Blood*, 99(11), pp. 4219–4221.

Andrews, R. K. and Berndt, M. C. (2013) 'Bernard – Soulier Syndrome: An Update', *Semin Thromb Hemost*, 39, pp. 656–662.

Arman, M. *et al.* (2014) 'Amplification of bacteria-induced platelet activation is triggered by FcγRIIA, integrin αIIbβ3, and platelet factor 4', *Blood*, 123(20), pp. 3166–3174.

Asselin, J. *et al.* (1999) 'Monomeric (glycine-proline-hydroxyproline)10 repeat sequence is a partial agonist of the platelet collagen receptor glycoprotein VI', *Biochemical Journal*, 339(2), pp. 413–418.

Axelrod, D. *et al.* (1976) 'Mobility measurement by analysis of fluorescence photobleaching recovery kinetics', *Biophysical Journal*, 16(9), pp. 1055–1069.

Axelrod, D. (1981) 'Cell-substrate contacts illuminated by total internal reflection fluorescence', *Journal of Cell Biology*, 89(1), pp. 141–145.

Badolia, R. *et al.* (2017) 'Gq pathway regulates proximal C-type lectin-like receptor-2 (CLEC-2) signaling in platelets', *Journal of Biological Chemistry*, 292(35), pp. 14516–14531.

Baell, J. B. and Holloway, G. A. (2010) 'New substructure filters for removal of pan assay interference compounds (PAINS) from screening libraries and for their exclusion in bioassays', *Journal of Medicinal Chemistry*, 53(7), pp. 2719–2740.

Bailey, S. R. *et al.* (2000) 'Actions and interactions of ADP, 5-HT, histamine and PAF on equine platelets', *Research in Veterinary Science*, 68(2), pp. 175–180.

Bajorath, J. (2002) 'Integration of virtual and high-throughput screening', *Nature Reviews Drug Discovery*, 1(11), pp. 882–894.

Baroletti, S. A. and Goldhaber, S. Z. (2006) 'Heparin-induced thrombocytopenia', *Circulation*, 114(8), pp. 355–357.

Beck, V., Pfitscher, A. and Jungbauer, A. (2005) 'GFP-reporter for a high throughput assay to monitor estrogenic compounds', *Journal of Biochemical and Biophysical Methods*, 64(1), pp. 19–37.

Bender, M. *et al.* (2013) 'Combined in vivo depletion of glycoprotein VI and C-type lectin-like receptor 2 severely compromises hemostasis and abrogates arterial thrombosis in mice', *Arteriosclerosis, Thrombosis, and Vascular Biology*, 33(5), pp. 926–934.

Berridge, M. J., Bootman, M. D. and Roderick, H. L. (2003) 'Calcium signalling: Dynamics, homeostasis and remodelling', *Nature Reviews Molecular Cell Biology*, 4(7), pp. 517–529.

Bertozzi, C. C. *et al.* (2010) 'Platelets regulate lymphatic vascular development through CLEC-2-SLP-76 signaling', *Blood*, 116(4), pp. 661–670.

Best, D. *et al.* (2003) 'GPVI levels in platelets: Relationship to platelet function at high shear', *Blood*, 102(8), pp. 2811–2818.

Blake, R. A. *et al.* (1994) 'Fcγ receptor II stimulated formation of inositol phosphates in human platelets is blocked by tyrosine kinase inhibitors and associated with tyrosine phosphorylation of the receptor', *FEBS Letters*, 342(1), pp. 15–18.

Bodin, S. *et al.* (2003) 'A critical role of lipid rafts in the organization of a key FcγRIIa-mediated signaling pathway in human platelets', *Thrombosis and Haemostasis*, 89(2), pp. 318–330.

Borgognone, A. *et al.* (2014) 'CLEC-2-dependent activation of mouse platelets is weakly inhibited by cAMP but not by cGMP', *Journal of Thrombosis and Haemostasis*, 12(4), pp. 550–559.

Born, G. V. R. (1962) 'Aggregation of blood platelets by adenosine diphosphate and its reversal', *Nature*, 194(4832), pp. 927–929.

Boulaftali, Y. *et al.* (2014) 'Platelet ITAM Signaling and Vascular Integrity', *Circulation Research*, 114(7), pp. 1174–1184.

Bourne, J. H. *et al.* (2021) 'Heme induces human and mouse platelet activation through C-type-lectin-like receptor-2', *Haematologica*, 106(2), pp. 626–629.

Boylan, B. *et al.* (2008) 'Identification of FcgammaRlla as the ITAM-bearing receptor mediating alphaIIbbeta3 outside-in integrin signaling in human platelets', *Blood*, 112(7), pp. 2780–2786.

Breiteneder-Geleff, S. *et al.* (1997) 'Podoplanin, novel 43-kd membrane protein of glomerular epithelial cells, is down-regulated in puromycin nephrosis', *American Journal of Pathology*, 151(4), pp. 1141–1152.

Breiteneder-Geleff, S. *et al.* (1999) 'Angiosarcomas express mixed endothelial phenotypes of blood and lymphatic capillaries: Podoplanin as a specific marker for lymphatic endothelium', *American Journal of Pathology*. American Society for Investigative Pathology, 154(2), pp. 385–394.

Bretscher, A., Edwards, K. and Fehon, R. G. (2002) 'ERM proteins and merlin: Integrators at the cell cortex', *Nature Reviews Molecular Cell Biology*, 3(8), pp. 586–599.

Brooks, D. G. *et al.* (1989) 'Structure and expression of human IgG (FcRII(CD32). Functional heterogeneity is encoded by the alternatively spliced products of multiple genes', *Journal of Experimental Medicine*, 170(4), pp. 1369–1385.

Burkhart, J. M. *et al.* (2012) 'The first comprehensive and quantitative analysis of human platelet protein composition allows the comparative analysis of structural and functional pathways', *Blood*, 120(15), pp. 73–82.

Caré, B. and Soula, H. (2013) 'Receptor clustering affects signal transduction at the membrane level in the reaction-limited regime. Bertrand', *Physical Review E : Statistical, Nonlinear, and Soft Matter Physics, American Physical Society*, 87(1), pp. 1–9.

Case, L. *et al.* (2019) 'Stoichiometry controls activity of phase separated clusters of actin signaling proteins', *Science*, 363(6431), pp. 1093–1097.

Chan, M. V., Armstrong, P. C. and Warner, T. D. (2018) '96-Well Plate-Based Aggregometry', *Platelets*. Taylor & Francis, 29(7), pp. 650–655.

Chang, Y. W. *et al.* (2015) 'Identification of a novel platelet antagonist that binds to CLEC-2 and suppresses podoplanin-induced platelet aggregation and cancer metastasis', *Oncotarget*, 6(40), pp. 42733–42748.

Choi, E. S. *et al.* (1995) 'Platelets generated in vitro from proplatelet-displaying human megakaryocytes are functional', *Blood*. American Society of Hematology, 85(2), pp. 402–413.

Christou, C. M. *et al.* (2008) 'Renal cells activate the platelet receptor CLEC-2 through podoplanin', *Biochemical Journal*, 411(1), pp. 133–140.

Chung, C. H., Au, L. C. and Huang, T. F. (1999) 'Molecular cloning and sequence analysis of aggretin, a collagen-like platelet aggregation inducer', *Biochemical and Biophysical Research Communications*, 263(3), pp. 723–727.

Cines, D. B. and McMillan, R. (2007) 'Pathogenesis of chronic immune thrombocytopenic purpura', *Current Opinion in Hematology*, 14(5), pp. 511–514.

Clark, J. C. *et al.* (2021) 'Evidence that GPVI is Expressed as a Mixture of Monomers and Dimers, and that the D2 Domain is not Essential for GPVI Activation', *Thrombosis and Haemostasis*.

Clements, J. L. *et al.* (1999) 'Fetal hemorrhage and platelet dysfunction in SLP-76-deficient mice', *Journal of Clinical Investigation*, 103(1), pp. 19–25.

Clemetson, J. M. *et al.* (1999) 'The platelet collagen receptor glycoprotein VI is a member of the immunoglobulin superfamily closely related to FcαR and the natural killer receptors', *Journal of Biological Chemistry*, 274(41), pp. 29019–29024.

Clemetson, K. J. (2010) 'Snaclecs (snake C-type lectins) that inhibit or activate platelets by binding to receptors', *Toxicon*. Elsevier Ltd, 56(7), pp. 1236–1246.

Colonna, M., Samaridis, J. and Angman, L. (2000) 'Molecular characterization of two novel C-type lectin-like receptors, one of which is selectively expressed in human dendritic cells', *European Journal of Immunology*, 30, pp. 697–704.

Crocke, E. L. (1998) 'Cholesterol function in plasma membranes from ectotherms: Membrane-specific roles in adaptation to temperature', *American Zoologist*, 38(2), pp. 291–304.

Cueni, L. N. and Detmar, M. (2009) 'Galectin-8 interacts with podoplanin and modulates lymphatic endothelial cell functions', *Experimental Cell Research*, 315(10), pp. 1715–1723.

Cutler, L., Rodan, G. and Feinstein, M. B. (1978) 'Cytochemical localization of adenylate cyclase and of calcium ion, magnesium ion-activated ATPases in the dense tubular system of human blood platelets.', *Biochim Biophys Act*, 542(3), pp. 357–371.

David, L. *et al.* (2019) 'Identification of Compounds That Interfere with High-Throughput Screening Assay Technologies', *ChemMedChem*, 14(20), pp. 1795–1802.

Davis, S. J. and van der Merwe, P. A. (2011) 'Lck and the nature of the T cell receptor trigger', *Trends in Immunology*, 32(1), pp. 1–5.

Debrincat, M. A. *et al.* (2012) 'Mcl-1 and Bcl-xL coordinately regulate megakaryocyte survival', *Blood*, 119(24), pp. 5850–5858.

Dickeson, S. K., Walsh, J. J. and Santoro, S. A. (1998) 'Binding of the α2 integrin I domain to extracellular matrix ligands: Structural and mechanistic differences between collagen and laminin binding', *Cell Adhesion and Communication*, 5(4), pp. 273–281.

Diller, D. J. and Merz, K. M. (2001) 'High throughput docking for library design and library prioritization', *Proteins: Structure, Function and Genetics*, 43(2), pp. 113–124.

Du, X. *et al.* (1987) 'Glycoprotein Ib and glycoprotein IX are fully complexed in the intact platelet membrane', *Blood*. American Society of Hematology, 69(5), pp. 1524–1527.

Dunster, J. L. *et al.* (2019) 'Interspecies differences in protein expression do not impact the spatiotemporal regulation of glycoprotein VI mediated activation', *Journal of Thrombosis and Haemostasis*, (October), pp. 1–12.

Durocher, Y. and Butler, M. (2009) 'Expression systems for therapeutic glycoprotein production', *Current Opinion in Biotechnology*, 20(6), pp. 700–707.

Dustin, M. L. *et al.* (2007) 'Supported Planar Bilayers for Study of the Immunological Synapse', *Current Protocols in Immunology*, pp. 1–35.

Dustin, M. L. and Groves, J. T. (2012) 'Receptor signaling clusters in the immune synapse', *Annual Review of Biophysics*, 41(1), pp. 543–556.

Dustin, M. L. and Pollitt, A. Y. (2018) 'The Study of Platelet Receptors Using Artificial Lipid Bilayers', in Gibbins, J. M. and Mahaut-Smith, M. (eds) *Platelets and Megakaryocytes : Volume 4, Advanced Protocols and Perspectives*. New York, NY: Springer New York, pp. 127–137.

Ebbe, S. (1976) 'Biology of megakaryocytes', *Prog. Hemost. Thromb.*, 3, pp. 211–229.

Edward Quach, M., Chen, W. and Li, R. (2018) 'Mechanisms of platelet clearance and translation to improve platelet storage', *Blood*, 131(14), pp. 1512–1521.

Eggeling, C. *et al.* (2003) 'Highly sensitive fluorescence detection technology currently available for HTS', *Drug Discovery Today*, 8(14), pp. 632–641.

Eggert, U. S. *et al.* (2004) 'Parallel chemical genetic and genome-wide RNAi screens identify cytokinesis inhibitors and targets', *PLoS Biology*, 2(12).

Eglen, R. M. *et al.* (2008) 'The Use of AlphaScreen Technology in HTS: Current Status', *Current Chemical Genomics*, 1, pp. 2–10.

Elokely, K. and Doerksen, R. (2013) 'Docking challenge: Protein sampling and molecular docking performance', *J Chem Inf Model*, 53(8), pp. 1934–1945.

Erlandsen, S. L. *et al.* (2001) 'High-resolution CryoFESEM of individual cell adhesion molecules (CAMs) in the glycocalyx of human platelets: Detection of P-selectin (CD62P), GPI-IX complex (CD42a/CD42bα,bβ), and integrin GPIIbIIIa (CD41/CD61) by immunogold labeling and stereo imaging', *Journal of Histochemistry and Cytochemistry*, 49(7), pp. 809–819.

Feizi, T. (1985) 'Demonstration by monoclonal antibodies that carbohydrate structures of glycoproteins and glycolipids are onco-developmental antigens', *Nature*, 314(6006), pp. 53–57.

Feng, J. *et al.* (2005) 'Convergence on a distinctive assembly mechanism by unrelated families of activating immune receptors', *Immunity*, 22(4), pp. 427–438.

Finney, B. A. *et al.* (2012) 'CLEC-2 and Syk in the megakaryocytic/platelet lineage are essential for development', *Blood*, 119(7), pp. 1747–1756.

Fooksman, D. R. *et al.* (2010) 'Functional Anatomy of T Cell Activation and Synapse Formation', *Annu Rev Immunol.*, 28, pp. 79–105.

Fratantoni, J. C. and Poindexter, B. J. (1990) 'Measuring platelet aggregation with microplate reader. A new technical approach to platelet aggregation studies', *American Journal of Clinical Pathology*, 94(5), pp. 613–617.

Frearson, J. A. and Collie, I. T. (2009) 'HTS and hit finding in academia - from chemical genomics to drug discovery', *Drug Discovery Today*, 14(23–24), pp. 1150–1158.

Friesner, R. A. *et al.* (2006) 'Extra precision glide: Docking and scoring incorporating a model of hydrophobic enclosure for protein-ligand complexes', *Journal of Medicinal Chemistry*, 49(21), pp. 6177–6196.

Fu, J. *et al.* (2008) 'Endothelial cell O-glycan deficiency causes blood/lymphatic misconnections and consequent fatty liver disease in mice', *Journal of Clinical Investigation*, 118(11), pp. 3725–3737.

Garcia-Parajo, M. F. *et al.* (2014) 'Nanoclustering as a dominant feature of plasma membrane organization', *Journal of Cell Science*, 127(23), pp. 4995–5005.

Gashaw, I. *et al.* (2012) 'What makes a good drug target?', *Drug Discovery Today*. Elsevier Ltd, 17(SUPPL.), pp. S24–S30.

Gibbins, J. M. *et al.* (1997) 'Glycoprotein VI is the collagen receptor in platelets which underlies tyrosine phosphorylation of the Fc receptor γ-chain', *FEBS Letters*. Federation of European Biochemical Societies, 413(2), pp. 255–259.

Gibbins, J. M. *et al.* (1998) 'The p85 subunit of phosphatidylinositol 3-kinase associates with the Fc receptor γ-chain and linker for activitor of T cells (LAT) in platelets stimulated by collagen and convulxin', *Journal of Biological Chemistry*. Â© 1998 ASBMB, 273(51), pp. 34437–34443.

Gillissen, M. A. *et al.* (2016) 'The modified FACS calcein AM retention assay: A high throughput flow cytometer based method to measure cytotoxicity', *Journal of Immunological Methods*, 434, pp. 16–23.

Gitz, E. *et al.* (2014) 'CLEC-2 expression is maintained on activated platelets and on platelet microparticles', *Blood*, 124(14), pp. 2262–2270.

Golebiewska, E. M. and Poole, A. W. (2015) 'Platelet secretion: From haemostasis to wound healing and beyond', *Blood Reviews*. Elsevier B.V., 29(3), pp. 153–162.

Goto, S. *et al.* (2002) 'Involvement of glycoprotein VI in platelet thrombus formation on both collagen and von Willebrand factor surfaces under flow conditions', *Circulation*, 106(2), pp. 266–272.

Graeve, L. *et al.* (1988) 'Polarized apical distribution of glycosyl-phosphatidylinositol-anchored proteins in a renal epithelial cell line.', *Proceedings of the National Academy of Sciences*, 85(24), pp. 9557–9561.

Gratacap, M. P. *et al.* (1998) 'Phosphatidylinositol 3,4,5-trisphosphate-dependent stimulation of phospholipase C-γ2 is an early key event in FcγRIIA-mediated activation of human platelets', *Journal of Biological Chemistry*, 273(38), pp. 24314–24321.

Grove, E. L. *et al.* (2015) 'Antiplatelet therapy in acute coronary syndromes', *Expert Opinion on Pharmacotherapy*, 16(14), pp. 2133–2147.

Haining, E. J. *et al.* (2017) 'CLEC-2 contributes to hemostasis independently of classical hemITAM signaling in mice', *Blood*, 130(20), pp. 2224–2228.

Haining, E. J. *et al.* (2021) 'Lymphatic blood filling in CLEC-2-deficient mouse models', *Platelets.* Taylor & Francis, 32(3), pp. 352–367.

Hamid, R. *et al.* (2004) 'Comparison of alamar blue and MTT assays for high through-put screening', *Toxicology in Vitro*, 18(5), pp. 703–710.

Hancock, J. F. (2006) 'Lipid rafts: Contentious only from simplistic standpoints', *Nature Reviews Molecular Cell Biology*, 7(6), pp. 456–462.

Harbi, M. H. *et al.* (2021) 'Novel antiplatelet strategies targeting GPVI, CLEC-2 and tyrosine kinases', *Platelets.* Taylor & Francis, 32(1), pp. 29–41.

Harker, L. A. and Finch, C. A. (1969) 'Thrombokinetics in man.', *The Journal of clinical investigation*, 48(6), pp. 963–974.

Hartman, N. C., Nye, J. A. and Groves, J. T. (2009) 'Cluster size regulates protein sorting in the immunological synapse', *Proceedings of the National Academy of Sciences of the United States of America*, 106(31), pp. 12729–12734.

Hartwig, J. H. (1992) 'Mechanisms of actin rearrangements mediating platelet activation', *Journal of Cell Biology*, 118(6), pp. 1421–1441.

Hato, T., Pampori, N. and Shattil, S. J. (1998) 'Complementary roles for receptor clustering and conformational change in the adhesive and signaling functions of integrin α(IIb)β3', *Journal of Cell Biology*, 141(7), pp. 1685–1695.

Hertzberg, R. P. and Pope, A. J. (2000) 'High-throughput screening: New technology for the 21st century', *Current Opinion in Chemical Biology*, 4(4), pp. 445–451.

Hess, P. R. *et al.* (2014) 'Platelets mediate lymphovenous hemostasis to maintain blood-lymphatic separation throughout life', *Journal of Clinical Investigation*, 124(1), pp. 273–284.

Hitchcock, J. R. *et al.* (2015) 'Inflammation drives thrombosis after Salmonella infection via CLEC-2 on platelets', *Journal of Clinical Investigation*, 125(12), pp. 4429–4446.

Hodivala-Dilke, K. M. *et al.* (1999) 'β3-integrin-deficient mice are a model for Glanzmann thrombasthenia showing placental defects and reduced survival', *Journal of Clinical Investigation*, 103(2), pp. 229–238.

Holinstat, M. *et al.* (2006) 'PAR4, but Not PAR1, Signals Human Platelet Aggregation via Ca2+ Mobilization and Synergistic P2Y12 Receptor Activation', *J Biol Chem*, 281(36), pp. 26665–26674.

Holinstat, M. (2017) 'Normal platelet function', *Cancer and Metastasis Reviews*, 36(2), pp. 195–198.

Holtkötter, O. *et al.* (2002) 'Integrin α 2-deficient mice develop normally, are fertile, but display partially defective platelet interaction with collagen', *Journal of Biological Chemistry*, 277(13), pp. 10789–10794.

Hoofnagle, A. and Wener, M. (2009) 'The Fundamental Flaws of Immunoassays and Potential Solutions Using Tandem Mass Spectrometry', *J Immunol Methods*, 347(1–2), pp. 3–11.

Horii, K., Kahn, M. L. and Herr, A. B. (2006) 'Structural basis for platelet collagen responses by the immune-type receptor glycoprotein VI', *Blood*, 108(3), pp. 936–942.

Hotchkiss, R. S. and Karl, I. E. (2003) 'The Pathophysiology and Treatment of Sepsis', *New England Journal of Medicine*, 348(2), pp. 138–150.

Hou, T. Z. *et al.* (2010) 'A distinct subset of podoplanin (gp38) expressing F4/80+ macrophages mediate phagocytosis and are induced following zymosan peritonitis', *FEBS Letters*. Federation of European Biochemical Societies, 584(18), pp. 3955–3961.

Huang, W. Y. C. *et al.* (2019) 'A molecular assembly phase transition and kinetic proofreading modulate Ras activation by SOS', *Science*, 363(6431), pp. 1098–1103.

Huggins, M. L. (1954) 'The structure of collagen', *Journal of the American Chemical Society*, 76(15), pp. 4045–4046.

Hughes, C. E. *et al.* (2010) 'CLEC-2 is not required for platelet aggregation at arteriolar shear', *Journal of Thrombosis and Haemostasis*, 8(10), pp. 2328–2332.

Huysamen, C. and Brown, G. D. (2009) 'The fungal pattern recognition receptor, Dectin-1, and the associated cluster of C-type lectin-like receptors', *FEMS Microbiology Letters*, 290(2), pp. 121–128.

Hynes, R. O. (2002) 'Integrins: Bidirectional, allosteric signaling machines', *Cell*, 110(6), pp. 673–687.

Hyvönen, M. and Saraste, M. (1997) 'Stucture of the PH domain and Btk motif from Bruton's tyrosine kinase: Molecular explanations for X-linked agammaglobulinaemia', *EMBO Journal*, 16(12), pp. 3396–3404.

Ishikawa-Ankerhold, H., Ankerhold, R. and Drummen, G. (2014) 'Fluorescence recovery after photobleaching', *eLS. John Wiley & Sons*, pp. 1–11.

Italiano, J. E. *et al.* (1999) 'Blood platelets are assembled principally at the ends of proplatelet processes produced by differentiated megakaryocytes', *Journal of Cell Biology*, 147(6), pp. 1299–1312.

Ito, T. *et al.* (1996) 'Recombinant human c-Mpl ligand is not a direct stimulator of proplatelet formation in mature human megakaryocytes', *British Journal of Haematology*, 94(2), pp. 387–390.

Izquierdo, I. *et al.* (2019) 'Platelet membrane lipid rafts protein composition varies following GPVI and CLEC-2 receptors activation', *Journal of Proteomics*. Elsevier, 195(December 2018), pp. 88–97.

Izquierdo, I. *et al.* (2020) 'A Comprehensive Tyrosine Phosphoproteomic Analysis Reveals Novel Components of the Platelet CLEC-2 Signaling Cascade', *Thrombosis and Haemostasis*, 120(2), pp. 262–276.

Jackson, C. W. and Edwards, C. C. (1977) 'Biphasic Thrombopoietic Response to Severe Hypobaric Hypoxia', *British Journal of Haematology*, 35(2), pp. 233–244.

Josefsson, E. C. *et al.* (2011) 'Megakaryocytes possess a functional intrinsic apoptosis pathway that must be restrained to survive and produce platelets', *Journal of Experimental Medicine*, 208(10), pp. 2017–2031.

Josefsson, E. C. *et al.* (2013) 'The Regulation of Platelet Life Span', *Platelets*. Elsevier Inc., pp. 51–65.

Judd, B. A. *et al.* (2002) 'Differential requirement for LAT and SLP-76 in GPVI versus T cell receptor signaling', *Journal of Experimental Medicine*, 195(6), pp. 705–717.

Jung, S. M. and Moroi, M. (2000) 'Activation of the platelet collagen receptor integrin α2β1. Its mechanism and participation in the physiological functions of platelets', *Trends in Cardiovascular Medicine*, 10(7), pp. 285–292.

Jung, S. M., Tsuji, K. and Moroi, M. (2009) 'Glycoprotein (GP) VI dimer as a major collagen-binding site of native platelets: Direct evidence obtained with dimeric GPVI-specific Fabs', *Journal of Thrombosis and Haemostasis*, 7(8), pp. 1347–1355.

Kahn, M. L. *et al.* (1999) 'Protease-activated receptors 1 and 4 mediate activation of human platelets by thrombin', *Journal of Clinical Investigation*, 103(6), pp. 879–887.

Kamath, S., Blann, A. D. and Lip, G. Y. H. (2001) 'Platelet activation: Assessment and quantification', *European Heart Journal*, 22(17), pp. 1561–1571.

Kaneko, M. K. *et al.* (2007) 'Functional glycosylation of human podoplanin: Glycan structure of platelet aggregation-inducing factor', *FEBS Letters*, 581(2), pp. 331–336.

Karas, S., Rosse, W. and Kurlander, R. (1982) 'Characterization of the IgG-Fc receptor on human platelets', *Blood*. American Society of Hematology, 60(6), pp. 1277–1282.

Kato, K. *et al.* (2003) 'The contribution of glycoprotein VI to stable platelet adhesion and thrombus formation illustrated by targeted gene deletion', *Blood*, 102(5), pp. 1701–1707.

Kato, Y. *et al.* (2003) 'Molecular Identification of Aggrus/T1α as a Platelet Aggregation-inducing Factor Expressed in Colorectal Tumors', *Journal of Biological Chemistry*, 278(51), pp. 51599–51605.

Kaushansky, K. *et al.* (1994) 'Promotion of megakaryocyte progenitor expansion and differentiation by the c-Mpl ligand thrombopoietin', *Nature*, 369(6481), pp. 568–571.

Kaushansky, K. (2005) 'The molecular mechanisms that control thrombopoiesis', *The Journal of Clinical Investigation*, 115(12), pp. 3339–3347.

Kauskot, A. and Hoylaerts, M. F. (2012) *Platelets: Past, present and future. Platelet Receptors*, *Handbook of Experimental Pharmacology*.

Kerjaschki, D. *et al.* (2004) 'Lymphatic Neoangiogenesis in Human Kidney Transplants Is Associated with Immunologically Active Lymphocytic Infiltrates', *Journal of the American Society of Nephrology*, 15(3), pp. 603–612.

Khan, M. S., Dosoky, N. S. and Williams, J. D. (2013) 'Engineering lipid bilayer membranes for protein studies', *International Journal of Molecular Sciences*, 14(11), pp. 21561–21597.

Kingston, R. E., Chen, C. A. and Okayama, H. (1999) 'Calcium Phosphate Transfection', *Current Protocols in Immunology*, 31(1), pp. 10.13.1-10.13.9.

Kisucka, J. *et al.* (2006) 'Platelets and platelet adhesion support angiogenesis while preventing excessive hemorrhage', *Proceedings of the National Academy of Sciences of the United States of America*, 103(4), pp. 855–860.

Koedam, J. A. *et al.* (1992) 'P-selectin, a granule membrane protein of platelets and endothelial cells, follows the regulated secretory pathway in AtT-20 cells', *Journal of Cell Biology*, 116(3), pp. 617–625.

Krishnan, H. *et al.* (2018) 'Podoplanin: An emerging cancer biomarker and therapeutic target', *Cancer Science*, 109(5), pp. 1292–1299.

Kumaraswamy, S. and Tobias, R. (2015) *Chapter 10. Label-Free Kinetic Analysis of an Antibody–Antigen Interaction Using Biolayer Interferometry*, *Protein-Protein Interactions: Methods and Applications: Second Edition*.

Kunita, A. *et al.* (2007) 'The platelet aggregation-inducing factor aggrus/podoplanin promotes pulmonary metastasis', *American Journal of Pathology*, 170(4), pp. 1337–1347.

Lanza, F. (2006) 'Bernard-Soulier syndrome (Hemorrhagiparous thrombocytic dystrophy)', *Orphanet Journal of Rare Diseases*, 1(1), pp. 1–6.

Lecut, C. *et al.* (2004) 'Identification of residues within human glycoprotein VI involved in the binding to collagen: Evidence for the existence of distinct binding sites', *Journal of Biological Chemistry*, 279(50), pp. 52293–52299.

Lefrançais, E. *et al.* (2017) 'The lung is a site of platelet biogenesis and a reservoir for hematopoietic progenitors Emma', *Nature*, 544(7648), pp. 105–109.

Li, S. De *et al.* (2006) 'Hemin-mediated hemolysis in erythrocytes: Effects of ascorbic acid and glutathione', *Acta Biochimica et Biophysica Sinica*, 38(1), pp. 63–69.

Li, X. *et al.* (2007) 'Functional characterization of cell lines for high-throughput screening of human neuromedin U receptor subtype 2 specific agonists using a luciferase reporter gene assay', *European Journal of Pharmaceutics and Biopharmaceutics*, 67(1), pp. 284–292.

Li, Z. *et al.* (2006) 'Sequential activation of p38 and ERK pathways by cGMP-dependent protein kinase leading to activation of the platelet integrin α IIbβ3', *Blood*, 107(3), pp. 965–972.

Li, Z. *et al.* (2010) 'Signaling during platelet adhesion and activation', *Arteriosclerosis, Thrombosis, and Vascular Biology*, 30(12), pp. 2341–2349.

Liebman, P. and Entine, G. (1974) 'Lateral Diffusion of Visual Pigment in Rod Disk Membranes', *Science*, 185, pp. 457–559.

Lingwood, D. and Simons, K. (2010) 'Lipid rafts as a membrane-organizing principle', *Science*, 327(5961), pp. 46–50.

Lipinski, C. *et al.* (1997) 'Experimental and computational approaches to estimate solubility and permeability in drug discovery and development settings', *Advanced Drug Delivery Reviews*, 23(1–3), pp. 3–25.

Locke, D. *et al.* (2002) 'Lipid rafts orchestrate signaling by the platelet receptor glycoprotein VI', *Journal of Biological Chemistry*. Â© 2002 ASBMB, 277(21), pp. 18801–18809.

López, J. *et al.* (1998) 'Bernard-Soulier Syndrome', *The Journal of The American Society of Hematology*, 91(12), pp. 4397–4418.

Loyau, S. *et al.* (2012) 'Platelet glycoprotein VI dimerization, an active process inducing receptor competence, is an indicator of platelet reactivity', *Arteriosclerosis, Thrombosis, and Vascular Biology*, 32(3), pp. 778–785.

Ma, Y. Q., Qin, J. and Plow, E. F. (2007) 'Platelet integrin $\alpha IIb\beta 3$: Activation mechanisms', *Journal of Thrombosis and Haemostasis*, 5(7), pp. 1345–1352.

Macarron, R. and Hertzberg, R. (2009) *High Throughput Screening. Chapter 1. Design and Implementation of High-Throguhput Screening assays*, *Methods and Protocols*.

Mammadova-Bach, E. *et al.* (2015) 'Platelet glycoprotein VI binds to polymerized fibrin and promotes thrombin generation', *Blood*, 126(5), pp. 683–691.

Mammadova-Bach, E. *et al.* (2020) 'Platelet glycoprotein VI promotes metastasis through interaction with cancer cell–derived galectin-3', *Blood*, 135(14), pp. 1146–1160.

Mangin, P. H. *et al.* (2018) 'Immobilized fibrinogen activates human platelets through glycoprotein VI', *Haematologica*, 103(5), pp. 898–907.

Manne, B. K. *et al.* (2013) 'Fucoidan is a novel platelet agonist for the C-type lectin-like receptor 2 (CLEC-2)', *Journal of Biological Chemistry*, 288(11), pp. 7717–7726.

Manne, B. K. *et al.* (2015) 'Distinct pathways regulate Syk protein activation downstream of immune tyrosine activation motif (ITAM) and hemITAM receptors in platelets', *Journal of Biological Chemistry*, 290(18), pp. 11557–11568.

Martín-Villar, E. *et al.* (2006) 'Podoplanin binds ERM proteins to activate RhoA and promote epithelial-mesenchymal transition', *Journal of Cell Science*, 119(21), pp. 4541–4553.

Martín-Villar, E. *et al.* (2010) 'Podoplanin associates with cd44 to promote directional cell migration', *Molecular Biology of the Cell*, 21(24), pp. 4387–4399.

Mason, K. D. *et al.* (2007) 'Programmed Anuclear Cell Death Delimits Platelet Life Span', *Cell*, 128(6), pp. 1173–1186.

Mattheyses, A. L., Simon, S. M. and Rappoport, J. Z. (2010) 'Imaging with total internal reflection fluorescence microscopy for the cell biologist', *Journal of Cell Science*, 123(21), pp. 3261–3628.

Maxwell, K. F. *et al.* (1999) 'Crystal structure of the human leukocyte Fc receptor, FcγRIIa', *Nature Structural Biology*, 6(5), pp. 437–442.

May, F. *et al.* (2009) 'CLEC-2 is an essential platelet-activating receptor in hemostasis and thrombosis', *Blood*, 114(16), pp. 3464–3472.

Mayr, L. M. and Bojanic, D. (2009) 'Novel trends in high-throughput screening', *Current Opinion in Pharmacology*, 9(5), pp. 580–588.

Mazet, F. *et al.* (2015) 'A high-density immunoblotting methodology for quantification of total protein levels and phosphorylation modifications', *Scientific Reports*. Nature Publishing Group, 5(October), pp. 1–8.

McGovern, S. L. *et al.* (2002) 'A common mechanism underlying promiscuous inhibitors from virtual and high-throughput screening', *Journal of Medicinal Chemistry*, 45(8), pp. 1712–1722.

van Meer, G. *et al.* (1987) 'Sorting of sphingolipids in epithelial (Madin-Darby canine kidney) cells.', *The Journal of cell biology*, 105(4), pp. 1623–1635.

van Meer, G., Voelker, D. R. and Feigenson, G. W. (2008) 'Membrane lipids: where they are and how they behave', *Nat Rev Mol Cell Biol*, 9(2), pp. 112–124.

Miura, Y. *et al.* (2000) 'Cloning and expression of the platelet-specific collagen receptor glycoprotein VI', *Thrombosis Research*, 98(4), pp. 301–309.

Miura, Y. *et al.* (2002) 'Analysis of the interaction of platelet collagen receptor glycoprotein VI (GPVI) with collagen: A dimeric form of GPVI, but not the monomeric form, shows affinity to fibrous collagen', *Journal of Biological Chemistry*, 277(48), pp. 46197–46204.

Modderman, P. W. *et al.* (1992) 'Glycoproteins V and Ib-IX form a noncovalent complex in the platelet membrane', *Journal of Biological Chemistry*, 267(1), pp. 364–369.

Moroi, A. J. and Watson, S. P. (2015) 'Impact of the PI3-kinase/Akt pathway on ITAM and hemITAM receptors: Haemostasis, platelet activation and antithrombotic therapy', *Biochemical Pharmacology*. Elsevier Inc., 94(3), pp. 186–194.

Moroi, M. and Jung, S. M. (2004) 'Platelet glycoprotein VI: Its structure and function', *Thrombosis Research*, 114(4), pp. 221–233.

Mossman, K. D. *et al.* (2005) 'Immunology: Altered TCR signaling from geometrically repatterned immunological synapses', *Science*, 310(5751), pp. 1191–1193.

Nagae, M. *et al.* (2014a) 'A platform of C-type lectin-like receptor CLEC-2 for binding O-glycosylated podoplanin and nonglycosylated rhodocytin', *Structure*. Elsevier Ltd, 22(12), pp. 1711–1721.

Nagae, M. *et al.* (2014b) 'A platform of C-type lectin-like receptor CLEC-2 for binding O-glycosylated podoplanin and nonglycosylated rhodocytin', *Structure*. Elsevier Ltd, 22(12), pp. 1711–1721.

Nakazawa, Y. *et al.* (2008) 'Tetraspanin family member CD9 inhibits Aggrus/podoplanin-induced platelet aggregation and suppresses pulmonary metastasis', *Blood*, 112(5), pp. 1730–1739.

Nakazawa, Y. *et al.* (2011) 'Prevention of hematogenous metastasis by neutralizing mice and its chimeric anti-Aggrus/podoplanin antibodies', *Cancer Science*, 102(11), pp. 2051–2057.

Navarro-Núñez, L. *et al.* (2015) 'Platelet adhesion to podoplanin under flow is mediated by the receptor CLEC-2 and stabilised by Src/Syk-dependent platelet signalling', *Thrombosis and Haemostasis*, 113(5), pp. 1109–1120.

Naveenkumar, S. K. *et al.* (2018) 'The Role of Reactive Oxygen Species and Ferroptosis in Heme-Mediated Activation of Human Platelets', *ACS Chemical Biology*, 13(8), pp. 1996–2002.

Nguyen, D. and Coull, B. M. (2017) 'Thrombosis', *Primer on Cerebrovascular Diseases*, pp. 108–113.

Nicolson, Phillip L.R. *et al.* (2020) 'A rationale for blocking thromboinflammation in COVID-19 with Btk inhibitors', *Platelets*. Taylor & Francis, 31(5), pp. 685–690.

Nicolson, Phillip L R *et al.* (2020) 'Low dose Btk inhibitors selectively block platelet activation by CLEC-2', *Hematologica*.

Nieswandt, B. *et al.* (2000) 'Expression and function of the mouse collagen receptor glycoprotein VI is strictly dependent on its association with the FcRγ chain', *Journal of Biological Chemistry*. Â© 2000 ASBMB. 275(31), pp. 23998–24002.

Nieswandt, B. and Watson, S. P. (2003) 'Platelet-collagen interaction: Is GPVI the central receptor?', *Blood*, 102(2), pp. 449–461.

Nowosad, C. R. and Tolar, P. (2017) *The Immune Synapse. Chapter 6. Plasma Membrane Sheets for Studies of B Cell Antigen Internalization from Immune Synapses*.

Nurden, A. T. (2006) 'Glanzmann thrombasthenia', *Orphanet Journal of Rare Diseases*, 1(1), pp. 1–8.

O'Brien, J. R. (1961) 'The adhesiveness of native platelets and its prevention.', *Journal of clinical pathology*, 14, pp. 140–149.

Offermanns, S. (2006) 'Activation of platelet function through G protein-coupled receptors', *Circulation Research*, 99(12), pp. 1293–1304.

Oishi, S. *et al.* (2021) 'Heme activates platelets and exacerbates rhabdomyolysis-induced acute kidney injury via CLEC-2 and GPVI/FcRγ', *Blood Advances*, 5(7), pp. 2017–2026.

Ozaki, Y. *et al.* (2005) 'Platelet GPIb-IX-V-dependent signaling', *Journal of Thrombosis and Haemostasis*, 3, pp. 1745–1751.

Parham, F. *et al.* (2009) 'Dose-Response Modeling of High-Throughput Screening Data', *J Biomol Screen*, 14(10), pp. 1216–1227.

Pasquet, J.-M. *et al.* (1999) 'LAT Is Required for Tyrosine Phosphorylation of Phospholipase Cγ2 and Platelet Activation by the Collagen Receptor GPVI', *Molecular and Cellular Biology*, 19(12), pp. 8326–8334.

Patankar, M. S. *et al.* (1993) 'A revised structure for fucoidan may explain some of its biological activities', *Journal of Biological Chemistry*, 268(29), pp. 21770–21776.

Patel, R. Y. and Balaji, P. V. (2011) 'Structure and Dynamics of Glycosphingolipids in Lipid Bilayers: Insights from Molecular Dynamics Simulations', *International Journal of Carbohydrate Chemistry*, 2011(3), pp. 1–9.

Payne, H. *et al.* (2017) 'Mice with a deficiency in CLEC-2 are protected against deep vein thrombosis', *Blood*, 129(14), pp. 2013–2020.

Pearce, A. C. *et al.* (2004) 'Vav1 and Vav3 have critical but redundant roles in mediating platelet activation by collagen', *Journal of Biological Chemistry*. Â© 2004 ASBMB. Currently published by Elsevier Inc; originally published by American Society for Biochemistry and Molecular Biology., 279(52), pp. 53955–53962.

Peppard, J. *et al.* (2003) 'Development of a high-throughput screening assay for inhibitors of aggrecan cleavage using luminescent oxygen channeling (AlphaScreen^{TM})', *Journal of Biomolecular Screening*, 8(2), pp. 149–156.

Pike, L. J. (2006) 'Rafts defined: A report on the Keystone symposium on lipid rafts and cell function', *Journal of Lipid Research*. © 2006 ASBMB. 47(7), pp. 1597–1598.

Polasek, J. (2005) 'Platelet secretory granules or secretory lysosomes?', *Platelets*, 16(8), pp. 500–501.

Pollitt, A. Y. *et al.* (2010a) 'Phosphorylation of CLEC-2 is dependent on lipid rafts, actin polymerization, secondary mediators, and Rac', *Blood*, 115(14), pp. 2938–2946.

Pollitt, A. Y. *et al.* (2010b) 'Phosphorylation of CLEC-2 is dependent on lipid rafts, actin polymerization, secondary mediators, and Rac', *Blood*, 115(14), pp. 2938–2946.

Pollitt, A. Y. *et al.* (2014) 'Syk and src family kinases regulate c-type lectin receptor 2 (clec-2)-mediated clustering of podoplanin and platelet adhesion to lymphatic endothelial cells', *Journal of Biological Chemistry*, 289(52), pp. 35695–35710.

Poo, M. and Cone, R. A. (1974) 'Lateral diffusion of rhodopsin in the visual receptor membrane', *Nature*, 247, pp. 438–441.

Quintanilla, M. *et al.* (2019) 'Podoplanin in inflammation and cancer', *International Journal of Molecular Sciences*, 20(3), pp. 1–38.

Rand, M. L. and Israels, S. J. (2017) *Molecular Basis of Platelet Function*. Seventh Ed, *Hematology: Basic Principles and Practice*. Seventh Ed. Elsevier Inc.

Rayes, J. *et al.* (2017) 'The podoplanin-CLEC-2 axis inhibits inflammation in sepsis', *Nature Communications*. Springer US, 8(1).

Reimhult, E. *et al.* (2010) 'Advances in nanopatterned and nanostructured supported lipid membranes and their applications', *Biotechnology and Genetic Engineering Reviews*, 27(1), pp. 185–216.

Rey, E. *et al.* (2017) 'Mitigating the hook effect in lateral flow sandwich immunoassays using real-time reaction kinetics', *Anal Chem.*, 89(9), pp. 5095–5100.

Riaz, A. *et al.* (2012) 'Human platelets efficiently kill IgG-opsonized E. coli', *FEMS Immunol Med Microbiol.*, 65(1), pp. 78–83.

Richter, R. P., Bérat, R. and Brisson, A. R. (2006) 'Formation of solid-supported lipid bilayers: An integrated view', *Langmuir*, 22(8), pp. 3497–3505.

Rivera, J. *et al.* (2009) 'Platelet receptors and signaling in the dynamics of thrombus formation', *Haematologica*, 94(5), pp. 700–711.

Ross, G. M. S. *et al.* (2020) 'Unraveling the Hook Effect: A Comprehensive Study of High Antigen Concentration Effects in Sandwich Lateral Flow Immunoassays', *Analytical Chemistry*, 92(23), pp. 15587–15595.

Salaita, K. *et al.* (2010) 'Restriction of Receptor Movement Alters Cellular Response: Physical Force Sensing by EphA2', *Science*, 327(5971), pp. 1380–1385.

Sandmann, R. and Köster, S. (2016) 'Topographic Cues Reveal Two Distinct Spreading Mechanisms in Blood Platelets', *Scientific Reports*. Nature Publishing Group, 6(February), pp. 1–11.

De Sauvage, F. J. *et al.* (1994) 'Stimulation of megakaryocytopoiesis and thrombopoiesis by the c-Mpl ligand', *Nature*, 369(6481), pp. 533–538.

Schacht, V. *et al.* (2005) 'Up-regulation of the lymphatic marker podoplanin, a mucin-type transmembrane glycoprotein, in human squamous cell carcinomas and germ cell tumors', *American Journal of Pathology*, 166(3), pp. 913–921.

Schmaier, A. A. *et al.* (2009) 'Molecular priming of Lyn by GPVI enables an immune receptor to adopt a hemostatic role', *Proceedings of the National Academy of Sciences of the United States of America*, 106(50), pp. 21167–21172.

Schrödinger (2015) *Glide 6.7 User Manual*.

Schuck, S. *et al.* (2003) 'Resistance of cell membranes to different detergents', *Proceedings of the National Academy of Sciences of the United States of America*, 100(10), pp. 5795–5800.

Sekiguchi, T. *et al.* (2016) 'Targeting a novel domain in podoplanin for inhibiting plateletmediated tumor metastasis', *Oncotarget*, 7(4), pp. 3934–3946.

Seltzer, S. and Gregoriadis, G. (1988) 'Evaluation of Dehydration-Rehydation Method for Production of Contrast-Carrying Liposomes', *Invest Radiol.*, 23(2), pp. 131–138.

Senis, Y. A. *et al.* (2009) 'The tyrosine phosphatase CD148 is an essential positive regulator of platelet activation and thrombosis', *Blood*, 113(20), pp. 4942–4954.

Senis, Y. A., Mazharian, A. and Mori, J. (2014) 'Src family kinases: At the forefront of platelet activation', *Blood*, 124(13), pp. 2013–2024.

Séverin, S. *et al.* (2011) 'Syk-dependent phosphorylation of CLEC-2: A novel mechanism of hem-immunoreceptor tyrosine-based activation motif signaling', *Journal of Biological Chemistry*, 286(6), pp. 4107–4116.

Shah, B. H. *et al.* (2001) 'Molecular mechanisms involved in human platelet aggregation by synergistic interaction of platelet-activating factor and 5-hydroxytryptamine', *Experimental and Molecular Medicine*, 33(4), pp. 226–233.

Shibahara, J. *et al.* (2006) 'Podoplanin is expressed in subsets of tumors of the central nervous system', *Virchows Archiv*, 448(4), pp. 493–499.

Shilts, K. and Naumann, C. A. (2018) 'Tunable cell-surface mimetics as engineered cell substrates', *Biochimica et Biophysica Acta - Biomembranes*. Elsevier, 1860(10), pp. 2076–2093.

Shirai, T. *et al.* (2017) 'C-type lectin-like receptor 2 promotes hematogenous tumor metastasis and prothrombotic state in tumor-bearing mice', *Journal of Thrombosis and Haemostasis*, 15(3), pp. 513–525.

Shoichet, B. K. (2006) 'Virtual screening of chemical libraries Problems with virtual screening', *Nature*, 432(7019), pp. 862–865.

Simon, M. I., Strathmann, M. P. and Gautam, N. (1991) 'Diversity of G proteins in Signal Transduction', *Science*, 252(1971), pp. 802–808.

Simons, K. and Ikonen, E. (1997) 'Functional rafts in cell membranes', *Nature*, 387(6633), pp. 569–572.

Simons, K. and Toomre, D. (2000) 'Lipid rafts and signal transduction', *Nat Rev Mol Cell Biol*, Oct 1(1), pp. 31–39.

Singer, S. . and Nicolson, G. L. (1972) 'The Fluid Mosaic Model of the Structure of Cell Membranes', *Science*, 175, pp. 720–731.

Singh, R. *et al.* (2002) 'Pathogenesis of atherosclerosis: A multifactorial process', *Exp Clin Cardiol.*, 7(1), pp. 40–53.

Smethurst, P. A. *et al.* (2004) 'Identification of the primary collagen-binding surface on human glycoprotein VI by site-directed mutagenesis and by a blocking phage antibody', *Blood*, 103(3), pp. 903–911.

Smith, K. G. C. and Clatworthy, M. R. (2010) 'FcγRIIB in autoimmunity and infection: evolutionary and therapeutic implications', *Nat Rev Immunol.*, 10(5), pp. 328–343.

Spalton, J. C. *et al.* (2009) 'The novel Syk inhibitor R406 reveals mechanistic differences in the initiation of GPVI and CLEC-2 signaling in platelets', *Journal of Thrombosis and Haemostasis*, 7(7), pp. 1192–1199.

Springer, T. A., Zhu, J. and Xiao, T. (2008) 'Structural basis for distinctive recognition of fibrinogen γC peptide by the platelet integrin αIIbβ3', *Journal of Cell Biology*, 182(4), pp. 791–800.

Sugiyama, T. *et al.* (1987) 'A novel platelet aggregating factor found in a patient with defective collagen-induced platelet aggregation and autoimmune thrombocytopenia', *Blood*. American Society of Hematology, 69(6), pp. 1712–1720.

Sundberg, S. A. (2000) 'High-throughput and ultra-high-throughput screening: Solution- and cell-based approaches', *Current Opinion in Biotechnology*, 11(1), pp. 47–53.

Suzuki-Inoue, K. *et al.* (2002) 'Association of Fyn and Lyn with the proline-rich domain of glycoprotein VI regulates intracellular signaling', *Journal of Biological Chemistry*, 277(24), pp. 21561–21566.

Suzuki-Inoue, K. *et al.* (2003) 'Murine GPVI stimulates weak integrin activation in PLCγ2 -/- platelets: Involvement of PLCγ1 and PI3-kinase', *Blood*, 102(4), pp. 1367–1373.

Suzuki-Inoue, K *et al.* (2006) 'A novel Syk-dependent mechanism of platelet activation by the C-type lectin receptor CLEC-2', *Blood*, 107(2), pp. 542–549.

Suzuki-Inoue, Katsue *et al.* (2006) 'A novel Syk-dependent mechanism of platelet activation by the C-type lectin receptor CLEC-2', *Blood*, 107(2), pp. 542–549.

Suzuki-Inoue, K. *et al.* (2007) 'Involvement of the Snake Toxin Receptor CLEC-2, in Podoplanin-mediated Platelet Activation, by Cancer Cells', *Journal of Biological Chemistry*, 282(36), pp. 25993–26001.

Suzuki-Inoue, K. *et al.* (2010a) 'Essential in vivo roles of the C-type lectin receptor CLEC-2: Embryonic/neonatal lethality of CLEC-2-deficient mice by blood/lymphatic misconnections and impaired thrombus formation of CLEC-2-deficient platelets', *Journal of Biological Chemistry*, 285(32), pp. 24494–24507.

Suzuki-Inoue, K. *et al.* (2010b) 'Essential in vivo roles of the C-type lectin receptor CLEC-2: Embryonic/neonatal lethality of CLEC-2-deficient mice by blood/lymphatic misconnections and impaired thrombus formation of CLEC-2-deficient platelets', *Journal of Biological Chemistry*, 285(32), pp. 24494–24507.

Takagi, S. *et al.* (2013) 'Platelets Promote Tumor Growth and Metastasis via Direct Interaction between Aggrus/Podoplanin and CLEC-2', *PLoS ONE*, 8(8), pp. 1–11.

Takemoto, A. *et al.* (2017) 'A critical role of platelet TGF-β release in podoplanin-mediated tumour invasion and metastasis', *Scientific Reports*. Nature Publishing Group, 7(February), pp. 1–12.

Tang, Y. Q., Yeaman, M. R. and Selsted, M. E. (2002) 'Antimicrobial peptides from human platelets', *Infection and Immunity*, 70(12), pp. 6524–6533.

Tavassoli, M. and Aoki, M. (1989) 'Localization of megakaryocytes in the bone marrow', *Blood Cells*, 15, pp. 3–14.

Taylor, M. J. *et al.* (2017) 'A DNA-Based T Cell Receptor Reveals a Role for Receptor Clustering in Ligand Discrimination', *Cell*. Elsevier Inc., 169(1), pp. 108–119.

Thomas, M. R. and Storey, R. F. (2015) 'The role of platelets in inflammation', *Thrombosis and Haemostasis*, 114.3, pp. 449–458.

Tomiyama, Y. *et al.* (1992) 'Response of human platelets to activating monoclonal antibodies: Importance of FcγRII (CD32) phenotype and level of expression', *Blood*. American Society of Hematology, 80(9), pp. 2261–2268.

Tsukiji, N. *et al.* (2018) 'Cobalt hematoporphyrin inhibits CLEC-2–podoplanin interaction, tumor metastasis, and arterial/venous thrombosis in mice', *Blood Advances*, 2(17), pp. 2214–2225.

Turner, M. *et al.* (1995) 'Perinatal lethality and blocked B-cell development in mice lacking the tyrosine kinase Syk', *Nature*, 378, pp. 298–302.

Valvo, S. *et al.* (2017) *The Immune Synapse. Chapter 26. Comprehensive Analysis of Immunological Synapse Phenotypes Using Supported Lipid Bilayers*.

Varma, R. *et al.* (2006) 'T Cell Receptor-Proximal Signals Are Sustained in Peripheral Microclusters and Terminated in the Central Supramolecular Activation Cluster', *Immunity*, 25(1), pp. 117–127.

Wagner, C. L. *et al.* (1996) 'Analysis of GPIIb/IIIa receptor number by quantification of 7E3 binding to human platelets', *Blood*, 88(3), pp. 907–914.

Wagner, D. D. and Burger, P. C. (2003) 'Platelets in Inflammation and Thrombosis', *Arteriosclerosis, Thrombosis, and Vascular Biology*, 23(12), pp. 2131–2137.

Wandall, H. H. *et al.* (2017) ' Characterizing the O -glycosylation landscape of human plasma, platelets, and endothelial cells ', *Blood Advances*, 1(7), pp. 429–442.

Wang, D. *et al.* (2000) 'Phospholipase C gamma 2 Is Essential in the Functions of B Cell and Several Fc Receptors', *Immunity*, 13, pp. 25–35. Available at:

Wang, L. *et al.* (2012) 'Structural and functional conservation of CLEC-2 with the species-specific regulation of transcript expression in evolution', *Glycoconjugate Journal*, 29(5–6), pp. 335–345.

Watanabe, N. *et al.* (2019) 'A pull-down and slot blot-based screening system for inhibitor compounds of the podoplanin-CLEC-2 interaction', *PLoS ONE*, 14(9), pp. 1–13.

Watson, A. A. *et al.* (2007) 'The crystal structure and mutational binding analysis of the extracellular domain of the platelet-activating receptor CLEC-2', *Journal of Biological Chemistry*. Â© 2007 ASBMB. 282(5), pp. 3165–3172.

Watson, A. A. *et al.* (2009) 'The platelet receptor CLEC-2 is active as a dimer', *Biochemistry*, 48(46), pp. 10988–10996.

Watson, A. A., Eble, J. A. and O'Callaghan, C. A. (2008) 'Crystal structure of rhodocytin, a ligand for the platelet-activating receptor CLEC-2', *Protein Science*, 17(9), pp. 1611–1616.

Watson, S. P., Auger, J. M., McCarty, O. J. T., *et al.* (2005) 'GPVI and integrin alpha-IIb-beta-3 signaling in platelets', *Journal of Thrombosis and Haemostasis*, 3, pp. 1752–1762.

Watson, S. P., Auger, J. M., McCrty, O. J. T., *et al.* (2005) 'GPVI and integrin alphaIIbbeta3 signaling in platelets', *Journal of Thrombosis and Haemostasis*, 3, pp. 1752–1762.

Watson, S. P., Herbert, J. M. J. and Pollitt, A. Y. (2010) 'GPVI and CLEC-2 in hemostasis and vascular integrity', *Journal of Thrombosis and Haemostasis*, 8(7), pp. 1456–1467.

White, J. G. (1972) 'Interaction of membrane systems in blood platelets.', *The American journal of pathology*, 66(2), pp. 295–312.

White, J. G. (2013) *Platelet Structure*. Third Edit, *Platelets*. Third Edit. Elsevier Inc.

Whittle, B. J. R., Moncada, S. and Vane, J. R. (1978) 'Comparison of the effects of prostacyclin (PGI2), prostaglandin E1 and D2 on platelet aggregation in different species', *Prostaglandis*, 16(3), pp. 373–388.

Wicki, A. *et al.* (2006) 'Tumor invasion in the absence of epithelial-mesenchymal transition: Podoplanin-mediated remodeling of the actin cytoskeleton', *Cancer Cell*, 9(4), pp. 261–272.

Wicki, A. and Christofori, G. (2007) 'The potential role of podoplanin in tumour invasion', *British Journal of Cancer*, 96(1), pp. 1–5.

Wonerow, P. *et al.* (2002) 'Differential role of glycolipid-enriched membrane domains in glycoprotein VI- and integrin-mediated phospholipase Cγ2 regulation in platelets', *Biochemical Journal*, 364(3), pp. 755–765.

Woulfe, D. S. (2005) 'Platelet G protein-coupled receptors in hemostasis and thrombosis', *Journal of Thrombosis and Haemostasis*, 3(10), pp. 2193–2200.

Xiang, B. *et al.* (2013) 'Platelets protect from septic shock by inhibiting macrophage-dependent inflammation via the cyclooxygenase 1 signaling pathway', *Nat Commun*, 4(2657).

Yarrow, J. C. *et al.* (2005) 'Screening for cell migration inhibitors via automated microscopy reveals a Rho-kinase inhibitor', *Chemistry and Biology*, 12(3), pp. 385–395.

Yokosuka, T. *et al.* (2008) 'Spatiotemporal regulation of T cell co-stimulation by TCR-CD28 microclusters through PKCθ translocation', *Immunity*, 29(4), pp. 589–601.

Yu, C. H. *et al.* (2011) 'Early integrin binding to Arg-Gly-Asp peptide activates actin polymerization and contractile movement that stimulates outward translocation', *Proceedings of the National Academy of Sciences of the United States of America*, 108(51), pp. 20585–20590.

Yu, X. and Lazarus, A. H. (2016) 'Targeting FcγRs to treat antibody-dependent autoimmunity', *Autoimmunity Reviews*. Elsevier B.V., 15(6), pp. 510–512.

Yun, S. H. *et al.* (2016) 'Platelet activation: The mechanisms and potential biomarkers', *BioMed Research International*. Hindawi Publishing Corporation, 2016, pp. 10–14.

Zeiler, M., Moser, M. and Mann, M. (2014) 'Copy number analysis of the murine platelet proteome spanning the complete abundance range', *Molecular and Cellular Proteomics*, 13(12), pp. 3435–3445.

Zhang, D. *et al.* (2020) 'Glycoprotein VI is not a Functional Platelet Receptor for Fibrin Formed in Plasma or Blood', *Thrombosis and Haemostasis*, 120(6), pp. 977–993.

Zhang, J. H., Chung, T. D. Y. and Oldenburg, K. R. (1999) 'A simple statistical parameter for use in evaluation and validation of high throughput screening assays', *Journal of Biomolecular Screening*, 4(2), pp. 67–73.

Zhang, S. and Reinhard, B. M. (2019) 'Characterizing Large-Scale Receptor Clustering on the Single Cell Level: A Comparative Plasmon Coupling and Fluorescence Superresolution Microscopy Study', *Journal of Physical Chemistry B*, 123(26), pp. 5494–5505.

Zheng, Y. M. *et al.* (2001) 'Expression of the Platelet Receptor GPVI Confers Signaling via the Fc Receptor γ-Chain in Response to the Snake Venom Convulxin but Not to Collagen', *Journal of Biological Chemistry*, 276(16), pp. 12999–13006.

Zhi, H. *et al.* (2013) 'Cooperative integrin/ITAM signaling in platelets enhances thrombus formation in vitro and in vivo', *Blood*, 121(10), pp. 1858–1867.

Zhu, T. *et al.* (2013) 'Hit Identification and Optimization in Virtual Screening: Practical Recommendations Based Upon a Critical Literature Analysis', *ournal of medicinal chemistry*, 56(17), pp. 6560–6572.
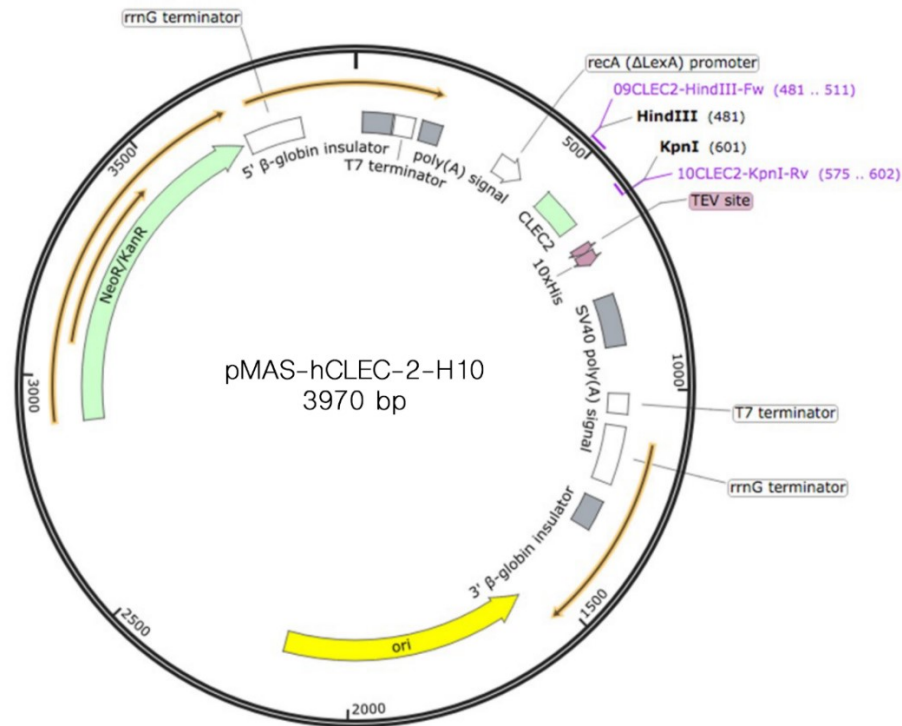
8. Appendix

Figure 8.1. Plasmid map of pMAS-hCLEC-2-H10.

The intracellular domain of human CLEC-2 (aa 1-33) was cloned in frame into pSF-OXB20-NH2-TEV-His10 containing a 10×His-tag

downstream of the multiple cloning sites using HindIII and KpnI. Map created in SnapGene.
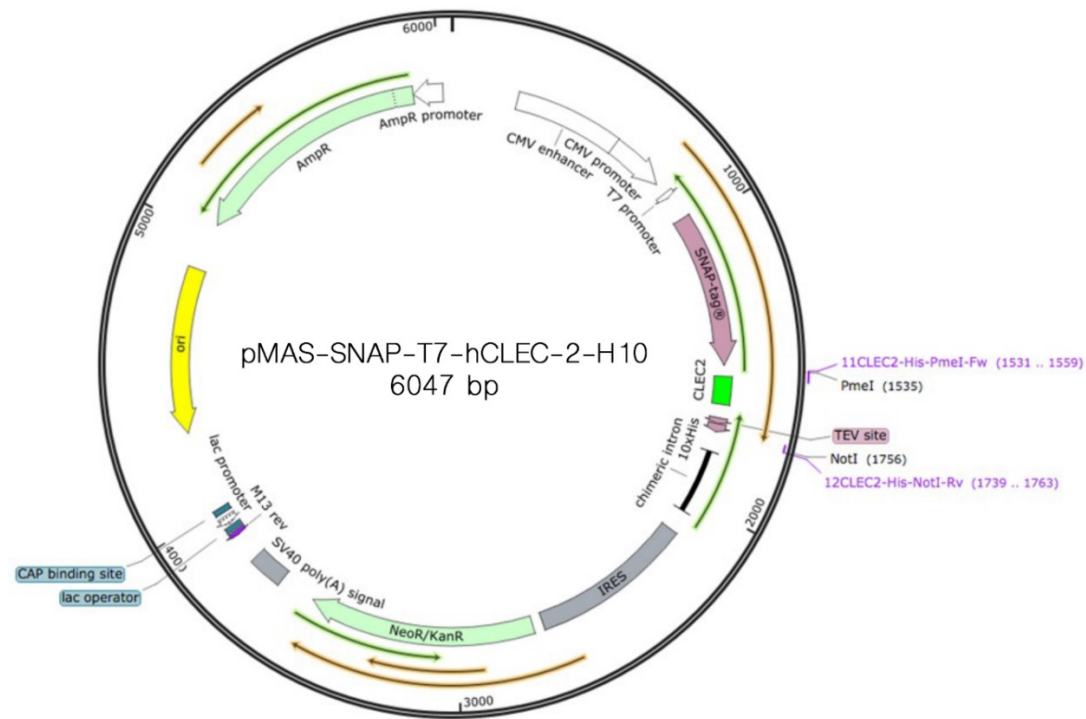
Figure 8.2. Plasmid map of pMAS-SNAP-T7-hCLEC-2-H10.

The intracellular domain of human CLEC-2 (aa 1-33) with C-terminal 10x His-tag was cloned in frame into pSNAP-tag® (T7)-2 vector containing a SNAP-tag protein gene sequence upstream of the multiple cloning sites using PmeI and NotI. Map created in SnapGene.
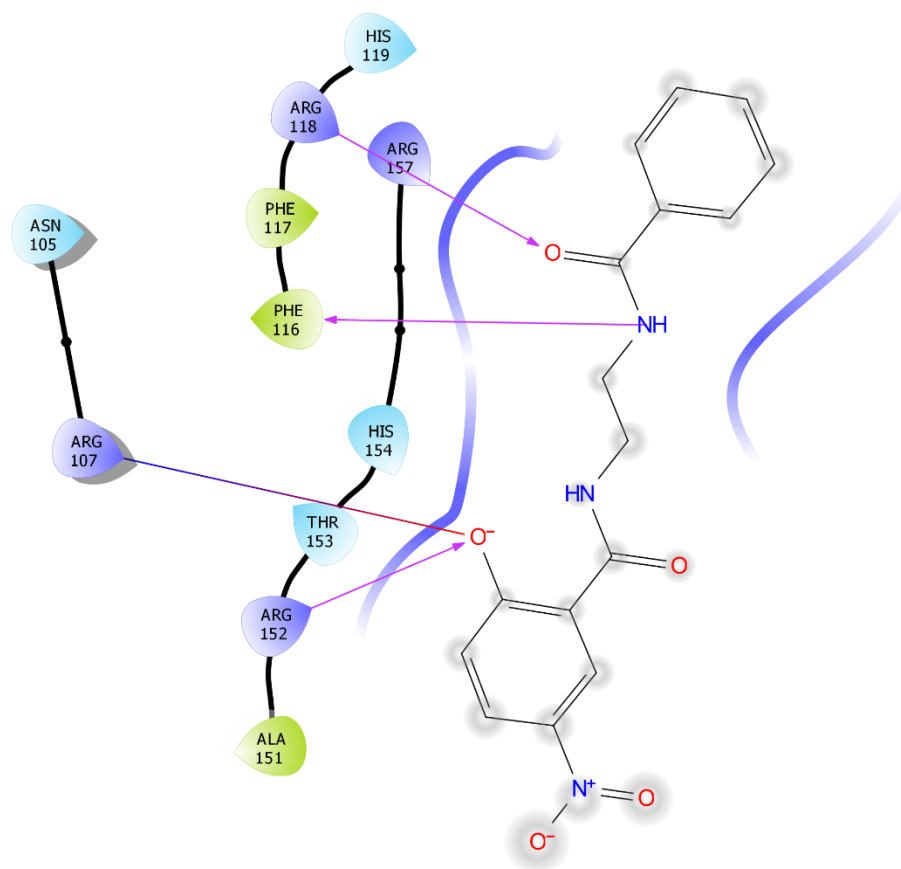
Figure 8.3. 2D diagram of 2CP binding to CLEC-2.

Interactions of CLEC-2 and 2CP are shown. 2CP is shown as stick diagram. H-bonds

between the receptor and ligands are shown as purple lines.